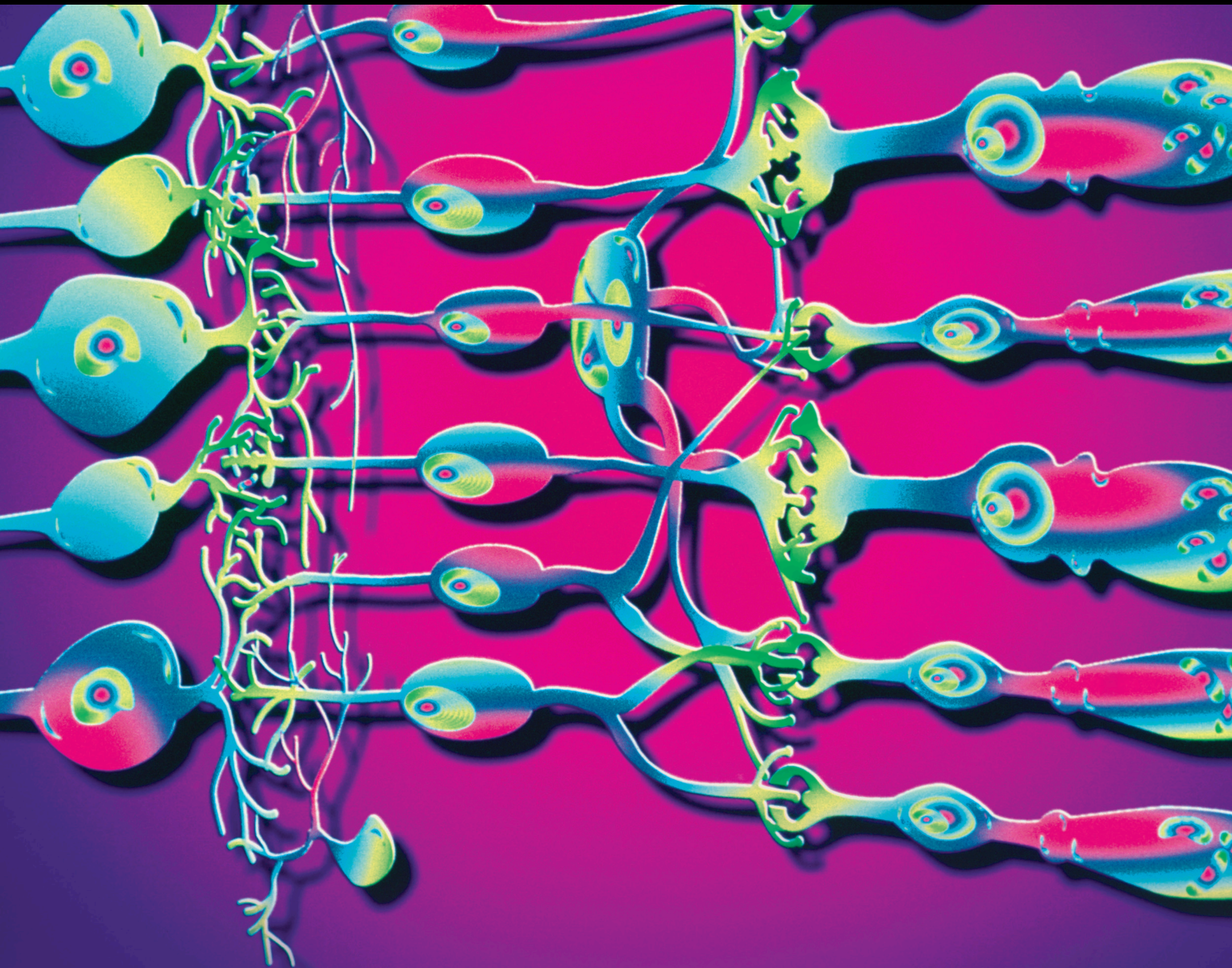# Advances and Clinical Applications of Anterior Segment Imaging Techniques 2021

Lead Guest Editor: Sang Beom Han
Guest Editors: Jodhbir S. Mehta, Yu-Chi Liu, and Karim Mohamed-Noriega

Advances and Clinical Applications of Anterior Segment Imaging Techniques 2021

Advances and Clinical Applications of Anterior Segment Imaging Techniques 2021

Lead Guest Editor: Sang Beom Han
Guest Editors: Jodhbir S. Mehta, Yu-Chi Liu, and Karim Mohamed-Noriega

Antonio Queiros, Portugal
Miguel Rechichi, Italy
Anthony G. Robson, United Kingdom
Mario R. Romano, Italy
Wataru Saito, Japan
Juan A. Sanchis-Gimeno, Spain
Dirk Sandner, Germany
Ana Raquel Santiago, Portugal
Rehman Siddiqui, Pakistan
Bartosz Sikorski, Poland
Shivalingappa K. Swamynathan, USA
Nóra Szentmáry, Hungary
Masaru Takeuchi, Japan
Suphi Taneri, Germany
Miguel Teus, Spain
Biju B. Thomas, USA
Oren Tomkins-Netzer, United Kingdom
Lisa Toto, Italy
Giacinto Triolo, Italy
Giacinto Triolo, Italy
Maurizio Uva, Italy
Manuel Vidal-Sanz, Spain
Paolo Vinciguerra, Italy
Nilufer Yesilirmak, Turkey
Vicente Zanon-Moreno, Spain
Tomasz Zarnowski, Poland
Yedi Zhou, China

Contents

Editorial

Advances and Clinical Applications of Anterior Segment Imaging Techniques 2021

Sang Beom Han ,[1] **Jodhbir S. Mehta** ,[2,3,4] **Yu-Chi Liu** ,[2,3,4] **and Karim Mohamed Noriega** [5]

[1]*Department of Ophthalmology, Kangwon National University College of Medicine, Kangwon National University Hospital, Chuncheon, Republic of Korea*
[2]*Singapore National Eye Centre, Singapore*
[3]*Singapore Eye Research Institute, Singapore*
[4]*Department of Ophthalmology, Yong Loo Lin School of Medicine, National University of Singapore, Singapore*
[5]*Department of Ophthalmology, University Hospital, Faculty of Medicine, Autonomous University of Nuevo Leon, Monterrey, Mexico*

Correspondence should be addressed to Sang Beom Han; m.sangbeom.han@gmail.com

This special issue covers the progress of imaging technologies of anterior segment of the eye, development of novel imaging devices of anterior segment, and the clinical and research application of the imaging modalities of anterior segment. In this annual issue, the authors contributed one review paper 10 research articles regarding the application of the various anterior segment imaging modalities in the diagnosis and treatment of various anterior segment diseases as well as in research of these diseases.

In this annual issue, the guest editorial team contributed a review paper regarding the following topic: application of intraoperative optical coherence tomography technology in anterior segment surgery. In this article, the authors summarized the recent development of intraoperative application of anterior segment optical coherence tomography technologies.

Authors from various countries conducted research on various imaging techniques and devices of anterior segment structures and contributed the results of their studies to this annual issue, as follows: (1) Changes of Lacrimal Puncta by Anterior Segment Optical Coherence Tomography after Topical Combined Antibiotic and Steroid Treatment in Cases of Inflammatory Punctual Stenosis; (2) Comparison of Consecutive Therapeutic Effects of Nanoemulsion and Emulsion Cyclosporin in Dry Eye Patients after Short-Term Treatment with Topical Fluorometholone; (3) The Efficacy of Clinical Tests to Diagnose Evaporative Dry Eye Disease Related to Meibomian Gland Dysfunction; (4) The Effectiveness of Laser Peripheral Iridotomy in Adolescent Eyes with Ocular Hypertension and Concave Configuration of the Peripheral Iris; (5) Evaluation of Intraocular Lens Tilt and Decentration in Congenital Ectopia Lentis by the Pentacam Scheimpflug System; (6) Specular Microscopic Corneal Endothelial Cell Changes following Uneventful Phacoemulsification in Patients with Gout; (7) Simultaneous Corneal Topography and Epithelial Thickness Mapping from a Single Measurement Using Optical Coherence Tomography; (8) Factors Related to Visual Outcomes after Lens Surgery in Isolated Microspherophakia; (9) Characteristics of Anterior Segment in Congenital Ectopia Lentis: An SS-OCT Study; (10) Characteristics of Optic Neuritis in South Korean Children and Adolescents: A Retrospective Multicenter Study.

Progress of imaging technologies of anterior segment of the eye and development of imaging devices of the anterior segment structures may allow optimal management of anterior segment diseases, such as corneal and conjunctival disorders, cataract, glaucoma, and diseases of the lacrimal system and eyelid.

Conflicts of Interest

Acknowledgments

Hindawi

Research Article

Characteristics of Optic Neuritis in South Korean Children and Adolescents: A Retrospective Multicenter Study

Kyung-Ah Park [ID],[1] **Hee Kyung Yang** [ID],[2] **Jinu Han** [ID],[3] **Seong-Joon Kim** [ID],[4] **Sung Eun Park,**[5] **Haeng-Jin Lee,**[6] **Sueng-Han Han,**[5] **Sei Yeul Oh,**[1] and **Jeong-Min Hwang** [ID][2]

[1]*Department of Ophthalmology, Samsung Medical Center, Sungkyunkwan University School of Medicine, Seoul, Republic of Korea*

[2]*Department of Ophthalmology, Seoul National University College of Medicine, Seoul National University Bundang Hospital, Seongnam, Republic of Korea*

[3]*Institute of Vision Research, Gangnam Severance Hospital, Department of Ophthalmology, Yonsei University College of Medicine, Seoul, Republic of Korea*

[4]*Department of Ophthalmology, Seoul National University College of Medicine, Seoul National University Hospital, Seoul, Republic of Korea*

[5]*Institute of Vision Research, Severance Hospital, Department of Ophthalmology, Yonsei University College of Medicine, Seoul, Republic of Korea*

[6]*Department of Ophthalmology, Jeonbuk National University College of Medicine, Jeonju, Republic of Korea*

Correspondence should be addressed to Jinu Han; jinuhan@yuhs.ac and Seong-Joon Kim; ophjun@snu.ac.kr

Academic Editor: Alessandro Meduri

Purpose. To analyze the clinical characteristics and prognosis of optic neuritis (ON) in pediatric patients aged <19 years in South Korea. *Methods*. This multicenter retrospective cohort study included 127 pediatric patients (median age: 10.3 (IQR: 7.3–14.2) years; female, 62.2%) who experienced ON for the first time between January 2004 and January 2018, with data obtained from five tertiary university-based hospitals in Korea. When ON was bilateral, the worse eye was selected for analysis. The baseline clinical characteristics and prognoses of patients, as well as the associations between these parameters, were analyzed. *Results*. The baseline clinical characteristics of the patients were as follows: best-corrected visual acuity (BCVA) < 20/200, 65.9%; pain on eye movement, 47.2%; optic disc swelling, 66.9%; and bilateral involvement, 41.7%. Among 101 patients who were followed up for ≥6 months, 48 (47.5%), 12 (11.9%), 19 (18.8%), 13 (12.9%), and 9 (8.9%) had been diagnosed with isolated ON, recurrent ON, multiple sclerosis (MS), neuromyelitis optica spectrum disorder (NMOSD), and acute disseminated encephalomyelitis (ADEM)-related ON, respectively. At the latest visit, 81.9% and 71.1% had achieved BCVA of ≥20/40 and ≥ 20/25, respectively. Only disc swelling at presentation was associated with poor baseline BCVA (coefficient: 0.31, $P = 0.004$) and greater improvement in BCVA (coefficient: 0.49, $P = 0.001P = 0.001$); there were no significant associations between the baseline factors and final BCVA. *Conclusions*. This study demonstrated pediatric ON-related clinical characteristics and visual outcomes in South Korea. Within this cohort, in about 40.6% of patients, ON was associated with other demyelinating diseases, namely, MS, NMOSD, and ADEM.

1. Introduction

Optic nerve inflammation has various causes, including infectious, granulomatous, paraneoplastic, or inflammatory demyelinating etiologies. Early determination of the cause of optic neuritis (ON) is an important aspect of providing appropriate treatment [1]. Demyelinating ON most commonly affects young adults. However, ON is less prevalent among children than it is among adults [2]. According to a population-based study, the annual incidence of ON among

pediatric patients in South Korea is 1.04 per 100,000 people [3], which is less than that among adults (2.21–3.29 per 100,000) [4, 5]. This is also slightly lower than the incidence of pediatric ON in Taiwan (1.79–2.46 per 100,000) [6] and higher than that in the US [7]. In terms of clinical manifestation, ON in children is reported to show more distinct features than in adults [8–24]. Children are likely to have a preceding viral illness, painless bilateral optic nerve swelling, and severe vision loss at presentation [8–24]. However, most available information about pediatric ON is based on retrospective studies with relatively small samples (up to 102) [8, 9, 15, 23, 25–27]. The Optic Neuritis Treatment Trial was performed on adults aged 18–46 years old, and because 85% of them were Caucasian [28], its findings cannot be generalized to Asian pediatric patients [28]. It has also been reported that the clinical features of patients with ON differ among different ethnicities in both adults [29] and children [30]. A multicenter prospective study on pediatric ON was conducted in the US, but only 9% of the included children were of Asian ethnicity [27]. In addition, large-scale studies on pediatric ON are rare in Asia [8, 9, 25–27]. To address these gaps in the literature, we conducted a multicenter study to investigate the clinical characteristics and prognoses of pediatric patients with ON in South Korea. We also analyzed prognostic factors associated with the visual outcomes of ON.

2. Methods

This multicenter retrospective case series included pediatric patients with ON from five tertiary university-based hospitals in Seoul and the Gyeongi province: Bundang Seoul National University Hospital, $n = 38$; Gangnam Severance Hospital, $n = 2$; Samsung Medical Center, $n = 28$; Seoul National University Hospital, $n = 36$; and Shinchon Severance Hospital, $n = 23$. All patients were aged <19 years at the time of the first presentation of ON between January 2004 and January 2018. Approval was obtained from the appropriate institutional review boards at individual centers.

The main inclusion criteria were as follows: (1) Diagnosis of ON in at least one eye based on clinical symptoms such as visual loss with or without pain on eye movement, (2) presence of relative afferent pupillary defect (RAPD) in the case of unilateral involvement, (3) presence of at least one of the following features in the affected eye: BCVA deficit that is at least two lines below the age-based norms; color vision reduction; visual field defect; or optic disc swelling. The exclusion criteria were as follows: evidence of metabolic, toxic, inherited, mitochondrial, vascular, infectious, or compressive etiology affecting the optic nerve; intracranial hypertension; clinical evidence indicating mitochondrial disorders; or previously diagnosed amblyopia [31]. Patients were excluded if they had pre-existing ocular abnormalities or previous episodes of ON.

Data on demographic characteristics such as sex, age at onset, history of vaccination, the occurrence of infection within one month before the onset of ON, BCVA at presentation, time to first recurrence from the onset of ON, bilateral optic nerve involvement, the number of

recurrences, the presence or absence of RAPD, pain on eye movement, optic disc swelling at presentation, white matter lesions (WMLs) on magnetic resonance (MR) images, and enhancement of the optic nerve on MR images were obtained. Serologic findings, including those of blood and cerebrospinal fluid (CSF) analyses, erythrocyte sedimentation rate, C-reactive protein, aquaporin-4 (AQP4) antibody, myelin oligodendrocyte glycoprotein (MOG) antibody, and anti-nuclear antibody, were also recorded. Serum levels of AQP4 and MOG antibodies were tested using a live cell-based assay [32, 33]. When ON was bilateral, the worse eye was selected for the analysis.

The final diagnoses were confirmed based on clinical and radiological information related to one of the following diagnostic categories: (1) isolated ON, (2) recurrent ON, and (3) multiple sclerosis (MS), in accordance with the 2013 International Pediatric Multiple Sclerosis Study Group consensus criteria [34], (4) neuromyelitis optica (NMO) spectrum disorder (NMOSD), in accordance with the 2015 International Panel for NMO diagnosis criteria, and (5) acute disseminated encephalomyelitis (ADEM) and ADEM-ON, in accordance with the 2013 International Pediatric Multiple Sclerosis Study Group consensus criteria [34].

Regression analyses were used to determine whether there were any associations between baseline characteristics and visual outcomes. We considered the following baseline factors: age at presentation, sex, disc swelling, final diagnosis (neurological associated, i.e., ADEM, NMO, or MS vs. isolated or recurrent ON), bilaterality, and the presence of WMLs on MR images. The visual outcomes were categorized as follows: good, the latest BCVA ≥20/40 with no visual field defect; fair, 20/200≤ BCVA <20/40 or ≥20/40 with permanent visual field defect; and poor, BCVA <20/200 [11, 35, 36]. Statistical analyses were conducted using Stata v.16.1 (StataCorp LLC, College Station, Texas, USA). Continuous variables were analyzed using the Kruskal-Wallis test. Categorical data were compared using the chi-square or Fisher's exact test. P values of <0.05 were considered to be statistically significant.

3. Results

3.1. Baseline Characteristics. In total, 127 children (62.2% female) who experienced the first occurrence of ON were included. The median age at presentation was 10.3 years (interquartile range [IQR], 7.3–14.2 years, Figure 1). The demographic and clinical features are listed in Table 1. The mean baseline BCVA was 1.26 logMAR (IQR, 0.82–1.7, range 0–1.7). Eighty-three patients (65.9%) presented with a BCVA <20/200 at the initial visit. Eye pain on movement was noted in 51 of the 108 (47.2%) patients, and disc swelling was noted in 83 of the 124 (66.9%) patients. Four patients had previous ADEM episodes, and the diagnosis of MS was made in one patient before the first episode of ON. Thirty-nine (36.1%) of the 109 children had a previous febrile illness within 1 month of the occurrence of ON. Seven (6.9%) of the 101 children had a vaccination history within 1 month of ON occurrence, and none of these seven patients were diagnosed with ADEM-ON. Because testing for AQP4 and MOG antibodies was not available during early study periods, the
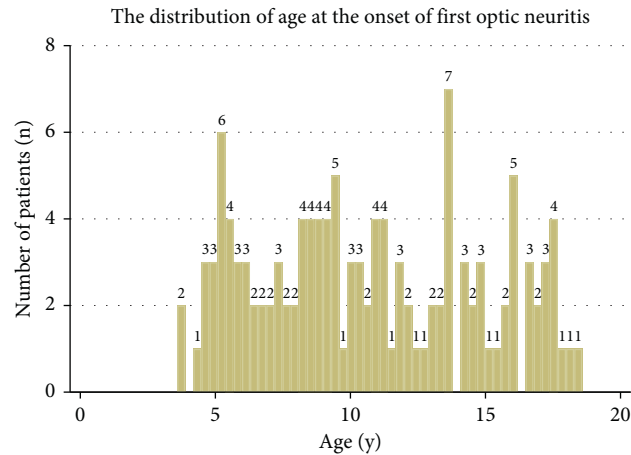
Figure 1: Age distribution of pediatric patients with optic neuritis at presentation.

Table 1: Clinical demographics of patients with pediatric onset optic neuritis.

	Numbers (total)	%, or SD (IQR)
Number of patients	127	100%
Sex (female)	79	62.2%
Age at onset (years)		
3–6	29	22.8%
7–9	32	25.2%
10–12	23	18.1%
≥13	43	33.9%
Mean (median)	10.7 (10.3)	4.1 (7.3–14.2)
Bilaterality	53 (127)	41.7%
Pain with eye movement	51 (108)	47.2%
Disc swelling at presentation	83 (124)	66.9%
Accompanying headache	37 (127)	29.1%
White matter lesions on MRI	41 (126)	32.5%
Preceding febrile illness within 1 month	39 (108)	36.1%
Vaccination history within 1 month	7 (101)	6.9%
Visual acuity at presentation	Total = 126	
≥20/20	4	3.2%
<20/20-≥ 20/40	11	8.7%
<20/40-≥ 20/200	28	22.2%
<20/200-> counting fingers	26	20.6%
Counting finger-no light perception	57	45.2%
Final visual outcome†	Total = 100	
Good	76	76%
Fair	15	15%
Poor	9	9%

SD = standard deviation, IQR = interquartile range. †Visual outcome was categorized as the latest BCVA ≥20/40 with no visual field defect (good), BCVA <20/40~≥ 20/200 or ≥ 20/40 with permanent visual field defect (fair), and BCVA less than 20/200 (poor).

former and latter were tested in 58 (45.7%) and 9 (7.1%) patients, respectively. Among these patients, seven patients (12.1%) and one patient (who was included in the isolated ON group in this study) (11.1%) tested positive for AQP4 and MOG, respectively. The anti-nuclear antibody was tested in 90 patients, 21 (23.3%) of whom tested positive. The CSF analyses were available for 69 children, and intrathecal oligoclonal bands (OCBs) and pleocytosis were respectively noted in three (4.4%) and six (8.7%) children. All three patients who tested positive for intrathecal OCBs were subsequently diagnosed with MS. Twenty-nine patients (22.1%) experienced recurrence of ON during the follow-up

period. The mean duration from the onset of ON to the first recurrence was 24.7 ± 39.2 months (range, 1–149 months).

Brain MR images of 126 patients (99.2%) were available at the initial visit. Optic nerve enhancement was detected in 102 patients (81.0%). The WMLs on MR images were noted in 41 (32.5%) patients at the time of presentation. The McDonald 2010 criteria and consensus definitions for pediatric MS, for dissemination in space and time, were met in 19 patients with subsequent follow-up MR images [37, 38]. The first treatment of ON was performed with 30 mg/kg or 1 g/day intravenous methylprednisolone for 3 days ($n = 104$, 81.9%) or 4–5 days ($n = 16$, 12.6%); seven patients (5.5%)

received no treatment. Among the patients who received intravenous steroid treatment, 66 children (55%) received a more extended slow tapering of oral steroids beyond 2 weeks.

The automated visual field test was available to 111 patients at the time of initial visit. The most frequent pattern of visual field defect was central scotoma ($n = 41$, 36.9%), followed in descending order by generalized depression ($n = 29$, 26.1%), generalized constriction ($n = 20$, 18.0%), cecocentral scotoma ($n = 11$, 9.9%), and altitudinal defect ($n = 10$, 9.0%).

3.2. Disease Groups. The median duration of follow-up was 24 months (IQR, 6–51). A total of 111, 101, and 84 patients were followed up for ≥3 months, ≥6 months, and ≥1 year, respectively. Among the 101 patients that were followed up for ≥6 months, the following diagnoses were noted: isolated ON (including one patient who tested positive for the MOG antibody and did not have any other abnormal neurologic finding except for ON), 48 (47.5%); recurrent ON, 12 (11.9%); MS, 19 (18.8%); NMOSD, 13 (12.9%); and ADEM-ON, 9 (8.9%). The proportion of female patients (83.3%) was highest in the NMOSD group, and the isolated ON group had an almost equal sex ratio (Table 2). The number of recurrences and durations of follow-ups were significantly different among these groups ($P < 0.001$ and 0.003, respectively).

3.3. Outcomes of Visual Acuity. BCVA data were available for 100 of the 101 patients who were followed up for ≥6 months. Among these, 76 patients (76.0%), 13 patients (13%), and 11 patients (11%) achieved good, fair, and poor visual outcomes, respectively, at the latest follow-up.

The mean baseline BCVA was 1.26 logMAR, which improved by a mean of 1.02 ± 0.70 logMAR (IQR, 0.30–1.7) to 0.22 ± 0.47 logMAR at the final visit (Figure 2). The mean final logMAR BCVAs in each group were as follows: isolated ON group, 0.16 ± 0.42; recurrent ON group, 0.34 ± 0.60; MS group, 0.12 ± 0.39; NMOSD group, 0.44 ± 0.62; and ADEM-ON group, 0.20 ± 0.48. The mean final logMAR BCVA was the worst in the NMOSD group, but there were no significant differences between the groups ($P = 0.250$). The visual outcomes as categorical variables (good, fair, and poor) were not significantly different among the groups either (Table 2, $P = 0.720$).

We analyzed the factors associated with a poor BCVA at presentation and improvement in BCVA. Only disc swelling at presentation was found to be associated with a poor BCVA at presentation (coefficient: 0.31, $P = 0.004$) and an improvement in BCVA (coefficient: 0.49, $P = 0.001$). Other factors such as age at presentation, sex, bilaterality, associated neurologic autoimmune diagnosis, and WMLs on MR images were not significantly associated with either of these two parameters. The data did not suggest a significant association between baseline characteristics and final BCVA.

4. Discussion

The current study, which included 127 children with ON from five tertiary centers who were treated over a 14-year period, is one of the largest multicenter studies conducted to date [8, 9, 15, 23, 25, 26]. The main findings of our study are as follows: (1) pain on eye movement was present in less than half of the pediatric patients (47.2%); (2) optic disc swelling was found in nearly two-thirds of pediatric patients (66.9%); (3) bilateral involvement was common (41.7%); (4) in a high percentage of pediatric patients (40.6%), ON was associated with other demyelinating diseases such as MS, NMOSD, and ADEM; (5) disc swelling was associated with both poor BCVA at presentation and greater improvement in BCVA; (6) there were no significant associations between baseline factors and final visual outcomes; and (7) NMOSD-related ON showed the highest rate of recurrence.

In our study, the overall clinical features of pediatric ON were similar to those reported in previous studies with Western and Asian children (Table 3) [8–24]. The median age at presentation in this study was 10.3 years, which is comparable to that in previous studies [8–24]. Moreover, the proportion of female patients (62.2%) along with the rates of optic disc swelling (66.9%) and bilateral involvement (41.7%) were higher, and the rate of pain on eye movement (47.2%) was relatively lower in our present study on pediatric patients than in previous studies on the adult population, and this finding is consistent with those of previous studies [8–24].

Optic nerve enhancement on MR images was detected in 81.0% of our patients. This feature is helpful for the clinical diagnosis of ON and is reported in up to 75–95% of adult patients with ON in Western countries [39–42]. This characteristic has been detected less frequently in Asian adults (30–74%) [43–46]. In a previous study on French children with ON, optic nerve enhancement was found in 29% (28 of 95) of the patients, which is much lower than that observed in our study [24]. These differences could be partly due to differences in the characteristics of the study subjects or the MR imaging protocols that were used in the study, or poor MR image quality for some young children. Moreover, WMLs on brain MR images were noted in 32.5% of the patients at presentation in our cohort, which was lower than the corresponding value of 45–52% reported in previous studies [24, 27]. In this regard, WMLs are closely associated with MS; the differences in the proportions of WMLs between studies may be related to the different proportions of patients with MS between the study cohorts.

Our study found that 18.8% and 12.9% of the patients who were followed up for ≥6 months had been diagnosed with MS and NMOSD, respectively. Although the rate of conversion to MS in our cohort (18.8%) was somewhat higher than that in previous Asian studies (4–10%) [8, 9, 15], it is still lower than that in prior studies conducted in Western countries (22–36%) [12, 22, 24]. The differences in the conversion rates to MS in adult patients with ON between Asian countries and Western countries have been well documented [47–49]. Similar differences may also be present in the pediatric population. The proportion of patients with NMOSD in this study was 12.9%, which was much higher than the corresponding value of 5–7% reported in Western counties [24, 27]. This could be related to the predisposition of non-Caucasians—especially Asians—to NMOSD [50–54]. Patients with NMOSD showed a higher rate of recurrence compared to patients with other etiologies.

TABLE 2: Demographic, clinical, and serologic features of 101 children who were followed up for more than 6 months according to their demyelination syndrome diagnosis.

Variables	Isolated ON (n = 48)	Recurrent ON (n = 12)	MS (n = 19)	NMOSD (n = 13)	ADEM-ON (n = 9)	P value
Age, median (IQR), y	9.3 (6.7–13.3)	10.1 (6.0–13.9)	10.6 (7.8–14.1)	11.8 (9.5–13.8)	7.8 (5.4–11.5)	0.495
Female, n (%)	22 (45.8%)	8 (66.7%)	15 (79.0%)	10 (83.3%)	6 (66.7%)	0.247
Disc swelling at presentation	32/47 (68.1%)	7/12 (58.3%)	10/19 (52.6%)	6/12 (50%)	7/9 (77.8%)	0.381
Intrathecal OCBs	0/19 (0%)	0/5 (0%)	3/14 (17.7%)	0/12 (0%)	0/7 (0%)	0.121
Total no. of optic neuritis, median (IQR)	0 (0–0)	1 (1–1)	0 (0–1)	1 (0–1)	0 (0–0)	<0.001
Bilateral involvement	19 (39.6%)	6 (50.0%)	8 (42.1%)	7 (53.9%)	2 (22.2%)	0.788
MRI enhancement	37/47 (78.7%)	8/12 (66.7%)	16/19 (84.2%)	11/13 (84.6%)	8/9 (88.9%)	0.834
Serologic testing						
AQP4 antibody	0/15	0/7	0/11	6/12 (50%)	0/1	
MOG antibody	1/2	0/1	0/2	0/1	0/1 (0%)	
ANA antibody	8/31 (25.8%)	3/8 (37.5%)	1/14 (7.1%)	3/13 (23.1%)	1/7 (14.3%)	
Visual outcome (n = 100)†						0.720
Good	40 (83.3%)	8 (66.7%)	14 (73.7%)	7 (58.3%)	7 (77.8%)	
Fair	5 (10.4%)	2 (16.7%)	4 (21.0%)	3 (25.0%)	1 (11.1%)	
Poor	3 (6.3%)	2 (16.7%)	1 (5.3%)	2 (16.7%)	1 (11.1%)	
logMAR visual acuity at latest visit (n = 100)†‡	0.16 ± 0.42	0.34 ± 0.60	0.12 ± 0.39	0.44 ± 0.62	0.20 ± 0.48	0.250
Follow-up duration, median (IQR)	30 (15–42)	47 (24–73)	32 (18–78)	54 (21–68)	47 (23–61)	0.003

ADEM = acute disseminated encephalomyelitis; ANA = anti-nuclear antibody; AQP4 = aquaporin-4; IQR = interquartile range; OCB = oligoclonal bands; ON = optic neuritis; MOG = myelin oligodendrocyte glycoprotein; MS = multiple sclerosis; NMO = neuromyelitis optica; NMOSD = neuromyelitis optica spectrum disorder. The percentages and interquartile ranges (IQR) are presented in parentheses. Continuous variables were analyzed by the Kruskal-Wallis test. Chi-square test or Fisher's exact test was used for categorical variables. †Visual outcome was only analyzed among 100 patients who were followed up for more than 6 months and whose BCVA data were available. ‡Visual outcome was categorized as the latest BCVA ≥20/40 with no visual field defect (good), BCVA <20/40~≥ 20/200 or ≥ 20/40 with permanent visual field defect (fair), and BCVA less than 20/200 (poor).
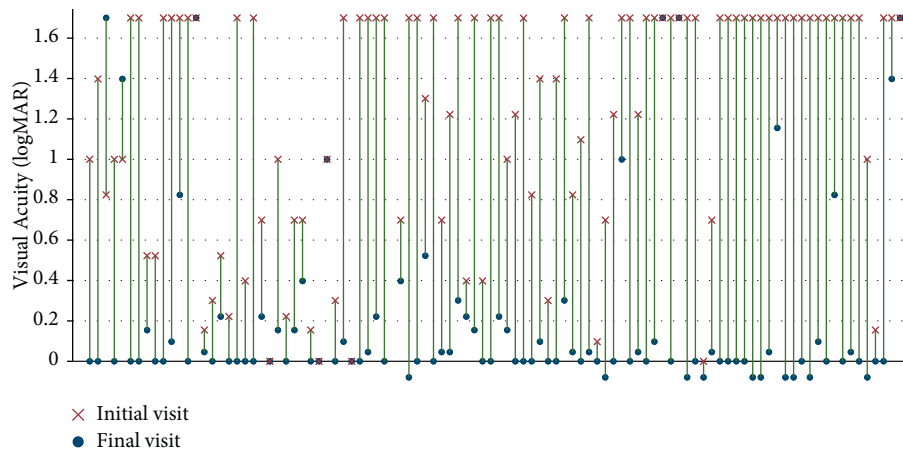
FIGURE 2: Paired dot plot showing initial and final best-corrected visual acuity (BCVA) in 100 patients with pediatric optic neuritis who were followed up for ≥6 months. BCVA presented as logMAR. BCVA improved from baseline to final visit by a mean value of 1.02 ± 0.70 logMAR (IQR, 0.30–1.7). BCVA of 20/800 or less was presented as 1.7 logMAR.

We investigated factors associated with visual outcomes in pediatric patients with ON. The only factor associated with an improvement of BCVA and poor BCVA at presentation in this study was the presence of disc swelling at presentation. However, no other factors were significantly associated with final visual outcomes. Wan et al. previously analyzed the visual outcomes and associated factors in a relatively large cohort of 36 patients with ON with at least 1 year of follow-up [11]. They found that none of the clinical characteristics, such as sex, baseline vision, laterality, treatment, or underlying diagnosis, predicted poor visual outcomes, which is consistent with the findings of our study [11]. A recent prospective study on pediatric ON demonstrated that baseline BCVA was worse in younger patients with associated neurologic autoimmune

TABLE 3: Comparison of patient demographics and clinical characteristics of pediatric optic neuritis.

Variable	Pineles et al. (n = 44) USA	Wan et al. (n = 46) USA	Averseng-peaureaux et al. (n = 102) France	Ambika et al. (n = 78) India	Chen et al. (n = 59) China	Present study (n = 127) Korea
Age, years (range)	10.2 (3.9–13.5)	12.6 (3.9–18.ct8)	11†	11.8 (2–18)	12.3 (5–18)	10.7 (3.6–18.6)
Gender (female), %	41%	72%	66%	54%	69%	62%
Pain with eye movement	—	43%	49%	46%	83%	47%
Bilateral involvement	36%	41%	37%	50%	63%	42%
Optic disc swelling	75%	67%	52%	50%	64%	67%
Severe visual loss at presentation (<20/200)	52%	50%	48%	NA	45%	66%
Final visual outcome						
≥20/40	85%	90%	72%‡	71%	85%	76%
<20/40-≥ 20/200	11%	8%	NA	NA	4%	15%
<20/200	4%	3%	NA	NA	11%	9%
Final diagnosis						
Isolated ON	48%	48%	58%	89%	69%	48%
Recurrent ON	18% (MOGAD)	—	6%	—	10%	12%
MS	11%	39%	21%	6%	3%	19%
NMOSD	7%	7%	5%	—	15%	13%
ADEM-ON	16%	7%	—	5%	3%	8%

ADEM = acute disseminated encephalomyelitis; NMOSD = neuromyelitis optica spectrum disorder; MOGAD = myelin oligodendrocyte glycoprotein-associated disorder; MS = multiple sclerosis; ON = optic neuritis. †The age in this study was presented as median. ‡72% of the patients had complete visual recovery (complete visual recovery defined as the recovery of normal visual acuity (20/20), or prior visual acuity if it was abnormal before optic neuritis occurrence).

diseases, those with WMLs on MR images, and those of non-White race and non-Hispanic ethnicity [27]. They also reported that there were no baseline factors associated with BCVA improvement. Their study did not analyze disc swelling. Based on our findings, we presume that pediatric patients with ON showing optic disc swelling, despite a relatively poor visual acuity at presentation, have a good prognosis that is comparable to that of patients without optic disc swelling.

This study has several limitations, including the retrospective design, variability of follow-up periods between patients, and unavailability of AQP4 and MOG antibody testing results in early study periods. Despite these limitations, our study provides important information on the baseline characteristics and visual outcomes of a relatively large number of Korean pediatric patients with ON. Although two-thirds of the patients experienced severe visual loss (<20/200) at presentation, 76% experienced good visual recovery at the final visit. Moreover, ON was associated with other neurological diseases (i.e., MS, NMOSD, and ADEM) in 40.6% of the pediatric patients.

In conclusion, our study is one of the largest multicenter studies summarizing the clinical characteristics and visual prognosis of pediatric ON. The baseline characteristics were similar to those reported in other countries. A relatively high proportion of pediatric ON showed optic disc swelling (67%), bilateral involvement (42%), and associations with other central nervous system demyelinating diseases (40%). NMOSD was found more frequently (12.9%) than it has been found in Western countries, showing the highest rate of recurrence among other etiologies. A more comprehensive future study investigating the seropositivity of MOG antibody testing in pediatric ON should extend our understanding of the clinical aspects of the disease in Koreans.

Data Availability

The data that support the findings of this study are available from the corresponding author upon reasonable request.

Conflicts of Interest

The authors declare that there are no conflicts of interest regarding the publication of this paper.

Authors' Contributions

Kyung Ah Park and Hee Kyung Yang contributed equally as first authors. Jinu Han and Seong-Joon Kim contributed equally as corresponding authors. Kyung Ah Park and Hee Kyung Yang equally contributed to the study.

Acknowledgments

References

[1] J. L. Bennett, "Optic neuritis," Continuum (Minneap Minn), vol. 25, no. 5, pp. 1236–1264, 2019.

[2] M. Rodriguez, A. Siva, S. A. Cross, P. C. O'Brien, and L. T. Kurland, "Optic neuritis: a population-based study in Olmsted County, Minnesota," Neurology, vol. 45, no. 2, pp. 244–250, 1995.

[3] D. D. Choi, M. S. Park, and K. A. Park, "Incidence of optic neuritis in Korean children and adolescents: a Nationwide survey and National Registry Analysis," *Journal of the Neurological Sciences*, vol. 408, Article ID 116554, 2020.

[4] J. Y. Lee, J. Han, M. Yang, and S. Y. Oh, "Population-based incidence of pediatric and adult optic neuritis and the risk of multiple sclerosis," *Ophthalmology*, vol. 127, no. 3, pp. 417–425, 2020.

[5] D. D. Choi, M. S. Park, and K. A. Park, "Seven-year nationwide incidence of optic neuritis requiring intravenous methylprednisolone injection in Korean adults," *Acta Ophthalmologica*, vol. 98, no. 4, pp. e523–e525, 2020.

[6] W. S. Lin, H. P. Wang, H. M. Chen, J. W. Lin, and W. T. Lee, "Epidemiology of pediatric multiple sclerosis, neuromyelitis optica, and optic neuritis in Taiwan," *Journal of Neurology*, vol. 267, no. 4, pp. 925–932, 2019.

[7] A. Langer-Gould, J. L. Zhang, J. Chung, Y. Yeung, E. Waubant, and J. Yao, "Incidence of acquired CNS demyelinating syndromes in a multiethnic cohort of children," *Neurology*, vol. 77, no. 12, pp. 1143–1148, 2011.

[8] S. Ambika, K. Padmalakshmi, V. Venkatraman, and O. V. Noronha, "Visual outcomes and clinical manifestations of pediatric optic neuritis in Indian population: an institutional study," *Journal of Neuro-Ophthalmology*, vol. 38, no. 4, pp. 462–465, 2018.

[9] R. Khadse, M. Ravindran, N. Pawar, P. Maharajan, and R. Rengappa, "Clinical profile and neuroimaging in pediatric optic neuritis in Indian population: a case series," *Indian Journal of Ophthalmology*, vol. 65, no. 3, pp. 242–245, 2017.

[10] J. Graves, V. Kraus, B. P. Soares, C. P. Hess, and E. Waubant, "Longitudinally extensive optic neuritis in pediatric patients," *Journal of Child Neurology*, vol. 30, no. 1, pp. 120–123, 2015.

[11] M. J. Wan, O. Adebona, L. A. Benson, M. P. Gorman, and G. Heidary, "Visual outcomes in pediatric optic neuritis," *American Journal of Ophthalmology*, vol. 158, no. 3, pp. 503–507.e2, 2014.

[12] A. T. Waldman, L. B. Stull, S. L. Galetta, L. J. Balcer, and G. T. Liu, "Pediatric optic neuritis and risk of multiple sclerosis: meta-analysis of observational studies," *Journal of American Association for Pediatric Ophthalmology and Strabismus*, vol. 15, no. 5, pp. 441–446, 2011.

[13] G. R. Bonhomme, A. T. Waldman, L. J. Balcer et al., "Pediatric optic neuritis: brain MRI abnormalities and risk of multiple sclerosis," *Neurology*, vol. 72, no. 10, pp. 881–885, 2009.

[14] N. Chirapapaisan and M. S. Borchert, "Pediatric optic neuritis," *Medical Journal of the Medical Association of Thailand*, vol. 91, no. 3, pp. 323–330, 2008.

[15] J-M. Hwang and Y. J. Lee, "Optic neuritis in Asian children," *Journal of Pediatric Ophthalmology & Strabismus*, vol. 39, no. 1, pp. 26–32, 2002.

[16] M. Absoud, C. Cummins, N. Desai et al., "Childhood optic neuritis clinical features and outcome," *Archives of Disease in Childhood*, vol. 96, no. 9, pp. 860–862, 2011.

[17] C. F. Lucchinetti, L. Kiers, A. O'Duffy et al., "Risk factors for developing multiple sclerosis after childhood optic neuritis," *Neurology*, vol. 49, no. 5, pp. 1413–1418, 1997.

[18] M. A. Lana-Peixoto and G. C. d. Andrade, "The clinical profile of childhood optic neuritis," *Arquivos de Neuro-Psiquiatria*, vol. 59, no. 2B, pp. 311–317, 2001.

[19] K. M. Brady, A. S. Brar, A. G. Lee, D. K. Coats, E. A. Paysse, and P. G. Steinkuller, "Optic neuritis in children: clinical features and visual outcome," *Journal of American Association for Pediatric Ophthalmology and Strabismus*, vol. 3, no. 2, pp. 98–103, 1999.

[20] G. Alper and L. Wang, "Demyelinating optic neuritis in children," *Journal of Child Neurology*, vol. 24, no. 1, pp. 45–48, 2009.

[21] G. Alvarez and M. Cárdenas, "Multiple sclerosis following optic neuritis in Chile," *Journal of Neurology, Neurosurgery & Psychiatry*, vol. 52, no. 1, pp. 115–117, 1989.

[22] M. Wilejto, M. Shroff, J. R. Buncic, J. Kennedy, C. Goia, and B. Banwell, "The clinical features, MRI findings, and outcome of optic neuritis in children," *Neurology*, vol. 67, no. 2, pp. 258–262, 2006.

[23] D. H. Jo, S. J. Kim, J. H. Chae, and Y. S. Yu, "The clinical characteristics of optic neuritis in Korean children," *Korean Journal of Ophthalmology*, vol. 25, no. 2, pp. 116–120, 2011.

[24] D. Averseng-Peaureaux, M. Mizzi, H. Colineaux et al., "Paediatric optic neuritis: factors leading to unfavourable outcome and relapses," *British Journal of Ophthalmology*, vol. 102, no. 6, pp. 808–813, 2018.

[25] Q. Chen, G. Zhao, Y. Huang et al., "Clinical characteristics of pediatric optic neuritis with myelin oligodendrocyte glycoprotein seropositive: a cohort study," *Pediatric Neurology*, vol. 83, pp. 42–49, 2018.

[26] H. Song, H. Zhou, M. Yang et al., "Clinical characteristics and prognosis of myelin oligodendrocyte glycoprotein antibody-seropositive paediatric optic neuritis in China," *British Journal of Ophthalmology*, vol. 103, no. 6, pp. 831–836, 2019.

[27] S. L. Pineles, M. X. Repka, G. T. Liu et al., "Assessment of pediatric optic neuritis visual acuity outcomes at 6 months," *JAMA Ophthalmology*, vol. 138, no. 12, pp. 1253–1261, 2020.

[28] C. K. Chan and D. S. Lam, "Optic neuritis treatment trial:10-year follow-up results," *American Journal of Ophthalmology*, vol. 138, no. 4, p. 695, 2004.

[29] H. E. Moss, W. Gao, L. J. Balcer, and C. E. Joslin, "Association of race/ethnicity with visual outcomes following acute optic neuritis: an analysis of the Optic Neuritis Treatment Trial," *JAMA Ophthalmology*, vol. 132, no. 4, pp. 421–427, 2014.

[30] A. Mizota, M. Niimura, and E. Adachi-Usami, "Clinical characteristics of Japanese children with optic neuritis," *Pediatric Neurology*, vol. 31, no. 1, pp. 42–45, 2004.

[31] S. A. Bagaglia, F. Passani, G. W. Oliverio et al., "Multimodal imaging in susac syndrome: a case report and literature review," *International Journal of Environmental Research and Public Health*, vol. 18, no. 7, p. 3435, 2021.

[32] E. M. Hennes, M. Baumann, K. Schanda et al., "Prognostic relevance of MOG antibodies in children with an acquired demyelinating syndrome," *Neurology*, vol. 89, no. 9, pp. 900–908, 2017.

[33] P. Waters, M. Woodhall, K. C. O'Connor et al., "MOG cell-based assay detects non-MS patients with inflammatory neurologic disease," *Neurol Neuroimmunol Neuroinflamm*, vol. 2, no. 3, p. e89, 2015.

[34] L. B. Krupp, M. Tardieu, M. P. Amato et al., "International Pediatric Multiple Sclerosis Study Group criteria for pediatric multiple sclerosis and immune-mediated central nervous system demyelinating disorders: revisions to the 2007 definitions," *Multiple Sclerosis*, vol. 19, no. 10, pp. 1261–1267, 2013.

[35] H. Zhou, W. Wang, Q. Xu et al., "Clinical features and visual outcomes of optic neuritis in Chinese children," *J Ophthalmol*, vol. 2016, Article ID 9167361, 7 pages, 2016.

[36] S. L. Pineles, R. J. Henderson, M. X. Repka et al., "The pediatric optic neuritis prospective outcomes study - two-year results," *Ophthalmology*, vol. 129, no. 8, pp. 856–864, 2022.

[37] M. Tardieu, B. Banwell, J. S. Wolinsky, D. Pohl, and L. B. Krupp, "Consensus definitions for pediatric MS and

other demyelinating disorders in childhood: Table," *Neurology*, vol. 87, pp. S8–s11, 2016.

[38] C. H. Polman, S. C. Reingold, B. Banwell et al., "Diagnostic criteria for multiple sclerosis: 2010 revisions to the McDonald criteria," *Annals of Neurology*, vol. 69, no. 2, pp. 292–302, 2011.

[39] R. W. Beck, R. L. Gal, M. T. Bhatti et al., "Visual function more than 10 years after optic neuritis: experience of the optic neuritis treatment trial," *American Journal of Ophthalmology*, vol. 137, no. 1, pp. 77–83, 2004.

[40] S. J. Hickman, K. A. Miszkiel, G. T. Plant, and D. H. Miller, "The optic nerve sheath on MRI in acute optic neuritis," *Neuroradiology*, vol. 47, no. 1, pp. 51–55, 2005.

[41] H. E. Fazzone, D. R. Lefton, and M. J. Kupersmith, "Optic neuritis: correlation of pain and magnetic resonance imaging," *Ophthalmology*, vol. 110, no. 8, pp. 1646–1649, 2003.

[42] M. J. Kupersmith, T. Alban, B. Zeiffer, and D. Lefton, "Contrast-enhanced MRI in acute optic neuritis: relationship to visual performance," *Brain*, vol. 125, no. 4, pp. 812–822, 2002.

[43] J. C. Wang, S. Tow, T. Aung, S. A. Lim, and J. F. Cullen, "The presentation, aetiology, management and outcome of optic neuritis in an Asian population," *Clinical and Experimental Ophthalmology*, vol. 29, no. 5, pp. 312–315, 2001.

[44] M. Wakakura, R. Minei-Higa, S. Oono et al., "Baseline features of idiopathic optic neuritis as determined by a multicenter treatment trial in Japan," *Japanese Journal of Ophthalmology*, vol. 43, no. 2, pp. 127–132, 1999.

[45] S. A. Lim, Y. Y. Sitoh, S. M. Chng, P. Y. Boey, and K. Y. Goh, "Magnetic resonance imaging in acute optic neuritis in Singapore," *Annals Academy of Medicine Singapore*, vol. 38, no. 9, pp. 821–826, 2009.

[46] H. Kim, K. A. Park, S. Y. Oh, J. H. Min, and B. J. Kim, "Association of optic neuritis with neuromyelitis optica spectrum disorder and multiple sclerosis in Korea," *Korean Journal of Ophthalmology*, vol. 33, no. 1, pp. 82–90, 2019.

[47] Y. Isayama, T. Takahashi, T. Shimoyoma, and A. Yamadori, "Acute optic neuritis and multiple sclerosis," *Neurology*, vol. 32, no. 1, pp. 73–76, 1982.

[48] S. A. Lim, K. Y. Goh, S. Tow et al., "Optic neuritis in Singapore," *Singapore Medical Journal*, vol. 49, no. 9, pp. 667–671, 2008.

[49] Y. C. Lin, M. Y. Yen, W. M. Hsu, H. C. Lee, and A. G. Wang, "Low conversion rate to multiple sclerosis in idiopathic optic neuritis patients in Taiwan," *Japanese Journal of Ophthalmology*, vol. 50, no. 2, pp. 170–175, 2006.

[50] H. T. Benamer, E. S. Ahmed, A. S. Al-Din, and D. G. Grosset, "Frequency and clinical patterns of multiple sclerosis in Arab countries: a systematic review," *Journal of the Neurological Sciences*, vol. 278, no. 1-2, pp. 1–4, 2009.

[51] P. Cabre, O. Heinzlef, H. Merle et al., "MS and neuromyelitis optica in Martinique (French West Indies)," *Neurology*, vol. 56, no. 4, pp. 507–514, 2001.

[52] J. S. Chopra, K. Radhakrishnan, B. B. Sawhney, S. R. Pal, and A. K. Banerjee, "Multiple sclerosis in north-west India," *Acta Neurologica Scandinavica*, vol. 62, no. 5, pp. 312–321, 2009.

[53] J. i. Kira, "Multiple sclerosis in the Japanese population," *The Lancet Neurology*, vol. 2, no. 2, pp. 117–127, 2003.

[54] R. M. Papais-Alvarenga, C. M. Miranda-Santos, M. Puccioni-Sohler et al., "Optic neuromyelitis syndrome in Brazilian patients," *Journal of Neurology Neurosurgery and Psychiatry*, vol. 73, no. 4, pp. 429–435, 2002.

Research Article

Characteristics of Anterior Segment in Congenital Ectopia Lentis: An SS-OCT Study

Haotian Qi,[1] Guangming Jin ⬤,[1] Minjie Zou,[1] Charlotte Young,[2] Liyan Liu,[1] Zhangkai Lian,[1] Dongwei Guo,[1] Zhenzhen Liu ⬤,[1] and Danying Zheng ⬤[1]

[1]*State Key Laboratory of Ophthalmology, Zhongshan Ophthalmic Center, Sun Yat-sen University, Guangdong Provincial Key Laboratory of Ophthalmology and Visual Science, Guangdong Provincial Clinical Research Center for Ocular Diseases, Guangzhou 510060, China*
[2]*Department of Ophthalmology, Third Affiliated Hospital, Nanchang University, Nanchang, Jiangxi Province, China*

Correspondence should be addressed to Guangming Jin; jingm@mail2.sysu.edu.cn, Zhenzhen Liu; liuzhenzhen@gzzoc.com, and Danying Zheng; zhengdyy@163.com

Purpose. To investigate the characteristics of anterior chamber angle parameters in congenital ectopia lentis (CEL) patients and to evaluate the sensitivity and specificity of anterior segment parameters in distinguishing CEL from healthy controls. *Setting.* Zhongshan Ophthalmic Center, Guangzhou, China. *Design.* Cross-sectional study. *Methods.* 35 CEL patients and 35 age- and sex-matched healthy controls were recruited. Axial length (AL) and anterior segment parameters including anterior chamber width (ACW), angle open distance (AOD), angle recess area (ARA), trabecular-iris space area (TISA), and trabecular-iris angle (TIA) were measured. All the above parameters and the ratio index of angle parameters, which was defined as the angle parameter value of the narrower side to that of the contralateral side, were compared between CEL and controls. Receiver operating characteristic (ROC) curves were also plotted to evaluate the diagnostic performance of anterior chamber angle parameters in CEL patients. *Results.* All angle parameters of the contralateral side to the dislocated lens side were significantly smaller than those of the dislocated lens side in CEL (all $P < 0.05$). For the diagnostic performance of anterior chamber angle parameters, the ratio index of TIAr500 combined with TIAr750 had the best diagnostic performance for CEL screening (AUC = 0.798), and TIAr500 of 0.887 and TIAr750 of 0.917 were detected to be the optimal cut-off points, representing a sensitivity of 89.8% and specificity of 68.7%. *Conclusion.* The contralateral side to the dislocated lens side in the CEL had a narrower anterior chamber angle. TIAr500 combined with TIAr750 is the optimal combination strategy for ectopia lentis screening.

1. Introduction

Congenital ectopia lentis (CEL) is a rare disease in which the lens dislocates from its normal position; it is a hereditary connective tissue disease [1]. CEL can not only lead to ocular symptoms such as severe refractive errors and amblyopia but also be associated with systemic diseases, such as such as Marfan's syndrome (MFS), homocystinuria, Weill–Marchesani syndrome, and sulfite oxidase deficiency syndrome [2].

For eyes with ectopia lentis, it has been reported that the dislocated lens can shallow the anterior chamber angle (ACA) and even cause acute secondary angle closure [3]. Zhang et al. [4] reported that CEL accounts for 2.4% of all causes of secondary glaucoma. However, little is known about the anterior segment characteristics of CEL patients, which hinders our understanding of the disease. While the slit lamp biomicroscope has been widely used for diagnosing ectopia lentis, this examination method may not detect early mild lesions without obvious signs; hence, objective and accurate diagnosis strategies for lens dislocation are needed.

In this study, we aimed to use the latest anterior segment swept-source optical coherence tomography (SS-OCT), a noncontact instrument with high-resolution imaging [5], to

investigate the anterior segment parameters of patients with CEL and to evaluate the sensitivity and specificity of anterior segment parameters in distinguishing ectopia lentis from healthy controls.

2. Methods

This cross-sectional study was conducted in accordance with the tenets of the Declaration of Helsinki and was approved by the Institutional Review Board of Zhongshan Ophthalmic Center. The CEL patients and the healthy controls were consecutively recruited from January 2021 to August 2021 in Zhongshan Ophthalmic Center, Sun Yat-sen University, Guangzhou, China. The included CEL patients were diagnosed according to the Ghent-2 criteria with genetic testing [6]. Exclusion criteria were as follows: (1) patients with ocular surgery history; (2) with other ocular diseases such as corneal diseases which would affect the measurement of anterior segment parameters. Age- and sex-matched individuals without ocular disease other than refractive error were included as the healthy controls. Written informed consent was obtained from all participants before enrolling.

All participants underwent a standardized ophthalmic examination including slit-lamp biomicroscopy, best corrected visual acuity, intraocular pressure (IOP) with Goldmann applanation, AL with IOL Master700 (Zeiss, Jena, Germany), and anterior segment SS-OCT images with the Casia SS-1000 OCT (Tomey, Nagoya, Japan).

3. Swept-Source Anterior Segment Optical Coherence Tomography Examination

The Casia SS-1000OCT (Tomey, Nagoya, Japan) is a commercially available swept-source OCT system with a swept-source laser wavelength of 1310 nm, using a monochromatic, tunable, fast scanning laser source and a photodetector to detect wavelength-resolved interference signals. During the examination, all the participants were asked to fixate on an internal fixation target during the scan. All images were obtained in a dark environment by the same observer before the participants received any pupil dilation or constriction medications. For the patients with mild subluxation, we also performed SS-OCT scanning both under nonmydriatic pupil (to collect the angle parameters) and mydriatic pupil (to confirm the direction of lens dislocation). To avoid lid artifact, participants were instructed to pull down the lower lid against the lower orbital rim to expose the lower limbus while the technician elevated the upper lid against the upper orbital rim to expose the upper limbus. All images with lid or motion artifacts were excluded from the analysis.

Anterior segment parameters of different axes were obtained from each participant. For CEL patients, the scans were performed on the dislocated lens axis (Figure 1). For healthy controls, the scans were performed on the horizontal axis (0–180 degrees) and vertical axis (90–270 degrees). For each image, the scleral spur (SS) and angle recess (AR) were both marked by the SS-OCT system first and then manually corrected to complete anterior chamber measurements by the same experienced ophthalmologist (Liu ZZ). The

scanned images were analyzed using custom software, and the obtained parameters included the following: anterior chamber dimension parameters (anterior chamber width (ACW)), angle parameters (angle opening distance (AOD), angle recess area (ARA), trabecular-iris space area (TISA), and trabecular-iris angle (TIA)). AOD, ARA, TISA, and TIA were all assessed at $250\,\mu m$, $500\,\mu m$, and $750\,\mu m$ from the scleral spur. All SS-OCT anterior chamber parameters are shown in Supplemental Figure 1. Of the above parameters, ACW was defined as the distance between the two scleral spurs. Angle opening distances at 250, 500, and $750\,\mu m$ (AOD250, AOD500, and AOD750) were defined as the distance between the posterior corneal surface and the anterior iris surface on a line perpendicular to the trabecular meshwork $250\,\mu m$, $500\,\mu m$, and $750\,\mu m$ from the scleral spur, respectively. Angle recess areas at 250, 500, and $750\,\mu m$ (ARA250, ARA500, and ARA750) were defined as the area of the angle recess bounded anteriorly by the AOD250, AOD500, and AOD750. Trabecular-iris space areas at 250, 500, and $750\,\mu m$ (TISA250, TISA500, and TISA750) were defined as the area bounded anteriorly by AOD250, AOD500, and AOD750 as determined posteriorly by a line drawn from the scleral spur vertical to the plane of the inner scleral wall to the iris, superiorly by the inner corneoscleral wall, and inferiorly by the iris surface. Trabecular-iris angles at 250, 500, and $750\,\mu m$ (TIA250, TIA500, and TIA750) were defined as an angle measured with the apex in the iris recess and the arms of the angle passing through a point on the trabecular meshwork $250\,\mu m$, $500\,\mu m$ and $750\,\mu m$ from the scleral spur and the point on the iris perpendicularly.

For the CEL patients and healthy controls, the ratio index of angle parameters, defined as the angle parameter value of the narrower side to that of the contralateral side, was also introduced as AODr, ARAr, TISAr, and TIAr in this study. The angle parameters are shown in Figure 1.

4. Statistical Analysis

All statistical analysis was performed using Stata MP 15.1 (Stata Corp LP, College Station, Texas, USA). Mean values with 95% confidence intervals (95% CI) were provided for normally distributed data. All data were tested for normality. Normally distributed parameters were compared between the CEL and healthy controls using the student's t test, while the rank sum test was used for nonnormal distribution data. The receiver operating characteristics (ROC) curve was plotted to evaluate the diagnostic value of each SS-OCT parameter in the differential diagnosis of CEL patients from healthy controls. A value of $P < 0.05$ was considered statistically significant unless otherwise specified.

5. Results

A total of 35 eyes from 35 CEL patients were recruited, of which 18 were male (51.43%) and 17 were female (48.57%). Meanwhile, 35 eyes from age- and sex-matched healthy controls were recruited, of which 17 were male (48.57%) and 18 were female (51.43%). The mean age of the CEL patients was 13.57 ± 8.37 years, and the healthy control group age was
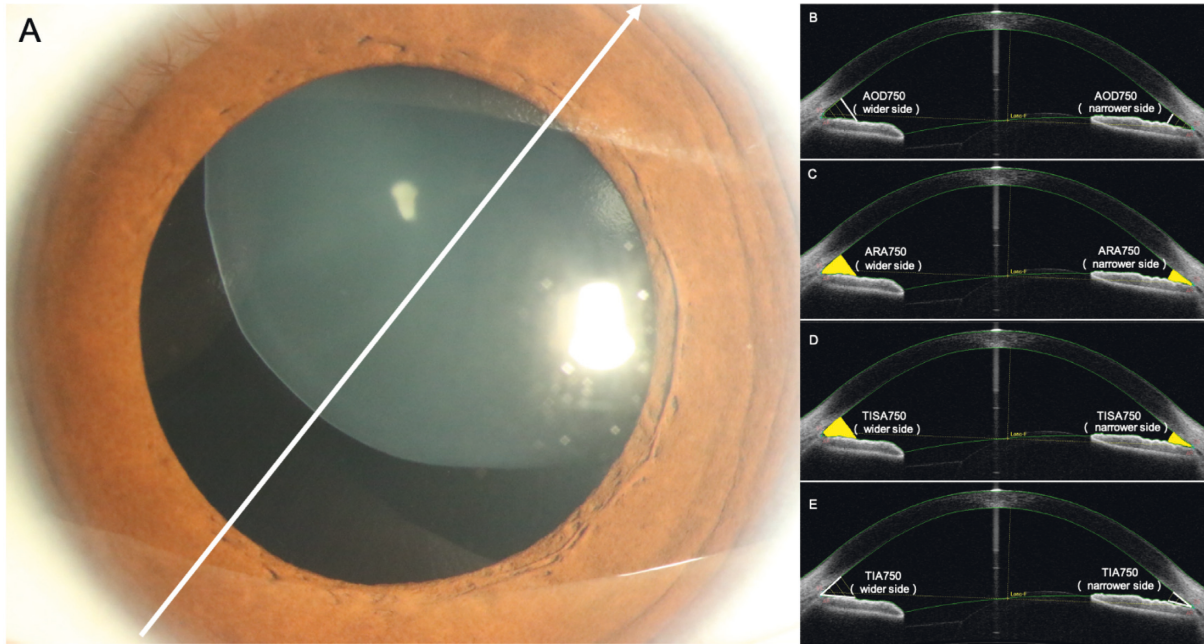
FIGURE 1: Diagram of the scan performed in CEL patients. (a) The scan was performed on the dislocated lens axis. (b–e) Different angle parameters of the dislocated lens side (wider side) and the contralateral side to the dislocated lens side (narrower side), and the ratio index of angle parameter was defined as the angle parameter value of the narrower side to that of the contralateral side.

11.11 ± 2.99 years. The mean AL was 25.01 ± 2.76 mm in the CEL and 25.01 ± 2.76 mm in the healthy controls, with no significant difference between the two groups were detected. Demographics and ocular biometric characteristics of participants are shown in Table 1.

The angle parameters (AOD, ARA, TISA, and TIA) at $250 \mu m$, $500 \mu m$, $500 \mu m$, and $750 \mu m$ of the dislocated lens side, the contralateral side to the dislocated lens side in the CEL patients, and those of the horizontal axis (0 degree and 180 degrees) and vertical axis (90 degree and 270 degrees) in the healthy controls are reported in Table 2. All angle parameters of the contralateral side to the dislocated lens side were significantly smaller than those of the dislocated lens side in the CEL patients and those of the horizontal axis (0–180 degrees) and vertical axis (90–270 degrees) in the healthy controls (all $P < 0.05$). As shown in Table 3, there were significant differences for all ratio indexes of angle parameters between the CEL patients and the healthy controls. To evaluate the sensitivity and specificity of the anterior segment parameters in distinguishing ectopia lentis from healthy controls, we calculated the area under the receiving operating characteristics curve (AUROC), which is presented in Figures 2 and 3. The ROC curve indicated that TIAr250, TIAr500, and TIAr750 had good discriminative performance (AUC = 0.720; AUC = 0.794; AUC = 0.741, respectively) for CEL. Meanwhile, the ratio index of TIAr500 combined with TIAr750 had the best diagnostic performance for CEL (AUC = 0.798); and TIAr500 of 0.887 and TIAr750 of 0.917 were found to be the optimal cut-offs.

Among the included CEL patients, FBN1 mutations account for more than 90% of the detected mutations. There was no statistical difference of anterior segment parameters among patients with different mutations.

TABLE 1: Demographics and ocular biometric characteristics of participants.

	CEL ($n = 35$)	Healthy controls ($n = 35$)
Age, years	13.571 ± 8.374	11.114 ± 2.988
Sex (male/female)	18/17	17/18
Eyes (right/left)	21/14	35/0
AL, mm	25.008 ± 2.764	24.651 ± 0.969
ACW, mm	11.966 ± 0.470	11.963 ± 0.357

AL = axial length; ACW = anterior chamber width.

6. Discussion

For CEL patients, the zonule of the lens is partially or completely slack or even broken, and the lens is often pushed forward to the iris which can change the anterior chamber angle structure. Until now, little is known about the characteristics of the anterior segment in CEL patients. Although changes in the anterior chamber depth can be easily detected in patients with severe lens dislocation, it is difficult to detect lens dislocation with traditional equipment such as a slit-lamp biomicroscope for patients with mild lens dislocation, and new detection strategies are needed for these patients.

At present, SS-OCT serves as a noncontact, easy-to-use, and quantitative evaluation of the anterior chamber device [7, 8] that utilizes much more data of the whole anterior chamber than can be obtained by the commonly used UBM. In addition, the noncontact nature of SS-OCT makes it more advantageous in pediatric patients with CEL. With the advancement of OCT technology, the current ultrahigh resolution of OCT can obtain very clear imaging of various structures in the anterior segment of the eye, and AS-OCT has been successfully used in the diagnosis of a variety of

TABLE 2: Comparison of angle parameters in different direction in CEL patients and healthy controls.

Angle parameters	CEL		Healthy controls			
	Contralateral side to dislocated lens side	Dislocated lens side (Mean ± SD, P^*)	0° (Mean ± SD, P^*)	90° (Mean ± SD, P^*)	180° (Mean ± SD, P^*)	270° (Mean ± SD, P^*)
AOD250, mm	0.27 ± 0.13	0.46 ± 0.16 <0.001	0.51 ± 0.13 <0.001	0.45 ± 0.15 <0.001	0.57 ± 0.18 <0.001	0.46 ± 0.14 <0.001
AOD500, mm	0.37 ± 0.15	0.63 ± 0.19 <0.001	0.74 ± 0.16 <0.001	0.67 ± 0.19 <0.001	0.82 ± 0.23 <0.001	0.66 ± 0.16 <0.001
AOD750, mm	0.51 ± 0.19	0.84 ± 0.22 <0.001	0.98 ± 0.18 <0.001	0.89 ± 0.21 <0.001	1.10 ± 0.25 <0.001	0.89 ± 0.22 <0.001
ARA250, mm^2	0.10 ± 0.06	0.17 ± 0.09 <0.001	0.18 ± 0.05 <0.001	0.15 ± 0.07 <0.001	0.19 ± 0.06 <0.001	0.16 ± 0.06 <0.001
ARA500, mm^2	0.17 ± 0.08	0.29 ± 0.13 <0.001	0.33 ± 0.09 <0.001	0.29 ± 0.10 <0.001	0.35 ± 0.11 <0.001	0.29 ± 0.10 <0.001
ARA750, mm^2	0.28 ± 0.12	0.48 ± 0.18 <0.001	0.55 ± 0.13 <0.001	0.48 ± 0.14 <0.001	0.59 ± 0.17 <0.001	0.48 ± 0.14 <0.001
TISA250, mm^2	0.057 ± 0.03	0.10 ± 0.04 <0.001	0.11 ± 0.03 <0.001	0.09 ± 0.04 <0.001	0.12 ± 0.04 <0.001	0.10 ± 0.03 <0.001
TISA500, mm^2	0.14 ± 0.06	0.24 ± 0.09 <0.001	0.27 ± 0.07 <0.001	0.24 ± 0.08 <0.001	0.30 ± 0.09 <0.001	0.24 ± 0.07 <0.001
TISA750, mm^2	0.25 ± 0.10	0.43 ± 0.14 <0.001	0.50 ± 0.11 <0.001	0.44 ± 0.12 <0.001	0.54 ± 0.15 <0.001	0.44 ± 0.11 <0.001
TIA250,°	33.51 ± 12.61	44.41 ± 8.40 <0.001	49.70 ± 11.36 <0.001	44.28 ± 12.11 <0.001	52.42 ± 11.59 <0.001	45.65 ± 11.61 <0.001
TIA500°	29.70 ± 8.13	41.45 ± 7.09 <0.001	47.29 ± 9.13 <0.001	43.37 ± 9.68 <0.001	49.92 ± 9.16 <0.001	43.41 ± 9.64 <0.001
TIA750°	28.99 ± 7.99	40.84 ± 6.99 <0.001	46.37 ± 7.19 <0.001	43.14 ± 7.95 <0.001	49.65 ± 7.57 <0.001	42.93 ± 8.49 <0.001

AOD, angle open distance; ARA, angle recess area; TISA, trabecular-iris space area; TIA, trabecular-iris angle; $^*t$-test for comparison of means with angle parameters of contralateral side to dislocated lens side in CEL patients.

TABLE 3: Comparison of the ratio index of different angle parameters in CEL patients with healthy controls (mean ± SD).

The ratio index of angle parameters	CEL	Healthy controls	Pvalue
AODr250	0.65 ± 0.47	1.02 ± 0.31	<0.001
AODr500	0.63 ± 0.31	1.03 ± 0.21	<0.001
AODr750	0.65 ± 0.35	1.04 ± 0.20	<0.001
ARAr250	0.64 ± 0.48	1.02 ± 0.44	<0.05
ARAr500	0.63 ± 0.40	1.01 ± 0.26	<0.001
ARAr750	0.64 ± 0.36	1.02 ± 0.22	<0.001
TISAr250	0.62 ± 0.42	1.02 ± 0.25	<0.001
TISAr500	0.63 ± 0.37	1.02 ± 0.21	<0.001
TISAr750	0.64 ± 0.35	1.03 ± 0.20	<0.001
TIAr250	0.79 ± 0.41	0.99 ± 0.14	<0.05
TIAr500	0.73 ± 0.26	1.02 ± 0.15	<0.001
TIAr750	0.72 ± 0.27	1.03 ± 0.13	<0.001

*The ratio index of angle parameter was defined as the ratio of the angle parameter value of the narrower side to that of the contralateral side.

anterior segment diseases [9–11]. Ma et al. [12] reported that SS-OCT showed excellent diagnostic ability in distinguishing primary angle closure disease (PACD) from the healthy population and showed moderate diagnostic performance in distinguishing primary angle closure/primary angle closure glaucoma (PAC/PACG) from primary angle closure suspect (PACS). However, the use of SS-OCT in the diagnosis of CEL patients has not been reported by far.

In this study, we detected that all angle parameters of the contralateral side to the dislocated lens side in CEL patients were significantly smaller than those of the healthy controls ($P < 0.05$). Specifically, the angle parameters of the contralateral side to the dislocated lens side in the CEL patients were statistically smaller than those of the opposite side ($P < 0.05$). The explanation of our results may lie in the fact that the dislocated lens could cause mechanical compression of the ACA, hence affecting the angle parameters. Previous studies have reported that angle parameters were significantly associated with angle closure [13–16]. Previous reports by Henriquez et al. [17] identified that TISA500 < 0.009 was risk factor for developing phacomorphic angle closure, and narrower angle width was an independent predictive factor for the development of angle closure after ten years [18]. Additionally, the smaller
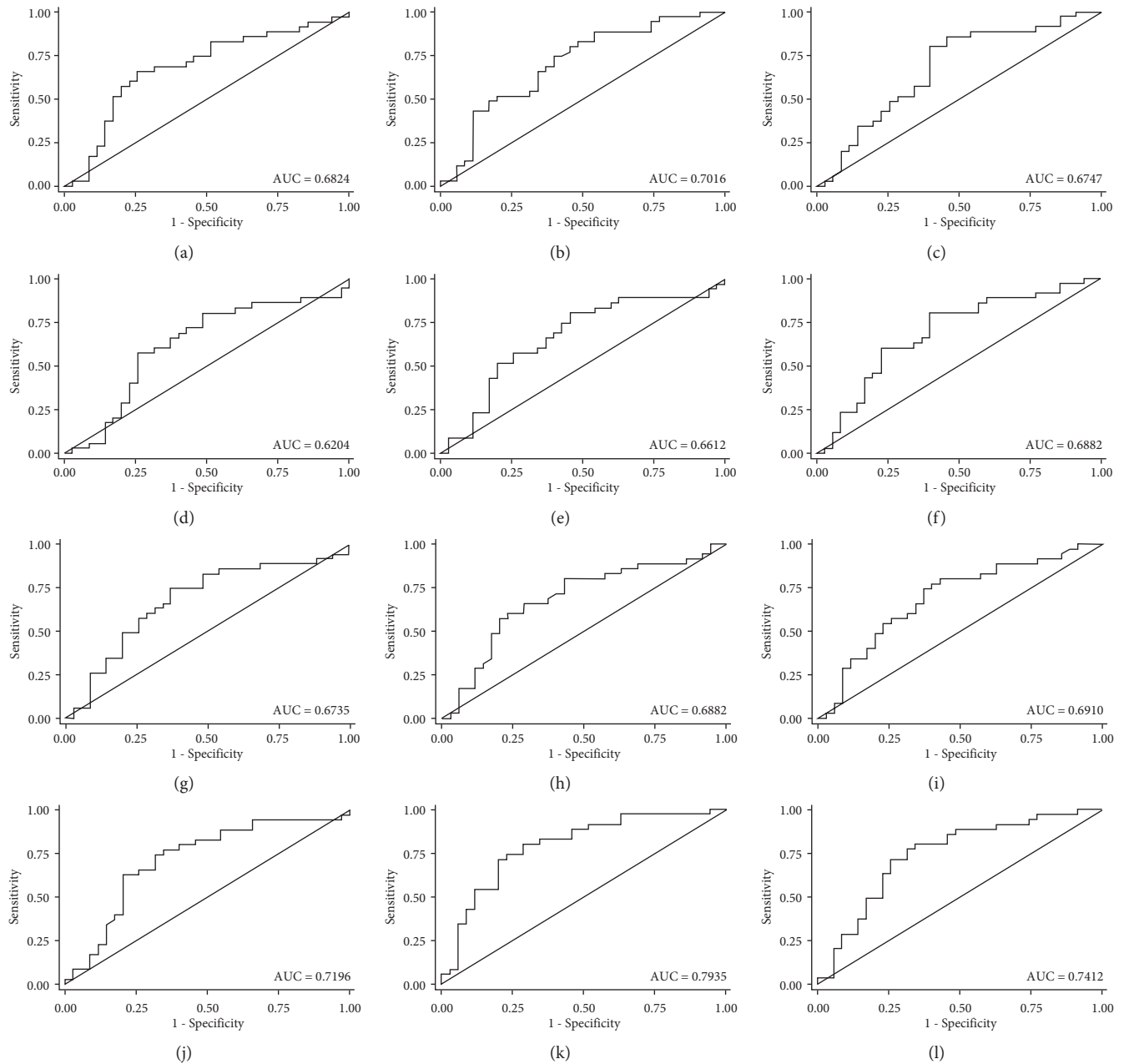
FIGURE 2: The receiving operating characteristics curve of single ratio index of angle parameter in differential diagnose of ectopia lentis. ((a) AODr250 (AUC = 0.682); (b) AODr500 (AUC = 0.701); (c) AODr750 (AUC = 0.675); (d) ARAr250 (AUC = 0.620); (e) ARAr500 (AUC = 0.661); (f) ARAr750 (AUC = 0.688); (g) TISAr250 (AUC = 0.674); (h) TISAr500 (AUC = 0.688); (i) TISAr750 (AUC = 0.691); (j) TIAr250 (AUC = 0.720); (k) TIAr500 (AUC = 0.794); (l) TIAr750 (AUC = 0.741).

AOD750 was also identified to be strongly associated with the development of incident angle closure in a previous study [19]. Due to the angle characteristics of the CEL patients, much more attention should be paid to the changes in angle parameters, and regular follow-up is recommended.

In this study, we also introduced a series ratio index of the angle parameters such as TIAr, AODr, ARAr, and TISAr. There was a significant difference between the CEL patients and the healthy controls for all angle parameter ratio indexes, of which the ratio indexes in CEL patients were smaller compared to the healthy controls. To explore the potential value of angle parameters in the differential diagnosis of lens dislocation, ROCs were plotted, and the results showed that TIAr had a higher power of discrimination compared with AODr, ARAr, and TISAr (all $P < 0.05$). The TIA is a parameter that represents the angle width, which has been commonly used in the evaluation of the ACA [20, 21]. In order to improve the diagnostic efficiency of the ratio parameters, TIAr250, TIAr500, and TIAr750 were combined, and the results showed that TIAr500 combined TIAr750 (AUC = 0.798) had a promising diagnostic performance for lens dislocation. This suggests
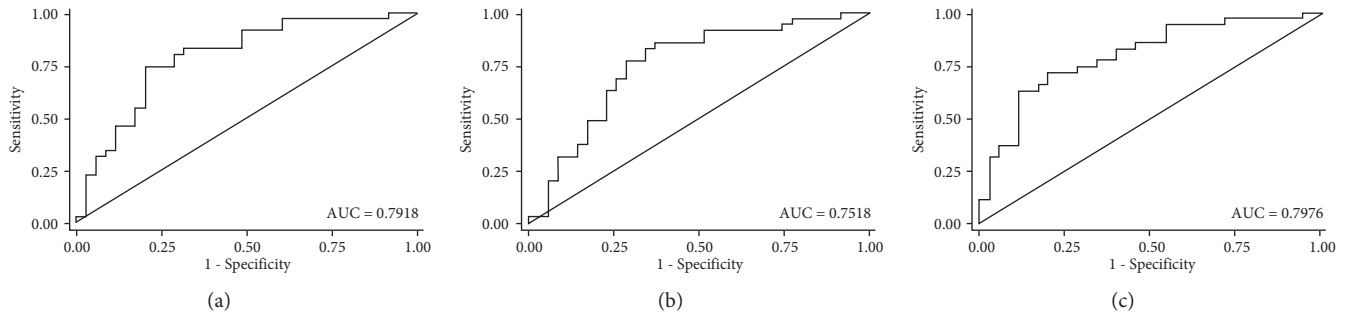
FIGURE 3: The receiving operating characteristics curve of combined ratio index of angle parameters in differential diagnose of ectopia lentis. ((a) TIAr250+TIAr500 (AUC = 0.792); (b) TIAr250+TIAr750 (AUC = 0.752); (c) TIAr500+TIAr750 (AUC = 0.798).

that TIAr500 combined with TIAr750 could serve as a screening tool for lens dislocation.

There are several limitations to this study. First, not all the cross-sectional images were analyzed, and the accuracy may be affected to some extent. Second, the scleral spur and angle recess required manual labeling. Although the investigator in this study had been well trained before the study, bias may still exist. Finally, since our participants were all from a single eye center, the generalization of our conclusion may be limited and further studies are needed. However, the value of our study is in the use of advanced SS-AS-OCT technology to evaluate the anterior segment characteristics of CEL patients and investigate the possibility of utilizing anterior angle parameters to differentiate and diagnose ectopia lentis patients from healthy controls, which could be a significant contribution to disease management.

In conclusion, the ACA of the contralateral side to the dislocated lens in CEL patients was significantly narrower than that of the healthy controls. We recommend that clinicians remain attentive to these changes in values, and regular follow-up is recommended for these patients. For the differential diagnosis of ectopia lentis, TIAr500 combined with TIAr750 could serve as a screening tool in clinical practice.

Data Availability

The data used to support the findings of this study are included within the article.

Additional Points

What Was Known. (i) For eyes with ectopia lentis, the dislocated lens can squeeze the anterior chamber angle and even cause acute secondary angle closure, but little is known about the anterior segment characteristics of CEL patients. *What This Paper Adds.* (i) The anterior chamber angle of the contralateral side to the dislocated lens in congenital ectopia lentis was significantly narrower than that of the healthy controls. (ii) TIAr500 combined with TIAr750 could serve as a screening tool in differential diagnosis of ectopia lentis form healthy population.

Disclosure

Haotian Qi and Guangming Jin are co-first authors.

Conflicts of Interest

The authors declare that there are no conflicts of interest. Acknowledgments

Acknowledgments

Supplementary Materials

Supplemental Figure 1: diagram of anterior chamber angle parameters in SS-OCT (a: anterior chamber width (ACW); b: angle opening distance (AOD) at 250, 500, and 750 μm; c–e: angle recess area (ARA) at 250, 500, and 750 μm; f–h: trabecular-iris space area (TISA) at 250, 500, and 750 μm; i–k: trabecular-iris angle (TIA) at 250, 500, and 750 μm). (*Supplementary Materials*)

References

[1] J. Fuchs and T. Rosenberg, "Congenital ectopia lentis. A Danish national survey," *Acta Ophthalmologica Scandinavica*, vol. 76, no. 1, pp. 20–26, 1998.

[2] M. A. Simon, C. A. Origlieri, A. M. Dinallo, B. J. Forbes, R. S. Wagner, and S. Guo, "New management strategies for ectopia lentis," *Journal of Pediatric Ophthalmology & Strabismus*, vol. 52, no. 5, pp. 269–281, 2015.

[3] J. W. Y. Lee, B. K. T. Wong, D. W. F. Yick, I. Y. H. Wong, C. Y. F. Yuen, and J. S. M. Lai, "Primary acute angle closure: long-term clinical outcomes over a 10-year period in the Chinese population," *International Ophthalmology*, vol. 34, no. 2, pp. 165–169, 2014.

[4] Y. Zhang, Y. Zong, Y. Jiang, C. Jiang, Y. Lu, and X. Zhu, "Clinical features and efficacy of lens surgery in patients with lens subluxation misdiagnosed as primary angle-closure glaucoma," *Current Eye Research*, vol. 44, no. 4, pp. 393–398, 2019.

[5] I. Riva, E. Micheletti, F. Oddone et al., "Anterior chamber angle assessment techniques: a review," *Journal of Clinical Medicine*, vol. 9, no. 12, p. 3814, 2020.

[6] B. L. Loeys, H. C. Dietz, A. C. Braverman et al., "The revised ghent nosology for the marfan syndrome," *Journal of Medical Genetics*, vol. 47, no. 7, pp. 476–485, 2010.

[7] H. Ishikawa, J. M. Liebmann, and R. Ritch, "Quantitative assessment of the anterior segment using ultrasound biomicroscopy," *Current Opinion in Ophthalmology*, vol. 11, no. 2, pp. 133–139, 2000.

[8] M. E. Nongpiur, B. A. Haaland, D. S. Friedman et al., "Classification algorithms based on anterior segment optical coherence tomography measurements for detection of angle closure," *Ophthalmology*, vol. 120, no. 1, pp. 48–54, 2013.

[9] J. Wang, M. Abou Shousha, V. L. Perez et al., "Ultra-high resolution optical coherence tomography for imaging the anterior segment of the eye," *Ophthalmic Surgery, Lasers and Imaging*, vol. 42, pp. S15–S27, 2011.

[10] M. A. Shousha, C. L. Karp, A. P. Canto et al., "Diagnosis of ocular surface lesions using ultra-high-resolution optical coherence tomography," *Ophthalmology*, vol. 120, no. 5, pp. 883–891, 2013.

[11] S. B. Han, Y. C. Liu, K. M. Noriega, and J. S. Mehta, "Applications of anterior segment optical coherence tomography in cornea and ocular surface diseases," *Journal of Ophthalmology*, vol. 2016, Article ID 4971572, 9 pages, 2016.

[12] P. Ma, Y. Wu, J. Oatts et al., "Evaluation of the diagnostic performance of swept-source anterior segment optical coherence tomography in primary angle closure disease," *American Journal of Ophthalmology*, vol. 233, 2021.

[13] B. Wang, L. M. Sakata, D. S. Friedman et al., "Quantitative iris parameters and association with narrow angles," *Ophthalmology*, vol. 117, no. 1, pp. 11–17, 2010.

[14] M. E. Nongpiur, M. He, N. Amerasinghe et al., "Lens vault, thickness, and position in Chinese subjects with angle closure," *Ophthalmology*, vol. 118, no. 3, pp. 474–479, 2011.

[15] R. Lavanya, T. Y. Wong, D. S. Friedman et al., "Determinants of angle closure in older singaporeans," *Archives of Ophthalmology*, vol. 126, no. 5, pp. 686–691, 2008.

[16] M. E. Nongpiur, L. M. Sakata, D. S. Friedman et al., "Novel association of smaller anterior chamber width with angle closure in singaporeans," *Ophthalmology*, vol. 117, no. 10, pp. 1967–1973, 2010.

[17] M. A. Henriquez, J. A. Mejías, M. Rincon, L. Izquierdo, and P. S. Binder, "Correlation between lens thickness and lens density in patients with mild to moderate cataracts," *British Journal of Ophthalmology*, vol. 104, no. 10, pp. 1350–1357, 2020.

[18] L. Wang, W. Huang, S. Huang et al., "Ten-year incidence of primary angle closure in elderly Chinese: the liwan eye study," *British Journal of Ophthalmology*, vol. 103, no. 3, pp. 355–360, 2019.

[19] M. E. Nongpiur, I. F. Aboobakar, M. Baskaran et al., "Association of baseline anterior segment parameters with the development of incident gonioscopic angle closure," *JAMA Ophthalmology*, vol. 135, no. 3, pp. 252–258, 2017.

[20] T. Nishida, T. Kojima, T. Kataoka, N. Isogai, Y. Yoshida, and T. Nakamura, "Prediction of the trabecular iris angle after posterior chamber phakic intraocular lens implantation," *Journal of Cataract & Refractive Surgery*, 2021.

[21] J. Lee, J. Lai, D. Yick, and C. Yuen, "Prospective case series on trabecular-iris angle status after an acute episode of phacomorphic angle closure," *International Journal of Ophthalmology*, vol. 6, no. 1, pp. 67–70, 2013.

Research Article

Factors Related to Visual Outcomes after Lens Surgery in Isolated Microspherophakia

Jialei Zheng [1,2,3] **Lina Cheng** [4,5] **Zexu Chen,** [1,2,3] **Tianhui Chen,** [1,2,3] **and Yongxiang Jiang** [1,2,3]

[1]*Eye Institute and Department of Ophthalmology, Eye & ENT Hospital, Fudan University, Shanghai 200031, China*
[2]*NHC Key Laboratory of Myopia (Fudan University), Key Laboratory of Myopia, Chinese Academy of Medical Sciences, Shanghai 200031, China*
[3]*Shanghai Key Laboratory of Visual Impairment and Restoration, Shanghai 200031, China*
[4]*Shaanxi Provincial Clinical Research Center for Ophthalmology Diseases, First Hospital of Xi'an, Xi'an, Shaanxi 710000, China*
[5]*Shaanxi Key Laboratory of Ophthalmology, Shaanxi Institute of Ophthalmology, Xi'an, Shaanxi, China*

Correspondence should be addressed to Yongxiang Jiang; yongxiang_jiang@163.com

Purpose. To evaluate the main factors influencing visual performance after lens subluxation surgery in subjects with isolated MSP. *Design*. Retrospective study. *Methods*. In this study, 38 eyes of subjects with isolated MSP (microspherophakia) were included and divided into two groups based on preoperative IOP (intraocular pressure), IOP <21 mmHg, or IOP ≧21 mmHg. Phacoemulsification and scleral-fixated modified capsular tension ring implantation were performed with or without goniosynechialysis according to the IOP. Some ocular biometric parameters, such as corneal curvature, corneal pachymetry, endothelial cell count (ECC), anterior chamber depth (ACD), and axial length, were evaluated. The best-corrected visual acuity (BCVA) and IOP of these subjects were measured before the surgery and during <1 month and 3- to 6-month postoperative follow-ups. *Results*. Compared with the high IOP group, the normal IOP group was significantly younger and had better preoperative BCVA, a higher ECC, deeper ACD, a lower postoperative IOP, and flatter total corneal refractive power K1. The multivariable analysis revealed that preoperative ACD ($b = -0.113$, $t = -2.070$, $P = 0.047$) and preoperative BCVA ($b = 0.153$, $t = 2.562$, $P = 0.015$) were significantly associated with postoperative BCVA at 3–6 months. A preoperative ACD of 1.86 mm was found to be the optimal cutoff point for 3- to 6-month postoperative BCVA of ≧20/63 (≤0.52 logMAR). *Conclusions*. In addition to the effect of normal IOP, better preoperative BCVA and deeper ACD also correlated with better visual outcomes after lens surgery. Preoperative ACD served as a warning for isolated MSP subjects, especially for the risk of irreversible loss of postoperative vision. This trial is registered with "ChiCTR2000039132."

1. Introduction

Microspherophakia (MSP) is a relatively rare condition in which the lens is smaller and more spherical than usual. The zonular fibers of MSP become weak and lack tension, which directly leads to the emergence of small spherical crystals [1]. According to previous reports [2], approximately 33% of subjects with MSP have incomplete dislocation and 9% have complete dislocation of the lens, and 20% of these subjects are blinded due to secondary glaucoma. During follow-up,

the blinding rate increases to 30% [2]. Due to the gradual progressive relaxation of the zonular fibers and the severity of damage to vision in MSP, the surgical effect could be various, which depends on the disease stages. Therefore, it is ideal if lens surgery is performed before the occurrence of secondary glaucoma to avoid irreversible damage caused by high IOP (intraocular pressure) on the optic nerve.

According to existing case reports, the following biological parameters may have specific effects on MSP. Because the spherical lens leads to a decreased anterior chamber

depth (ACD), the ACD of MSP ranges from 0.55 to 2.87 mm [3, 4]. The mean anteroposterior distance of the lenses ranges from 4.06 to 6.75 mm [4–7]. The axial length (AL) varies from 21.5 mm to 25 mm, and keratometry varies between 39.4 D and 45.6 D [5–8]. Muralidhar et al. [9] reported that half of MSP subjects had high IOP, and glaucoma developed in 44.4% of the subjects' eyes. Therefore, these may be used as specific biological parameters for evaluating the pathological stage of MSP. However, there is no scientific evidence describing the effectiveness of the biological parameters for assessing isolated MSP.

In our study, we compared how the biometric characteristics of age, corneal curvature, endothelial cell count (ECC), ACD, AL, preoperative and postoperative best-corrected visual acuity (BCVA), and IOP affect the outcome of surgery in isolated MSP. The influence of these factors and postoperative BCVA on these associations was further explored. Moreover, the principal factors driving vision loss distribution were also discussed. This study provides evidence of the high-risk stage of isolated MSP in the clinic.

2. Methods

2.1. Subject Selection. This is a retrospective study. Isolated MSP was diagnosed based on the methods of Chan RT [10]. The inclusion criteria were as follows. (1) Diagnostic criteria: bilateral involvement; lenticular myopia; after mydriasis, the equatorial edge of the lens could be seen under slit lamp or operating microscope; whole lens zonular fibers were found to be sparse and lax by ultrasound biomicroscopy; and the dislocation of lens can be seen in supine position. (2) The surgeries were completed successfully. (3) Those who completed the 1-month and 3–6-month follow-ups. Exclusion criteria were as follows. (1) Lenses fell into the anterior chamber or vitreous cavity. (2) History of ocular trauma. (3) History of other ophthalmic surgery, such as congenital cataract, retinal detachment, epiretinal membrane, or antiglaucoma surgery. (4) Those with systemic associations such as Marfan syndrome, Alport syndrome, homocysteinuria, Weill–Marchesani syndrome, etc. (5) Follow-ups were not completed, or IOP and BCVA data were missing.

Isolated MSP treated between July 2018 and February 2021 in the Eye and ENT Hospital of Fudan University were involved in the study; we enrolled 24 subjects (38 eyes). The subjects were divided into high IOP group and normal IOP group according to whether the initially diagnosed IOP was greater than 21 mmHg. Written informed consent was obtained from all participants or guardians of children. The study was approved by the Human Research Ethics Committee of the Eye and ENT Hospital of Fudan University and adhered to the tenets of the Declaration of Helsinki (ChiCTR2000039132).

2.2. Measurement of Ocular Biometric Parameters. The biometric parameters were collected before surgery. We measured the anterior corneal curvature (mean keratometry, Km), ACD, and AL by partial coherence interferometry

(IOLMaster 500 & 700, Carl Zeiss Meditec AG, Jena, Germany). The corneal pachymetry, anterior and posterior corneal curvature, and total corneal refractive power (TCRP) were assessed by rotating Scheimpflug camera (Pentacam, Oculus Optikgeräte GmbH, Wetzlar, Germany). During the postoperative visits at <1 and 3–6 months, BCVA was measured by the same experienced ophthalmologist with a comprehensive refractometer (NIDEK ARK 510, Japan). The noncontact tonometer (CT-80, Topcon Medical Systems, Japan) was used to measure the IOP. The logarithm of the minimum angle of resolution (logMAR) was used to describe BCVA. The data for all subjects were the average of measurements taken three times.

2.3. Surgical Technique. All surgeries of phacoemulsification (Phaco), goniosynechialysis, scleral-fixated modified capsular tension ring (MCTR) implantation, and sutured scleral fixation of an intraocular lens (IOL) were performed by an experienced doctor (Dr. YX Jiang) [11]. A 2.6 mm superior corneal incision was made after general anesthesia. A continuous curvilinear capsulorhexis (CCC) of 4.0–5.0 mm was applied manually. The capsular bag was suspended and fixed with four capsular hooks (CapsuleCare, Med Devices Lifesciences, India). In adult subjects, the stop and chop technique was performed to deal with nuclei over grade three. In children, the lens material was removed with a phacoemulsifier (Alcon Laboratories Inc, USA) using irrigation/aspiration under a low vacuum with a reduced bottle height of 65 cm. The MCTR (Morcher GmbH, Germany) was then sutured to the sclera 1.5–2 mm behind the limbus with 9-0 polypropylene (MANI Inc. Japan) using a modified knot-free z-suture technique. After removal of the capsular hooks, an IOL was delivered into the capsular bag. In the high IOP group, if the ACD <1.50 mm, it was too shallow to operate, and limited centric anterior vitrectomy was performed via the pars plana to decrease vitreous pressure, facilitating the injection of viscoelastic agent into the anterior chamber to deepen the anterior chamber at the beginning of the surgery. The peripheral part of the iris was pulled towards the center and back 360° with capsulorhexis forceps, and the adhesions of the angle were separated twice. Then, the viscoelastic agent was used to separate the anterior chamber angle again at 360°. If there was vitreous leakage into the anterior chamber, anterior vitrectomy was required. In the case of incomplete CCC and rupture of the posterior capsule, an IOL was fixed to the sclera with 9-0 polypropylene using the modified knotless z-suture technique [12]. The surgery flow chart for the subjects is shown in Figure 1. In the first week after the surgery, the subjects were treated with sodium hyaluronate, praprofen, and ofloxacin eye drops and prednisone acetate ophthalmic suspension 1% four times a day. The frequency was changed to three times a day in the 2nd week and reduced to two times a day in the 3rd week, and we continued to use this frequency for 1 month.

2.4. Statistical Analysis. Statistical analyses were performed with SPSS version 23.0 software (IBM Corp. Armonk, NY,
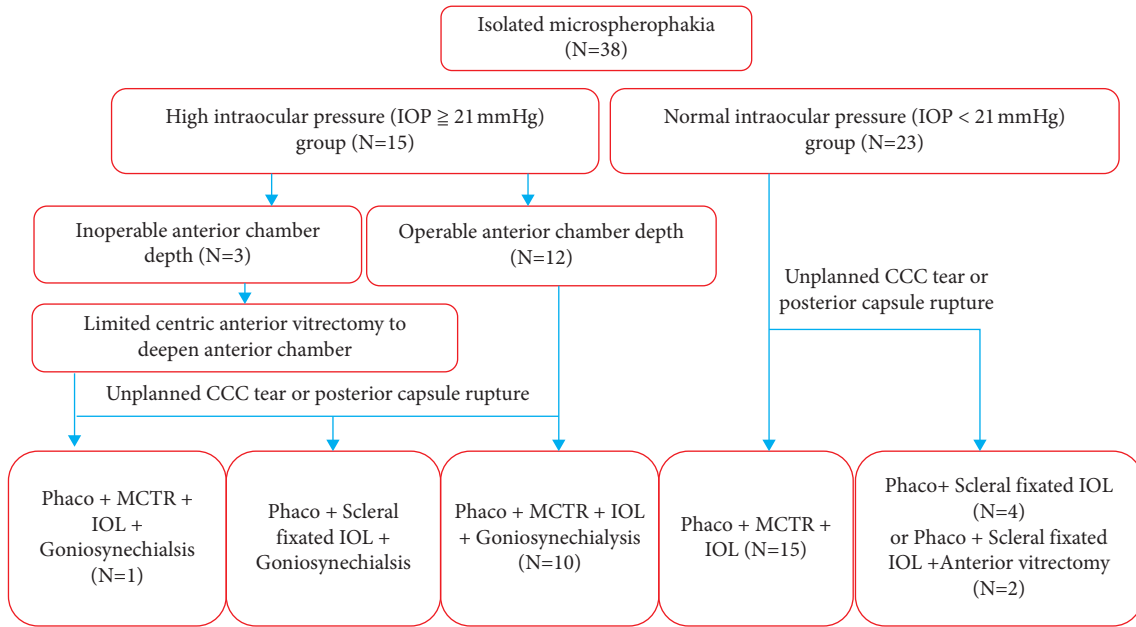
FIGURE 1: Subjects' surgery flow chart. IOP: intraocular pressure; phaco: phacoemulsification; CCC: continuous curvilinear capsulorhexis; MCTR: modified capsular tension rings; IOL: intraocular lens.

USA). A Kolmogorov–Smirnov test of normality was performed for all variables. Absolute frequency (n) and relative frequency (%) were used to describe categorical variables. The statistical results for the continuous variables included the mean ± standard deviation (SD) and median P_{50} (P_{25}, P_{75}) according to the normality of the data. The Student's t-test and Wilcoxon rank-sum test (Mann–Whitney U-test) were used, as appropriate, to compare continuous data. The Chi-square test and Fisher's test were used to compare categorical variables. Univariate linear regression analysis was used to evaluate correlations between ocular biometric parameters and postoperative BCVA. Multivariable linear regression analysis was performed to identify the predictors of postoperative BCVA at 3–6 months. The receiver operating characteristic (ROC) curve was used to evaluate the high-risk values of the preoperative ACD and preoperative BCVA. A P value of <0.05 was considered significant.

3. Results

3.1. Preoperative Characteristics of All Subjects.

This study included 38 eyes from 24 isolated MSP subjects treated between July 2018 and February 2021 at the Eye & ENT Hospital of Fudan University. The mean subjects age was 27 ± 19.24 years. The basic preoperative parameters of these eyes are shown in Table 1.

3.2. Surgical Outcomes.

Scleral suture fixation IOL surgery was performed in 10 eyes and MCTR implantation in 28 eyes. The mean BCVAs (logMAR) of the 38 eyes with MSP were 1.22 ± 1.0 (preoperative), 0.46 ± 0.49 (1 month), and 0.39 ± 0.33 (3–6 months). The mean IOPs (mmHg) were 20.2 ± 9.8 (preoperative), 15.62 ± 5.46 (1 month), and 16.92 ± 4.65 (3–6 months). The preoperative vs.

TABLE 1: Baseline characteristics of total subjects.

	Total
Subjects/eyes	24/38
Sex (female : male)	14 (58.33%) : 10 (41.67%)
Eyes (right : left)	18 (47.37%) : 20 (52.63%)
Age (years)	27 ± 19.24 (4~60)
Preoperative BCVA (logMAR)	1.22 ± 1.00 (0.22~4)
Preoperative IOP (mmHg)	20.21 ± 9.81 (9.0~53.5)
High IOP/normal IOP	15 (39.47%) : 23 (60.53%)
Central ECC (cells/mm^2)	2733.861 ± 475.9466 (1468~3818)
Corneal pachymetry (μm)	546.39 ± 46.39 (463~622)
Preoperative AL (mm)	24.82 ± 2.22 (21.99~30.14)
Preoperative SimK (D)	42.78 ± 1.99 (29.4~47.4)
Preoperative TRCP K_m (D)	43.04 ± 1.86 (39.2~46.2)
Preoperative ACD$_{ext}$ (mm)	2.76 ± 0.87 (1.01~4.62)
B/F ratio	78.72 ± 16.28 (77.4~85.7)

BCVA: best-corrected visual acuity; IOP: intraocular pressure; ECC: endothelial cell count; WTW: white to white; AL: axial length; km: mean keratometry; TCRP: total corneal refractive power; ACD: anterior chamber depth; B/F ratio: mean radius of the posterior corneal surface/mean radius of the anterior corneal surface ratio; SD: standard deviation.

postoperative differences in BCVA and IOP were statistically significant ($P < 0.05$). There was an improvement in BCVA and a reduction in IOP at 1-month and 3–6-month follow-ups compared with the preoperative measurements, but no significant differences between the 1-month follow-up and 3–6-month follow-up were observed ($P = 0.102$). The results are shown in Figure 2.

3.3. Postoperative Complications.

Posterior capsular opacification (PCO) was found in five eyes at follow-up. When the IOP was 21–30 mmHg (five eyes) after the surgery, one antiglaucoma eye drop was added to reduce the IOP. When the IOP was 30–40 mmHg (three eyes), two drugs were used.
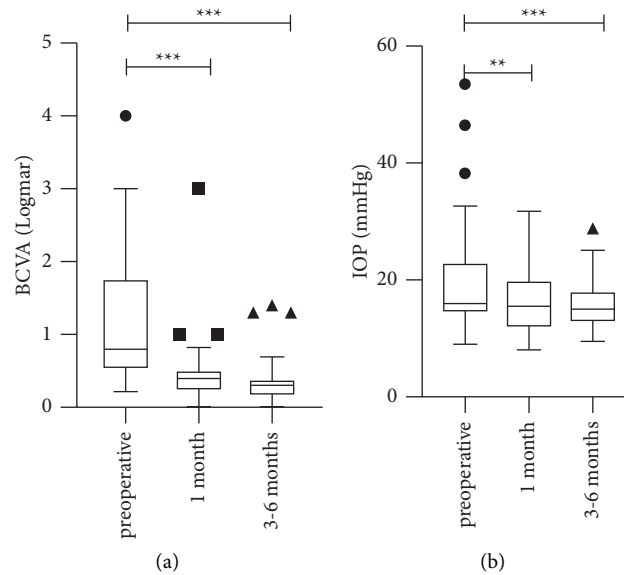
Figure 2: BCVA: best-corrected visual acuity; IOP: intraocular pressure. (a) Changes of BCVA in all subjects. (b) Changes of IOP in all subjects. $^{*}P < 0.05$; $^{**}P < 0.01$; $^{***}P < 0.001$.

After the IOP reached a normal value, the drugs were gradually reduced. In the process of drug reduction, changes in the IOP were monitored. During the 3–6-month follow-up, six eyes still needed antiglaucoma drugs to control IOP. There was no endophthalmitis, retinal detachment, or dislocation of the IOL by the end of follow-up.

3.4. Differences between High IOP and Normal IOP Groups.
The eyes were divided into two groups according to IOP. The normal IOP group was allocated based on a preoperative IOP of <21 mmHg without any IOP-lowering drugs and glaucoma surgery. The other subjects were entered into the high IOP group. There were 23 eyes in the normal IOP group and 15 eyes in the high IOP group. Differences between the two groups are summarized in Table 2. There were significant differences in age, preoperative BCVA, preoperative IOP, ECC, preoperative ACD, and preoperative TCRP K1. During the follow-up at 3–6 months, there were significant differences in postoperative IOP between the two groups.

3.5. Univariate and Multivariable Analyses of Various Factors Associated with Postoperative BCVA at 3–6 Months.
Univariate analysis of various factors (Table 3) associated with postoperative BCVA at 3–6 months revealed that preoperative BCVA, preoperative and postoperative IOP at 3–6 months, and preoperative ACD were significantly associated with postoperative BCVA. In the multivariable analysis (Table 4), preoperative BCVA and preoperative ACD were the variables significantly associated with the 3–6-month postoperative BCVA.

3.6. The Relationship between Preoperative ACD and 3–6-Month Postoperative BCVA ≥20/63 (0.52 LogMAR).
The ROC curve was analyzed to consider the potential risk values

for preoperative ACD that resulted in a 3–6-month postoperative BCVA of ≥20/63 (≤0.52 LogMAR), as shown in Figure 3. The area under the curve was 0.807. The value of preoperative ACD at 1.86 mm was found to be the optimal cut-off point for a 3–6-month postoperative BCVA of ≥20/63 (≤0.52 logMAR). The preoperative ACD presented a sensitivity of 93.8% and a specificity of 66.7% ($P = 0.018$).

4. Discussion

Subjects with MSP usually have poor vision and complications such as high refractive myopia, lens subluxation, glaucoma, corneal decompensation, and retinal detachment [9, 10]. The severity of the MSP determines the differences in postoperative visual function and prognosis of these subjects [9]. Therefore, this paper mainly discusses the application of MCTR in MSP and the factors affecting visual performance after surgery.

Due to the particularity of lens morphology and the complexity of the complications, the treatment methods used for MSP are variable [4, 13–15]. The abnormal lens should be removed surgically [13]. Lensectomy, anterior vitrectomy, and glaucoma surgery are common choices for managing secondary glaucoma in MSP [16]. However, the former surgical method tends to have more postoperative complications [17]. In Jarrete's study [17], including 166 dislocation lens cases, lens extraction was done in 114 eyes in the series. Vitreous was lost in 47 (41%) at surgery, and 12 retina detachments (11%) occurred following extraction of the dislocated lens. With the rapid development of phacoemulsification and lens capsule stabilizing devices, posterior chamber (PC) IOLs are also implanted with capsular tension rings (CTR) or capsular tension segments (CTS) [18]. The postoperative visual acuity recovered better, and the incidence of postoperative complications decreased. Yang et al. [4] did a 3-year research including 19 subjects with

TABLE 2: Differences of high IOP group and normal IOP group.

Characteristics	Normal IOP group	High IOP group	P value
Sex (female/male)	13 (56.52%)/10 (43.48%)	6 (40.0%)/9 (60.0%)	0.254
Eyes (right/left)	12 (52.17%)/11 (47.83%)	5 (33.33%)/10 (66.67%)	0.254
Age (years)	21.65 ± 19.90 (4~60)	35.2 ± 15.38 (15~59)	**0.032***
Preoperative BCVA (logMAR)	0.7 ± 0.51 (0.22~2.70)	2.02 ± 1.06 (0.5~4.0)	**<0.001***
Preoperative IOP (mmHg)	15.33 ± 2.5 (11.0~20.7)	27.36 ± 12.07 (9~53.5)	**<0.001***
Central ECC (cells/mm^2)	2969.0 ± 413.06 (2248~3818)	2404.67 ± 351.47 (1468~2776)	**<0.001***
Corneal pachymetry (μm)	541.26 ± 46.50 (503~612)	554.267 ± 38.3210 (526~605)	0.374
Preoperative AL (mm)	24.84 ± 2.07 (22.0~28.24)	24.84 ± 2.52 (21.99~30.14)	0.995
Preoperative ACD (mm)	3.12 ± 0.77 (1.51~4.80)	2.31 ± 0.81 (1.05~3.65)	**0.006***
Preoperative KI (D)	41.44 ± 6.74 (39.89~48.49)	43.65 ± 1.71 (40.53~46.40)	0.255
Preoperative K2 (D)	44.01 ± 2.29 (41.01~48.84)	44.61 ± 1.7 (42.29~46.96)	0.413
Preoperative SimK (D)	42.30 ± 1.94 (39.4~47.4)	43.53 ± 1.88 (40.5~46.4)	0.060
Preoperative TCRP K1 (D)	41.81 ± 1.69 (39.2~45.5)	43.26 ± 1.92 (41.1~46.2)	**0.019***
Preoperative TCRP K2 (D)	43.33 ± 2.05 (40.4~47.3)	44.28 ± 1.65 (41.8~46.4)	0.141
Preoperative TCRP Km (D)	42.58 ± 1.81 (40.2~46.1)	43.75 ± 1.75 (41.1~46.0)	0.055
B/F ratio	82.59 ± 2.53 (77.4~85.7)	82.27 ± 1.60 (78.8~84.9)	0.682
Postoperative IOP (mmHg) <1 month	13.91 ± 3.81 (10.1~19.0)	18.07 ± 6.43 (10.5~31.0)	0.059
Postoperative BCVA (logMAR) <1 month	0.33 ± 0.18 (0.04~0.69)	0.65 ± 0.75 (0~3)	0.193
Postoperative IOP (mmHg) (3–6 months)	13.64 ± 2.97 (10.6~22.5)	19.59 ± 4.13 (14.0~29.1)	**<0.001***
Postoperative BCVA (logMAR) (3–6 months)	0.26 ± 0.13 (0~0.52)	0.53 ± 0.47 (0.04~1.39)	0.124

BCVA: best-corrected visual acuity; IOP: intraocular pressure; ECC: endothelial cell count; WTW: white to white; AL: axial length; Km: mean keratometry; TCRP: total corneal refractive power; ACD: anterior chamber depth; B/F ratio: mean radius of the posterior corneal surface/mean radius of the anterior corneal surface ratio.

TABLE 3: Univariate analysis of factors associated with postoperative BCVA at 3–6 months.

Various factors	Beta coefficient (95% CI)	t value	P value
Age (years)	−0.005 (−0.01, 0.001)	−1.755	0.088
Preoperative BCVA (logMAR)	0.204 (0.115, 0.292)	4.650	**<0.001***
Preoperative IOP (mmHg)	0.019 (0.009, 0.029)	3.883	**<0.001***
Central ECC (cells/mm^2)	0.000 (0.000, 0.000)	−1.474	**0.015***
Corneal pachymetry (μm)	0.001 (−0.001, 0.004)	1.085	0.285
Preoperative ACD (mm)	−0.229 (−0.346, −0.113)	−4.021	**<0.001***
Preoperative AL (mm)	0.188 (−0.022, 0.078)	1.150	0.258
Preoperative km (D)	−0.035 (−0.091, 0.020)	−1.294	0.204
Preoperative TCRP Km (D)	−0.249 (−1.106, 0.014)	−1.542	0.132
B/F ratio	−0.004 (−0.053, 0.051)	−0.026	0.979
MCTR implantation/suture-fixated IOL	−0.190 (−0.434, 0.054)	−1.581	0.123
PCO	−0.081 (−0.409, 0.247)	−0.501	0.619
Postoperative IOP (mmHg) ≤1 month	0.254 (−0.010, 0.044)	1.315	0.200
Postoperative IOP (mmHg) 3–6 months	0.397 (0.006, 0.053)	2.561	**0.015***

CI: confidence interval; BCVA: best-corrected visual acuity; IOP: intraocular pressure; ECC: endothelial cell count; ACD: anterior chamber depth; AL: axial length; km: mean keratometry; TCRP: total corneal refractive power; B/F ratio: mean radius of the posterior corneal surface/mean radius of the anterior corneal surface ratio; MCTR: modified capsular tension ring; IOL: intraocular lens; PCO: posterior capsular opacification. *: $P < 0.05$; **: $P < 0.01$; ***: $P < 0.001$.

TABLE 4: Multivariate analysis of factors associated with postoperative BCVA at 3–6 months.

Various factors	Beta coefficient (95% CI) ($N = 38$)	T value	P value
Preoperative BCVA (logMAR)	0.153 (0.031, 0.275)	2.562	**0.015***
High/normal IOP	−0.093 (−0.376, 0.191)	−0.665	0.511
Preoperative ACD (mm)	−0.113 (−0.225, 0.002)	−2.070	**0.047***
Postoperative IOP (mmHg) 3–6 months	0.018 (0.008, 0.044)	1.436	0.161

TCI: confidence interval; BCVA: best-corrected visual acuity; IOP: intraocular pressure; high IOP: preoperative IOP ≧21 mmHg; normal IOP: preoperative IOP <21 mmHg; ACD: anterior chamber depth. *: $P < 0.05$; **: $P < 0.01$; ***: $P < 0.001$.

microspherophakia and glaucoma, 7 eyes underwent phacoemulsification and CTR, whereas 17 eyes underwent lensectomy with scleral-fixated posterior chamber (PC) IOL implantation. The postoperative BCVA increased from 0.79 ± 0.36 to 0.44 ± 0.38 (logMAR) in the CTR group and from 1.15 ± 0.75 to 0.43 ± 0.38 (logMAR) in the lensectomy
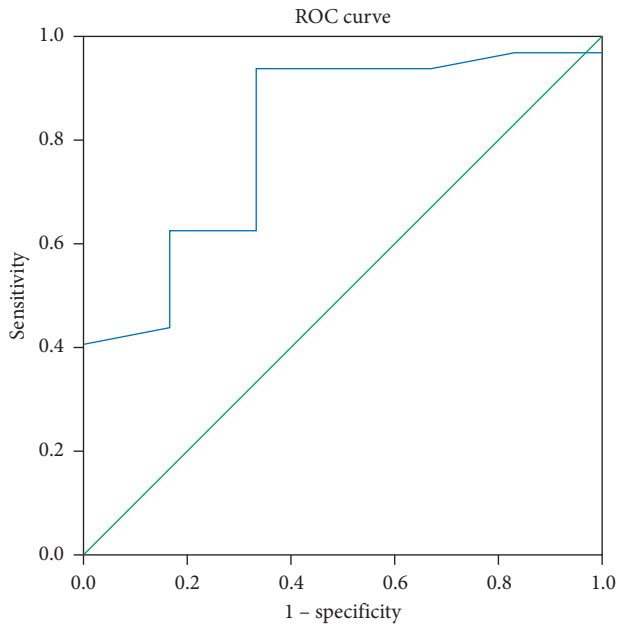
ROC curve

FIGURE 3: ROC curve for preoperative ACD in relation to the postoperative BCVA at 3–6 months. ROC: receiver operating characteristic; ACD: anterior chamber depth; BCVA: best-corrected visual acuity.

group at the 3-year follow-up. Six eyes (85.7%) in the CTR group developed different degrees of posterior capsular opacity. However, the follow-up of other complications was not reported.

MCTR has also been recognized as providing a fixed support for capsular bags with zonular dialysis [14]. Cionni et al. [19] reported a postoperative BCVA of 20/40 or better in 88.9% of subjects with congenital loss of zonular support by phacoemulsification with MCTR implantation, while the mean follow-up was 14.6 months (range 2 to 32 months). The incidence of retinal detachment (1%), mild persistent iritis (3.3%), and suture spontaneously broke (10.0%) was low.

With the support of the MCTR, capsular hooks [20, 21], and other new technology, our lens surgery of choice for isolated MSP has changed from lens extraction, which has more complications, to phacoemulsification and MCTR implantation, with fewer complications. In this study, we used MCTR implantation (28 eyes, 73.7%) and IOL scleral interlaminar surgery (10 eyes, 26.3%). Goniosynechialysis was carried out for subjects with high IOP. In our study group, 78.9% of subjects at 3- to 6-month follow-up achieved a vision of 0.48 logMAR or better, compared with 61.1% of subjects in previous studies in which lensectomy was done by the limbal route or by pars plana, while the mean follow-up was 8.55 ± 3.98 years [9]. The preoperative vs. postoperative differences in BCVA and IOP were statistically significant.

The findings suggest these surgical methods were effective. One month after the surgery, the visual performance of all eyes was significantly improved, and the improvement tended to be stable at 3- to 6-month follow-up. Compared with previous studies [17, 19], our surgery also had small probabilist intraocular complications. Thus, the surgical

procedure appeared safe over the short-term observation period.

Which factors are the main influences on visual performance in isolated MSP still needs to be determined. We further explored certain parameters; the surgical method; the occurrence of PCO which would affect the postoperative BCVA. As a result, the surgical method and PCO might not be a key index for determining the postoperative visual outcome.

In our study, 39.5% (15/38) of subjects with isolated MSP had a high IOP, which is comparable to 44% of subjects with MSP seen in previous studies [9]. Due to abnormal relaxation of the lens zonular fibers in MSP [22], lens dislocation or subluxation may occur, and the small lens is often displaced towards the anterior chamber, which may lead to shallowing of the ACD and the loss of corneal endothelial cells [23]. When the iris contacts the anterior surface of the lens repeatedly over a long time period, it causes repeated pupil block, resulting in the closure of angle adhesion and finally the formation of chronic angle-closure glaucoma [24]. This process occurs repeatedly and leads to continuous glaucoma development. Compared with the high IOP group, the normal IOP subjects were younger and had better preoperative BCVA, a higher ECC, a greater anterior chamber depth, lower postoperative IOP, and flatter TCRP K1. Therefore, these biological parameters should be important and meaningful in subjects with high IOP. During the 3- to 6-month follow-up period, six eyes still needed to be treated with two to three hypotensive drugs to maintain the IOP below 21 mmHg. Therefore, the alteration of the structure and function of the trabecular meshwork caused by the spherical lens was partly irreversible, suggesting that surgery should be performed before excessive goniosynechia. However, there was no significant linear correlation between the high/normal IOP group and postoperative BCVA. As a result, finding more sensitive and specific indicators to predict postoperative BCVA would be beneficial.

In this study, univariable and multivariable linear regression of various factors revealed that the preoperative ACD and BCVA were significantly associated with postoperative BCVA at 3–6 months, which suggested subjects with deeper ACD and better preoperative BCVA could achieve a better postoperative visual outcome. The ACD and BCVA measurements are easy to obtain on ophthalmic examination. The disadvantage of BCVA is that it is considered to be a subjective index, and crystal astigmatism, corneal astigmatism, and refractive amblyopia might also affect the results of optometry. Therefore, we did not take preoperative BCVA to be an evaluation parameter. On the other hand, preoperative ACD is an objective indicator that is measured directly by partial coherence interferometry, and it has good practicability and operability in the clinic. The results of the study showed that ACD can reflect the severity of the spherical lens and predict postoperative visual outcomes. We used a visual outcome of less than 20/63 as the diagnostic value because the diagnostic criterion of low vision is 20/63 according to the World Health Organization (WHO) criteria [25]. A preoperative ACD of 1.86 mm was the optimal cut-off point for poor

postoperative vision. This result reminded us that we should not only pay attention to the IOP of isolated MSP but also closely monitor the preoperative ACD, and surgical measures should be performed in time to avoid the occurrence of poor vision.

There were some limitations to this study. Firstly, only 24 subjects were enrolled; therefore, the sample size was rather small. Secondly, some of the follow-up periods were rather short and variable due to the COVID-19 pandemic in 2020. Therefore, the final follow-up results from 3 to 6 months after surgery were selected, instead of more exact time points, for the endpoint analysis. Thirdly, our findings might be biased because of the retrospective methodology and the lack of a control group for comparison.

In conclusion, phacoemulsification and scleral-fixated MCTR implantation for isolated MSP subjects was safe and effective in the short term. During the follow-up of isolated MSP, we also need to pay attention to changes in the BCVA and ACD in addition to the IOP. The critical value for the preoperative ACD could be used as a feasible reference to avoid the occurrence of low visual ability after the surgery. In future studies, it will be important to extend the follow-up time to observe the long-term complications of these surgical methods and the subsequent changes in BCVA and IOP.

Data Availability

Data are available in a public, open-access repository. All data relevant to the study are included in the article or uploaded as supplementary information.

Conflicts of Interest

The authors declare that they have no conflicts of interest.

Authors' Contributions

Jialei Zheng and Lina Cheng contributed equally to this work.

Acknowledgments

References

[1] P. A. Ndoye Roth, S. A. Toure, H. Kane et al., "Isolated microspherophakia in a senegalese family," *Journal Francais d'Ophtalmologie*, vol. 40, no. 2, pp. 110–114, 2017.

[2] S. Senthil, H. L. Rao, N. T. Hoang et al., "Glaucoma in microspherophakia: presenting features and treatment outcomes," *Journal of Glaucoma*, vol. 23, no. 4, pp. 262–267, 2014.

[3] J. Shakrawal, H. Selvan, A. Sharma, and D. Angmo, "Double trouble: microspherophakia with axenfeld-rieger anomaly," *Indian Journal of Ophthalmology*, vol. 67, no. 3, pp. 394-395, 2019.

[4] J. Yang, Q. Fan, J. Chen et al., "The efficacy of lens removal plus IOL implantation for the treatment of spherophakia with secondary glaucoma," *British Journal of Ophthalmology*, vol. 100, no. 8, pp. 1087–1092, 2016.

[5] M. Moshirfar, J. J. Meyer, J. A. Schliesser, L. Espandar, and J. C. Chang, "Iris-fixated phakic intraocular lens implantation for correction of high myopia in microspherophakia," *Journal of Cataract and Refractive Surgery*, vol. 36, no. 4, pp. 682–685, 2010.

[6] S. H. Lim, J. H. Son, and S. C. Cha, "Acute angle-closure glaucoma in a highly myopic patient secondary to Weill-Marchesani syndrome: histopathologic lens features," *International Ophthalmology*, vol. 36, no. 6, pp. 921–924, 2016.

[7] C. E. Willoughby and P. K. Wishart, "Lensectomy in the management of glaucoma in spherophakia," *Journal of Cataract and Refractive Surgery*, vol. 28, no. 6, pp. 1061–1064, 2002.

[8] R. T. Chan and H. B. Collin, "Microspherophakia," *Clinical and Experimental Optometry*, vol. 85, no. 5, pp. 294–299, 2002.

[9] R. Muralidhar, K. Ankush, P. Vijayalakshmi, and V. P. George, "Visual outcome and incidence of glaucoma in patients with microspherophakia," *Eye*, vol. 29, no. 3, pp. 350–355, 2015.

[10] X. Yu, W. Chen, and W. Xu, "Diagnosis and treatment of microspherophakia," *Journal of Cataract & Refractive Surgery*, vol. 46, no. 12, pp. 1674–1679, 2020.

[11] Z. Chen, M. Zhang, M. Deng et al., "Surgical outcomes of modified capsular tension ring and intraocular lens implantation in marfan syndrome with ectopia lentis," *European Journal of Ophthalmology*, vol. 32, no. 2, pp. 924–932, 2021.

[12] P. Szurman, K. Petermeier, S. Aisenbrey, M. S. Spitzer, and G. B. Jaissle, "Z-suture: a new knotless technique for trans-scleral suture fixation of intraocular implants," *British Journal of Ophthalmology*, vol. 94, no. 2, pp. 167–169, 2010.

[13] H. Guo, X. Wu, K. Cai, and Z. Qiao, "Weill-Marchesani syndrome with advanced glaucoma and corneal endothelial dysfunction: a case report and literature review," *BMC Ophthalmology*, vol. 15, no. 1, p. 3, 2015.

[14] S. Khokhar, S. Gupta, G. Kumar, and N. Rowe, "Capsular tension segment in a case of microspherophakia," *Contact Lens and Anterior Eye*, vol. 35, no. 5, pp. 230–232, 2012.

[15] S. Khokhar, S. Gupta, B. Nayak, and V. Gogia, "Capsular hook-assisted implantation of modified capsular tension ring," *BMJ Case Reports*, vol. 2016, Article ID bcr2015214274, 2016.

[16] S. Khokhar, G. Pillay, S. Sen, and E. Agarwal, "Clinical spectrum and surgical outcomes in spherophakia: a prospective interventional study," *Eye*, vol. 32, no. 3, pp. 527–536, 2018.

[17] W. H. Jarrett, "Dislocation of the lens. A study of 166 hospitalized cases," *Archives of Ophthalmology*, vol. 78, no. 3, pp. 289–296, 1967.

[18] S. Canabrava, A. C. Canedo Domingos Lima, A. E. L. Arancibia, L. F. Bicalho Dornelas, and G. Ribeiro, "Novel double-flanged technique for managing marfan syndrome and microspherophakia," *Journal of Cataract & Refractive Surgery*, vol. 46, no. 3, pp. 333–339, 2020.

[19] R. J. Cionni, R. H. Osher, D. M. Marques, F. F. Marques, M. E. Snyder, and S. Shapiro, "Modified capsular tension ring for patients with congenital loss of zonular support," *Journal of Cataract & Refractive Surgery*, vol. 29, no. 9, pp. 1668–1673, 2003.

[20] J. C. Merriam and L. Zheng, "Iris hooks for phacoemulsification of the subluxated lens," *Journal of Cataract & Refractive Surgery*, vol. 23, no. 9, pp. 1295–1297, 1997.

[21] R. J. Cionni and R. H. Osher, "Management of profound zonular dialysis or weakness with a new endocapsular ring designed for scleral fixation," *Journal of Cataract & Refractive Surgery*, vol. 24, no. 10, pp. 1299–1306, 1998.

[22] A. D. Jensen, H. E. Cross, and D. Paton, "Ocular complications in the weill-marchesani syndrome," *American Journal of Ophthalmology*, vol. 77, no. 2, pp. 261–269, 1974.

[23] S. Khokhar, M. S. Pangtey, P. Sony, and A. Panda, "Phacoemulsification in a case of microspherophakia," *Journal of Cataract & Refractive Surgery*, vol. 29, no. 4, pp. 845–847, 2003.

[24] A. Z. Burakgazi, Z. Ozbek, C. J. Rapuano, and D. J. Rhee, "Long-term complications of iris-claw phakic intraocular lens implantation in weill-marchesani syndrome," *Cornea*, vol. 25, no. 3, pp. 361–363, 2006.

[25] Y. Tang, X. Wang, J. Wang et al., "Prevalence and causes of visual impairment in a Chinese adult population," *Ophthalmology*, vol. 122, no. 7, pp. 1480–1488, 2015.

Research Article

Simultaneous Corneal Topography and Epithelial Thickness Mapping from a Single Measurement Using Optical Coherence Tomography

Bartosz L. Sikorski [1,2]

[1]*Department of Ophthalmology, Nicolaus Copernicus University, 9 M. Sklodowskiej-Curie Street, Bydgoszcz 85-309, Poland*
[2]*Oculomedica Eye Research and Development Centre, Ogrody 14 Street, Bydgoszcz 85-870, Poland*

Correspondence should be addressed to Bartosz L. Sikorski; sikorski@doctors.org.uk

Purpose. To evaluate the performance of corneal epithelial thickness mapping (ETM) and demonstrate simultaneous measurement of ETMs and corneal topography using REVO NX (Optopol Technology, Zawiercie, Poland)—an OCT device for anterior and posterior segment imaging. *Methods*. One hundred thirty-seven eyes of 137 normal subjects and patients with corneal diseases were recruited to the study. Each subject was scanned with REVO NX. ETMs and corneal topography maps were reconstructed from a single measurement. Corneal topography was also carried out using Pentacam (Oculus, Wetzlar, Germany). One hundred twenty-eight eyes were qualified for the final analysis. Forty healthy eyes were used to evaluate the performance of ETM, and 88 eyes were used to compare ETMs and corneal topography. The repeatability and reproducibility of ETMs in healthy subjects were assessed on the basis of 17 spatial zones derived from an 8-mm diameter corneal scan using within-subject standard deviation, test-retest repeatability, within-subject coefficient of variation (CoV), and intraclass correlation coefficient (ICC). *Results*. The ICC for both repeatability and reproducibility of ETMs for the central sector was 0.95. The ICC value for the other sectors was only moderately lower. However, the CoV for repeatability (≤1.55%) was slightly higher than the value reported for the RTVue device (Optovue, Inc, Fremont, California, USA), for which a CoV in the central zone of 1.07% was reported in unoperated eyes. The superior quadrants were found to be the thinnest while the inferior ones were the thickest. ETMs and topography maps created from a single OCT measurement present a complementary image of the cornea. *Conclusions*. ETMs obtained using REVO NX show high levels of repeatability and reproducibility in normal eyes. Because the topographic and epithelial thickness analyses are performed using the same data, which means they are based on the exact same 3D corneal model, they do not require reciprocal centration and map matching. This ensures a complete point-to-point correlation between ETMs and corneal topography maps, which paints a fuller picture of a given pathology.

1. Introduction

Accurate corneal imaging is critical for both diagnosis and effective management and treatment of patients with ocular surface diseases. As new diagnostic imaging modalities become more detailed and treatments for many eye diseases become more sophisticated, the ability to obtain a more complete picture of a condition through multimodal imaging becomes particularly important. In recent years, with the popularization of spectral domain optical coherence tomography (OCT), we have gained the ability to routinely perform corneal epithelial thickness mapping (ETM) in daily clinical practice, in addition to the classic OCT visualization of the corneal structure and corneal curvature and power in topography. The first commercially available device capable of creating ETMs was the RTVue 100 (Optovue Inc., Fremont, California, USA). The device demonstrated excellent repeatability of corneal epithelial thickness measurements in normal as well as in keratoconus (KCN) eyes, dry eye patients, and postlaser-assisted in situ keratomileusis eyes [1–4]. ETMs were also shown to be helpful in differentiation KCN from contact lens warpage in patients with abnormal topography [5]. The RTVue, however, did not have the capacity to perform corneal topography, which

could be correlated with an ETM to obtain a more complete picture of the pathology. The latest version of the device, Avanti (Optovue Inc., Fremont, California, USA), does not offer this possibility either. In order to compare ETMs with corneal topography, one needs to use data from other diagnostic devices, which brings the risk of nonideal spatial and temporal correlation of examinations. Recently, a novel stand-alone anterior segment OCT device, which provides the ability to perform imaging of the anterior segment and obtain ETMs combined with placido disc corneal topography, has been introduced into clinical practice (MS-39, CSO, Firenze, Italy) [6]. It delivers high repeatability of ETM measurements in healthy and KCN eyes [7]. However, as mentioned earlier, the device does not use the OCT technique to create corneal topography maps and thus also uses different data than those used to plot ETMs. Anterior segment-only OCTs using swept-source (SS-OCT) technology, such as the Casia 2 (Tomey Corporation, Nagoya, Japan) and Anterion (Heidelberg Engineering GmbH, Heidelberg, Germany) devices, are also commercially available for corneal topography. However, they have not released their ETM capabilities that are currently under clinical trials. This function is present only in its investigational software version and has not been released commercially [8].

The first device to offer full commercial corneal topography and ETMs derived from an OCT examination is REVO NX (Optopol Technology, Zawiercie, Poland). The device also gives the possibility to create topographic maps and ETMs from one data set obtained in a single measurement. The goal of this study is to evaluate the performance of ETMs and to demonstrate the implementation of ETM measurement with a simultaneous registration of corneal topography in the REVO NX device.

2. Methods

2.1. Subjects. The study was conducted from May 2020 to June 2021 and included 137 subjects (mean age: 41.4 ± 14.5 years; 65 females). Subjects showing no changes in the corneal structure in an examination using a slit lamp as well as patients with corneal diseases were qualified for the study. A complete ocular assessment was performed. All patients were examined using REVO NX (Optopol Technology S.A, Zawiercie, Poland) with the topography OCT (T-OCT) module with an add-on anterior adapter (software version 9.5). Topography maps and ETMs were produced using the topography protocol, which is a modified 8-mm anterior radial scanning protocol. During the examination, the center of the pupil was positioned at the center of the measurement window to keep the central reflection centered in both the horizontal and vertical preview windows of the tomogram. Participants were asked to blink to enable corneal tear film coverage before measurements and to concentrate on the fixation target during the scan and open the eye widely. Each measurement was checked for quality. If it did not meet the manufacturer's recommended total quality factor (TQF) value, the test was rejected and a new measurement was performed. The procedure was repeated up to three times. If

the quality of all measurements was not good enough, the eye was excluded from the analysis. Topography maps were also made for all patients using Pentacam AXL (Oculus, Wetzlar, Germany). Like in the case of REVO NX, the measurement was also repeated three times, if it did not meet the quality criteria. Maps of good quality were obtained on both devices in 88 of 97 subjects (the most common reason for examination rejection was lack of stable fixation or dropping eyelid). This included 32 healthy eyes (mean anterior K1, K2, and cylinder for REVO NX were 42.71 ± 1.05 D, 43.95 ± 1.30 D, and 1.20 ± 0.99 D, respectively; mean anterior K1, K2, and cylinder for Pentacam were 42.77 ± 0.99 D, 44.07 ± 1.35 D, and 1.31 ± 1.05 D, respectively; mean posterior K1, K2, and cylinder for REVO NX were -6.02 ± 0.27, -6.37 ± 0.33, and 0.35 ± 0.19, respectively; and mean posterior K1, K2, and cylinder for Pentacam were -6.10 ± 0.20, -6.47 ± 0.30, 0.39 ± 0.18, respectively) and 56 eyes with corneal pathologies (mean anterior K1, K2, and cylinder for REVO NX were 44.36 ± 5.61 D, 47.34 ± 7.51 D, and 3.00 ± 2.96 D, respectively; mean anterior K1, K2, and cylinder for Pentacam were 44.25 ± 5.58 D, 47.55 ± 7.79 D, and 3.29 ± 3.52 D, respectively; mean posterior K1, K2, and cylinder for REVO NX were -5.99 ± 0.92, -6.90 ± 1.35, and 0.93 ± 0.69, respectively; and mean posterior K1, K2, and cylinder for Pentacam were -6.19 ± 1.27, -6.81 ± 1.61, and 0.63 ± 0.63, respectively). Additionally, 40 healthy eyes (40 healthy volunteers, mean age 35.7 ± 8.38 years) were examined only with REVO NX in order to determine intraobserver repeatability and interobserver reproducibility of ETMs. Eight of these subjects had astigmatism <0.5 D, 16 subjects had astigmatism in the range of 0.5–1.0 D, and 16 subjects had astigmatism exceeding 1 D. Mean K1 and K2 [D] were 43.26 ± 0.99 and 44.46 ± 1.73, respectively. The values of K1 and K2 [mm] were 7.8 ± 0.18 and 7.6 ± 0.28, respectively. The cylinder [D] value was 1.2 ± 1.24 (with a range of: 0.2–7.6). The respective values of Min K [D] and Avg K [D] were 44.58 ± 1.76 and 43.85 ± 1.25 (with a range of 42.56–47.80). The respective values of Min K [D] and Avg K [D] were 7.58 ± 0.27 and 7.70 ± 0.20 (with a range of 7.06–7.93). Each measurement was taken three times by 2 operators in a random order, under ambient lighting conditions. Following each measurement, the subject head was repositioned on the chin rest and the REVO NX device was realigned. The study protocol was in accordance with the Declaration of Helsinki. The Institutional Ethics Committee approval was granted, and informed consent was obtained from all participants.

2.2. Creation of Topography Maps and ETMs. Topography maps and ETMs were reconstructed using REVO NX with the anterior adapter. It is an OCT device dedicated to posterior as well as anterior segment imaging, with the ability to analyze corneal curvature and a built-in optical biometry module using the split-window OCT method [9]. The device has the following technical parameters: the LED light source with central wavelengths of 830 nm, a scanning speed of 110 000 A-scan/sec, a scan depth window of 2.43 mm, a maximum anterior scan width of 16 mm, an axial

resolution of 5 μm (digital~2,5 μm), and the transverse resolution of 18 μm.

Topography maps and ETMs were produced using the topography protocol, which is a modified anterior radial scanning protocol. It consists of 16 evenly spaced meridian B-scans (8 mm in length each). Every B-scan consists of 1024 A-scans. The examination time is 0.17 sec. After collecting the data, the algorithm automatically recognizes the B-scans' 3 boundaries defining the edges of corneal layers: air and corneal boundary, the posterior epithelium boundary, and the posterior endothelium boundary, which makes it possible to create a thickness map of the whole cornea, epithelium, and stroma. The posterior border of the epithelium is detected as the border of the epithelium and the Bowman membrane. In the absence of the Bowman membrane, for example, in patients who have undergone photorefractive keratectomy, the posterior border is defined as the border of the corneal epithelium and stroma. Once the layers are recognized, the system dewarps the collected tomograms to reconstruct the actual shape and profile of the anterior and posterior corneal surfaces. Next, a 3D model of the corneal surface is created on the basis of the B-scans and the identified layers. The reconstructed corneal profile undergoes a qualitative assessment expressed as a summary TQF that determines whether the operator can trust the measurement. The TQF is based on the values of the following individual factors: the quality index, which is based on the signal-to-noise ratio of all tomograms, and the correlation index, which describes the quality of the tomogram correlation and the analyzed area index that indicates the percentage of the recognized area for anterior and posterior surfaces of the cornea. Metrics describing corneal curvature, topography maps, and ETMs are not displayed for scans with poor quality or with motion artifacts that cannot be compensated. The software also detects imaging artifacts and displays adequate warnings whenever on 3 consecutive scans. The system detects areas where there is no continuous corneal structure and the corneal layers cannot be recognized. This makes it easy to recognize artifacts caused by a closed eyelid, a ghost signal from the iris, a lack of signal due to long eyelashes, or a weak signal due to corneal opacity. If the quality of data is insufficient for analysis, the system does not display the data or marks the area as interpolated with a texture of different transparency. The corneal vertex is determined on the 3D model, which is followed by the creation of 16 maps describing the curvature and thickness of the cornea in relation to the vertex (Figure 1). The maps include the following: Axial map [Anterior], Axial map [Posterior], Tangential map [Anterior], Tangential map [Posterior], Refractive Power map [Anterior], Refractive Power map [Posterior], Refractive Power map [Kerato], Refractive Power map [Total], Net map, Axial True Net, Equivalent Keratometer map, Elevation map [Anterior], Elevation Map [Posterior], Height map, and Pachymetry map. An ETM is also created on the basis of the same data and the 3D model of the cornea. Quantitative data for topography maps are displayed in 3 zones, i.e., 3 mm, 5 mm, and 7 mm. Also, the simulated keratometry value (Sim K) is calculated for the anterior and posterior corneal surfaces, and real power is calculated according to the thick lens formula. ETMs display an averaged epithelial thickness across 17 sectors. Around the central sector with the diameter of 2 mm, the following paracentral sectors are found: Superior, Superior-temporal, Temporal, Inferior-temporal, Inferior, Inferior-nasal, Nasal, and Superior-nasal. Outwards from these, there are the following sectors: Superior_Out, Superior-temporal_Out, Temporal_Out, Inferior-temporal_Out, Inferior_Out, Inferior-nasal_Out, Nasal_Out, or Superior-nasal_Out. The limits of the zones outside the central 2-mm sector are 2–5 mm and 5–7 mm, respectively.

2.3. Statistical Analysis. Statistical analysis was performed using Statistica 13.1 software (Dell Inc., USA). To determine the intraobserver repeatability and interobserver reproducibility of the REVO ETMs, the within-subject standard deviation (Sw), test-retest repeatability (TRT), coefficient of variation (CoV), and intraclass correlation coefficient (ICC) were calculated and analyzed. The Sw was the square root of the residual mean square in the one-way analysis of variance. The TRT was defined as 2.77 Sw, which shows the interval within which 95% of the differences between measurements are expected to lie [10]. The percentage of CoV was calculated as the ratio of the Sw to the mean. The ICC represented the consistency in data measurement: high agreement is indicated by a value higher than 0.9 [11]. To assess agreement between REVO NX and Pentacam AXL topography for anterior K1, anterior K2, anterior cylinder, posterior K1, posterior K2, and posterior cylinder, the paired samples t-test and Bland–Altman analyses were performed, and 95% limits of agreement were calculated by the mean difference ± 1.96 SD [12]. A p value of less than 0.05 was considered statistically significant.

3. Results

3.1. Repeatability and Reproducibility of ETMs. The results of intraobserver repeatability and interobserver reproducibility assessment in 17 sectors of ETMs using REVO NX in 40 healthy eyes are shown in Tables 1 and 2. The ICC of repeatability for the central sector was ≥0.95. The ICC values for the sectors immediately surrounding the central sector were the following: Superior ≥0.88, Superior-temporal ≥0.82, Temporal ≥0.86, Inferior-temporal ≥0.91, Inferior ≥0.89, Inferior-nasal ≥0.85, Nasal ≥0.91, and Superior-nasal ≥0.88. The ICC value for the peripheral sectors were as follows: Superior_Out ≥0.76, Superior-temporal_Out ≥0.79, Temporal_Out ≥0.69, Inferior-temporal Out ≥0.74, Inferior_Out ≥0.81, Inferior-nasal_Out 0.79, Nasal_Out ≥0.89, and Superior-nasal_Out ≥0.64. The value of the ICC of reproducibility for the central sector was 0.95, while for the inner sectors, it showed the following values: Superior=0.92, Superior-temporal=0.87, Temporal=0.90, Inferior-temporal=0.91, Inferior=0.90, Inferior-nasal=0.87, Nasal=0.91, Superior-nasal=0.86, Superior_Out=0.76, Superior-temporal_Out=0.77, Temporal_Out=0.69, Inferior-temporal_Out=0.77, Inferior_Out=0.77, Inferior-nasal_Out=0.79, Nasal_Out=0.77, and Superior-nasal_Out=0.60.
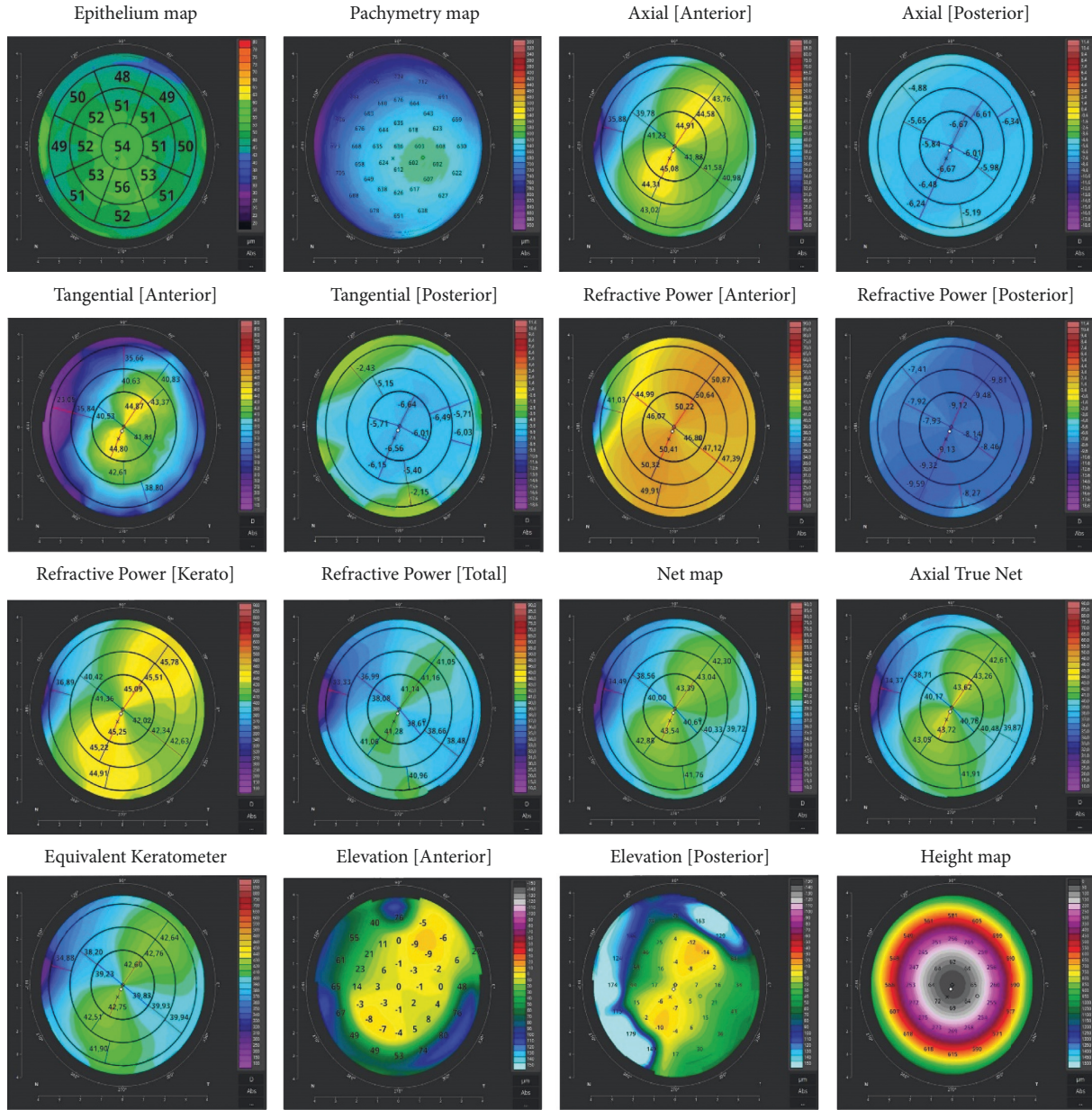
Figure 1: Topography maps and ETMs generated during a simultaneous measurement by REVO NX with 16 evenly spaced meridian B-scans of 8-mm width. To the right of each map are the color scales used to represent the analyzed parameter.

Table 1: Intraobserver repeatability results for ETMs using REVO NX based on three measurements taken by 2 operators in a sample of 40 eyes.

Sector	Operator	Mean ± SD	TRT	Sw	CoV (%)	ICC
Superior (μm)	1st	51.53 ± 3.45	1.60	0.58	1.12	0.98
	2nd	51.27 ± 3.22	3.36	1.21	2.36	0.88
Superior-temporal (μm)	1st	51.47 ± 3.28	1.89	0.68	1.33	0.96
	2nd	51.30 ± 3.00	3.89	1.40	2.73	0.82
Temporal (μm)	1st	51.43 ± 3.26	1.82	0.66	1.28	0.97
	2nd	51.33 ± 2.99	3.36	1.21	2.36	0.86
Inferior-temporal (μm)	1st	51.23 ± 3.09	2.77	1.00	1.95	0.91
	2nd	51.53 ± 3.12	2.09	0.75	1.46	0.95
Inferior (μm)	1st	51.13 ± 3.04	3.12	1.13	2.20	0.89
	2nd	51.47 ± 3.07	2.37	0.86	1.66	0.94
Inferior-nasal (μm)	1st	51.07 ± 2.98	3.51	1.26	2.48	0.85
	2nd	51.57 ± 2.99	2.53	0.91	1.77	0.92

TABLE 1: Continued.

Sector	Operator	Mean ± SD	TRT	Sw	CoV (%)	ICC
Nasal (μm)	1st	51.20 ± 3.06	2.53	0.91	1.78	0.93
	2nd	51.43 ± 3.05	2.77	1.00	1.94	0.91
Superior-nasal (μm)	1st	51.17 ± 3.07	2.86	1.03	2.02	0.91
	2nd	51.73 ± 2.83	3.04	1.10	2.12	0.88
Central (μm)	1st	51.50 ± 3.22	1.96	0.71	1.37	0.96
	2nd	51.43 ± 3.34	2.21	0.80	1.55	0.95
Superior_Out (μm)	1st	51.13 ± 2.96	3.95	1.43	2.79	0.81
	2nd	51.67 ± 2.67	3.98	1.44	2.78	0.76
Superior-temporal_Out (μm)	1st	51.20 ± 2.80	3.89	1.40	2.74	0.79
	2nd	51.80 ± 2.62	3.51	1.26	2.44	0.81
Temporal_Out (μm)	1st	51.10 ± 2.87	4.08	1.47	2.88	0.78
	2nd	51.67 ± 2.44	4.11	1.48	2.87	0.69
Inferior-temporal_Out (μm)	1st	51.53 ± 2.61	4.05	1.46	2.83	0.74
	2nd	51.87 ± 2.47	2.95	1.06	2.05	0.85
Inferior_Out (μm)	1st	51.20 ± 2.80	3.58	1.29	2.52	0.82
	2nd	51.80 ± 2.62	3.51	1.26	2.44	0.81
Inferior-nasal_Out (μm)	1st	51.93 ± 2.74	3.36	1.21	2.33	0.79
	2nd	52.03 ± 2.63	3.36	1.21	2.33	0.82
Nasal_Out (μm)	1st	51.57 ± 2.58	2.26	0.82	1.58	0.92
	2nd	51.43 ± 3.00	2.99	1.08	2.10	0.89
Superior-nasal_Out (μm)	1st	51.30 ± 2.20	4.05	1.46	2.85	0.64
	2nd	51.67 ± 3.24	3.61	1.30	2.52	0.87

TABLE 2: Interobserver reproducibility results for ETMs using REVO NX based on the first readings from each session taken by 2 operators in a sample of 40 eyes.

Sector	Mean ± SD	TRT	Sw	CoV (%)	ICC
Superior (μm)	51.40 ± 3.31	2.63	0.95	1.85	0.92
Superior-temporal (μm)	51.38 ± 3.11	3.07	1.11	2.16	0.87
Temporal (μm)	51.38 ± 3.10	2.70	0.97	1.90	0.90
Inferior-temporal (μm)	51.38 ± 3.08	2.48	0.90	1.74	0.91
Inferior (μm)	51.30 ± 3.03	2.69	0.97	1.89	0.90
Inferior-nasal (μm)	51.32 ± 2.97	2.95	1.06	2.07	0.87
Nasal (μm)	51.32 ± 3.03	2.46	0.89	1.73	0.91
Superior-nasal (μm)	51.45 ± 2.94	2.97	1.07	2.08	0.86
Central (μm)	51.47 ± 3.25	2.00	0.72	1.40	0.95
Superior_Out (μm)	51.40 ± 2.81	3.78	1.36	2.65	0.76
Superior-temporal_Out (μm)	51.50 ± 2.70	3.59	1.30	2.52	0.77
Temporal_Out (μm)	51.38 ± 2.66	4.06	1.46	2.85	0.69
Inferior-temporal_Out (μm)	51.70 ± 2.53	3.36	1.21	2.34	0.77
Inferior_Out (μm)	51.50 ± 2.70	3.59	1.30	2.52	0.77
Inferior-nasal_Out (μm)	51.98 ± 2.66	3.36	1.21	2.33	0.79
Nasal_Out (μm)	51.50 ± 2.78	3.66	1.32	2.57	0.77
Superior-nasal_Out (μm)	51.48 ± 2.75	4.80	1.73	3.37	0.60

3.2. Clinical Cases. The comparison of the ETMs and topography maps obtained using REVO NX and Pentacam AXL was based on a group of 88 patients. The mean anterior K1 [D] measurement difference in 32 healthy eyes was -0.06 ± 0.15 ($p = 0.09$, the 95% limits of agreement (LoA) on Bland–Altman plots ranged from -0.35 to 0.25); the mean anterior K2 [D] difference was -0.12 ± 0.26 ($p = 0.05$, 95% LoA -0.60 to 0.40); the mean anterior cylinder [D] difference was -0.12 ± 0.26 D ($p = 0.05$, 95% LoA -0.60 to 0.40); the mean posterior K1 [D] difference was 0.08 ± 0.18 D ($p = 0.05$, 95% LoA -0.25 to 0.45); the mean posterior K2 [D] difference was 0.10 ± 0.24 ($p = 0.06$, 95% LoA -0.35 to

0.60); and the mean posterior cylinder [D] difference was -0.04 ± 0.08 ($p = 0.04$, 95% LoA -0.20 to 0.10). The mean anterior K1 [D] measurement difference in 56 eyes with corneal diseases was 0.11 ± 0.22 ($p = 0.05$, 95% LoA -0.30 to 0.50); the mean anterior K2 [D] difference was -0.21 ± 0.87 ($p = 0.17$, 95% LoA -1.90 to 1.50); the mean anterior cylinder [D] difference was -0.29 ± 0.78 ($p = 0.08$, 95% LoA -1.80 to 1.25); the mean posterior K1[D] difference was 0.20 ± 0.70 ($p = 0.44$, 95% LoA -1.20 to 1.60); the mean posterior K2 [D] difference was -0.09 ± 0.59 ($p = 0.69$, 95% LoA -1.25 to 1.05); and the mean posterior cylinder [D] difference was 0.30 ± 0.52 ($p = 0.15$, 95% LoA -0.75 to 1.35).
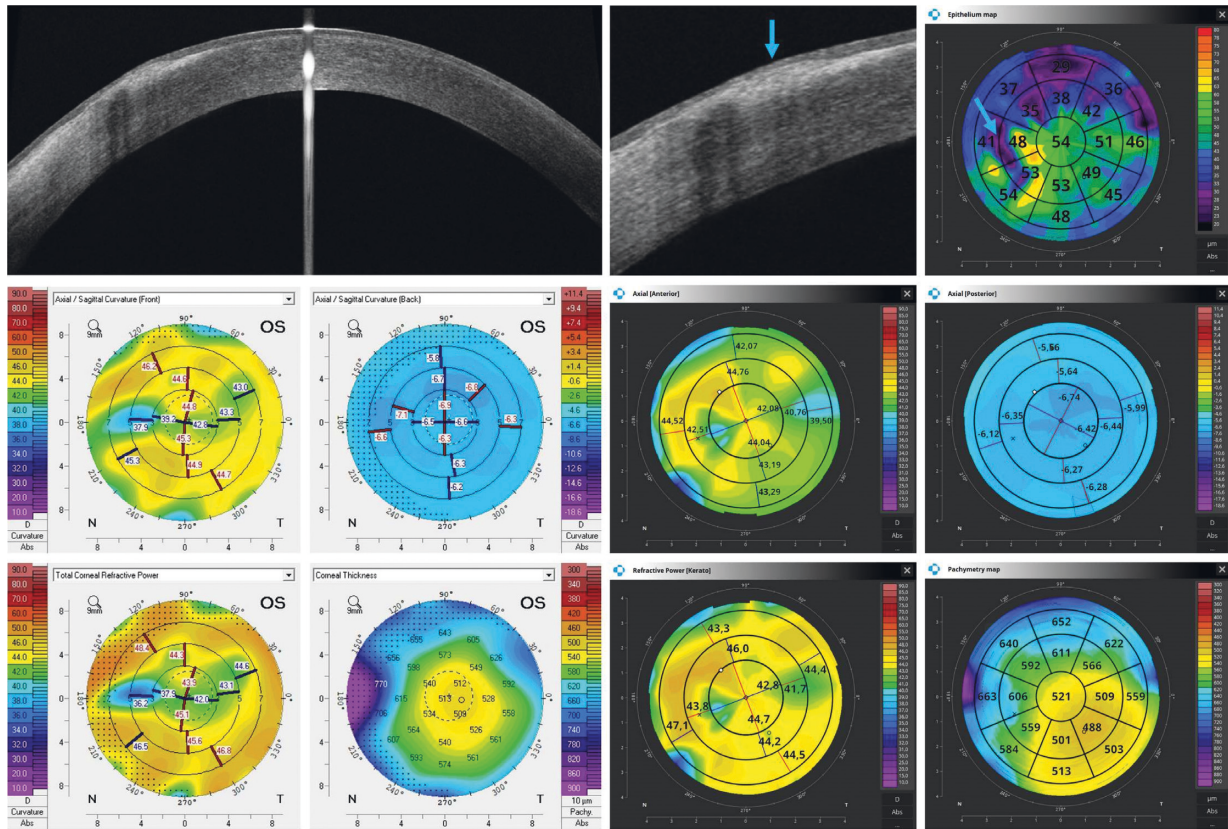
FIGURE 2: Postpterygium surgery OCT tomogram shows an irregular reduction in the epithelial thickness across the entire upper and partially nasal portions of the central cornea on the ETM (blue arrows). Topography maps reveal irregular astigmatism of the anterior surface of the cornea while the posterior surface is regular. The measurements performed with Pentacam have a white background, and the ones performed with REVO NX have a black background. The K1, K2, and astigmatism values for the anterior surface of the cornea obtained using Pentacam are 41.2 D, 44.8 D, and 3.6 D, respectively, while the values obtained using REVO NX are 41.4 D, 44.5 D, and 3.1 D, respectively. The values of analogous parameters for the posterior corneal surface from Pentacam are −6.5 D, −6.6 D, and 0.1 D and the values from REVO NX are −6.2 D −6.5 D 0.3 D.

Figures 2–7 show representative examples of corneal pathologies, selected from the group of eyes mentioned above, imaged with REVO NX using simultaneous corneal topography (dark background) and ETMs from a single measurement together with corresponding topography maps created using Pentacam (white background).

Figure 2 shows the condition after pterygium surgery that resulted in an irregular astigmatism. An OCT tomogram depicts an irregular reduction in the epithelial thickness across the entire upper and partially nasal portions of the central cornea on the ETM (blue arrows). The Axial Anterior and Refractive Power maps reveal that the anterior surface of the cornea is damaged and the posterior surface is regular. In the area of the removed pterygium, the cornea is thicker due to scarring, as shown by pachymetry. The same relationship is also evident on maps created using Pentacam.

Figure 3 shows ulcerative keratitis with extensive corneal stromal scarring. In the area of the disease process, ETM reveals a thickening of the epithelium (red arrow) accompanied by an increase in corneal thickness on the pachymetry map. Again, the Axial Anterior and Refractive Power

maps demonstrate that the patient's irregular astigmatism originates from the anterior corneal surface. The posterior corneal surface is normal. Corneal topography performed with Pentacam shows similar results.

Figure 4 shows the ocular surfaces of a patient with corneal ectasia. The decrease in corneal epithelial thickness (blue arrow) corresponds to the increase in corneal thickness on the pachymetry map in a manner typical for KNC. Axial Anterior and Tangential Anterior as well as Tangential Posterior maps show that both the anterior and posterior corneal surfaces have irregular curvature. They are represented in the same way on the Pentacam maps.

The example in Figure 5 shows an intracorneal ring segment. OCT reveals epithelial thinning immediately above the ring (blue arrow), with the thickness increasing toward the ring (red arrow). This relationship is clearly visible in the en face image on the ETM. The Axial Anterior, Tangential Anterior, and Refractive Power maps show anterior corneal surface abnormalities, which correlate well with the results from Pentacam.

Figure 6 shows a postradial keratotomy eye. The OCT en face reconstruction depicts corneal incisions spreading
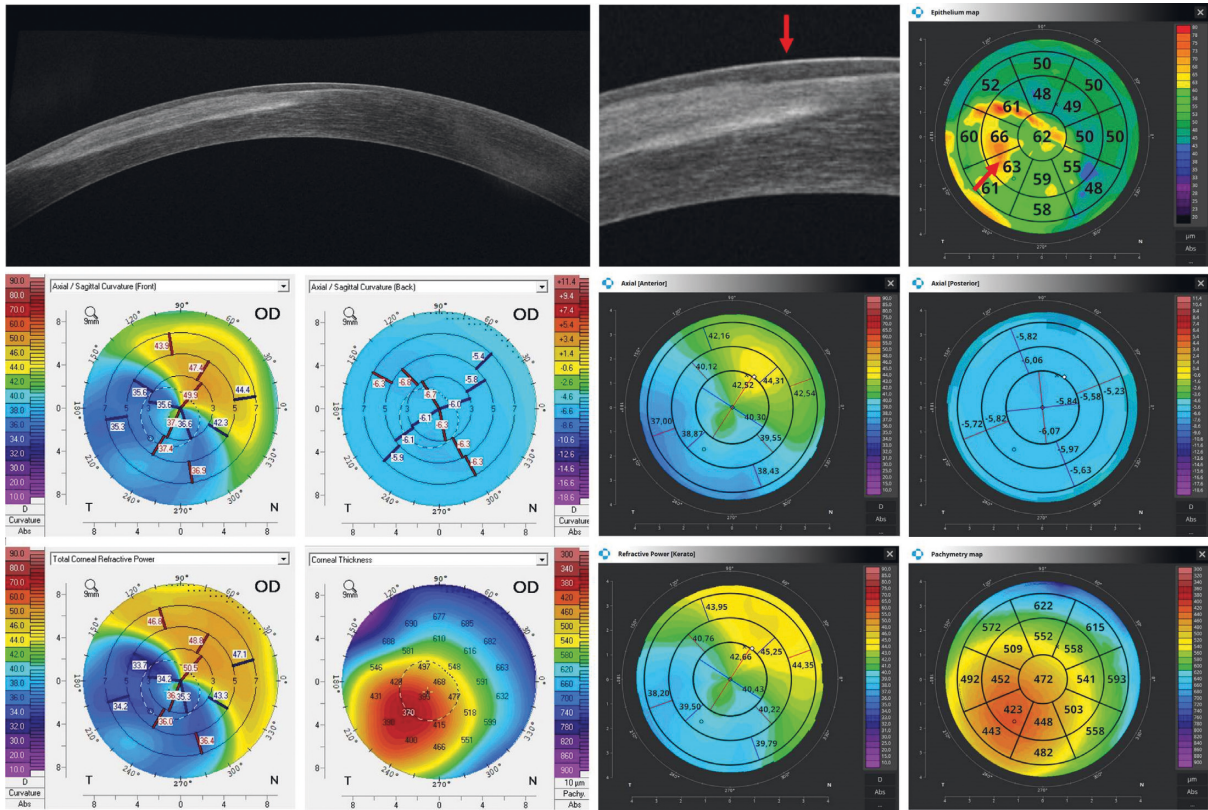
FIGURE 3: Ulcerative keratitis with extensive corneal stromal scarring. ETM shows thickening of the epithelium in the area of the disease process (red arrow). Topography maps depict irregular astigmatism of the anterior surface of the cornea while the posterior surface is regular. The measurements performed with Pentacam have a white background, and the ones performed with the REVO NX have a black background. The K1, K2, and astigmatism values for the anterior surface of the cornea obtained using Pentacam are 36.8 D, 42.9 D, and 6.1 D, respectively, while the values obtained using REVO NX are 37.6 D, 42.9 D, and 5.3 D, respectively. The values of analogous parameters for the posterior corneal surface from Pentacam are −6.0 D, −6.3 D, and 0.3 D and the values from the REVO NX are −5.8 D, −6.0 D, and 0.2 D.

radially. The Axial Anterior and Refractive Power maps show the flattening of the central cornea that is typical for this procedure. A similar pattern can be observed on the Pentacam maps. Both devices present a small paracentral island with the reduced curvature of the posterior corneal surface. On the ETM, one can observe an increase in epithelial thickness (red arrow) exactly in the same place (red arrow).

The final example shows the patient's eye on the first and fifth days after cataract surgery (Figure 7). At the first follow-up visit, one can observe a large corneal oedema on the pachymetry map (red arrow) and an irregularity of the anterior corneal surface on the Axial Anterior map. At the next visit, the oedema is no longer visible. Despite a significant change in the corneal thickness and curvature between examinations, ETMs show a similar image.

4. Discussion

The analysis of the distribution of the epithelial thickness is a valuable diagnostic and follow-up tool when dealing with patients presenting corneal abnormalities caused by such factors as the presence of pathogenic changes, wearing contact lenses, or undergoing refractive surgeries. For this reason, ETMs have been increasingly used in recent years to evaluate the ocular surface. It can be assumed, therefore, that as new devices featuring ETM functionality come on the market, its popularity will continue to increase. Since the diagnostic value of ETMs is more complete when combined with corneal topography (which provides complementary information about the ocular surface), it would be very practical to have a tool capable of performing both examinations simultaneously. However, the OCT devices available on the market provide either ETMs (Avanti, Optovue Inc., Fremont, California, USA; MS-39, CSO, Firenze, Italy) or topography maps (Heidelberg Engineering GmbH, Heidelberg, Germany; Casia 2, Tomey Corporation, Nagoya, Japan). The world's first commercially available OCT device that can perform a simultaneous measurement of both epithelial thickness and corneal topography is REVO NX, and it is not a trivial task.

Performing reliable ETMs using commercially available OCT devices can be difficult due to several aspects. First of all, the corneal epithelium has a relatively small thickness in relation to the optical axial resolution of OCT devices. The majority of devices on the market that operate at the
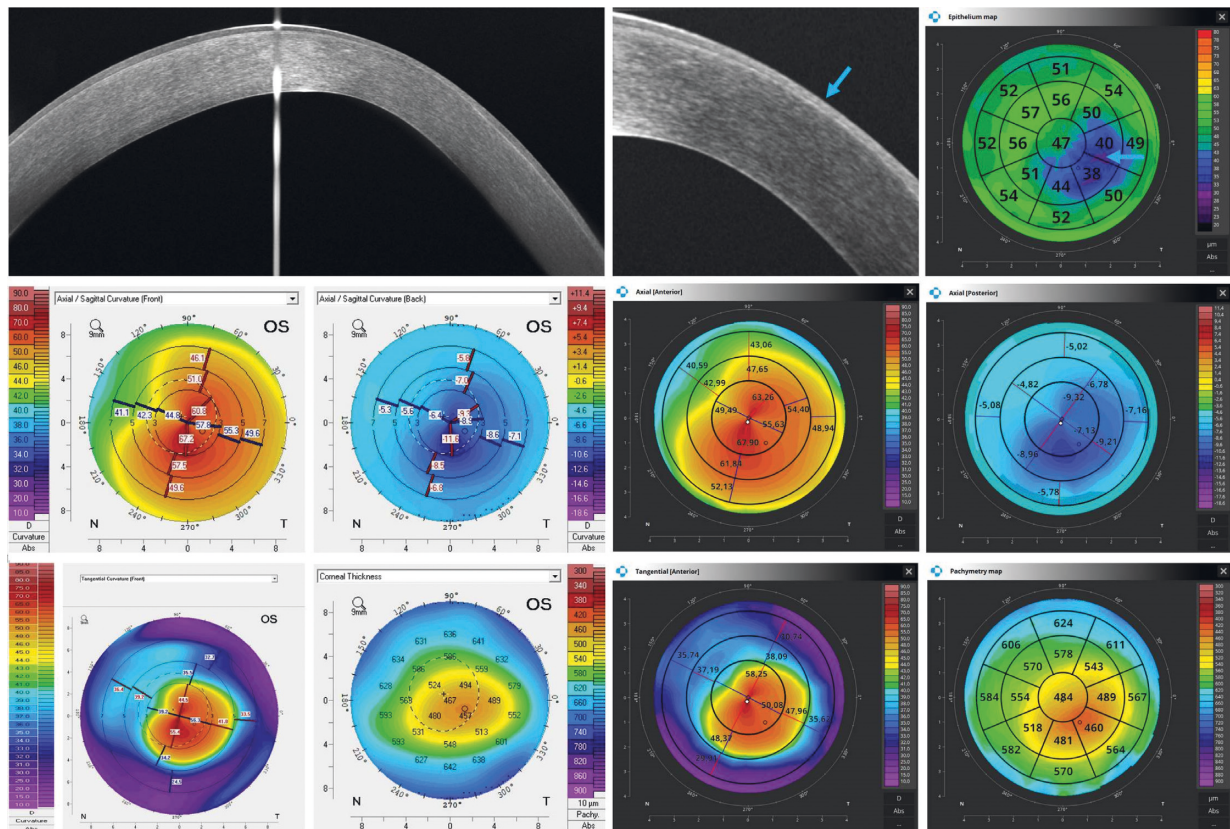
FIGURE 4: Cornea with keratoconus. The decrease in corneal epithelial thickness (blue arrow) corresponds to the increase in corneal thickness on the pachymetry map. Topography maps show that both the anterior and posterior corneal surfaces have irregular curvature. The measurements performed with Pentacam have a white background, and the ones performed with the REVO NX have a black background. The K1, K2, and astigmatism values for the anterior surface of the cornea obtained using Pentacam are 51.0 D, 62.9 D, and 11.9 D, respectively, while the values obtained using the REVO NX are 50.9 D, 61.9 D, and 11.0 D, respectively. The values of analogous parameters for the posterior corneal surface from Pentacam are −7.7 D, −9.7 D, and 2.0 D and the values from REVO NX are −7.2 D, −9.4 D, and 2.2 D.

wavelengths in the range of 830–850 nm typically features an optical axial resolution of around 5 μm (e.g., REVO NX), effectively delivering digital image resolution of around 2.5 μm. What is more, the transverse resolution of OCT devices is much lower than their axial resolution, which makes it more difficult to visualize small and local changes in epithelial thickness. This problem can become even more pronounced in SS-OCT devices, which offer less axial resolution due to their longer wavelength. Also, the low reflectivity of the boundary between the epithelium and the Bowman membrane can make it difficult to properly segment the corneal layers. When this boundary disappears, only the interface between the epithelium and the stroma is visible. Scanning the cornea several times at the same locations and averaging the tomograms may be helpful to overcome the difficulties described above. This, however, increases scanning time and can lead to difficulties in building correlations between consecutive B-scans, between which involuntary eye movements occur [13].

Also, OCT topography methods must overcome a challenge connected with the movement of the eye that can occur during serial image acquisition. Even during fixation,

eye movements, such as drift and microsaccades, occur [14]. Especially microsaccades, which are larger (0–2 deg) and more rapid (~40 deg/s) eye movements occurring at a rate of 1–2 times per second, if not handled properly, can cause significant distortions in topography maps and adversely impact measurement accuracy and repeatability [13, 15, 16]. One should also keep in mind that building a reliable 3D model of the cornea and performing its spatial alignment, which is essential for creating topography maps, is particularly difficult when it is based on data from OCT devices dedicated to posterior segment imaging. Apart from REVO NX, no other such commercially available OCT device offers the functionality of corneal topography. The Avanti device in the corneal power scan mode (8 radial scans with 6-mm scan length of 1024 A-scans) only provides mean Net, Anterior, and Posterior power measurements, representing the net corneal power, anterior corneal power, and posterior corneal power, respectively. The corneal curvature radii, on the other hand, are derived based only on the best fit sphere to the central 3 mm for anterior and posterior surfaces.

Since topography maps and ETMs are generated by REVO NX from exactly the same data set and are based on
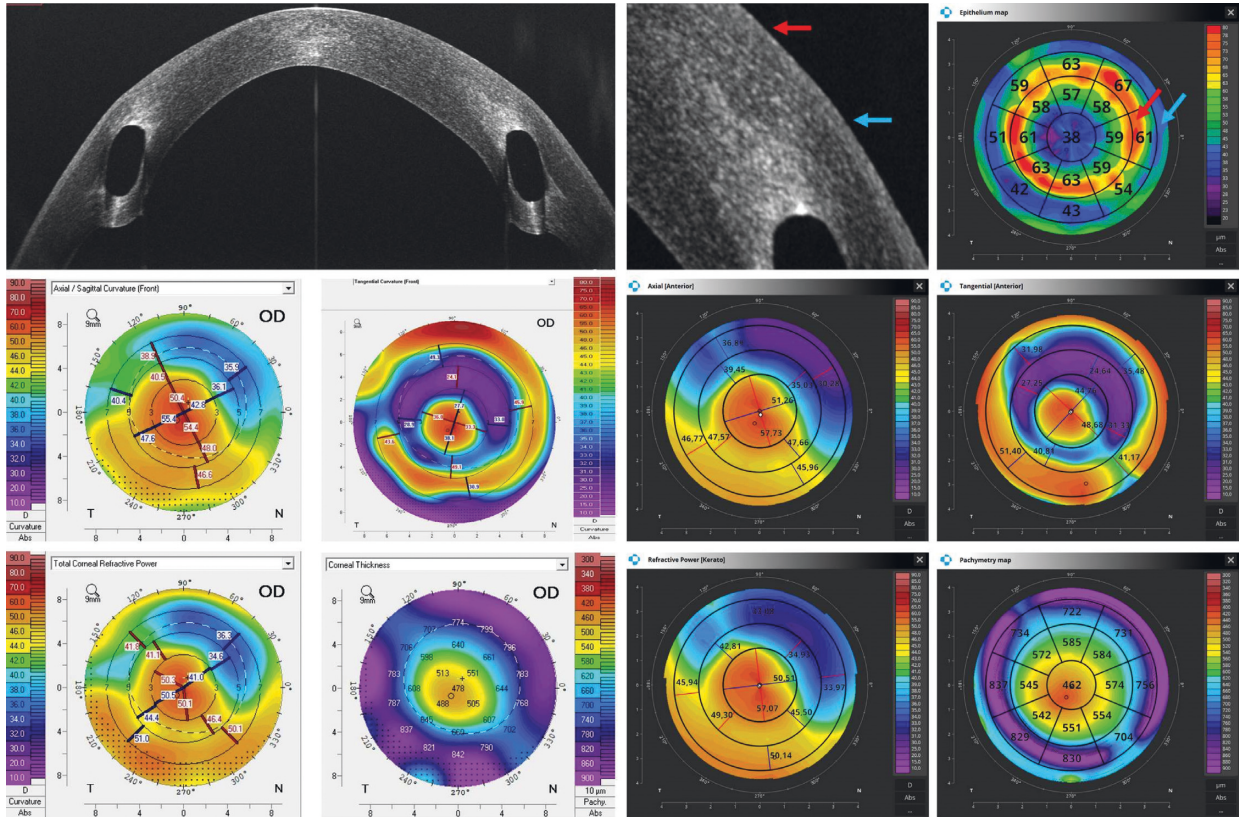
FIGURE 5: Cornea with an intracorneal ring segment. OCT reveals epithelial thinning immediately above the ring (blue arrow) with the thickness increasing toward the ring (red arrow). Topography maps reveal abnormalities in the anterior surface of the cornea. The measurements performed with Pentacam have a white background, and the ones performed with REVO NX have a black background. The K1, K2, and astigmatism values for the anterior surface of the cornea obtained using Pentacam are 48.9 D, 52.8 D, and 4.0 D, respectively, while the values obtained using REVO NX are 48.6 D, 52.4 D, and 3.8 D, respectively. The values of analogous parameters for the posterior corneal surface from Pentacam are −9.1 D, −9.5 D, and 0.3 D and the values from REVO NX are −9.1 D, −9.7 D, and 0.6 D.

the same 3D corneal model, the spatial correlation between them is complete, enabling a point-to-point comparison. As shown in the presented clinical examples (Figures 2–7), ETMs obtained in this way are perfectly complementary to topography maps. For example, in Figure 6, we can see a nonobvious correlation of an area of increased epithelial thickness with an island of decreased curvature of the posterior corneal surface. The topography maps obtained with REVO NX correspond well with the topography maps from Pentacam. When ETMs and topography maps are created from different OCT examinations, there is a risk of a nonideal fit and centration of the examinations as well as differences in the two 3D corneal models.

It should be mentioned that REVO NX also features the anterior radial scan functionality for more precise reproduction of the epithelial course on single B-scans. It includes a smaller number of tomograms, which are 7 mm wide (8 B-scans versus 16 B-scans) but their resolution is higher (2560 A-scans), and they are repeated 3 times. In this case, therefore, ETMs and topography maps are created from different data. With more A-scans and several repetitions of the scan at a single location (averaged B-scans), the visibility of the epithelium-Bowman membrane boundary is improved, making it easier to detect the corneal layers. The

downside of this scanning protocol is the longer measurement time and lower angular density of the scan, potentially reducing the sensitivity of ETMs in the visualization of small local changes within the epithelium. The protocol is similar to the one of the Avanti device.

The ICC index for ETMs obtained with REVO NX in this study, for both intraobserver repeatability and interobserver reproducibility, has lower values for the outer sectors. This may be connected with the decreasing precision of epithelial thickness measurements as one moves away from the center of the cornea due to a weaker signal at the periphery of the image. It is difficult to directly compare the obtained results with the results from other devices due to the different area of the sectors analyzed. In the case of the MS-39 device, the authors evaluated the repeatability of the central epithelial thickness reading over an area of 3.0 mm and the 4 paracentral measurements (nasal, temporal, superior, and inferior), with a diameter between 3.0 mm and 6.0 mm. However, for the central sector (which is larger than in REVO NX), they obtained an ICC value of 0.957 and CoV on the level of 1.87%. [6] The values are similar to the ones obtained in this study (ICC ≥ 0.95; CoV ≤ 1.55%). The ICC value for the other sectors was only slightly lower. However, the CoV was slightly higher than the one reported for the
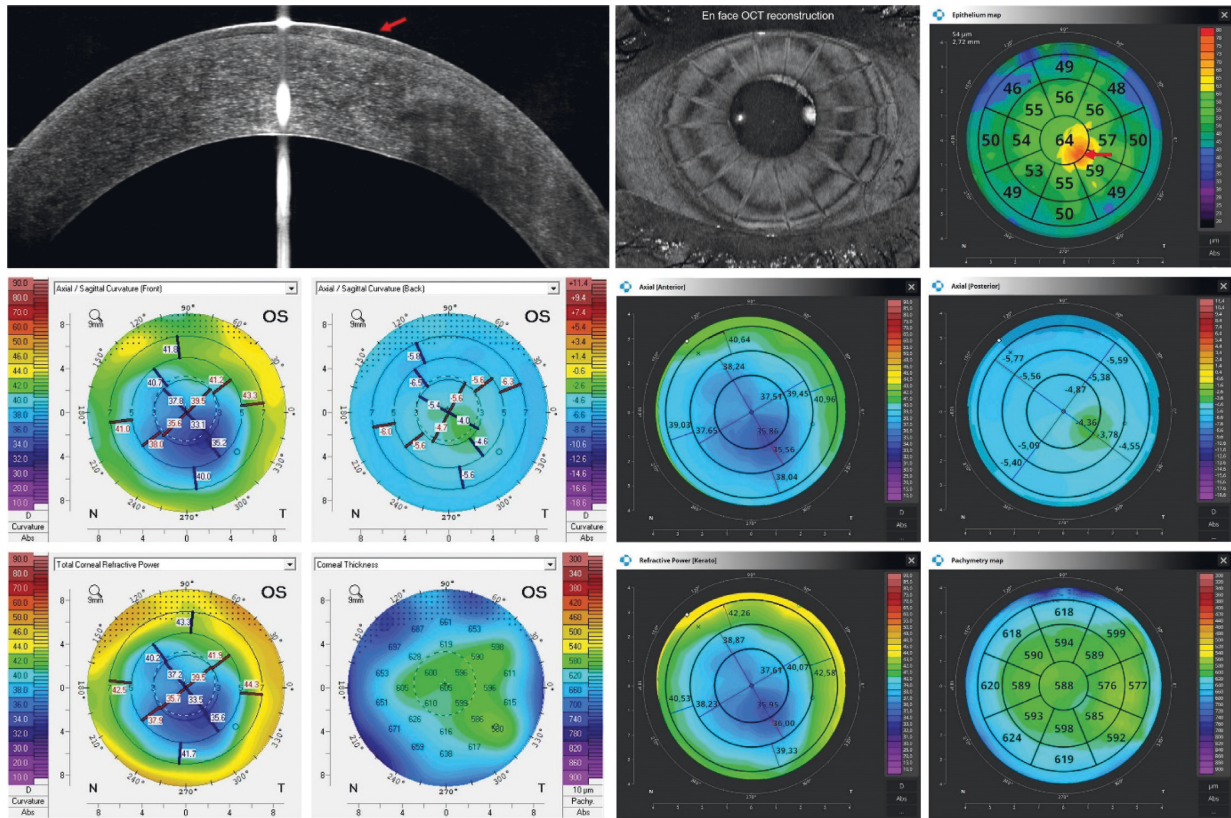
Figure 6: Postradial keratotomy eye. ETM shows a small paracentral island of increased epithelial thickness (red arrow). Topography maps show an area of reduced curvature of the posterior corneal surface at this location. Also, a flattening of the anterior surface of the cornea can be observed. The measurements performed with Pentacam have a white background, and the ones performed with REVO NX have a black background. The K1, K2, and astigmatism values for the anterior surface of the cornea obtained using Pentacam are 35.5 D, 37.5 D, and 1.9 D, respectively, while the values obtained using REVO NX are 35.6 D, 37.5 D, and 1.9 D, respectively. The values of analogous parameters for the posterior corneal surface from Pentacam are −4.5 D, −5.0 D, and 0.5 D and the values from the REVO NX are −4.2 D, −5.0 D, and 0.8 D.

RTVue device, for which a CoV in the central zone of 1.07% has been reported in unoperated eyes [4]. The repeatability of the REVO NX ETMs found in this study cannot be directly compared to the values reported in the literature by other authors using REVO NX because they made maps based on a 5-mm averaged radial scan without an anterior adapter [17]. Like in other studies, the superior quadrants were found to be the thinnest while the inferior was the thickest [18].

The study has some limitations. First of all, the repeatability and reproducibility were assessed on the basis of a relatively small group of subjects, which did not include patients with corneal pathologies. Also, the parameters were not tested using a higher resolution averaging scanning protocol. Further study should aim to better estimate the limits of the simultaneous corneal topography and ETM applicability in corneal diseases. It would also be particularly valuable to evaluate the exact sensitivity and specificity of the REVO NX ETMs for detecting corneal diseases and their comparison with ETMs obtained from OCT data from other OCT devices (e.g., Avanti). Future studies will need to include larger populations, with different ocular conditions.

In conclusion, the study demonstrated high precision (intraobserver repeatability and interobserver reproducibility) of the epithelial thickness measurement using REVO NX. However, increasing the distance from the corneal center is accompanied by a slight decrease in precision. The study also demonstrated excellent spatial correlation between ETMs and corneal topography exams performed simultaneously, which stems from the fact that both map types are created from the same OCT data, they are based on the same 3D model, and they are ideally centered in the same way. This way of analyzing the surface, curvature, and thickness of the cornea and its epithelium may become a routine procedure in the near future.

Post-op day 1
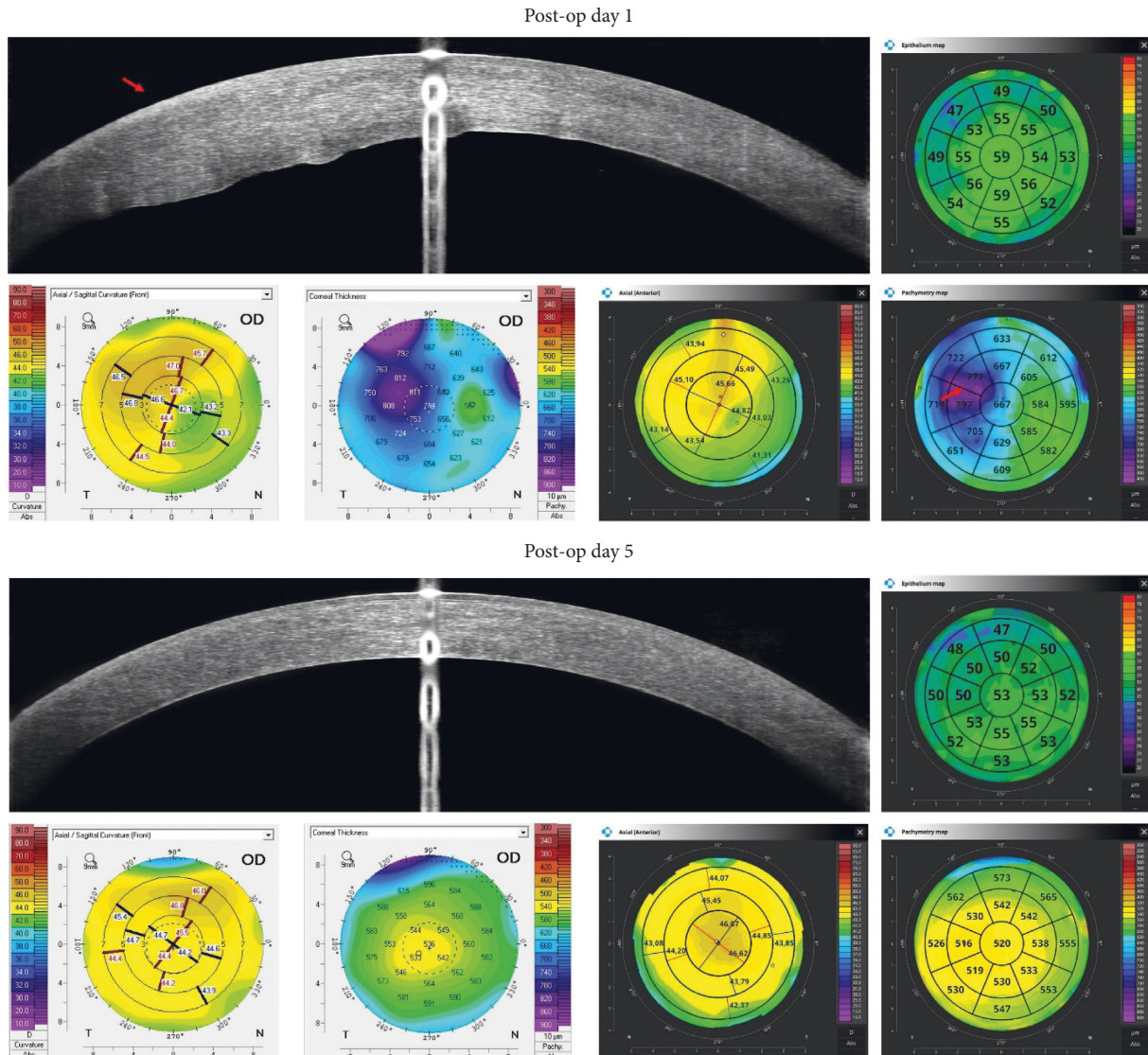
Post-op day 5

FIGURE 7: Condition after cataract surgery. On postop day 1, corneal oedema is visible on the pachymetry map (red arrow) and a disruption of the regularity of the anterior corneal surface can be observed on the result of corneal topography. On postop day 5, the oedema regressed. Despite a significant change in the corneal thickness and curvature between examinations, ETMs show a similar image. The measurements performed with Pentacam have a white background, and the ones performed with REVO NX have a black background.

Data Availability

The data are available on request.

Conflicts of Interest

The author declares that he has no conflicts of interest and no commercial relationship with Optopol Technology and Oculus. Dr. Sikorski has provided clinical consultation to Optopol Technology, free of charge.

References

[1] A. J. Kanellopoulos and G. Asimellis, "In vivo three-dimensional corneal epithelium imaging in normal eyes by anterior-segment optical coherence tomography," *Cornea*, vol. 32, no. 11, pp. 1493–1498, 2013.

[2] A. J. Kanellopoulos and G. Asimellis, "In vivo 3-dimensional corneal epithelial thickness mapping as an indicator of dry eye: preliminary clinical assessment," *American Journal of Ophthalmology*, vol. 157, no. 1, pp. 63–68, 2014.

[3] M. Tang, Y. Li, W. Chamberlain, D. J. Louie, J. M. Schallhorn, and D. Huang, "Differentiating keratoconus and corneal warpage by analyzing focal change patterns in corneal topography, pachymetry, and epithelial thickness maps," *Investigative Opthalmology & Visual Science*, vol. 57, no. 9, pp. 544–549, 2016.

[4] X. J. Ma, L. Wang, and D. D. Koch, "Repeatability of corneal epithelial thickness measurements using fourier-domain optical coherence tomography in normal and post-LASIK eyes," *Cornea*, vol. 32, no. 12, pp. 1544–1548, 2013.

[5] J. M. Schallhorn, M. Tang, Y. Li, D. J. Louie, W. Chamberlain, and D. Huang, "Distinguishing between contact lens warpage and ectasia: usefulness of optical coherence tomography

epithelial thickness mapping," *Journal of Cataract and Refractive Surgery*, vol. 43, no. 1, pp. 60–66, 2017.

[6] G. Savini, D. Schiano-Lomoriello, and K. J. Hoffer, "Repeatability of automatic measurements by a new anterior segment optical coherence tomographer combined with Placido topography and agreement with 2 Scheimpflug cameras," *Journal of Cataract and Refractive Surgery*, vol. 44, no. 4, pp. 471–478, 2018.

[7] A. Vega-Estrada, M. Mimouni, E. Espla, J. Alió del Barrio, and J. L. Alio, "Corneal epithelial thickness intrasubject repeatability and its relation with visual limitation in keratoconus," *American Journal of Ophthalmology*, vol. 200, pp. 255–262, 2019.

[8] A. Stojanovic, "The rise of epithelial thickness mapping. ETM is an essential tool for the diagnosis and management of keratoconus," *Ophthalmology Management*, vol. 25, 2021.

[9] B. L. Sikorski and P. Suchon, "OCT biometry (B-Oct): a new method for measuring ocular axial dimensions," *Journal of Ophthalmology*, vol. 2019, Article ID 9192456, 10 pages, 2019.

[10] J. M. Bland and D. G. Altman, "Statistics notes: measurement error," *BMJ*, vol. 313, no. 7059, p. 744, 1996.

[11] R. Müller and P. Büttner, "A critical discussion of intraclass correlation coefficients," *Statistics in Medicine*, vol. 13, no. 23-24, pp. 2465–2476, 1994.

[12] J. Martin Bland and D. Altman, "Statistical methods for assessing agreement between two methods of clinical measurement," *The Lancet*, vol. 327, no. 8476, pp. 307–310, 1986.

[13] E. Pavlatos, D. Huang, and Y. Li, "Eye motion correction algorithm for OCT-based corneal topography," *Biomedical Optics Express*, vol. 11, no. 12, pp. 7343–7356, 2020.

[14] E. Kowler, "Eye movements: the past 25 years," *Vision Research*, vol. 51, no. 13, pp. 1457–1483, 2011.

[15] J. Otero-Millan, X. G. Troncoso, S. L. Macknik, I. Serrano-Pedraza, and S. Martinez-Conde, "Saccades and microsaccades during visual fixation, exploration, and search: foundations for a common saccadic generator," *Journal of Vision*, vol. 8, pp. 21 1–21 18, 2008.

[16] M. Rolfs, "Microsaccades: small steps on a long way," *Vision Research*, vol. 49, no. 20, pp. 2415–2441, 2009.

[17] Y. Li, A. Gokul, C. McGhee, and M. Ziaei, "Repeatability of corneal and epithelial thickness measurements with anterior segment optical coherence tomography in keratoconus," *PLoS One*, vol. 16, no. 6, Article ID e0248350, 2021.

[18] N. Hashmani, S. Hashmani, and C. M. Saad, "Wide corneal epithelial mapping using an optical coherence tomography," *Investigative Opthalmology & Visual Science*, vol. 59, no. 3, pp. 1652–1658, 2018.

Review Article

Application of Intraoperative Optical Coherence Tomography Technology in Anterior Segment Surgery

Sang Beom Han [ID],[1] **Yu-Chi Liu,**[2,3,4] **Karim Mohamed-Noriega,**[5] **and Jodhbir S. Mehta** [ID][2,3,4]

[1]*Department of Ophthalmology, Kangwon National University School of Medicine, Kangwon National University Hospital, Chuncheon, Republic of Korea*
[2]*Singapore National Eye Centre, Singapore*
[3]*Singapore Eye Research Institute, Singapore*
[4]*Department of Ophthalmology, Yong Loo Lin School of Medicine, National University of Singapore, Singapore*
[5]*Department of Ophthalmology, University Hospital, Faculty of Medicine, Autonomous University of Nuevo Leon, Monterrey, Mexico*

Correspondence should be addressed to Jodhbir S. Mehta; jodmehta@gmail.com

The use of optical coherence tomography (OCT) technology in anterior segment diseases allows for precise assessment of the changes following anterior segment surgery. Advances in microscope-integrated OCT systems have allowed the utilization of intraoperative OCT (iOCT) in anterior segment surgeries, i.e., cornea, cataract, and refractive surgery. iOCT has enabled real-time precise visualization of anterior segment tissues as well as interactions between surgical instruments and ocular tissue; thus, the device can facilitate surgical procedures and provide valuable information for decision-making during anterior segment surgeries. In this review, the authors will introduce studies regarding the development of iOCT technology and its application in various anterior segment surgeries. Multiple studies have shown the efficacy of the iOCT for intraoperative assistance and guidance, suggesting the potential of the device for optimizing the surgical outcomes after cornea, cataract, and refractive surgery.

1. Introduction

To date, evaluation of ocular tissues and tissue-instrument interactions during anterior segment surgery has depended on directing visualization using an operating microscope. Although technological development enables coaxial operating microscopes to show high-resolution images, they cannot provide detailed three-dimensional (3D) visualization of the anterior segment structures. [1, 2] Hence, operating microscopes have limited ability to provide depth information for anterior segment tissues. [1–3] Although intraoperative slit beam examination can be helpful for depth evaluation, it does not have a high enough resolution for precise measurement of tissue depth. [1] In addition, tissues behind the cloudy media, such as opaque cornea, cannot be visualized using traditional operating microscopes, which may be problematic in cases with corneal edema or haze. [1–4].

The application of optical coherence tomography (OCT) technology, which can provide high-resolution cross-sectional images of anterior segment structures, has allowed precise assessment of anterior segment tissues; this may be advantageous for the diagnosis and treatment of various anterior segment diseases. [2, 3, 5] Introduction of the intraoperative OCT (iOCT) technology to anterior segment surgery is expected to allow real-time precise visualization of anterior segment tissues and tissue-instrument interactions, which may contribute to improved anatomical and visual outcomes. [2, 3, 5–7] In particular, iOCT can be advantageous in cases with corneal opacity in which structures underneath the cornea are difficult to visualize with an operating microscope. [2, 3, 5, 7] Detailed intraoperative visualizations of these tissues can be helpful for more precise surgical procedures and improved visual outcomes in various anterior segment surgeries, such as corneal surgeries

including penetrating keratoplasty (PK), deep anterior lamellar keratoplasty (DALK), Descemet stripping automated endothelial keratoplasty (DSAEK), and Descemet membrane endothelial keratoplasty (DMEK), cataract, and refractive surgery. [1–3, 5, 7].

In this review, we provide an overview of the advances in iOCT systems and the application of these devices in various anterior segment surgeries. The potential future developments and applications of iOCT are also discussed.

2. Development of Intraoperative OCT Technology

Several developments have been made to overcome the barriers to the intraoperative use of OCT. [2, 7, 8] First, conventional OCT modalities are stationary table top systems and lack portability; thus, integration into the ophthalmic surgical microscope is difficult. [2]To address this problem, intraoperative imaging using lightweight handheld OCT was first introduced. [9] However, handheld OCT can never provide "real-time" intraoperative imaging because surgeons must cease surgical procedures when obtaining OCT images or request an assistant to take the images. [7, 9] Limited stability of the handheld device and involuntary hand movement can be associated with difficulty in image acquisition and decreased image quality. [2] Introduction of a nonsterile handheld device to a sterile surgical field can also increase the risk of infection. [2, 5].

To address this problem, researchers introduced a method of mounting a lightweight handheld OCT probe to the operating microscope, which can enable improved stability, higher image quality, faster image acquisition, and enhanced sterility. [10, 11] However, the mounted OCT system needs extra space for the machine in the operating room and an additional foot switch to control the OCT probe. [2, 5] Moreover, in the microscope-mounted OCT system, surgeons still need to discontinue the procedures before image capture.10. To allow "real-time" intraoperative image acquisition without surgical delay, microscope-integrated OCT (MIOCT), in which OCT probes are integrated into the microscopic optics, have been developed (Figure 1). [1, 2] In MIOCT systems, surgeons can control the pattern of OCT image scan, such as the region of interest, orientation, and size, with a microscope foot-pedal in which the OCT system is also integrated. [12, 13].

To date, three systems of MIOCT are commercially available: Rescan® 700 (Cirrus OCT system built on Lumera 700 microscope; Carl Zeiss Meditec, Oberkochen, Germany), [12, 14] OPMedT® (OPMedT OCT system, Haag-Streit Hi-R 1000G-microscope, Haag-Streit Surgical GmbH, Wedel, Germany) [15], and EnFocus® (Bioptigen, Leica, Wetzlar, Germany). [1, 2].

3. Application of Intraoperative OCT in Anterior Segment Surgery

Several studies have shown the efficacy of iOCT in various anterior segment surgeries [1, 2, 5, 7, 8, 10, 13–37]. Researchers indicated that information obtained using iOCT

FIGURE 1: Display of an image of the intraoperative optical coherence tomography (iOCT) integrated into the microscope during the cataract surgery.

was helpful for intraoperative decision-making and selection of surgical procedures [1, 14, 15, 19, 38].

In a large prospective study including 275 eyes, Ehlers et al. [10] revealed that a portable OCT system mounted on a microscope can be helpful for visualization of anterior segment structures during anterior segment surgery, particularly in lamellar keratoplasty procedures [10]. In a subsequent study, they demonstrated that the MIOCT enabled real-time visualization of anterior segment tissues and tissue-instrument interaction [12, 14].

3.1. iOCT in Corneal Transplantation. In PK, iOCT can enable the visualization of structures beneath the hazy and irregular cornea that are difficult to identify with an operating microscope [7]. During PK, iOCT can allow real-time display of the host-graft interface, which can be helpful for appropriate apposition at the interface.8. Eguchi et al. [39] showed that iOCT can be useful for the detection of iridocorneal adhesion and iris incarceration that can occur during PK [39]. iOCT can also provide information regarding the location of the suture needle penetrating the corneal layers, which can lead to a secure suture by adjusting the needle depth [7].

In DALK, iOCT can display all surgical steps and facilitate intraoperative decision-making [10, 12, 14, 20, 35, 40]. During the DALK procedure, iOCT can provide real-time cross-sectional visualization of deep needle injection, intrastromal bubbles, deep dissection plane, residual stromal bed, Descemet's membrane (DM), and interface fluid (Figure 2) [7, 10, 12, 14, 17, 20, 26, 35, 40]. Scorcia et al. [31] demonstrated that the iOCT enabled detailed evaluation of the dissection depth of the corneal stroma, which may improve the success rate for big-bubble formation in DALK [31]. In cases in which big bubble was difficult to attain, e.g., cases with corneal scars involving DM, iOCT enables precise assessment of the depth and uniformity of the stromal dissection plane, which is critical for the achievement of a residual bed with appropriate thickness and smooth surface. [1] In DALK cases, in which viscodissection is performed for stromal dissection, iOCT may be particularly helpful as it can visualize the tissues underneath the cloudy cornea caused by viscoelastic bubbles [20]. De Benitos et al. [20] also showed

(a)

(b)

(c)
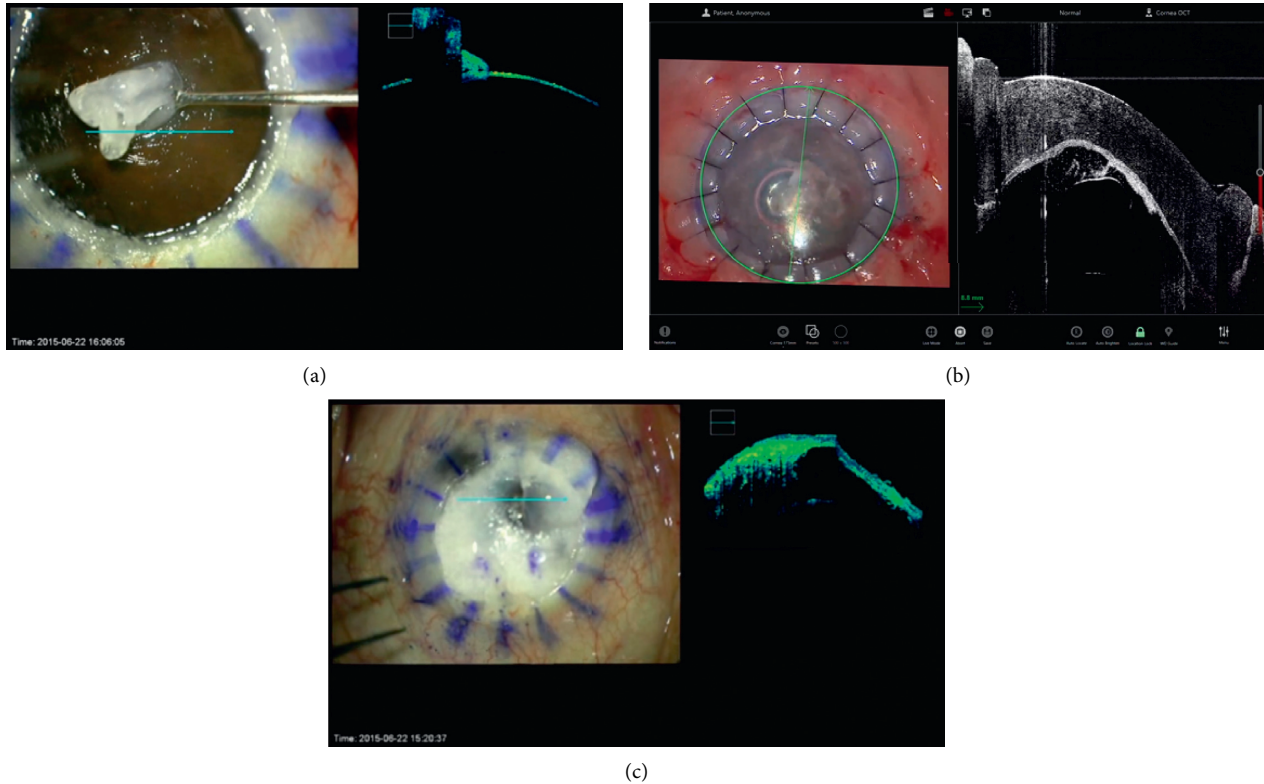
FIGURE 2: Application of the iOCT in DALK surgery. (a) Visualization of the residual stromal bed. (b) Confirmation of the attachment between the graft cornea and recipient bed (c) visualization of the tissue underneath the cloudy cornea using the iOCT during the viscodissection.

that iOCT enabled the achievement of big-bubble and completely detached DM in a case with irregular corneal thinning and scarring (Figure 2(c)). [20] They also reported that iOCT enabled visualization of intrastromal fluid retention that was invisible with the operating microscope in a case with diffuse corneal scarring due to chemical injury [20]. Eguchi et al. [39] demonstrated that iOCT can also detect iris protrusion caused by misdirected air into the posterior chamber at the end of DALK that can lead to acute intraocular pressure elevation due to angle closure [39].

In DSAEK and DMEK, iOCT can provide critical information from intraoperative decision-making in all surgical steps [7, 12, 14, 19, 29, 41, 42], which may lead to enhanced anatomical and visual outcomes. [10, 12–15, 19, 38] In both DSAEK and DMEK, iOCT can visualize donor-recipient attachment and residual interface fluid, which may help achieve tight apposition and prevent graft dislocation (Figure 3) [1, 7, 10, 14]. Shazly et al. [32] reported that iOCT may be advantageous for confirming the attachment of the endothelial graft to the host cornea, particularly in cases with severe corneal opacity. Studies have revealed discordance between surgeon's impressions using the operating microscope and information obtained using iOCT in 18–50% of cases, suggesting a potentially critical role of iOCT in endothelial keratoplasty procedures [10, 14]. A prospective study revealed that information provided by iOCT regarding graft malposition or presence of interface fluid led to the modification of intraoperative decision-

making or additional surgical maneuvers, such as corneal sweeping, anterior chamber re-bubbling, graft reposition, or additional peeling of residual host DM in 43% of DSAEK or DMEK cases [14].

Juthani et al. [43] demonstrated that transient residual interface fluid quantified using iOCT during DSAEK had correlation with textural interface opacity postoperatively [43]. Moreover, the amount of residual interface fluid measured using iOCT was associated with an increased rate of early graft nonadherence, indicating the potentially critical role of iOCT for immediate detection and removal of interface fluid [44, 45]. iOCT can also be helpful for confirmation of central placement of endothelial grafts and detection of abnormal tissue particles between the graft and host cornea, which may result in an increased success rate and decreased rejection risk [1, 7]. iOCT can be advantageous in cases with abnormal anterior segment structures after multiple ocular surgeries, such as corneal irregularity and opacity, peripheral anterior synechiae, and vitreous incarceration, particularly for determining the relationship between the endothelial graft and the iris or vitreous [7].

In DMEK, iOCT can be a valuable tool for verification of graft orientation, particularly in cases with severe corneal edema or haze [5, 7, 14, 15, 19, 38]. Based on the scrolling configuration of the endothelial graft visualized using iOCT, the DMEK orientation can be easily confirmed prior to the identification of the orienting marker (Figure 3(d) [14, 15, 19, 38, 41, 46]. Thus, with the use of iOCT, the

(a)

(b)

(c)

(d)
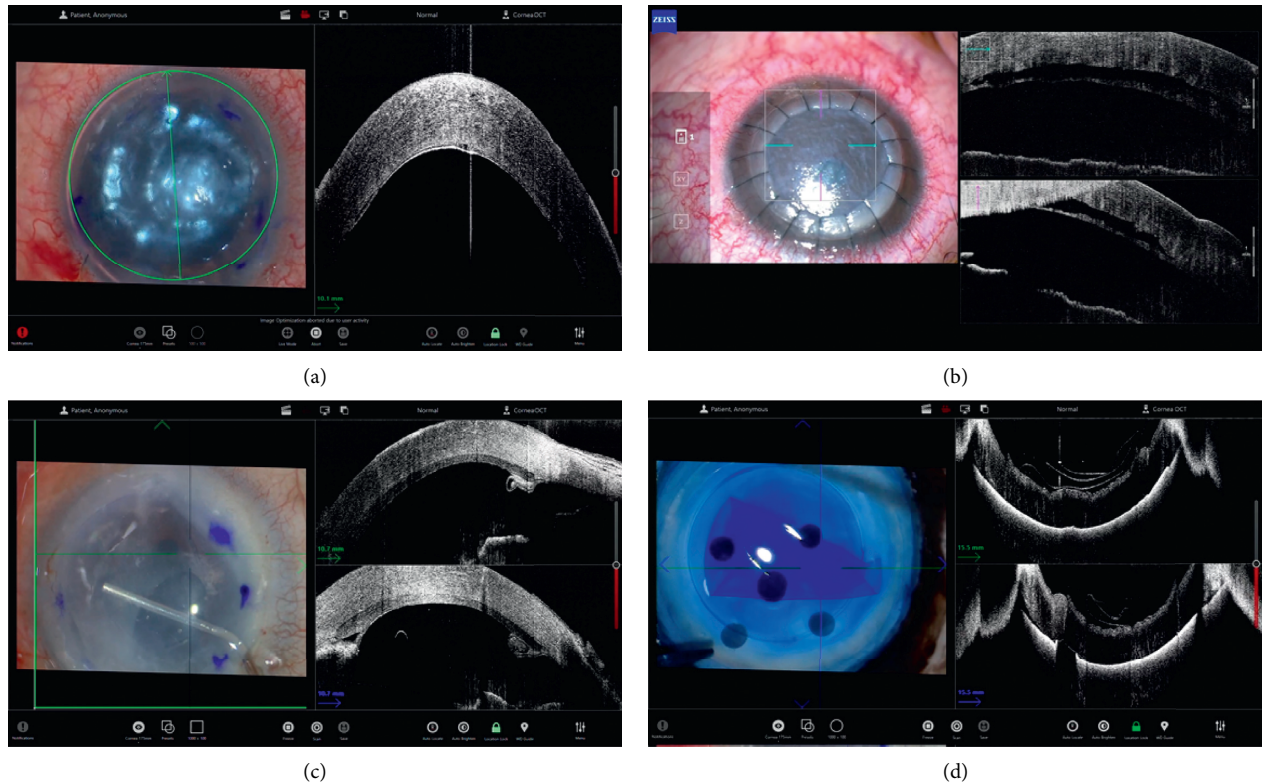
FIGURE 3: Application of the iOCT in DSAEK and DMEK surgery. (a) Confirmation of the attachment of the endothelial graft during DMEK. (b) Visualization of the detached endothelial graft cornea in DMEK. (c) Visualization of the peripheral anterior synechiae during DSAEK. (d) Visualization of the donor fold before donor graft insertion in DMEK.

marking of the donor tissue may become unnecessary, which can be beneficial for the preservation of donor corneal endothelial cells [1, 14, 15, 19, 38, 41]. iOCT can also help shorten the learning curve for DMEK [12].

3.2. Corneal Trauma and Other Corneal Surgeries. iOCT can be helpful in emergency surgery for corneal trauma. In cases of corneal laceration, iOCT can facilitate secure corneal sutures by demonstrating the needle depth during suture procedures [7]. The modality can also be useful for assessment of the depth of the foreign body in the cornea, which can facilitate effective removal of the foreign body and reduce the risk of complications, such as damage to the surrounding corneal tissue or displacement of the foreign body to the anterior chamber [7]. The depth of corneal opacity can be precisely estimated using iOCT during emergency operations in cases of chemical or thermal burns.[7].

iOCT can help visualize the cleavage plane between the nodule and underlying corneal tissue in image-guided lamellar keratectomy for the surgical treatment of the Salzmann nodular degeneration [14]. In the Bowman layer transplantation, a new procedure for the treatment of advanced keratoconus, iOCT might enable the visualization of the dissection plane in spite of the air-endothelial reflex being obscured [47]. Siebelmann et al. [48] reported that iOCT enabled assessment of corneal opacity and surface

smoothness through real-time imaging during phototherapeutic keratectomy [48].

Intracorneal pathology can also be precisely isolated and located for biopsy using iOCT [49]. Ruland et al. [50] showed that iOCT was helpful for the identification and excision of retrocorneal fibrous membranes following PK. In cases of acute corneal hydrops in keratoconus, iOCT facilitated the micropuncture of intrastromal fluid pockets combined with compression sutures and gas tamponade, which resulted in immediate reattachment of DM [33]. During insertion of Intacs® for keratoconus, iOCT can be used for assessment of the depth of the corneal incision and visualization of the corneal channel for the implant [14]. In the corneal cross-linking for keratoconus, iOCT can be used for the measurement of changes in corneal pachymetry [23, 28].

4. Refractive Surgery

In small-incision lenticule extraction (SMILE), iOCT can allow real-time visualization of the desired dissection plane [51]. It can also enable intraoperative identification of the intrastromal lenticule and the distinguishment of the lenticule from the overlying stromal cap and underlying stromal bed, resulting in complete isolation of the lenticule [37]. This can be particularly advantageous in difficult cases, for example, cases with an edematous overlying cap [51]. Intraoperative complications, such as incomplete lenticule

separation, cap-lenticule adhesion, lenticule remnants, and creation of false planes, can be easily detected using iOCT, which can lead to immediate corrective procedures and enhanced surgical outcomes [37, 51].

During the implantation of an implantable collamer lens (ICL), iOCT can be used for the visualization and assessment of the vault of the ICL. [1] Titiyal et al. [36] reported that intraoperative vaulting measured with iOCT had a close correlation with postoperative vaulting and can be helpful for the detection of extreme vaulting. [36] It enhances the safety of the surgical procedure by providing a real-time display of intraoperative manipulations. [36].

5. Cataract Surgery

Corneal incisions for cataract surgery can be visualized with iOCT. [12] As iOCT can easily identify the location of implants, it can be helpful for verification of correct placement of the intraocular lens (IOL). [10, 14] Nagpal et al. [52] recently revealed that the gap between the IOL and the posterior capsule can be successfully measured using iOCT, which may be helpful for evaluation of the dynamics for the space between the IOL and the posterior capsule.

The device can also provide information regarding calculations of optimal IOL. [12] Hirnschall et al. [53] reported that iOCT enabled more accurate measurement of anterior chamber depth and determination of postoperative lens position, which resulted in better refractive outcomes. In patients with a previous radial keratotomy scar, application of the iOCT during cataract surgery may be helpful for monitoring of the stability of the radial scar and early detection of the dehiscence of the scar, which requires immediate sutures [54, 55].

In cases of posterior polar cataracts, iOCT can be a valuable tool to improve the safety of the surgery by detecting pre-existing posterior capsular dehiscence during cataract surgery and preventing lens drop [56]. In pediatric patients with posterior lens opacities, iOCT can allow the categorization of the morphology of the posterior capsule and the posterior lens cortex, as well as the determination of the integrity of the posterior capsule, which can provide guidance for surgical strategy and increase the safety of the surgery [57]. Similarly, iOCT can be useful for categorization of the white cataract into four types and predicting the intraoperative dynamics according to the type, which can provide valuable information for the selection of surgical strategies for safe surgery, particularly in cases of uneventful completion of capsulorhexis [58].

During IOL scleral fixation, iOCT can enable visualization of the scleral flap preparation and assessment of the preparation depth, which results in enhanced stability of the fixated IOL [25]. iOCT can also be helpful in the adjustment of the IOL tilt during the IOL scleral fixation [22]. Using RESCAN 700, Fukumoto et al. [22] demonstrated that the use of iOCT was associated with the significantly reduced angle of the IOL tilt, which might result in decreased lenticular astigmatism and improved visual outcome. [22].

With the development of robotic surgery for cataracts, iOCT integrated with an intraocular robotic surgical system can help improve the safety and efficacy of automated robotic cataract surgery. [18, 59] The images obtained with iOCT can enable real-time intraoperative monitoring and intervention of robotic surgery by ophthalmic surgeons. [18] With further technological development, iOCT integrated with the robotic surgical system is expected to contribute to the enhanced precision and safety of fully automated robotic cataract surgery. [59].

6. Future Developments

Although iOCT must be beneficial for the success of various anterior segment surgeries, the cost has been the biggest hurdle for its widespread use. [1] In addition, all three commercially available iOCT devices are integrated into the operating microscope produced by the same manufacturer. Thus, an additional cost is incurred for the utilization of the devices in the operating room. [1] With the rapid increase in the intraoperative application of iOCT, we expect that technological development and mass production may lower the cost of the device.

During the use of iOCT, light scattering and shadowing caused by metallic surgical instruments can seriously limit visualization of the interaction between ocular tissues and instruments and a detailed view of tissues under the instruments. [2, 12, 60] Thus, the development of novel materials for minimizing the impact of instruments is necessary. [61] Compensation of the disturbing effect of the surgical instruments using software methods, such as image processing or adjustment using artificial intelligence, can be an alternative. [6].

The development of a software platform that enables automated tracking of the region of interest and automated analysis of the captured image is also necessary. [2] Automated tracking can allow surgeons to concentrate on the surgical procedures without the burden of manual aiming for the region of interest. [62] Protocols for automated analysis of captured images may enable precise assessment of the changes in the ocular tissues associated with surgical procedures. [45] For instance, an automated protocol for segmentation and quantification of interface fluid during DSAEK can be used for the prediction of anatomical and visual outcomes. [45].

With advances in technology of corneal tomography, new iOCT systems that can provide more precise images with minimal delays are being developed. Instead of the currently used spectral-domain OCT system, swept-source OCT is expected to provide more detailed images of ocular tissues during surgery with enhanced acquisition speed. [2] In addition, the application of ultrahigh resolution OCT can enable visualization of anterior segment structures at a microscopic level, which may result in more precise surgical procedures and enhanced surgical outcomes. [63].

7. Conclusion

The development of iOCT technology may allow real-time precise visualization of ocular tissues and tissue-instrument interactions during anterior segment surgery, which can

contribute to improved visual and anatomical outcomes. [2, 8] The device can be significantly advantageous in cases with corneal opacity, particularly during lamellar keratoplasties, such as DALK, DSAEK, and DMEK. [8] Application of the iOCT in cataract and refractive surgery can also enable precise measurement of the ocular parameters, which may lead to optimal visual outcomes. With further developments, iOCT systems may be essential for optimizing surgical outcomes by facilitating surgical procedures and intraoperative decision-making in corneal, cataract, and refractive surgery. [2].

Data Availability

The data supporting this systemic review are from previously reported studies and datasets, which have been cited in this article.

Conflicts of Interest

The authors declare that they have no conflicts of interest.

Acknowledgments

References

[1] F. W. Price Jr., "Intraoperative optical coherence tomography: game-changing technology," *Cornea*, vol. 40, no. 6, pp. 675–678, 2021.

[2] J. P. Ehlers, "Intraoperative optical coherence tomography: past, present, and future," *Eye*, vol. 30, no. 2, pp. 193–201, 2016.

[3] S. B. Han, J. S. Mehta, Y. C. Liu, and K. Mohamed-Noriega, "Advances and clinical applications of anterior segment imaging techniques," *Journal of ophthalmology*, vol. 2016, Article ID 8529406, 2 pages, 2016.

[4] A. Meduri, L. Bergandi, P. Perroni, F. Silvagno, and P. Aragona, "Oral l-cysteine supplementation enhances the long term-effect of topical basic fibroblast growth factor (bFGF) in reducing the corneal haze after photorefractive keratectomy in myopic patients," *Pharmaceuticals*, vol. 13, no. 4, 2020.

[5] M. B. Muijzer, P. Schellekens, H. J. M. Beckers, J. H. de Boer, S. M. Imhof, and R. P. Wisse, "Clinical applications for intraoperative optical coherence tomography: a systematic review," *Eye*, vol. 36, no. 2, pp. 379–391, 2022.

[6] J. P. Ehlers, Y. K. Tao, S. Farsiu, R. Maldonado, J. A. Izatt, and C. A. Toth, "Visualization of real-time intraoperative maneuvers with a microscope-mounted spectral domain optical coherence tomography system," *Retina*, vol. 33, no. 1, pp. 232–236, 2013.

[7] H. Eguchi, F. Hotta, S. Kusaka, and Y. Shimomura, "Intraoperative optical coherence tomography imaging in corneal surgery: a literature review and proposal of novel applications," *Journal of ophthalmology*, vol. 2020, p. 1497089, 2020.

[8] J. S. Titiyal, M. Kaur, S. Nair, and N. Sharma, "Intraoperative optical coherence tomography in anterior segment surgery," *Survey of Ophthalmology*, vol. 66, no. 2, pp. 308–326, 2021.

[9] P. B. Knecht, C. Kaufmann, M. N. Menke, S. L. Watson, and M. M. Bosch, "Use of intraoperative fourier-domain anterior segment optical coherence tomography during descemet stripping endothelial keratoplasty," *American Journal of Ophthalmology*, vol. 150, no. 3, pp. 360–365, 2010.

[10] J. P. Ehlers, W. J. Dupps, P. K. Kaiser et al., "The prospective intraoperative and perioperative ophthalmic ImagiNg with optical CoherEncE TomogRaphy (PIONEER) study: 2-year results," *American Journal of Ophthalmology*, vol. 158, no. 5, pp. 999–1007, 2014.

[11] R. Ray, D. E. Barañano, J. A. Fortun et al., "Intraoperative microscope-mounted spectral domain optical coherence tomography for evaluation of retinal anatomy during macular surgery," *Ophthalmology*, vol. 118, no. 11, pp. 2212–2217, 2011.

[12] J. P. Ehlers, J. Goshe, W. J. Dupps et al., "Determination of feasibility and utility of microscope-integrated optical coherence tomography during ophthalmic surgery," *JAMA Ophthalmology*, vol. 133, no. 10, pp. 1124–1132, 2015.

[13] J. P. Ehlers, P. K. Kaiser, and S. K. Srivastava, "Intraoperative optical coherence tomography using the RESCAN 700: preliminary results from the DISCOVER study," *British Journal of Ophthalmology*, vol. 98, no. 10, pp. 1329–1332, 2014.

[14] J. P. Ehlers, Y. S. Modi, P. E. Pecen et al., "The DISCOVER study 3-year results," *Ophthalmology*, vol. 125, no. 7, pp. 1014–1027, 2018.

[15] P. Steven, C. Le Blanc, K. Velten et al., "Optimizing descemet membrane endothelial keratoplasty using intraoperative optical coherence tomography," *JAMA Ophthalmology*, vol. 131, no. 9, pp. 1135–1142, 2013.

[16] M. I. Asif, R. K. Bafna, N. Sharma et al., "Microscope integrated optical coherence tomography guided descemet stripping automated endothelial keratoplasty in congenital hereditary endothelial dystrophy," *Clinical Ophthalmology*, vol. 15, pp. 3173–3181, 2021.

[17] J. Au, J. Goshe, W. J. Dupps Jr., S. K. Srivastava, and J. P. Ehlers, "Intraoperative optical coherence tomography for enhanced depth visualization in deep anterior lamellar keratoplasty from the PIONEER study," *Cornea*, vol. 34, no. 9, pp. 1039–1043, 2015.

[18] C. W. Chen, Y. H. Lee, M. J. Gerber et al., "Intraocular robotic interventional surgical system (IRISS): semi-automated OCT-guided cataract removal," *The international journal of medical robotics + computer assisted surgery : MRCAS*, vol. 14, no. 6, Article ID e1949, 2018.

[19] B. Cost, J. M. Goshe, S. Srivastava, and J. P. Ehlers, "Intraoperative optical coherence tomography-assisted descemet membrane endothelial keratoplasty in the DISCOVER study," *American Journal of Ophthalmology*, vol. 160, no. 3, pp. 430–437, 2015.

[20] L. De Benito-Llopis, J. S. Mehta, R. I. Angunawela, M. Ang, and D. T. H. Tan, "Intraoperative anterior segment optical coherence tomography: a novel assessment tool during deep anterior lamellar keratoplasty," *American Journal of Ophthalmology*, vol. 157, no. 2, pp. 334–341, 2014.

[21] W. Fang, Q. Li, J. Fan et al., "Microscope-integrated intraoperative optical coherence tomography for anterior segment surgical maneuvers," *Translational Vision Science & Technology*, vol. 9, no. 7, p. 18, 2020.

[22] R. Fukumoto, M. Inoue, T. Ishida, T. Koto, and A. Hirakata, "Adjustment of intraocular lens tilt during intrascleral

fixation assisted by intraoperative OCT," *Journal of Cataract and Refractive Surgery*, vol. 47, no. 10, pp. 1308–1313, 2021.

[23] R. Ghaffari, M. Mortazavi, P. Anvari et al., "Intraoperative optical coherence tomography to evaluate the effect of the eyelid speculum on corneal pachymetry during accelerated corneal cross-linking (9 mW/cm2)," *Eye*, vol. 32, no. 3, pp. 579–585, 2018.

[24] L. Juergens, S. Michiels, M. Borrelli et al., "Intraoperative OCT—real-world user evaluation in routine surgery," *Klinische Monatsblatter fur Augenheilkunde*, vol. 238, no. 6, pp. 693–699, 2021.

[25] S. J. Lang, S. Heinzelmann, D. Böhringer, T. Reinhard, and P. Maier, "Indications for intraoperative anterior segment optical coherence tomography in corneal surgery," *International Ophthalmology*, vol. 40, no. 10, pp. 2617–2625, 2020.

[26] Y.-C. Liu, V. V. Wittwer, N. Z. B. M. Yusoff et al., "Intraoperative optical coherence tomography-guided femtosecond laser-assisted deep anterior lamellar keratoplasty," *Cornea*, vol. 38, no. 5, pp. 648–653, 2019.

[27] L. M. Lytvynchuk, C. G. Glittenberg, C. I. Falkner-Radler et al., "Evaluation of intraocular lens position during phacoemulsification using intraoperative spectral-domain optical coherence tomography," *Journal of Cataract and Refractive Surgery*, vol. 42, no. 5, pp. 694–702, 2016.

[28] C. Mazzotta and S. Caragiuli, "Intraoperative corneal thickness measurement by optical coherence tomography in keratoconic patients undergoing corneal collagen cross-linking," *American Journal of Ophthalmology*, vol. 157, no. 6, pp. 1156–1162, 2014.

[29] M. B. Muijzer, N. Soeters, D. A. Godefrooij, C. M. van Luijk, and R. P. L. Wisse, "Intraoperative optical coherence tomography-assisted descemet membrane endothelial keratoplasty: toward more efficient, safer surgery," *Cornea*, vol. 39, no. 6, pp. 674–679, 2020.

[30] S. Nair, M. Kaur, and J. S. Titiyal, "Intraoperative optical coherence tomography guided imaging of incision-site descemet membrane dynamics during phacoemulsification," *JAMA Ophthalmology*, vol. 139, no. 8, pp. 917-918, 2021.

[31] V. Scorcia, M. Busin, A. Lucisano, J. Beltz, A. Carta, and G. Scorcia, "Anterior segment optical coherence tomography-guided big-bubble technique," *Ophthalmology*, vol. 120, no. 3, pp. 471–476, 2013.

[32] T. A. Shazly, L. K. To, I. P. Conner, and L. Espandar, "Intraoperative optical coherence tomography-assisted descemet stripping automated endothelial keratoplasty for anterior chamber fibrous ingrowth," *Cornea*, vol. 36, no. 6, pp. 757-758, 2017.

[33] S. Siebelmann, A. Händel, M. Matthaei, B. Bachmann, and C. Cursiefen, "Microscope-integrated optical coherence tomography-guided drainage of acute corneal hydrops in keratoconus combined with suturing and gas-aided reattachment of descemet membrane," *Cornea*, vol. 38, no. 8, pp. 1058–1061, 2019.

[34] S. Siebelmann, M. Matthaei, L. M. Heindl, B. O. Bachmann, and C. Cursiefen, "Intraoperative optical coherence tomography (MI-OCT) for the treatment of corneal dystrophies," *Klin Monbl Augenheilkd*, vol. 235, no. 6, pp. 714–720, 2018.

[35] P. Steven, C. Le Blanc, E. Lankenau et al., "Optimising deep anterior lamellar keratoplasty (DALK) using intraoperative online optical coherence tomography (iOCT)," *British Journal of Ophthalmology*, vol. 98, no. 7, pp. 900–904, 2014.

[36] J. S. Titiyal, M. Kaur, S. Sahu, N. Sharma, and R. Sinha, "Real-time assessment of intraoperative vaulting in implantable collamer lens and correlation with postoperative vaulting," *European Journal of Ophthalmology*, vol. 27, no. 1, pp. 21–25, 2017.

[37] J. Urkude, J. S. Titiyal, and N. Sharma, "Intraoperative optical coherence tomography-guided management of cap-lenticule adhesion during SMILE," *Journal of Refractive Surgery*, vol. 33, no. 11, pp. 783–786, 2017.

[38] A. Saad, E. Guilbert, A. Grise-Dulac, P. Sabatier, and D. Gatinel, "Intraoperative OCT-assisted DMEK," *Cornea*, vol. 34, no. 7, pp. 802–807, 2015.

[39] H. Eguchi, S. Kusaka, E. Arimura-Koike et al., "Intraoperative optical coherence tomography (RESCAN 700) for detecting iris incarceration and iridocorneal adhesion during keratoplasty," *International Ophthalmology*, vol. 37, no. 3, pp. 761–765, 2017.

[40] S. Siebelmann, P. Steven, and C. Cursiefen, "[Intraoperative optical coherence tomography in deep anterior lamellar keratoplasty]," *Klin Monbl Augenheilkd*, vol. 233, no. 6, pp. 717–721, 2016.

[41] A. S. Patel, J. M. Goshe, S. K. Srivastava, and J. P. Ehlers, "Intraoperative optical coherence tomography-assisted descemet membrane endothelial keratoplasty in the DISCOVER study: first 100 cases," *American Journal of Ophthalmology*, vol. 210, pp. 167–173, 2020.

[42] A. Kobayashi, H. Yokogawa, N. Mori, and K. Sugiyama, "Visualization of precut DSAEK and pre-stripped DMEK donor corneas by intraoperative optical coherence tomography using the RESCAN 700," *BMC Ophthalmology*, vol. 16, no. 1, p. 135, 2016.

[43] V. V. Juthani, J. M. Goshe, S. K. Srivastava, and J. P. Ehlers, "Association between transient interface fluid on intraoperative OCT and textural interface opacity after DSAEK surgery in the PIONEER study," *Cornea*, vol. 33, no. 9, pp. 887–892, 2014.

[44] K. M. Hallahan, B. Cost, J. M. Goshe, W. J. Dupps, S. K. Srivastava, and J. P. Ehlers, "Intraoperative interface fluid dynamics and clinical outcomes for intraoperative optical coherence tomography-assisted descemet stripping automated endothelial keratoplasty from the PIONEER study," *American Journal of Ophthalmology*, vol. 173, pp. 16–22, 2017.

[45] D. Xu, W. J. Dupps Jr., S. K. Srivastava, and J. P. Ehlers, "Automated volumetric analysis of interface fluid in descemet stripping automated endothelial keratoplasty using intraoperative optical coherence tomography," *Investigative Opthalmology & Visual Science*, vol. 55, no. 9, pp. 5610–5615, 2014.

[46] Y. Dai, L. Luo, and Y. Liu, "Intraoperative optical coherence tomography guided imaging of incision-site descemet membrane dynamics during phacoemulsification-reply," *JAMA Ophthalmology*, vol. 139, no. 8, p. 918, 2021.

[47] C. M. Tong, J. S. Parker, P. W. Dockery, R. S. Birbal, and G. R. J. Melles, "Use of intraoperative anterior segment optical coherence tomography for bowman layer transplantation," *Acta Ophthalmologica*, vol. 97, no. 7, 2019.

[48] S. Siebelmann, J. Horstmann, P. Scholz et al., "Intraoperative changes in corneal structure during excimer laser phototherapeutic keratectomy (PTK) assessed by intraoperative optical coherence tomography," *Graefe's Archive for Clinical and Experimental Ophthalmology*, vol. 256, no. 3, pp. 575–581, 2018.

[49] E. M. Schmidt, H. C. Stiefel, D. C. Houghton, and W. D. Chamberlain, "Intraoperative optical coherence tomography to guide corneal biopsy: a case report," *Cornea*, vol. 38, no. 5, pp. 639–641, 2019.

[50] K. Ruland, T. W. Bouldin, R. M. Davis, and D. Fleischman, "Intraoperative optical coherence tomography-assisted retrocorneal fibrous membrane biopsy and excision," *American Journal of Ophthalmology Case Reports*, vol. 11, pp. 101–104, 2018.

[51] N. Sharma, J. Urkude, M. Chaniyara, and J. S. Titiyal, "Microscope-integrated intraoperative optical coherence tomography-guided small-incision lenticule extraction: new surgical technique," *Journal of Cataract and Refractive Surgery*, vol. 43, no. 10, pp. 1245–1250, 2017.

[52] R. Nagpal, C. Shakkarwal, R. Agarwal, R. K. Bafna, P. K. Maharana, and N. Sharma, "Quantitative analysis of gap between the intraocular lens and posterior capsule using microscope-integrated optical coherence tomography in eyes undergoing phacoemulsification," *Clinical Ophthalmology*, vol. 15, pp. 1965–1970, 2021.

[53] N. Hirnschall, S. Norrby, M. Weber, S. Maedel, S. Amir-Asgari, and O. Findl, "Using continuous intraoperative optical coherence tomography measurements of the aphakic eye for intraocular lens power calculation," *British Journal of Ophthalmology*, vol. 99, no. 1, pp. 7–10, 2015.

[54] A. Meduri, G. Oliverio, A. A. Severo, U. Camellin, M. Rechichi, and P. Aragona, "Double safe suture during cataract surgery on post radial keratotomy patients using clear corneal incisions," *European Journal of Ophthalmology*, Article ID 11206721221083799, 2022.

[55] A. Meduri, M. Urso, G. A. Signorino, M. Rechichi, C. Mazzotta, and S. Kaufman, "Cataract surgery on post radial keratotomy patients," *International Journal of Ophthalmology*, vol. 10, no. 7, pp. 1168–1170, 2017.

[56] M. S. Sachdev, R. Malik, H. Gupta, R. Sachdev, and G. S. Sachdev, "Femtosecond laser-integrated anterior segment optical coherence tomography to detect preexisting posterior capsular dehiscence and increase safety in posterior polar cataracts," *Journal of Cataract and Refractive Surgery*, vol. 46, no. 2, pp. 235–240, 2020.

[57] W. Chen, Z. Lin, Q. Zhu et al., "Intraoperative optical coherence tomography for the assessment of posterior capsular integrity in pediatric cataract surgery," *Journal of Cataract & Refractive Surgery*, vol. 48, 2021.

[58] J. S. Titiyal, M. Kaur, F. Shaikh, S. Goel, and L. M. S. Bageshwar, "Real-time intraoperative dynamics of white cataract-intraoperative optical coherence tomography-guided classification and management," *Journal of Cataract and Refractive Surgery*, vol. 46, no. 4, pp. 598–605, 2020.

[59] C.-W. Chen, A. A. Francone, M. J. Gerber et al., "Semi-automated optical coherence tomography-guided robotic surgery for porcine lens removal," *Journal of Cataract and Refractive Surgery*, vol. 45, no. 11, pp. 1665–1669, 2019.

[60] J. P. Ehlers, Y. K. Tao, S. Farsiu, R. Maldonado, J. A. Izatt, and C. A. Toth, "Integration of a spectral domain optical coherence tomography system into a surgical microscope for intraoperative imaging," *Investigative Opthalmology & Visual Science*, vol. 52, no. 6, pp. 3153–3159, 2011.

[61] J. P. Ehlers, S. K. Srivastava, D. Feiler, A. I. Noonan, A. M. Rollins, and Y. K. Tao, "Integrative advances for OCT-guided ophthalmic surgery and intraoperative OCT: microscope integration, surgical instrumentation, and heads-up display surgeon feedback," *PLoS One*, vol. 9, no. 8, Article ID e105224, 2014.

[62] M. T. El-Haddad and Y. K. Tao, "Automated stereo vision instrument tracking for intraoperative OCT guided anterior segment ophthalmic surgical maneuvers," *Biomedical Optics Express*, vol. 6, no. 8, pp. 3014–3031, 2015.

[63] S. B. Han, Y. C. Liu, K. Mohamed-Noriega, and J. S. Mehta, "Advances in imaging technology of anterior segment of the eye," *Journal of Ophthalmology*, vol. 2021, Article ID 9539765, 9 pages, 2021.

Research Article

Specular Microscopic Corneal Endothelial Cell Changes following Uneventful Phacoemulsification in Patients with Gout

Mortada Abozaid [iD],[1] **Rana Saad-eldin,[2] Mahmoud Farouk,[1] Mohamed Anbar,[1] and Ehab Wasfi[3]**

[1]*Department of Ophthalmology, Sohag University, Sohag, Egypt*
[2]*Department of Rheumatology and Rehabilitation, Sohag University, Sohag, Egypt*
[3]*Department of Ophthalmology, Assiut University, Assiut, Egypt*

Correspondence should be addressed to Mortada Abozaid; mourtada_abdelaal@med.sohag.edu.eg

Purpose. To assess the effects of phacoemulsification on the corneal endothelium in patients with gout and age-related cataracts. *Methods.* Eighty-eight patients who underwent uneventful phacoemulsification for age-related cataracts were included in this retrospective comparative study. The patients were divided into two groups: group A included 31 patients with gout and tight control of uric acid levels and group B included 57 patients without gout or any other systemic disease. All patients completed follow-up assessments over 6 months, and the two groups were compared in terms of changes to their specular microscopic values. *Results.* Both groups showed marked improvement in uncorrected and best-corrected visual acuity at the end of the follow-up period. Corneal endothelial cell loss was more severe in group A than in group B, with a mean difference of 221.35 ± 43.87 in group A and 169.88 ± 52.67 in group B at the sixth month ($p < 0.001$). The difference between the two groups in terms of other specular microscopic values did not reach statistical significance. *Conclusion.* Patients with gout are more prone to corneal endothelial cell damage after phacoemulsification than those without gout. To confirm these results, future studies with a prospective design and longer durations of follow-up are needed.

1. Introduction

Gout is an inflammatory condition caused by metabolic dysfunction, which can lead to elevated body uric acid levels (≥6.8 mg/dL), in turn triggering deposition of monosodium urate (MSU) crystals in different tissues, especially the joints. This condition mostly affects postmenopausal women and middle-aged men [1–4]. Changes in lifestyle and increasing rates of obesity are probably responsible for the doubling of gout prevalence over the past couple of decades.

Tophi are lesions resulting from the deposition of MSU crystals in the eye, especially in the ocular adnexa and anterior segment. Patients with tophi usually present with bilateral acute or chronic conjunctivitis and hyperaemic vessels. They may also develop cataracts caused by hyperuricaemia itself or from drugs used in the treatment of gout,

such as steroids and allopurinol. Other ocular manifestations of gout include dry eye syndrome, uveitis, scleritis, and glaucoma [5–7]. Gout is also known to be associated with endothelial dysfunction of the blood vessels and renal tubules, and high levels of uric acid in the anterior chamber may accelerate apoptosis of the corneal endothelial cells, thus increasing corneal thickness [8–10].

The frequency of phacoemulsification cataract surgery is increasing these days because of its several advantages, including rapid rehabilitation, fewer complications, and reasonable cost. However, one of the primary limitations of this procedure is the potential for postoperative damage to the corneal endothelium. The integrity of the corneal endothelium is very important for dehydration of the corneal stroma and clarity of the cornea. Any compromise in the barrier function or active pump mechanism of the

endothelium can result in corneal oedema [11]. Severe damage to the endothelium after phacoemulsification may cause corneal decompensation with a marked drop in vision, which may necessitate corneal transplantation and its related complications. Considering the decline in endothelial function with advancing age, great attention should be paid to the corneal endothelium before and during cataract surgery in elderly people, especially those with systemic comorbidities, to achieve the main goal of surgery, which is an improvement of vision [12, 13].

The aim of this study was to evaluate the effect of uneventful phacoemulsification on the corneal endothelium of patients with gout and compare the results with those obtained in a group of patients without gout or any other systemic disease. Endothelial cell density (ECD), coefficient of variation (CV), hexagonality (HEX), and central corneal thickness (CCT) were the parameters compared between the two groups.

2. Patients and Methods

This retrospective comparative study was conducted using the charts of 88 patients who had undergone uneventful phacoemulsification for visually significant age-related cataracts at the Ophthalmology Department of Sohag University Hospital and Assiut University Hospital. The patients were treated in collaboration with the respective rheumatology departments. The Ethics Committee of the Sohag Faculty of Medicine approved the study (approval number: soh-Med-21-03–14), which adhered to the tenets of the Declaration of Helsinki, and written informed consent was obtained from all patients before surgery. The study eyes were divided into two groups: group A, which included 31 eyes from 31 patients with age-related cataracts and gout defined according to the American College of Rheumatology 2015 gout classification criteria [14], and group B, which included 57 eyes from 57 patients with age-related cataracts without gout or any other systemic disease. The inclusion criteria included cataracts with nuclear grades N2 or N3 according to the Lens Opacities Classification System III [15] and a normal fundus and normal intraocular pressure (IOP). In contrast, we excluded patients with corneal pathology or a low endothelial cell count (<2000 cells/mm), contact lens wear, poor pupillary dilatation, pseudoexfoliation syndrome, glaucoma, uveitis, history of eye trauma, surgery, or any systemic disease that could have affected the endothelium, such as diabetes mellitus.

All study patients underwent a complete ophthalmic examination before and after surgery, including measurements of uncorrected visual acuity (UCVA) and best-corrected visual acuity (BCVA) in the logarithm of minimum angle of resolution (logMAR) values, evaluation of manifest refraction, slit-lamp and fundus examinations, IOP measurement using an applanation tonometer, noncontact specular microscopy using CEM-530 (Nidek, Gamagori, Japan), and measurement of the axial length (AL), anterior chamber depth (ACD), corneal power (K1, K2, $K_{average}$, and keratometric cylinder), and intraocular lens (IOL) power using IOLMaster$^®$ 500 (Carl Zeiss Meditec AG, Jena, Germany).

2.1. Sample Size Calculation.
In the absence of previous similar studies, we relied on a pilot study to calculate the sample size. Using a small set of preliminary data collected from five patients with gout (group 1) and 10 nongout patients (group 2), the mean and standard deviation of the difference between the preoperative and 6-month postoperative values of the endothelial cell density were calculated to be 209.4 ± 110.2 in group 1 and 143.7 ± 89.3 in group 2. Then, a G* Power software (Dusseldorf University, Germany) was used to calculate the effect size which is utilised in a priori analysis together with an alpha error of 0.05 and a power of 0.8 to detect the sample size required to reveal a significant change in the endothelial cell density. The allocation ratio was set as 2 to increase the statistical confidence. We found that the study should include 30 patients with gout and 60 patients without gout.

2.2. Surgical Procedures.
All patients were operated on by two surgeons (MA and EW) who conducted stop-and-chop phacoemulsification using the Infiniti$^®$ Ozil continuous phacomachine (Alcon, Fort Worth, Texas, USA) with intelligent phacoemulsification (IP) software. To obtain adequate pupillary dilation before surgery, a topical mixture of cyclopentolate hydrochloride (1%) and phenylephrine hydrochloride (10%) was instilled into the eye every 10 min for 30 minutes. The surgery started with instillation of the topical anaesthetic benoxinate hydrochloride 0.4% into the conjunctival sac, which was followed by retrobulbar and facial nerve blocks using 2% lidocaine HCl injection.

Two paracentesis incisions were performed using a microvitreoretinal knife (20 gauge) followed by injection of a cohesive ophthalmic viscoelastic device (OVD); injection of sodium hyaluronate ophthalmic solution 1.4% into the anterior chamber; and a clear typical triplanar corneal incision using a 2.2 mm keratome. After forceps-aided capsulorrhexis, hydrodissection was performed and a dispersive viscoelastic fluid, 2% hydroxypropylmethylcellulose, was injected into the anterior chamber for endothelial protection.

Nucleotomy was performed in all cases by using the stop-and-chop technique followed by irrigation-aspiration of the cortical matter and implantation of a foldable intraocular lens. After aspiration of the residual viscoelastic material, the incisions were sealed by hydration without using sutures. Finally, we administered topical moxifloxacin hydrochloride 0.5% eye drops and prednisolone acetate 1% eye drops followed by eye patching. At the end of the surgery, the cumulative dissipated energy (CDE) and estimated fluid used were recorded, as shown in Figure 1.

2.3. Postoperative Care and Follow-Up.
Patients were instructed to instil moxifloxacin eye drops five times daily for one week and prednisolone eye drops five times daily with gradual withdrawal within four weeks. Slit-lamp examinations were routinely performed during the entire follow-up period. All patients underwent postoperative UCVA, BCVA, subjective refraction, and specular microscopy assessments at 1, 3, and 6 months postoperatively.
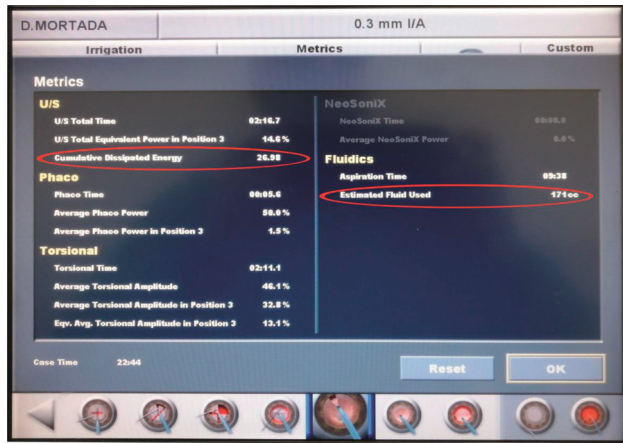
Figure 1: Summary of phacoemulsification parameters at the end of surgery, with the CDE and estimated fluid used highlighted.

2.4. Statistical Analysis. Data were analysed using IBM SPSS Statistics for Windows version 20.0. Quantitative data were expressed as mean ± standard deviation, median, and range, while qualitative data were expressed as numbers and percentages. The data were tested for normality using the Shapiro–Wilk test, in which significant results indicated that the findings of nonparametric tests were not normally distributed. Independent-sample t-tests and repeated-measures ANOVA with pairwise comparisons were applied for normally distributed data. The nonparametric Mann–Whitney test, Friedman test with pairwise comparisons, and Spearman correlation were used for data that were not normally distributed. The chi-square (χ^2) test and Fisher's exact test were used for the comparison of qualitative variables as appropriate. A 5% level was chosen to indicate significance in all the statistical tests used in the study.

3. Results

This retrospective comparative study included 88 eyes from 88 patients (38 men (43.2%) and 50 women (56.8%)) who underwent uneventful phacoemulsification cataract surgery for age-related cataracts (grade N2 or N3). The right eye was operated on in 46 patients (52.3%), while the left eye was operated on in 42 patients (47.7%). The patients were divided into two groups: group A included 31 patients with gout and group B included 57 patients who had no gout or any other systemic disease. Preoperative parameters were matched between the two groups. The mean patient age in group A was 58.23 ± 3.91 years, while that in group B was 59.61 ± 5.99 years. The two groups showed no statistically significant differences in the nuclear grade of cataracts, average keratometry findings, ACD, AL, and IOL power (biometry), as given in Table 1. The specular microscopy values in group A were as follows: mean ECD, 2761 ± 327.17; mean CV, 35.45 ± 4.61; mean HEX, 51.58 ± 8.21; and mean CCT, 512.13 ± 29.22. The corresponding values in group B were as follows: mean ECD, 2844.46 ± 335.1; mean CV, 36.39 ± 4.32; mean HEX, 47.86 ± 7.26; and mean CCT, 515.44 ± 22.9, respectively. In the assessment of

intraoperative parameters, the CDE and the estimated fluid used did not differ between the two groups, as given in Table 1.

Comparisons of visual acuity before and after surgery in the two groups showed significant improvement in both UCVA and BCVA after the surgery throughout the follow-up period, with no significant differences between the two groups. After surgery, the ECD showed a significant progressive decline in both groups, with mean values of 2622.52 ± 329.08, 2571.06 ± 326.09, and 2539.65 ± 324.7 after 1, 3, and 6 months, respectively, in group A and mean values of 2738.32 ± 342.28, 2697.91 ± 344.41, and 2674.58 ± 342.77, respectively, in group B. This decline was more significant in group A (gout group) than in group B (normal group), with a mean difference of 138.48 ± 41.2, 189.94 ± 50.18, and 221.35 ± 43.87 at 1, 3, and 6 months, respectively, in group A and a mean difference of 106.14 ± 32.62, 146.54 ± 43.3, and 169.88 ± 52.67, respectively, in group B, as shown in Figures 2 and 3 and Table 2. Spearman correlation analysis of the ACD, CDE, and estimated fluid used with the ECD change after the 6th month postoperatively revealed a significant correlation only with ACD ($r = -0.318$ and $p = 0.003$).

The other specular microscopic values also showed significant changes after surgery in the two groups, with CV values showing an initial rise followed by a decline, HEX values showing an initial decline followed by an increase, and CCT values showing an initial rise followed by a plateau and a final return to preoperative values. However, the mean differences did not reach statistical significance when the two groups were compared.

With regard to postoperative complications, no differences were noted between the two groups, with posterior capsule opacification (PCO) developing in three cases in each group and macular oedema developing in one case in group A and two cases in group B.

4. Discussion

The increasing prevalence of gout may signal the onset of a worldwide epidemic. This condition affects 8.3 million adults in the United States, and its prevalence is expected to increase with the spread of obesity. Considering the increasing use of phacoemulsification surgeries together with the rise in life expectancy and the global increase in gout prevalence, eye surgeons should be aware of the importance of corneal endothelial care in such patients.

In this retrospective comparative study, we evaluated the stress exerted on the corneal endothelium in patients with gout who underwent uneventful phacoemulsification surgery for age-related cataract (group A) and compared them to a control group (group B) with no gout or any other systemic disease.

The two groups showed no differences in their preoperative or intraoperative characteristics. Conversely, the postoperative corneal endothelial characteristics showed significant differences, with more damage to the endothelium observed in the gout group than in the normal group. These differences in the ECD values were significant over the

TABLE 1: Comparison of preoperative and intraoperative characteristics between study groups.

Characteristics	Group		P value
	Gout ($N = 31$)	Normal ($N = 57$)	
Gender			<0.001*
Female	27 (87.1%)	23 (40.4%)	
Male	4 (12.9%)	34 (59.6%)	
Age (year)			0.165
Mean ± S.D.	58.23 ± 3.91	59.61 ± 5.99	
Median (IQ range)	57 (55–62)	60 (55–65)	
Laterality			0.590*
Left	16 (51.6%)	26 (45.6%)	
Right	15 (48.4%)	31 (54.4%)	
Grade			0.314*
N2	13 (43.4%)	23 (40.4%)	
N3	17 (56.6%)	34 (59.6%)	
Preaverage K			0.544
Mean ± S.D.	45.37 ± 1.87	44.73 ± 1.42	
CI of mean	44.69–46.06	44.35–45.11	
Median (IQ range)	44.36 (43.75–47.25)	45.08 (44.06–45.99)	
Preaxial L			0.047
Mean ± S.D.	22.96 ± 1.07	23.77 ± 1.68	
CI of mean	22.56–23.35	23.32–24.21	
Median (IQ range)	23.11 (22.21–23.6)	23.53 (22.37–24.19)	
Pre-AC depth			0.763
Mean ± S.D.	3.23 ± 0.37	3.23 ± 0.32	
CI of mean	3.09–3.36	3.14–3.31	
Median (IQ range)	3.25 (3.06–3.37)	3.26 (2.95–3.45)	
Biometry			0.046
Mean ± S.D.	20.48 ± 3.91	18.44 ± 4.45	
CI of mean	19.05–21.92	17.26–19.62	
Median (IQ range)	21 (19–22)	20 (18–21)	
Cumulative dissipated energy CDE			0.389
Mean ± S.D.	4.62 ± 3.02	6.23 ± 5.33	
CI of mean	3.51–5.73	4.82–7.64	
Median (IQ range)	4.61 (1.47–6.07)	4.19 (3.09–8.53)	
Estimated fluid used			0.313
Mean ± S.D.	110.06 ± 34.19	100.04 ± 28.95	
CI of mean	97.52–122.61	92.35–107.72	
Median (IQ range)	103 (80–141)	95 (83–114.5)	

P values were calculated using the Mann–Whitney U test. *P values were calculated using the Chi-square test. P values of <0.05 indicated statistical significance.

entire follow-up period (6 months) but did not reach statistical significance with regard to CCT, CV, and HEX values.

Sahu et al. [16] studied the effect of uneventful phacoemulsification on the corneal endothelium of 60 patients with controlled diabetes mellitus (type 2 with glycosylated haemoglobin< 7.0) and compared them to the findings in 60 nondiabetic patients. Both groups showed a decline in ECD and HEX and a rise in CV and CCT at the end of the follow-up period of 3 months; however, the changes were more significant in the diabetic group, indicating more endothelial dysfunction. However, this study did not exclude other systemic diseases such as gout from the control group, which may have biased the results.

Kosekahya et al. [17] investigated corneal endothelial changes in 50 patients with gout compared to an age and sex-matched group of healthy individuals. They found that the gout group had a lower mean ECD and HEX and higher CV

and CCT than the control group. In addition, they reported a negative correlation between gout duration and both ECD and HEX ($r = -0.400$, $p = 0.019$ and $r = -0.348$, $p = 0.043$, respectively), while the uric acid level was positively correlated with CCT ($r = 0.355$, $p = 0.003$) and negatively correlated with HEX ($r = -0.245$, $p = 0.044$). They concluded that patients with gout might have corneal endothelial dysfunction which is proportional to disease duration and uric acid levels. They urged eye surgeons to consider such endothelial dysfunction when treating patients with cataracts or glaucoma and having gout.

The same group [18] evaluated the characteristics of the cornea and tear film in 41 patients with gout in comparison with healthy individuals. They studied corneal densitometry findings in both groups by using Pentacam corneal tomography and reported significantly higher values in the 0–2 mm and 2–6 mm zones of both anterior and central layers in the gout group compared to the control group,
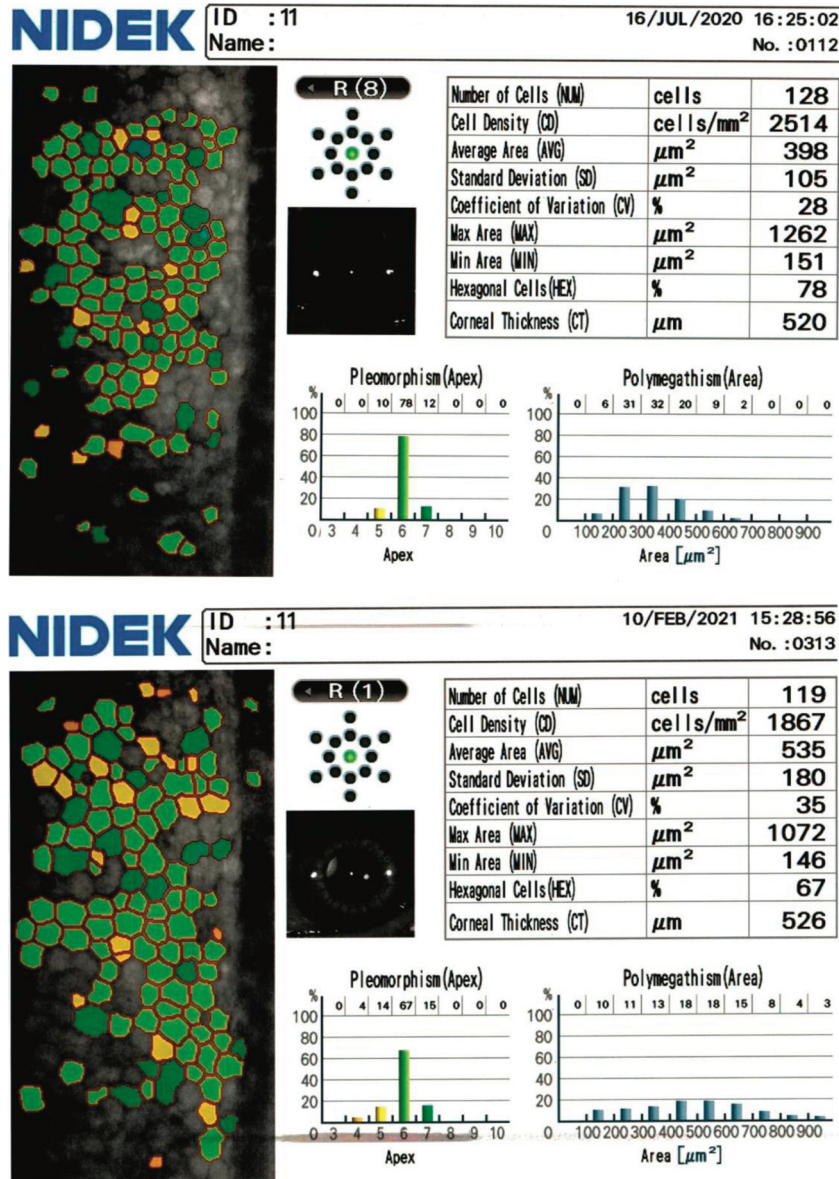
FIGURE 2: Preoperative and 6-month postoperative specular microscopy findings in a female patient in group A (gout group). The reduction is in ECD and HEX and the increase is in CV and CCT values.

while the densitometric values of the 0–2 mm and 2–6 mm zones of the posterior layer were similar in both groups. The 6–10 mm and 10–12 mm zones of all layers showed similar values in two groups. In addition, they noted a strong positive correlation between the anterior and central 0–2 mm and 2–6 mm zones and both uric acid levels and duration of gout.

To the best of our knowledge, this is the first study to investigate the effects of phacoemulsification cataract surgery on the corneal endothelium in patients with gout. Endothelial cell loss was more severe in patients with gout than in patients without gout or any other systemic disease, indicating the need for greater attention during surgery in such patients.

Hyperuricemia induced in rats was linked to damage of the renal tubular endothelium due to decrease in Na, K-ATPase activity. Higher levels of serum uric acid were associated with a higher decline in enzyme activity [19]. Such mechanisms relating to endothelial dysfunction may also explain the excessive loss of corneal endothelial cells in patients with gout after phacoemulsification cataract surgery.

The main limitations of this study are its retrospective design, small sample size, and relatively short follow-up duration. Although the study included a small number of cases, it can be used as a pilot study to calculate the sample size of more powerful studies. Future randomised controlled clinical trials with larger samples and longer durations of follow-up are needed to confirm the results of this study.
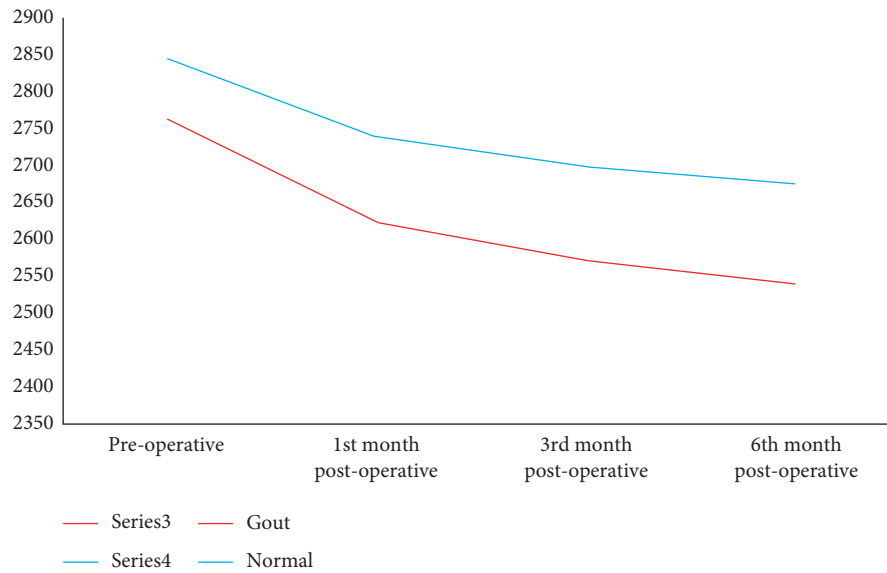
FIGURE 3: A chart comparing repeated cell density measures in the two groups.

TABLE 2: Comparison of changes in study measures between the study groups six months postoperatively.

Characteristics	Group		P value
	Gout ($N = 31$)	Normal ($N = 57$)	
UCVA			0.608
Mean ± S.D.	−0.48 ± 0.2	−0.5 ± 0.22	
CI of mean	−0.56–0.41	−0.56–0.44	
Median (IQ range)	−0.45 (−0.57–0.4)	−0.45 (−0.62–0.4)	
BCVA			0.492
Mean ± S.D.	−0.62 ± 0.24	−0.64 ± 0.23	
CI of mean	−0.71–0.53	−0.70–0.58	
Median (IQ range)	−0.58 (−0.9–0.4)	−0.58 (−0.9–0.47)	
Cell density			<0.001
Mean ± S.D.	221.35 ± 43.87	169.88 ± 52.67	
CI of mean	205.26–237.45	155.90–183.85	
Median (IQ range)	210 (198–255)	172 (148–191)	
CV			0.03
Mean ± S.D.	−1.77 ± 2.92	−3.46 ± 4.34	
CI of mean	−2.84–0.70	−4.61–2.30	
Median (IQ range)	−1 (−3–0)	−3 (−6–1)	
Hex			0.82
Mean ± S.D.	5.45 ± 4.21	5.72 ± 5.62	
CI of mean	3.91–7	4.23–7.21	
Median (IQ range)	5 (2–8)	5 (2–9)	
CCT			0.234
Mean ± S.D.	−2.65 ± 6.75	−1.39 ± 14.17	
CI of mean	−5.12–0.17	−5.15–2.37	
Median (IQ range)	−1 (−7–2)	−1 (−7–5.5)	

P values were calculated by the Mann–Whitney U test. P values of <0.05 indicated statistical significance.

5. Conclusions

In conclusion, patients with gout, such as those with diabetes, are probably more prone to corneal endothelial dysfunction postcataract surgery. Thus, surgeries in these patients should be performed using more protective viscoelastic devices or less damaging nuclear-dividing techniques, with more attention to intraoperative phaco parameters.

Data Availability

The datasets used and/or analysed during the current study are available from the corresponding author upon request.

Conflicts of Interest

Acknowledgments

References

[1] N. Dalbeth, T. R. Merriman, and L. K. Stamp, "Gout," *The Lancet*, vol. 388, no. 10055, pp. 2039–2052, 2016.

[2] T. Bardin, S. Bouée, P. Clerson et al., "Prevalence of gout in the adult population of France," *Arthritis Care & Research*, vol. 68, no. 2, pp. 261–266, 2016.

[3] R. Terkeltaub, "Update on gout: new therapeutic strategies and options," *Nature Reviews Rheumatology*, vol. 6, no. 1, pp. 30–38, 2010.

[4] J. A. Singh, "Gout: will the "King of Diseases" be the first rheumatic disease to be cured?" *BMC Medicine*, vol. 14, no. 1, p. 180, 2016.

[5] J. Lin, G. Q. Zhao, C. Y. Che, S. S. Yang, Q. Wang, and C. G. Li, "Characteristics of ocular abnormalities in gout patients," *International Journal of Ophthalmology*, vol. 6, pp. 307–311, 2013.

[6] B. Bernad, J. Narvaez, C. Diaz-Torné, M. Diez-Garcia, and J. Valverde, "Clinical image: corneal tophus deposition in gout," *Arthritis & Rheumatism*, vol. 54, no. 3, p. 1025, 2006.

[7] P. Sarma, D. Das, P. Deka, and A. C. Deka, "Subconjunctival urate crystals: a case report," *Cornea*, vol. 29, no. 7, pp. 830–832, 2010.

[8] U. M. Khosla, S. Zharikov, J. L. Finch et al., "Hyperuricemia induces endothelial dysfunction," *Kidney International*, vol. 67, no. 5, pp. 1739–1742, 2005.

[9] W. Cai, X. M. Duan, and Y. Liu, "Uric acid induces endothelial dysfunction by activating the HMGB1/RAGE signaling pathway," *BioMed Research International*, vol. 2017, Article ID 4391920, 11 pages, 2017.

[10] M. Coassin, O. Piovanetti, W. J. Stark, and W. R. Green, "Urate deposition in the iris and anterior chamber," *Ophthalmology*, vol. 113, no. 3, pp. 462–465, 2006.

[11] S. P. Srinivas, "Dynamic regulation of barrier integrity of the corneal endothelium," *Optometry and Vision Science: Official Publication of the American Academy of Optometry*, vol. 87, pp. E239–E254, 2010.

[12] K. Inoue, Y. Tokuda, Y. Inoue, S. Amano, T. Oshika, and J. Inoue, "Corneal endothelial cell morphology in patients undergoing cataract surgery," *Cornea*, vol. 21, no. 4, pp. 360–363, 2002.

[13] Y. Majima, H. Nogawa, and E. Yussa, "The specular microscopic studies of the corneal endothelium. The change with age and the change between pre and post cataract extraction," *Acta Societatis Ophthalmologicae Japonicae*, vol. 83, pp. 936–946, 1979.

[14] T. Neogi, T. L. T. A. Jansen, N. Dalbeth et al., "2015 gout classification criteria: an American College of rheumatology/European league against rheumatism collaborative initiative," *Arthritis & Rheumatology*, vol. 67, no. 10, pp. 2557–2568, 2015.

[15] L. T. Chylack, J. K. Wolfe, and D. M. Singer, "The lens Opacities classification System III," *Archives of Ophthalmology*, vol. 111, no. 6, pp. 831–836, 1993.

[16] P. Sahu, G. Das, S. Agrawal, and S. Kumar, "Comparative evaluation of corneal endothelium in patients with diabetes undergoing phacoemulsification," *Middle East African Journal of Ophthalmology*, vol. 24, no. 2, pp. 74–80, 2017.

[17] P. Kösekahya, C. Üçgül Atılgan, K. G. Atılgan et al., "Corneal endothelial morphology and thickness changes in patients with gout," *Turkish Journal of Orthodontics*, vol. 49, no. 4, pp. 178–182, 2019.

[18] P. Kosekahya, K. G. Atilgan, C. U. Atilgan et al., "Could corneal densitometry be used as a diagnostic and screening tool for ocular involvement in patients with gout?" *International Ophthalmology*, vol. 39, no. 5, pp. 991–1001, 2019.

[19] J. Xiao, X. Zhang, and C. Fu, "Impaired Na+-K+- ATPase signaling in renal proximal tubule contributes to hyperuricemiainduced renal tubular injury," *Experimental & Molecular Medicine*, vol. 50, p. 452, 2018.

Research Article

Evaluation of Intraocular Lens Tilt and Decentration in Congenital Ectopia Lentis by the Pentacam Scheimpflug System

Huiwen Ye, Zhenzhen Liu, Qianzhong Cao, Zhangkai Lian, Xinyu Zhang, Danying Zheng ⓘD, and Guangming Jin ⓘD

State Key Laboratory of Ophthalmology, Zhongshan Ophthalmic Center, Sun Yat-sen University,
Guangdong Provincial Key Laboratory of Ophthalmology and Visual Science,
Guangdong Provincial Clinical Research Center for Ocular Disease, Guangzhou 510060, China

Correspondence should be addressed to Danying Zheng; zhengdyy@163.com and Guangming Jin; jingm@mail2.sysu.edu.cn

Purpose. The purpose of this study was to quantify the characteristics of the tilt and decentration of the IOL after trans-scleral suture fixation surgery in congenital ectopia lentis (CEL) patients. *Methods.* The clinical characteristics of 70 CEL patients at Zhongshan Ophthalmic Center in China were retrospectively analyzed. The tilt and decentration of intraocular lens (IOL) were measured by using a Pentacam and compared between different axial length (AL) subgroups. The correlation between IOL tilt, decentration, and ocular characteristics was investigated using Spearman's correlation analysis. *Results.* The postoperative IOL position of CEL patients was mainly located nasally inferiorly. The average tilt of the IOL in CEL patients was less than 7° (for temporal: $2.21 \pm 1.53°$, for nasal: $-1.84 \pm 2.04°$, for superior: $2.22 \pm 2.18°$, and for inferior: $-1.70 \pm 1.62°$), and the average decentration of the IOL in CEL patients was larger than 0.4 mm (for temporal: 0.49 ± 0.38 mm, for nasal: -0.69 ± 0.46 mm, for superior: 0.72 ± 0.58 mm, and for inferior: -0.68 ± 0.54 mm). The decentration of CEL patients in the $AL \geq 26$ subgroup was greater than those with $AL < 24$ mm and AL 24 to 26 mm subgroups (for superior: 0.72 ± 0.28 mm vs. 0.46 ± 0.25 mm and 0.48 ± 0.22 mm, all $P < 0.05$; for inferior: -0.94 ± 0.56 mm vs. -0.44 ± 0.26 mm and -0.44 ± 0.46 mm, all $P < 0.05$). IOL decentration was positively correlated with AL (for superior: $r = 0.44$, $P = 0.019$; for inferior: $r = 0.54$, $P = 0.006$). IOL tilt was positively correlated with AL on the superior side ($r = 0.38$, $P = 0.041$). *Conclusions.* The extent of IOL decentration after trans-scleral suture fixation was great in CEL patients, and the IOL decentration in CEL patients was significantly associated with AL.

1. Introduction

Congenital ectopia lentis (CEL) is a rare disease that is defined as the dislocation or displacement of the natural crystalline lens [1]. CEL can occur as an ocular symptom of many systemic or hereditary diseases such as homocystinuria, Weill–Marchesani syndrome, and sulfite oxidase deficiency [2–4] with Marfan syndrome being the most common etiology [1, 5, 6].

Scleral suture-fixed posterior chamber intraocular lens (IOL) surgery is one of the most commonly performed surgical procedures for CEL patients. Although most patients can achieve good visual outcomes with this surgical technology, more complications have been reported

compared to the traditional surgery method, in which the IOL is implanted into the capsular bag, and the position of the IOL is one of the most important complications affecting visual quality [7, 8]. As previous studies have shown, IOL decentration greater than 0.4 mm and tilt greater than 7° could induce a lower visual performance [9]. Korynta found that an IOL tilt of 12° and decentration of 3 mm could result in a postoperative myopia of −7.0D and astigmatism of +4.0D [10]. Hence, the position of the IOL is important for a good visual prognosis.

However, few studies have focused on the characteristics and factors associated with IOL tilt and decentration in CEL patients. Hence, this study was conducted to evaluate the characteristics of IOL tilt and decentration three months

postoperatively and to investigate the factors associated with IOL tilt and decentration in CEL patients.

2. Methods

2.1. Design. This retrospective study was conducted at the Zhongshan Ophthalmic Center. All participants had signed an informed consent form. The study was approved by the Human Research Ethics Committee of the Zhongshan Ophthalmic Center and followed the principles of the Declaration of Helsinki.

2.2. Patients. The data from baseline and routine follow-up at three months postoperatively were obtained by reviewing the medical records of CEL patients who underwent scleral suture-fixed posterior chamber intraocular lens surgery from April 2019 to March 2021, and for those who underwent binocular surgery, the first eye at three months postoperatively was selected in this study. The included CEL patients were stratified into three categories according to AL: AL < 24 mm group, 24<AL < 26 mm group, and AL ≥ 26 mm group. The inclusion criteria were as follows: (1) patients diagnosed with bilateral EL; (2) patients younger than 40 years old; (3) patients who underwent trans-scleral suture fixation surgery; and (4) patients with adequately and asymmetrically dilated pupils during the Pentacam examination. The exclusion criteria were as follows: (1) patients with secondary lens dislocations or lens dislocations caused by ocular trauma; (2) patients with ocular surgery history; (3) patients with ocular trauma history; (4) patients who cannot cooperate in the examination; and (5) patients with unclear Pentacam images. The study was approved by the institutional review board of Zhongshan Ophthalmic Center and conducted in accordance with the Declaration of Helsinki.

2.3. Study Procedures. During the three months of postoperative routine follow-up, nonmydriatic and mydriatic photographs of the anterior segment were collected. AL and anterior chamber depth (ACD) were measured using an IOLMaster 700 (Carl Zeiss Meditec AG). The tilt and decentration of the IOLs were measured using the Pentacam HR system (Oculus Inc., Wetzlar, Germany). The Pentacam exam requires the patient to sit in front of the instrument with the pupil sufficiently dilated to obtain scanned slit images in 25 directions to obtain an image of the anterior and posterior segments of the lens. Image processing software (MATLAB) was used to fit the anterior and posterior surfaces of the IOL and the iris plane in each image, and the corresponding tilt and decentration were then calculated according to previously reported methods [11, 12]. The midpoint of the line connecting the two ends of the iris segment is considered as the pupil center, and the line passing through the pupil center and the anterior corneal center of curvature is defined as the pupillary axis. The perpendicular line at the midpoint of the intersection of the fitted lines on the anterior and posterior surfaces of the IOL is defined as the IOL axis. The IOL tilt is defined as the angle between the IOL axis and the pupillary axis around the *x*-axis or *y*-axis, while the decentration of the

IOL is defined as the vertical distance from the IOL axis to the pupillary axis [13]. The vertical meridian is defined as the 90-degree meridian, and the horizontal meridian is defined as the 180-degree meridian. Positive values indicate the temporal side in the horizontal meridian and the superior side in the vertical meridian, while negative values indicate the nasal and inferior sides, respectively [14].

2.4. Surgical Technique. All patients underwent trans-scleral suture-fixed posterior chamber intraocular lens IOL implantation right after the crystalline lens extraction by a single experienced surgeon (DY Z). The fixation of the IOL haptic occurred using an 8–0 polypropylene suture (Johnson and Johnson, USA) with a 26-G needle, and the needles were pierced from the ciliary sulcus to the sclera of the 150-degree meridian and the 330-degree meridian from 2 mm posterior to the surgical limbus. All patients were implanted with 970 C/920H (Rayner, UK) one-piece IOLs. The bilateral sutures were evenly tightened so that the IOL was centered as much as possible. The end of the suture under the scleral flap was knotted in turn to bury the knot under the sclera. The scleral flap was closed with a 10/0 nylon suture.

2.5. Statistical Analysis. Statistical analysis of the quantitative data was performed for all variables, and the differences in ocular data between the three subgroups were tested by one-way Anova analysis. A Spearman correlation analysis was used to evaluate the correlation between the positions of the IOL and AL. All data were analyzed by using SPSS 23.0 (SPSS, IBM Corp, Armonk, NY, USA). The P value less than 0.05 was considered statistically significant.

3. Results

3.1. Demographic and Ocular Characteristics. The demographic data and ocular biometric parameters of the patients are shown in Table 1. A total of 70 eyes of 70 patients were enrolled. The mean age of CEL patients was 9.77 years ±5.13 (SD), and 88.57% (62/70) of patients were over 6 years. The mean AL was 24.86 ± 1.80 mm, and the mean ACD was 4.67 ± 1.45 mm, and six patients (8.57%) had undergone anterior segment vitrectomy during surgery.

3.2. IOL Tilt and Decentration. Figure 1 illustrates the definition of IOL tilt and decentration. Tilt and decentration represent the angle and distance around the *x*-axis or *y*-axis of the IOL axis from the pupillary axis. Positive values indicate tilt and decentration exist on the nasal or temporal side, while negative values indicate tilt and decentration exist on the superior side or inferior side. Figure 2 shows that the IOL tilt and decentration of CEL patients were mainly distributed nasally inferiorly (for tilt and decentration: both 23/70 (32.86%)). The average values of the IOL tilt and decentration in the CEL patients are shown in Table 2 and Figure 3. The mean tilt of the IOL in CEL patients was less than 7° (for temporal: $2.21 \pm 1.53°$, for nasal: $-1.84 \pm 2.04°$, for superior: $2.22 \pm 2.18°$, and for inferior: $-1.70 \pm 1.62°$), and the

TABLE 1: The demographic and clinical features of 70 CEL patients.

Characteristics	Value
Patients/eyes, n	70/70
Age (yrs), mean (SD)	9.77 (5.13)
Male/female, n	33/37
Axial length (mm), mean (SD)	24.86 (1.80)
WTW (mm), mean (SD)	4.67 (1.45)
SE (D)	−1.625
Anterior vitrectomy (n, %)	6 (8.57)

SD = standard deviation.
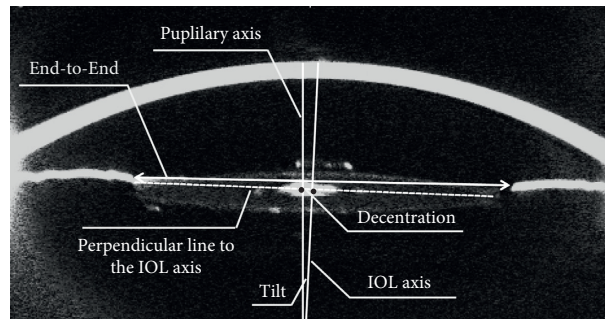
FIGURE 1: Fitted circumferences, pupillary axis, and IOL axis merged on a Scheimpflug cross-section image. Decentration is calculated from the distance between the IOL axis and pupillary axis. The IOL tilt was calculated from the angle between the axes.
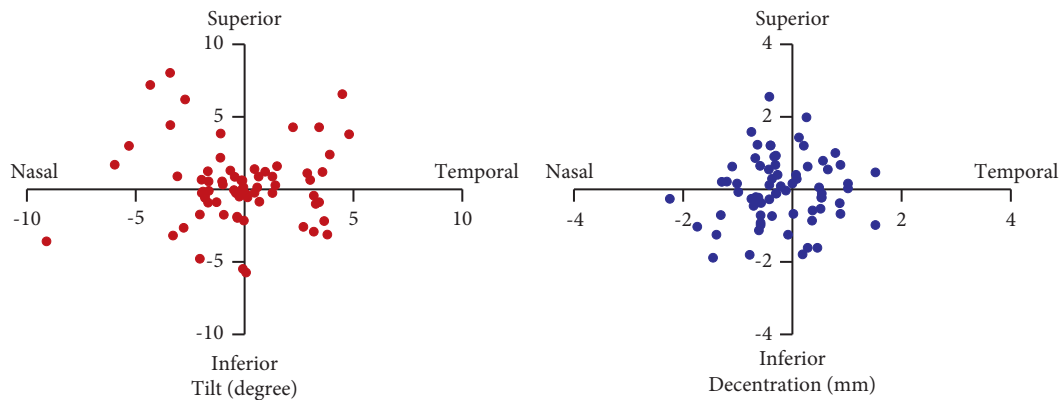
FIGURE 2: Degree and distribution of IOL tilt and decentration in CEL patients.

TABLE 2: IOL position parameters of CEL patients according to axial length.

	Total	AL < 24 mm	24 mm ≤ AL < 26 mm	AL ≥ 26 mm	P value
			Tilt (degree)		
Temporally	2.21 ± 1.53	2.22 ± 1.46	2.38 ± 1.64	2.19 ± 1.58	0.963
Nasally	−1.84 ± 2.04	−1.56 ± 1.52	−1.39 ± 1.27	−1.83 ± 1.66	0.897
Superiorly	2.22 ± 2.18	1.34 ± 1.77	1.89 ± 2.00	3.50 ± 2.71	0.031
Inferiorly	−1.70 ± 1.62	−1.19 ± 1.63	−1.65 ± 1.72	−1.88 ± 1.65	0.523
			Decentration (mm)		
Temporally	0.49 ± 0.38	0.46 ± 0.25	0.38 ± 0.39	0.52 ± 0.41	0.795
Nasally	−0.69 ± 0.46	−0.53 ± 0.27	−0.74 ± 0.37	−0.56 ± 0.19	0.194
Superiorly	0.72 ± 0.58	0.46 ± 0.25	0.48 ± 0.22	0.72 ± 0.28	0.045
Inferiorly	−0.68 ± 0.54	−0.44 ± 0.26	−0.44 ± 0.46	−0.94 ± 0.56	0.033

average decentration of the IOL in CEL patients was larger than 0.4 mm (for temporal: 0.49 ± 0.38 mm, for nasal: −0.69 ± 0.46 mm, for superior: 0.72 ± 0.58 mm, and for inferior: −0.68 ± 0.54 mm). The decentration in the AL ≥ 26 subgroup was greater than those with AL < 24 mm and 24<AL < 26 mm subgroups. (for superior: 0.72 ± 0.28 mm vs.
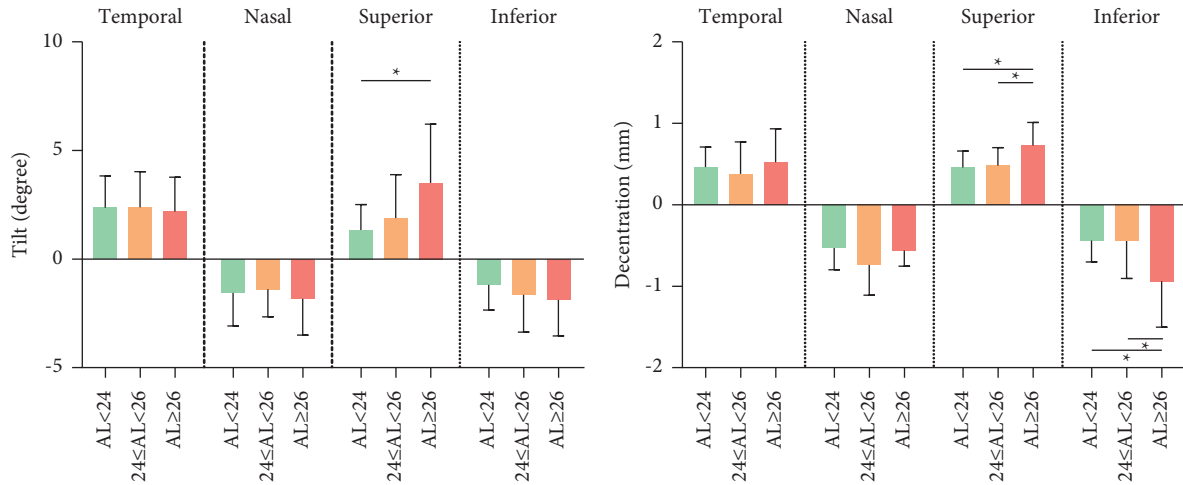
FIGURE 3: Comparisons of IOL tilt and decentration according to axial length in CEL patients.

TABLE 3: Spearman correlation between clinical features and IOL position.

| | Age (yrs) | | Sex (female) | | WTW (mm) | | SE (D) | | AL (mm) | | ACD (mm) | |
	R value	P value	R value	P value	R value	P value	R value	P value	R value	P value	R value	P value
						Tilt						
Temporally	0.06	0.572	0.33	0.171	0.612	0.312	0.21	0.209	0.02	0.926	0.04	0.462
Nasally	−0.35	0.156	−0.14	0.233	0.526	0.440	0.11	0.621	0.09	0.571	0.10	0.701
Superiorly	0.17	0.725	−0.12	0.501	0.307	0.105	0.10	0.715	0.382	0.041	0.12	0.124
Inferiorly	0.18	0.236	0.09	0.325	0.235	0.303	0.21	0.269	0.07	0.702	0.17	0.506
						Decentration						
Temporally	0.15	0.314	−0.13	0.163	0.31	0.178	0.14	0.270	−0.08	0.700	0.13	0.423
Nasally	−0.18	0.205	0.23	0.421	−0.27	0.590	0.06	0.19	−0.08	0.635	0.11	0.502
Superiorly	0.23	0.604	0.10	0.121	0.11	0.231	0.12	0.352	0.44	0.019	0.21	0.787
Inferiorly	−0.31	0.215	−0.17	0.304	−0.19	0.331	0.13	0.639	0.542	0.006	−0.31	0.169

0.46 ± 0.25 mm and 0.48 ± 0.22 mm, all $P < 0.05$; for inferior: $−0.94 \pm 0.56$ mm vs. $−0.44 \pm 0.26$ mm and -0.44 ± 0.46 mm, all $P < 0.05$). The results of the correlations between the IOL position and the ocular meters are shown in Table 3 and Figure 4. AL was positively associated with IOL decentration at the superior and inferior side (for superiorly: $r = 0.44$, $P = 0.019$; for inferiorly: $r = 0.54$, $P = 0.006$), and AL was positively associated with IOL tilt at the superior side ($r = 0.38$, $P = 0.041$).

4. Discussion

In recent years, Pentacam has been commonly used in clinical practice to measure IOL tilt and decentration. By using the Scheimpflug camera scanning principle, Pentacam can obtain a three-dimensional image of the anterior segment of the eye in less than two seconds, as well as automatically track and correct the patient's eye movements during the examination, and its measurements have been popularly commercialized [15]. In this study, by using Pentacam, we found that the postoperative IOL positions in CEL patients were mainly located nasally inferiorly, while the average tilt of IOLs in CEL patients was less than 7° in all four directions. However, the IOL decentration in CEL patients was larger than 0.4 mm. Moreover, patients with the

longer AL had a greater IOL decentration than those with the shorter AL.

Previous studies have suggested that although small tilt and decentration of the IOL will not lead to abnormal visual experiences, large tilt and decentration can cause higher-order aberrations and changes in refractive status, which can affect the visual quality of patients [16–18]. Hence, maintaining a central position of the IOL in the visual axis region is particularly critical for postoperative visual prognosis. Although previous studies have suggested that the AL, ACD, and IOL types are related to IOL tilt and decentration, to our knowledge, studies on the distribution of IOL tilt and decentration in CEL patients after IOL scleral suture loop fixation and related factors are still rare.

Hayashi K's study showed that the tilt and decentration of the IOL after out-of-the-bag implantation were significantly greater than those after in-the-bag implantation, and the extent of both tilt and decentration after scleral suture fixation was greater than that observed after either out-of-the-bag or in-the-bag implantation [19, 20], which was consistent with part of our findings. In comparison with data in the published literature, our study showed that the tilt of the IOL after trans-scleral fixation in CEL patients was not significantly greater than that after in-the-bag implantation in cataract patients, whereas the decentration of the IOL in CEL patients was significantly greater [21]. The

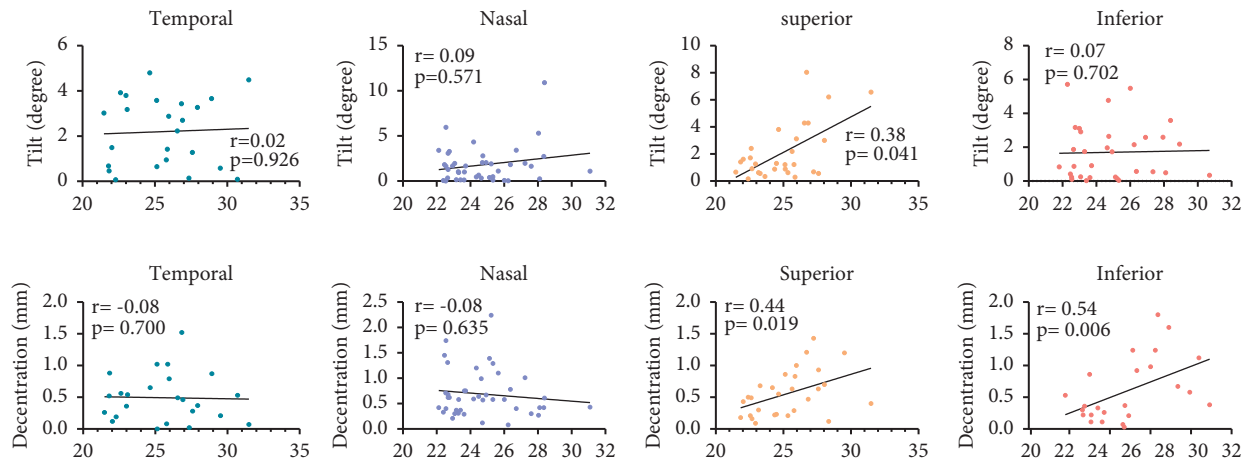FIGURE 4: The scatter plots show the correlations between IOL position and AL at different directions.

abovementioned findings may be explained by the fact that since our surgical operation required tensioning and fixation of the bilateral sutures, it was difficult to ensure a completely uniform force on both sides with only the surgeon's experience, so it was prone to greater decentration; as most of our patients did not undergo vitrectomy, the more complete vitreous support may explain the lesser tilt.

Zhang F's study showed that IOL tilt and decentration in most patients were distributed on the temporal-inferiorly side [14], and our results showed that the tilt and decentration were mainly nasally inferiorly, which suggests the distribution of IOL positions after trans-scleral sutures was different from that of in-the-bag implantation. In our study, 5.71% (4/70) of CEL patients had an IOL tilt greater than 7°; all four patients had an AL > 26 mm; and the maximum tilt was 9.18° on the nasal side. This patient had an AL > 26 mm and a history of intraoperative anterior vitrectomy. The reason for this patient's large IOL tilt may lie in the fact that the IOL was less supported after the anterior vitrectomy.

We divided the CEL patients into three groups according to the AL, as shown in Table 2 and Figure 3. The postoperative IOL decentration was greater in the CEL patients with an AL $\geq$ 26 mm than in patients with an AL of less than 26 mm, both on the superior and inferior side. And the IOL tilt was greater in the CEL patients with AL $\geq$ 26 mm than in patients with AL less than 26 mm on the superior side. This may be explained by the fact that the growth of the eye with a long AL may have stretched the suture of the lens loop fixed to the sclera, thus increasing the chance of postoperative IOL decentration and tilt. As shown in Table 3 and Figure 4, the decentration in superior and inferiority was positively correlated with the AL. This conclusion could be explained by the fact that due to the poorly developed zonular support in CEL patients, the common surgical approach is to fix the IOL in the ciliary sulcus through scleral suture instead of directly into the lens capsule, in the eye with long AL, the IOL may be easily stretched and hence more likely to lead to a large decentration.

There are several limitations in this study. Although the patients came from different regions of China, most were from southern China, which might not represent the whole population with CEL. Although the majority of patients in

this study were older than 6 years old, there was still a large age span in our patients and the accuracy of our conclusions may be affected to some extent. More studies are needed in the future to further investigate the relationship between age and IOL position. And this study is a cross-sectional study, and more relevant longitudinal studies are still needed in the future to better understand the distribution and changing trend of tilt and decentration of IOL in CEL patients. However, this study is important as it uses a large sample size focused on the characteristics of the tilt and decentration of the IOL after trans-scleral fixation in CEL patients.

5. Conclusion

The results of this study indicate that the trans-scleral sutured posterior-chamber IOL in CEL patients may lead to great decentration. In addition, IOL decentration is positively associated with AL in CEL patients. In future clinical practice, improvements in the surgical approach to CEL patients should be enhanced to reduce the decentration of the IOL. Emphasis should be placed on individualized evaluation and treatment of patients, especially those with long eye axes, to minimize IOL decentration.

Data Availability

The data used to support the findings of this study are available from the corresponding author upon request.

Consent

Informed consent was obtained from all subjects involved in the study.

Disclosure

Huiwen Ye and Zhenzhen Liu share first authorship.

Conflicts of Interest

The authors declare no conflicts of interest.

Authors' Contributions

GM Jin and DY Zheng designed the study, initiated the collaborative project, and revised the paper; HW Ye and Zhenzhen Liu contributed to data acquisition, data analysis/interpretation, and drafting the manuscript; HW Ye, QZ Cao, and ZK Lian cleaned and analyzed the data; XY Zhang was responsible for administrative, technical, or logistic support; and DY Zheng and GM Jin gave final approval.

Acknowledgments

References

[1] J. Fuchs and T. Rosenberg, "Congenital ectopia lentis, A Danish national survey," *Acta Ophthalmologica Scandinavica*, vol. 76, no. 1, pp. 20–26, 1998.

[2] L. B. Nelson and I. H. Maumenee, "Ectopia lentis," *Survey of Ophthalmology*, vol. 27, no. 3, pp. 143–160, 1982.

[3] P. Dureau, "Pathophysiology of zonular diseases," *Current Opinion in Ophthalmology*, vol. 19, no. 1, pp. 27–30, 2008.

[4] R. S. Hoffman, M. E. Snyder, F. Devgan, Q. B. Allen, R. Yeoh, and R. Braga-Mele, "Management of the subluxated crystalline lens," *Journal of Cataract and Refractive Surgery*, vol. 39, no. 12, pp. 1904–1915, 2013.

[5] J. Fuchs, "Marfan syndrome and other systemic disorders with congenital ectopia lentis, A Danish national survey," *Acta paediatrica (Oslo, Norway)*, vol. 86, pp. 947–952, 1997.

[6] A. Chandra, D. Patel, fnm Aragon-Martin et al., "The revised ghent nosology; reclassifying isolated ectopia lentis," *Clinical Genetics*, vol. 87, no. 3, pp. 284–287, 2015.

[7] E. G. Buckley, "Safety of transscleral-sutured intraocular lenses in children," *Journal of American Association for Pediatric Ophthalmology and Strabismus*, vol. 12, no. 5, pp. 431–439, 2008.

[8] D. Madrid-Costa, J. Ruiz-Alcocer, fnm Pérez-Vives, T. Ferrer-Blasco, N. López-Gil, and R. Montés-Micó, "Visual simulation through different intraocular lenses using adaptive optics: effect of tilt and decentration," *Journal of Cataract & Refractive Surgery*, vol. 38, no. 6, pp. 947–958, 2012.

[9] J. T. Holladay, P. A. Piers, F Koranyi, M. van der Mooren, and N. E. S. Norrby, "A new intraocular lens design to reduce spherical aberration of pseudophakic eyes," *Journal of Refractive Surgery*, vol. 18, no. 6, pp. 683–691, 2002.

[10] J. Korynta, J. Bok, and J. Cendelin, "Changes in refraction induced by change in intraocular lens position," *Journal of Refractive Surgery*, vol. 10, no. 5, pp. 556–564, 1994.

[11] M. M. Uzel, S. Ozates, A. G. Taslipinar Uzel, and P. Yılmazbaş, "Decentration and tilt of intraocular lens after posterior capsulotomy," *Seminars in Ophthalmology*, vol. 33, no. 6, pp. 766–771, 2018.

[12] X. Wang, J. Dong, fnm Wang, and Q. Wu, "IOL tilt and decentration estimation from 3 dimensional reconstruction of OCT image," *PLoS One*, vol. 8, no. 3, Article ID e59109, 2013.

[13] A. de Castro, P. Rosales, and S. Marcos, "Tilt and decentration of intraocular lenses in vivo from Purkinje and Scheimpflug imaging," *Journal of Cataract & Refractive Surgery*, vol. 33, no. 3, pp. 418–429, 2007.

[14] F. Zhang, J. Zhang, L. Zhou et al., "Correlative comparison of three ocular axes to tilt and decentration of intraocular lens and their effects on visual acuity," *Ophthalmic Research*, vol. 63, no. 2, pp. 165–173, 2020.

[15] I. Kovács, K. Kránitz, M. C. Knorz, E. D. Donnenfeld, R. M. Nuijts, and Z. Z. Nagy, "The effect of femtosecond laser capsulotomy on the development of posterior capsule opacification," *Journal of Refractive Surgery*, vol. 30, no. 3, pp. 154–158, 2014.

[16] J. McKelvie, B. McArdle, and C. McGhee, "The influence of tilt, decentration, and pupil size on the higher-order aberration profile of aspheric intraocular lenses," *Ophthalmology*, vol. 118, no. 9, pp. 1724–1731, 2011.

[17] R. Montés-Micó, N. López-Gil, V. Pérez, S. Bonaque, and T. Ferrer-Blasco, "In vitro optical performance of nonrotational symmetric and refractive-diffractive aspheric multifocal intraocular lenses: impact of tilt and decentration," *Journal of Cataract & Refractive Surgery*, vol. 38, no. 9, pp. 1657–1663, 2012.

[18] X. Zhu, W. He, and Y. Lu, "Factors influencing 1-year rotational stability of AcrySof Toric intraocular lenses," *British Journal of Ophthalmology*, vol. 100, no. 2, pp. 263–268, 2016.

[19] K. Hayashi, H. Hayashi, and F. Hayashi, "Intraocular lens tilt and decentration, anterior chamber depth, and refractive error after trans-scleral suture fixation surgery11The authors have no proprietary interest in any of the materials described in this article," *Ophthalmology*, vol. 106, no. 5, pp. 878–882, 1999.

[20] K. Hayashi, A. Hirata, and H. Hayashi, "In-the-bag scleral suturing of intraocular lens in eyes with severe zonular dehiscence," *Eye*, vol. 26, no. 1, pp. 88–95, 2012.

[21] Y. L. Wang, Y. Z. Liu, and Y. Q. Wang, "[Comparison of stability of acrylic intraocular lens and transparency of lens capsule using Pentacam Scheimpflug System]," *Zhonghua Yan Ke Za Zhi*, vol. 47, pp. 298–302, 2011.

Research Article

The Effectiveness of Laser Peripheral Iridotomy in Adolescent Eyes with Ocular Hypertension and Concave Configuration of the Peripheral Iris

Alina Bakunowicz-Łazarczyk [ID],[1] **Beata Urban** [ID],[1] **and Małgorzata Krętowska** [ID][2]

[1]*Department of Paediatric Ophthalmology and Strabismus, Medical University of Bialystok, Waszyngtona 17, Bialystok 15-274, Poland*
[2]*Faculty of Computer Science, Bialystok University of Technology, Wiejska 45A, Białystok 15-351, Poland*

Correspondence should be addressed to Beata Urban; urbanbea@umb.edu.pl

Purpose. To evaluate the efficacy of laser peripheral iridotomy (LPI) in preventing deterioration in eyes with ocular hypertension (OHT) and concave configuration of the iris. *Materials and Methods*. This was a retrospective study, which was carried out within a period of 3–5 years. Twenty-four patients with OHT and concave irises were treated with LPI and followed up periodically. IOP, central corneal thickness (CCT), anterior chamber depth (ACD), scleral spur angle (SSA), global neuroretinal rim (NRR) thickness, and global retinal nerve fiber layer (RNFL) were examined before and after LPI. *Results*. The average age of the 24 patients was 14.21 ± 1.41 (13–17.5) years on admission. The initial IOP of the 48 eyes was 23.21 ± 1.56 mmHg in RE and 22.96 ± 2.1 mmHg in LE before LPI. All 48 eyes had concave irises in both eyes. All eyes treated with LPI have shown iris flattening, which has persisted during follow-up (mean 1.54 ± 0.9 years). At the last follow-up visit, the average IOP was 17.58 ± 2.63 (14–21) mmHg in RE and 17.58 ± 2.86 (14–21) mmHg in LE, which was statistically lower than that of the baseline ($p < 0.001$). There were significant changes in SSA in both eyes and global RNFL in RE after LPI. *Conclusions*. In the current study, LPI resulted in an IOP-lowering effect and iris flattening in adolescent eyes with a concave configuration of the peripheral iris.

1. Introduction

The pigment dispersion syndrome (PDS) is characterized by structural changes in the anterior segment, especially a structural disturbance in the iris pigment epithelium, that lead to the shedding of the pigment from the posterior surface of the iris into the anterior segment and its deposition on various ocular structures [1, 2]. In PDS, the iris has a concave configuration and is often inserted into the posterior ciliary body band. Anomalous iridozonular contact leads to rubbing of the pigmented iris epithelium against the zonular fibers and pigment release throughout the anterior segment [3, 4]. Pigment dispersion results in an accumulation of pigment granules within the aqueous humor and the outflow tissue. PDS can lead to a secondary elevation

of IOP and cause PG. Other clinical presentations of PDS include Krukenberg spindle, radial iris transillumination defects, diffuse pigmentation of the anterior chamber angle, Sampaolesi-like line, Scheie/Zentmayer stripe, and sometimes pigment deposition on the posterior lens capsule [1–4]. When IOP in patients with PDS is high or when signs of glaucomatous optic nerve develop, treatment should be initiated. Topical antiglaucoma medications are the first choice. Sometimes, laser procedures are considered. However, their current role is still unclear. Laser peripheral iridotomy (LPI)—an alternate treatment of elevated IOP—is one such method. This procedure creates an opening in the iris tissue and inhibits pigment release.

Ocular hypertension (OHT) is defined as the presence of intraocular pressure higher than 21 mmHg, with no optic

nerve damage or visual field loss. OHT is considered the most important risk factor for glaucoma. Without proper intervention, over 10% of the patients with ocular hypertension would develop glaucoma in the following 5 to 10 years [5]. Therefore, lowering IOP is the main strategy for preventing glaucoma in patients who are at risk. Regrettably, patients with OHT usually have none or very few ocular symptoms and little disturbance in visual acuity, making its diagnosis and treatment a huge challenge [6]. In addition, there is no consensus concerning the management of OHT.

The aim of this study was to assess the effects of LPI on lowering IOP in adolescents with OHT and concave configuration of the iris visible in anterior segment optical coherence tomography (AS-OCT). We assumed that peripheral iris concavity may be a risk factor for the development of PDS in adolescents, making pigment release easier. We also wanted to investigate whether laser therapy results in any changes in the anterior segment parameters and in the optic disc and retinal parameters, as assessed by optical coherence tomography.

2. Materials and Methods

Twenty-four patients with ocular hypertension and concave configuration of the iris were treated with laser peripheral iridotomy and followed up periodically in the Department of Paediatric Ophthalmology and Strabismus. None of the patients had PDS. Inclusion criteria were as follows: IOP >21 mmHg, age between 12 and 18 years, no signs of glaucoma, best-corrected visual acuity 1.0, no history of ocular or systemic disorders, and good quality of OCT images. The exclusion criterion was peripapillary atrophy. All patients underwent a full-eye examination, including best-corrected Snellen visual acuity, IOP measurement by TonoPen, visual field, corneal pachymetry, slit-lamp examination, and stereoscopic optic disc examination with a 78-diopter lens, gonioscopy, AS-OCT, and SLO/OCT Spectralis imaging.

The main items of investigation included evaluation of IOP and selected parameters of the anterior and posterior segments before and 2 months after laser treatment. To examine the iris configuration, central corneal thickness (CCT), anterior chamber depth (the distance between the anterior surface of the cornea and the anterior border of the lens capsule (ACD)), and scleral spur angle (SSA, a measurement of the angle formed at the apex of the iris recess), with the arms of the angle passing through the angle-opening distance/AOD/ at $500\,\mu m$ anterior to the scleral spur/AOD500 line/) in the nasal and temporal quadrants, all subjects underwent anterior segment optical coherence tomography (AS-OCT Visante, Carl Zeiss Meditec AG, Oberkochen, Deutschland) (Figures 1 and 2).

The AS-OCT was performed by an ophthalmic imaging technician. To perform the global neuroretinal rim (NRR, the neuroretinal tissue between the optic disc margin and the cup margin around the entire circumference of the optic nerve head) thickness and global retinal nerve fiber layer thickness (RNFL) measurements, optical coherence tomography (SLO/OCT Spectralis) has been used by the same ophthalmic imaging technician. The decision on whether LPI was clinically indicated was made by the ophthalmologist based on the AS-OCT images obtained during the first visit.

The LPI was performed using the Laser LightLas SLT/ YAG/577 (LightMed). All eyes were instilled with 2% pilocarpine prior. The LPI was placed in the superior region (between 11 and 1 o'clock) of the iris, as peripherally as possible, by the same ophthalmologist, and 8–12 shots of 3.0–3.5 mJ power were applied. After the procedure, patients were given a 5-day course of topical loteprednol etabonate 0.5% to relieve postlaser inflammation. At the last follow-up visit, AS-OCT was repeated for each patient to evaluate the iris configuration.

2.1. Statistical Analysis. The Shapiro–Wilk test was used to verify the hypotheses of normal distribution of the analyzed parameters. For comparing the parameter values before and after the treatment, the paired t-test and Wilcoxon signed-rank tests were applied. In addition, Pearson's rank correlation coefficient was used as a correlation measure between variables. The unpaired t-test was used to compare the two groups of patients. The Holm–Bonferroni method was applied for multiple comparisons. In all the comparisons, a 0.05 significance level was applied.

2.2. Ethical Issues. The study was conducted according to the tenets of the Declaration of Helsinki and had received approval from the Local Ethics Committee. All parents signed a consent form before the inclusion in the study.

3. Results

The study included 48 eyes of 24 patients with OHT. The average age of adolescents (14 boys and 10 girls) was 14.21 ± 1.41 years (13–17.5 years) on admission. All patients had best-corrected visual acuity of 1.0. Fourteen adolescents had myopia (4 cases-mild myopia, 2 cases-moderate myopia, and 8 cases-high myopia), and 10 people were emmetropic. The initial IOP of the 48 eyes was 23.21 ± 1.56 mmHg in RE and 22.96 ± 2.1 mmHg in LE before LPI. In addition, all 48 eyes had a concave configuration of the iris in AS-OCT. The selected examined parameters of the anterior and posterior segments are presented in Table 1. The iris became flat in all treated eyes after the laser treatment. There were no adverse postlaser complications. At the last follow-up visit, the average IOP was 17.58 ± 2.64 (14–21) mmHg in RE and 17.58 ± 2.86 mmHg (14–21) in LE, which was statistically lower than that of baseline ($p < 0.001$ and $p < 0.001$, respectively; Table 2).

There were statistically significant differences in SSA in the nasal and temporal quadrants in both the eyes before and after the laser treatment (Table 1). There were no essential changes in CCT and ACD in both the eyes after the laser procedure.

Image Analysis Report

ZEISS

Patient name:

Date of birth:
Patient ID:

Exam date: 4/24/2019 7:20:58 AM

Rx: Sphere: 0.0
Cylinder: 0.0
Axis: 0.0
Fixation Angle: 0.0
Polarization: 0.0
Orientation: 0.0

Protocol: All Scans
Scan: Anterior Segment Single

OD
Visante™OCT
ANTERIOR SEGMENT IMAGING

180°
0°

IC Angle - 180°
AOD500 : 0.769 mm
AOD750 : 1.113 mm
TISA500 : 0.233 mm²
TISA750 : 0.466 mm²
Scleral Spur Angle : 56.4 °

IC Angle - 0°
AOD500 : 0.771 mm
AOD750 : 0.939 mm
TISA500 : 0.245 mm²
TISA750 : 0.439 mm²
Scleral Spur Angle : 55.2 °

550 µm

3.06 mm
240 µm
12.42 mm
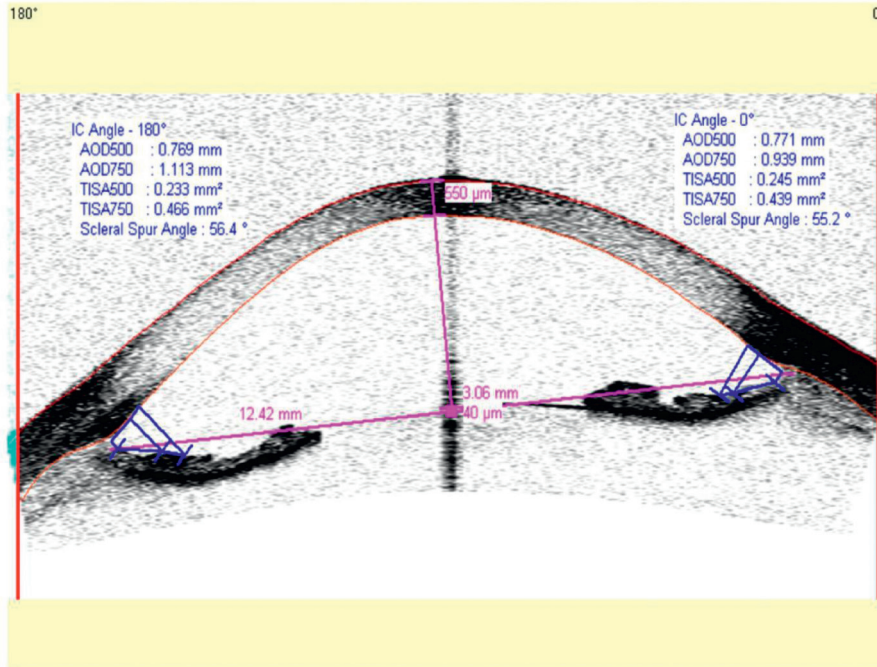
Planning
Institution: UDSK Bialystok
Planner: VisanteTech
Date: 2/14/2020 9:10:16 AM
Station: Klinika Okulistyki Dziecięcej
Serial Number: 1000-2030
Software Ver: 3.0.0.139

Acquisition
Institution: UDSK Bialystok
Operator: Visante operator
Station: Klinika Okulistyki Dziecięcej
Serial Number: 1000-2030
Software Ver: 3.0.0.139

Report Date: 12/9/2021 3:58:51 PM   Page: 1

FIGURE 1: Concave configuration of the iris before LPI.

Apart from the global retinal nerve fiber layer (RNFL) thickness in RE ($p = 0.003$), differences in global RNFL in LE and global neuroretinal rim (NRR) thickness in both eyes on OCT before and after LPI were not significant (Table 3).

We analyzed the effect of gender, age, and observation time on the intraocular pressure reduction after LPI. There were no differences in IOP reduction after LPI depending on gender (Table 4). There was also no correlation between age and IOP reduction after LPI (Table 5). We omitted the impact of myopia presence on the results of LPI due to limited sample size.

4. Discussion

Reverse pupillary block has been considered as one possible pathogenetic mechanism for backward bowing of the iris, leading to iris-zonular rubbing and distribution of melanin granules in the anterior chamber in PDS [1, 3, 7]. Karickhoff was the first to suggest that LPI may relieve the posterior bowing of the peripheral iris by equalizing the pressure between the anterior and posterior chambers [4]. LPI is an alternative treatment to medications, because it can reverse backward bowing of the iris and thus may prevent further

FIGURE 2: Flattening of the iris after LPI.

melanin dispersion and development of pigmentary glaucoma. The effect of Nd:YAG laser iridotomy as a prophylactic and potentially causal treatment in PDS can be effortlessly visualized by OCT [8]. However, the usability of LPI has not been completely established in both PDS and PG. Besides, nearly all publications are concerned with adult patients. Areaux and Grajewski reported the clinical and ultrasound biomicroscopic findings of PDS in a 14-year-old girl with Marfan syndrome and its favorable response to bilateral LPI [9].

In the present study, we have evaluated the effect of LPI in adolescents with ocular hypertension and a concave configuration of the iris visualized by optical coherence tomography. We assumed that the concave iris may contribute to the development of PDS, especially in myopic adolescents. Therefore, making the hole in the iris will protect from IOP elevation by relieving iridozonular contact and diminishing pigment release. We are conscious that although laser iridotomy produces a planar iris configuration, some eyes may retain a concave iris configuration. Iris flattening and a decrease in IOP were observed in all eyes treated with LPI. IOP was reduced by 5.5 mmHg after LPI with a mean follow-up of 1.54 ± 0.9 years. The mean decline after laser treatment was 5.6 mmHg in the right eyes and 5.4 mmHg in the left eyes.

Table 1: Changes in parameters of the anterior segment: central corneal thickness (CCT), anterior chamber depth (ACD), and scleral spur angle (SSA) before and after the laser treatment.

Parameter on AS-OCT	Before LPI	After LPI	p value
CCT-RE (μm)	548 ± 43	551 ± 45	0.565[a]
CCT-LE (μm)	552 ± 42	545 ± 36	0.18[b]
ACD-RE (mm)	3.38 ± 0.29	3.39 ± 0.27	0.41[a]
ACD-LE (mm)	3.35 ± 0.27	3.37 ± 0.22	0.53[a]
SSA in nasal quadrant-RE (°)	54.54 ± 5.62	46.58 ± 7.08	<0.001[a#]
SSA in temporal quadrant-RE (°)	49.29 ± 6.73	44.29 ± 8.6	0.004[a#]
SSA in nasal quadrant-LE (°)	53.42 ± 6.02	48.92 ± 6.04	0.006[a#]
SSA in temporal quadrant-LE (°)	52 ± 6.69	43.63 ± 9.19	<0.001[a#]

[a]p value for the paired t-test, [b]p value for the Wilcoxon signed-rank test, and [#]statistically significant differences at the 0.05 significance level.

Table 2: Values of intraocular pressure (IOP) before and after laser peripheral iridotomy.

	Before LPI	After LPI	p value
Mean intraocular pressure (IOP) RE (mmHg)	23.21 ± 1.56	17.58 ± 2.64	<0.001[a#]
Mean intraocular pressure (IOP) LE (mmHg)	22.96 ± 2.1	17.58 ± 2.86	<0.001[a#]

[a]p value for the paired t-test and [#]statistically significant differences at the 0.05 significance level.

Table 3: Changes in global retinal nerve fiber layer (RNFL) and global neuroretinal rim (NRR) thickness on OCT before and after the laser peripheral iridotomy.

Parameter on SLO/OCT	Before LPI	After LPI	Significance
Global RNFL-RE (μm)	94.63 ± 10.46	96.63 ± 9.64	0.003[b#]
Global RNFL-LE (μm)	95.54 ± 9.6	97.96 ± 11.52	0.07[b]
Global NRR-RE (μ)	307.67 ± 50.26	316.75 ± 53.83	0.038[b]
Global NRR-LE (μ)	316.92 ± 57. 39	324.63 ± 55.17	0.047[b]

[a]p value for the paired t-test and [#]statistically significant differences at the 0.05 significance level.

Table 4: Comparison between gender and IOP reduction after LPI.

	Male ($n = 14$) Mean ± Std	Female ($n = 10$) Mean ± Std	p value[a]
IOP in RE after LPI (mmHg)	16.71 ± 2.23	18.8 ± 2.78	0.07
IOP in LE after LPI (mmHg)	16.86 ± 2.6	18.6 ± 3.03	0.16

[a]p value for the unpaired t-test.

Table 5: Correlation between age and IOP reduction after LPI.

	Pearson's correlation coefficient	p value
IOP in RE after LPI (mmHg)	−0.316	0.13
IOP in LE after LPI (mmHg)	−0.172	0.42

Gandolfi and Vecchi have proved that YAG laser iridotomy may reduce the incidence of ocular hypertension in eyes affected by PDS. In their opinion, this effect, being less pronounced after 40 years of age, may be of clinical relevance in young subjects [10]. Similar results were obtained by Qing et al., who noted that LPI effectively prevents progression in eyes with PDS [11]. However, at the end of the 10-year follow-up, approximately one-third of the whole PDS patient population treated with LPI showed an IOP increase of 5 mmHg or higher in at least 1 eye [12]. Similar observations were made by Scott et al., who showed that there was no benefit of LPI in preventing progression from PDS with ocular hypertension to pigmentary glaucoma within 3 years of follow-up [13]. The lack of reduction in IOP after LPI in patients with PDS/PG may be explained by the fact that this procedure cannot correct structural abnormalities or changes in trabecular meshwork. Besides, among five trials assessing the effectiveness of LPI, no clear benefit was reported for this procedure compared with no laser in eyes with PG for visual field loss or PDS as regards preventing visual field progression [14].

We have observed an increase in ACD and a decrease in CCT in both eyes after LPI, but these changes were not statistically significant (Table 1). In the current study, the mean CCT was $548 \pm 43 \,\mu$m in the right eyes and $552 \pm 42 \,\mu$m in the left eyes, so the corneas were rather thin. The ophthalmologist should consider thin corneal thickness measurements as one of the key risk factors for developing glaucoma. The Ocular Hypertension Treatment Study (OHTS) determined that a thin cornea is a very important factor that can predict the transformation of ocular hypertension in primary open-angle glaucoma [15]. Five-year follow-up has shown that patients with CCT lower than $555 \,\mu$m had a 3 times higher risk of developing the disease in comparison with a subject with a CCT higher than $588 \,\mu$m. This could mean the possibility that some of our patients have an additionally increased risk of developing POAG in the future.

In the current study, we observed the significant reduction of SSA as the result of iris flattening (Table 1). SSA in both nasal and temporal quadrants were significantly smaller after LPI. This post-LPI narrowing of the scleral spur angles

may be explained by the iris flattening. In the current study, we observed the iris flattening in all eyes after the laser treatment and it persisted during the last follow-up (mean 1.54 ± 0.9 years). Aptel et al. evaluated anterior chamber volume, iris volume, and iridolenticular contact area before and after LPI in eyes with PDS using AS-OCT [16]. After estimating the biometric parameters, they concluded that PDS eyes show little resistance to an iris that is stretched and pushed against the lens when there is a pressure difference across the iris. It is possible to assume that all eyes of our patients have a normal structure of iris, which responds to LPI with flattening, leading to significant lowering of IOP.

The assessment of circumpapillary RNFL thickness serves as an important tool in the diagnosis and follow-up of glaucoma. SD-OCT is one of the imaging modalities that is most often used worldwide to evaluate the optic nerve head and the neuroretinal rim. We have observed that the flattening of the iris in examined eyes was associated with both a lowering of intraocular pressure and an improvement in both global RNFL thickness and global NRR thickness in both eyes after the laser treatment, but only changes in RNFL in RE were significant (Table 3). In the current study, the mean peripapillary RNFL thickness was $94.63 \pm 10.46\,\mu m$ in the right eyes and $95.54 \pm 9.6\,\mu m$ in the left eyes and this corresponds with RNFL values reported in other studies [17–19]. To our astonishment, we observed $2\,\mu m$ RNFL thickening in the right eyes ($p = 0.003$) and $2.42\,\mu m$ RNFL thickening in the left eyes (NS) after LPI. One of the explanations may be the decentration of the circle scan during OCT—its displacement by just $0.1\,mm$ can result in a $2.3 \pm 2.0\,\mu m$ error in average RNFL thickness [20]. It is also possible that ageing itself may be the reason for these changes in the paediatric population. Another reason is the fact that RNFL mainly consists of the axons of the retinal ganglion cells, but it is also composed of glial cells and blood vessels [21]. Numerous studies have shown that ocular blood flow increases after a significant decline in IOP [22, 23]. In the study of Ch'ng at al., peripapillary RNFL thickness was transiently increased in a total of 40 eyes 1 month after glaucoma surgery, but in their opinion, RNFL thickness was completely IOP independent [23]. Our patients were adolescents, and we can theoretically assume that perhaps the lowering of IOP after LPI increased their ocular blood flow and it could thus contribute to RNFL thickening. Certainly, further research is essential for the evaluation of ocular blood flow in OHT using OCTA.

The improvement of global NRR could be a comparable occurrence to congenital glaucoma, although we know that such a comparison is controversial. The phenomenon of reversing the glaucomatous cupping of the optic disc following lowering of the IOP was originally recognized in infants [24]. Wu et al. observed a reduction in optic disc cupping after trabeculotomy in primary congenital glaucoma [25]. Similar results were obtained by Meirelles et al., who noted that there was a significant difference between the preoperative and postoperative C/D in childhood glaucoma [26]. One of the mechanisms of cupping reversal seen after lowering IOP in paediatric glaucoma is the shrinkage of a stretched scleral canal [27]. Gietzelt et al. reported that

structural reversal of disc cupping after trabeculectomy markedly influences the Bruch membrane opening-based parameters for even more than 1 year [28].

In the current study, none of our patients had side effects after LPI. However, the possibility of postlaser adverse events should be considered before deciding on the laser procedure. Postoperative inflammation, halos, transient hemorrhage, elevated IOP, posterior synechiae, retinal detachment, or cataract may happen [14, 28, 29]. Scott et al. reported 1 case of cataract out of 52 patients after laser treatment in a prospective, randomized, controlled 3-year trial [13]. The most commonly reported adverse event, besides cataract, was mild iritis.

Although the risks of LPI may be minimal, the systematic review by Michelessi and Lindsley found no high-quality evidence for or against the usefulness of iridotomy for improving long-term outcomes of visual field loss in PG and visual field progression in PDS [14]. A possible reduction in iris concavity and iridozonular contact with less pigment dispersion may not mitigate existing dysfunction of the trabecular meshwork nor lead to a significant reduction in long-term visual function loss. However, LPI may have long-term beneficial effects on IOP in eyes with PDS and in eyes at high risk of IOP decompensation. On the other hand, Buffault et al. analyzed randomized controlled trials and two cohort studies (286 eyes of 218 participants), which tried to assess the effects of LPI for PDS and PG [30]. They noticed that the effects of LPI on visual field changes or progression have not been established in PG and PDS. They concluded that there is no scientific evidence to advocate PI as a treatment for PDS and PG.

It is estimated that up to 60–80% of patients with PDS and PG are myopes [7, 31]. Interestingly, increasing myopia is a predictor of increasing iridolenticular contact, independent of the presence of PDS [32]. Campbell suggested that the enlargement of the myopic eye in young patients creates more space for the peripheral iris to bow posteriorly [33]. In the current study, among our 24 patients, more than half of them (14/58, 3%) were myopic and the other 10 had emmetropia at baseline. The results of the last follow-up showed that the number of emmetropic patients has not changed and the percentage of myopic patients was the same as at the start of the study. The degree of myopia has increased in 10 patients (by a mean of $-0.83\,D$), and in 4 patients, their refractive error have remained unchanged. We noticed no significant differences in the effectiveness of LPI in myopic eyes compared with emmetropic eyes. Unfortunately, we omitted the impact of myopia presence on the effect of LPI due to the small sample size.

The main limitation of this study is the small sample size, the COVID-19 pandemic being the main reason. Secondly, there is a relatively short time period of observation of our patients, again due to the pandemic. In the study with a follow-up period of 10–20 years, the relationship between the concave iris configuration and possible PDS development/prevention might be objectifiable. We are aware that additional randomized controlled trials on LPI should be compared to other forms of treatment (or no treatment) in eyes with OHT and iris concavity. We also realize that

TonoPen is not the gold standard technique to determine IOP. Furthermore, we do not have a control group, which could consist of patients with one eye after LPI and another with no treatment.

5. Conclusion

In the current study, laser peripheral iridotomy resulted in an IOP-lowering effect and iris flattening in adolescent eyes with a concave configuration of the peripheral iris.

Data Availability

The statistical data used to support the findings are available from the corresponding author upon request.

Conflicts of Interest

The authors declare that they have no conflicts of interest.

Acknowledgments

References

[1] N. Niyadurupola and D. C. Broadway, "Pigment dispersion syndrome and pigmentary glaucoma-a major review," *Clinical & Experimental Ophthalmology*, vol. 36, no. 9, pp. 868–882, 2008.

[2] C. Y. Mardin, M. Küchle, N. X. Nguyen, P. Martus, and G. O. Naumann, "Quantification of aqueous melanin granules, intraocular pressure and glaucomatous damage in primary pigment dispersion syndrome," *Ophthalmology*, vol. 107, no. 3, pp. 435–440, 2000.

[3] G. Scuderi, M. T. Contestabile, L. Scuderi, A. Librando, V. Fenicia, and S. Rahimi, "Pigment dispersion syndrome and pigmentary glaucoma: a review and update," *International Ophthalmology*, vol. 39, no. 7, pp. 1651–1662, 2019.

[4] J. R. Karickhoff, "Pigmentary dispersion syndrome and pigmentary glaucoma: a new mechanism concept, a new treatment, and a new technique," *Ophthalmic Surgery*, vol. 23, no. 4, pp. 269–277, 1992.

[5] Y. Y. Sun, W. W. Chen, and N. L. Wang, "Diagnosis and treatment of ocular hypertension," *Zhonghua Yan Ke Za Zhi*, vol. 52, no. 7, pp. 542–546, 2016.

[6] X. H. Sun, "Management of juvenile ocular hypertension," *Zhonghua Yan Ke Za Zhi*, vol. 48, no. 6, pp. 481–484, 2012.

[7] S. M. Farrar, M. B. Shields, K. N. Miller, and C. M. Stoup, "Risk factors for the development and severity of glaucoma in the pigment dispersion syndrome," *American Journal of Ophthalmology*, vol. 108, no. 3, pp. 223–229, 1989.

[8] Y. Siddiqui, R. D. Ten Hulzen, J. D. Cameron, D. O. Hodge, and D. H. Johnson, "What is the risk of developing pigmentary glaucoma from pigment dispersion syndrome?" *American Journal of Ophthalmology*, vol. 135, no. 6, pp. 794–799, 2003.

[9] R. G. Areaux Jr and A. L. Grajewski, "Pigment dispersion syndrome and response to laser peripheral iridotomies in a child with Marfan syndrome," *Journal of American Association for Pediatric Ophthalmology and Strabismus*, vol. 23, no. 5, pp. 300–302, 2019.

[10] S. A. Gandolfi and M. Vecchi, "Effect of a YAG laser iridotomy on intraocular pressure in pigment dispersion syndrome," *Ophthalmology*, vol. 103, no. 10, pp. 1693–1695, 1996.

[11] G. Qing, S. Zhang, H. Wang et al., "Long-term efficacy of laser peripheral iridotomy in preventing progression in eyes with pigment dispersion syndrome," *Zhonghua Yan Ke Za Zhi*, vol. 50, no. 7, pp. 536–540, 2014.

[12] S. A. Gandolfi, N. Ungaro, M. G. Tardini, S. Ghirardini, A. Carta, and P. Mora, "A 10-year follow-up to determine the effect of YAG laser iridotomy on the natural history of pigment dispersion syndrome," *JAMA Ophthalmology*, vol. 132, no. 12, pp. 1433–1438, 2014.

[13] A. Scott, A. Kotecha, C. Bunce et al., "YAG laser peripheral iridotomy for the prevention of pigment dispersion glaucoma: a prospective, randomized, controlled trial," *Ophthalmology*, vol. 118, no. 3, pp. 468–473, 2011.

[14] M. Michelessi and K. Lindsley, "Peripheral iridotomy for pigmentary glaucoma," *Cochrane Database of Systematic Reviews*, vol. 2, Article ID CD005655, 2016.

[15] M. O. Gordon, J. A. Beiser, J. D. Brandt et al., "The ocular hypertension treatment study: baseline factors that predict the onset of primary open-angle glaucoma," *Archives of Ophthalmology*, vol. 120, no. 6, pp. 714–720, 2002.

[16] F. Aptel, S. Beccat, V. Fortoul, and P. Denis, "Biometric analysis of pigment dispersion syndrome using anterior segment optical coherence tomography," *Ophthalmology*, vol. 118, no. 8, pp. 1563–1570, 2011.

[17] T. Alasil, K. Wang, P. A. Keane et al., "Analysis of normal retinal nerve fiber layer thickness by age, sex, and race using spectral domain optical coherence tomography," *Journal of Glaucoma*, vol. 22, no. 7, pp. 532–541, 2013.

[18] L. E. Vazquez, J.-C. Mwanza, G. Triolo et al., "Separation and thickness measurements of superficial and deep slabs of the retinal nerve fiber layer in healthy and glaucomatous eyes," *Ophthalmology Glaucoma*, vol. 3, no. 1, pp. 66–75, 2020.

[19] D. Li, F. G. Rauscher, E. Y. Choi et al., "Sex-specific differences in circumpapillary retinal nerve fiber layer thickness," *Ophthalmology*, vol. 127, no. 3, pp. 357–368, 2020.

[20] C. Y. L. Cheung, C. K. F. Yiu, R. N. Weinreb et al., "Effects of scan circle displacement in optical coherence tomography retinal nerve fibre layer thickness measurement: a RNFL modelling study," *Eye*, vol. 23, no. 6, pp. 1436–1441, 2009.

[21] D. C. Hood and R. H. Kardon, "A framework for comparing structural and functional measures of glaucomatous damage," *Progress in Retinal and Eye Research*, vol. 26, no. 6, pp. 688–710, 2007.

[22] M. C. Grieshaber and J. Flammer, "Blood flow in glaucoma," *Current Opinion in Ophthalmology*, vol. 16, no. 2, pp. 79–83, 2005.

[23] T. W. Ch'ng, K. Gillmann, K. Hoskens, H. L. Rao, A. Mermoud, and K. Mansouri, "Effect of surgical intraocular pressure lowering on retinal structures-nerve fibre layer, foveal avascular zone, peripapillary and macular vessel density: 1 year results," *Eye*, vol. 34, no. 3, pp. 562–571, 2020.

[24] A. L. Ely, M. A. El-Dairi, and S. F. Freedman, "Cupping reversal in pediatric glaucoma-evaluation of the retinal nerve fiber layer and visual field," *American Journal of Ophthalmology*, vol. 158, no. 5, pp. 905–915, 2014.

[25] S. C. Wu, S. C. M. Huang, C. L. Kuo, K. K. Lin, and S. M. Lin, "Reversal of optic disc cupping after trabeculotomy in primary congenital glaucoma," *Canadian Journal of Ophthalmology*, vol. 37, no. 6, pp. 337–341, 2002.

[26] S. H. S. Meirelles, C. R. Mathias, R. R. Bloise et al., "Evaluation of the factors associated with the reversal of the disc cupping

after surgical treatment of childhood glaucoma," *Journal of Glaucoma*, vol. 17, no. 6, pp. 470–473, 2008.

[27] H. Mochizuki, A. G. Lesley, and J. D. Brandt, "Shrinkage of the scleral canal during cupping reversal in children," *Ophthalmology*, vol. 118, no. 10, pp. 2008–2013, 2011.

[28] C. Gietzelt, J. Lemke, F. Schaub et al., "Structural reversal of disc cupping after trabeculectomy alters Bruch membrane opening-based parameters to assess neuroretinal rim," *American Journal of Ophthalmology*, vol. 194, pp. 143–152, 2018.

[29] P. A. Newman-Casey and J. D. Stein, "Yag laser peripheral iridotomy for the prevention of pigment dispersion glaucoma: a prospective, randomized, controlled trial," *Evidence-Based Ophthalmology*, vol. 12, no. 4, pp. 194-195, 2011.

[30] J. Buffault, B. Leray, A. Bouillot, C. Baudouin, and A. Labbé, "Role of laser peripheral iridotomy in pigmentary glaucoma and pigment dispersion syndrome: a review of the literature," *Journal Français d'Ophtalmologie*, vol. 40, no. 9, pp. e315–e321, 2017.

[31] S. M. Farrar and M. B. Shields, "Current concepts in pigmentary glaucoma," *Survey of Ophthalmology*, vol. 37, no. 4, pp. 233–252, 1993.

[32] J. M. Liebmann, C. Tello, S. J. Chew, H. Cohen, and R. Ritch, "Prevention of blinking alters iris configuration in pigment dispersion syndrome and in normal eyes," *Ophthalmology*, vol. 102, no. 3, pp. 446–455, 1995.

[33] D. G. Campbell, "Pigmentary dispersion and glaucoma: a new theory," *Archives of Ophthalmology*, vol. 97, no. 9, pp. 1667–1672, 1979.

Hindawi

Research Article

The Efficacy of Clinical Tests to Diagnose Evaporative Dry Eye Disease Related to Meibomian Gland Dysfunction

Jerry R. Paugh [1], **Tiffany Nguyen,**[1] **Alan Sasai** [1], **Elaine Chen** [1], **Melinda Thomas De Jesus** [1], **Justin Kwan,**[1] **Andrew Loc Nguyen,**[2] **Marjan Farid** [3], **Sumit Garg** [3], **and James V. Jester**[3,4]

[1]Southern California College of Optometry, Marshall B. Ketchum University, Fullerton, CA, USA
[2]Department of Mathematics, California State University, Fullerton, CA, USA
[3]Gavin Herbert Eye Institute, University of California, Irvine, CA, USA
[4]Biomedical Engineering, University of California, Irvine, CA, USA

Correspondence should be addressed to Jerry R. Paugh; jpaugh@ketchum.edu

Objectives. To determine the efficacy of widely available subtype clinical tests to characterize evaporative dry eye disease (EDED) related to meibomian gland dysfunction (MGD) compared to normal and to validate those clinical cut points in an independent sample. *Methods.* A diagnostic accuracy study (52 subjects), an investigator-masked study, was followed by a larger independent sample (364 subjects) analysis to confirm efficacy in normal and EDED subjects. All subjects were 18 years of age and older and were classified using a battery of clinical tests for dry eye that included symptoms, tear meniscus height, tear stability, ocular staining, evaporative-specific tests, and the Schirmer I test. *Results.* Normal (nondry eye; $n = 26$) and EDED ($n = 26$) subjects completed the efficacy study. The global tests of tear breakup time, staining, and symptoms all produced AUCs ≥ 0.70, representing acceptable discrimination. EDED-specific tests of eyelid marginal signs, gland secretion quality, and gland loss did not demonstrate acceptable test efficacy or differences between normal and EDED subjects. In a larger, independent sample of normal and EDED subjects, gland secretion quality and eyelid marginal score achieved acceptable diagnostic levels: AUCs of 0.789 (CI: 0.734–0.844) and 0.729 (CI: 0.648–0.810), respectively, but not lipid interferometry grade or lower eyelid gland dropout estimated using meiboscopy. *Conclusions.* Meibomian gland secretion quality is an efficient and useful functional indicator in EDED and should be incorporated into core outcome sets for this dry eye subtype.

1. Introduction

Dry eye disease (DED) is a common clinical condition, affecting 5 to 50% of the population, depending on the sampling approach and diagnostic criteria [1]. Of all the dry eye diseases, evaporative dry eye disease (EDED) related to meibomian gland dysfunction (MGD) appears to be the more prevalent subtype [2]. The prevalence of EDED may be much greater in Asian populations compared to other ethnicities [1, 3, 4].

As a common subtype of dry eye, EDED is a condition with major health and quality of life impacts that requires diagnostic methods that can also monitor treatment. In medical specialties, sets of clinical outcome criteria including those important to patients are developed by consensus groups into core outcome sets (COSs) [5]. COSs are used to standardize randomized clinical trials so that the effects of treatments can be uniformly assessed across trials such as in systematic reviews of treatment efficacy [5]. The parameters that comprise the COSs must be efficacious in diagnosing the medical condition and also quantitative to establish the severity of the condition and to monitor the response to treatment. Despite several consensus recommendations to diagnose EDED, [2, 6] tests have not been globally adopted that might comprise a COS battery for EDED related to MGD.

The 2011 MGD workshop report (diagnostic subcommittee [6]) suggested tests for EDED related to MGD diagnosis appropriate to a general clinic and additional tests for more specialized ocular surface clinics that may engage

in clinical research. The tests for a general clinic included symptoms, lower tear meniscus height, tear osmolarity (if available), fluorescein breakup time, corneal and conjunctival staining, and the Schirmer I test. The general clinic recommendations also included observation of eyelid morphological features, gland expression/expressibility, and meibography. Recent surveys suggest that these general clinic tests are commonly used by ophthalmic practitioners [7, 8].

It was the purpose of this investigation to determine the test efficacy (sensitivity and specificity) of widely available clinical tests to characterize EDED related to MGD compared to normal and to validate those preliminary clinical cut points in an independent sample.

2. Methods

This was a two-part investigation: an initial rigorous efficacy study (adhering to the STARD 2015 statement (Bossuyt et al. [9]), as shown in the flow diagram, Figure 1) and an independent sample conducted with identical methods and classification criteria. Both subject groups comprised a convenience sample of clinic-based subjects. Subjects were over the age of 18 years and provided written consent prior to the start of the study. These studies were approved by the Institutional Review Boards of Marshall B. Ketchum University and the University of California at Irvine.

Participant flow and investigator masking for diagnostic efficacy samples. The index test was the summed MGD score (as shown in the text) at a cut point of 5.4 on the 0–12 scale. The reference standard was clinical diagnosis of normal or EDE via the third masked examiner.

Major inclusion criteria were normal or dry eyes as determined by global DED tests, over age 18, and willingness to discontinue topical ocular drop use on the day of the assessment. Subjects were included if their dry eye management was stable for 30 days prior to enrollment. EDED was classified using either the lower eyelid gland secretion score ≥1.0 [10] or gland dropout using meiboscopy ≥1.0 [11]. Major exclusion criteria were blepharitis, ocular surgeries within 12 months of study start; active ocular allergy or infection; greater than mild ectropion, entropion, or ptosis; use of topical ocular medications except artificial tears; contact lens use; and punctal plugs within 30 days of study start. Aqueous deficient dry eye disease (ADDED) subjects were excluded based on the Schirmer I test for less than 5 mm of wetting in 5 minutes (without anesthesia) and tear meniscus height <0.20 mm [2].

Subjects for both studies underwent a comprehensive dry eye evaluation using the same tests from least to most invasive. For the efficacy study, separate masked examiners collected the global dry eye data (such as ocular history, tear stability, corneal, and conjunctival staining) or the specific meibomian gland data (such as lid marginal signs, gland expression, and meiboscopy). Symptoms (modified Schein, OSDI, and MGD-specific [12]), eyelid marginal signs (0 or 1 for present or absent orifice metaplasia, vascularity, capped glands, ridging, and marginal irregularity), fluorescein tear breakup time (TBUT; 2.0 μl of 1.0% NaFl; yellow filter used,

mean of three values), corneal (fluorescein) and conjunctival (lissamine green) staining with NEI and Oxford schemes, gland secretion (average score, entire lower eyelid, using the Bron 0–3 scale [10] using a cotton bud with gentle expression), lower eyelid meiboscopy (entire lower eyelid; percentage gland loss based on ½ and whole glands missing) [13], and the Schirmer I test without anesthesia were assessed. The central 8 glands of each eyelid were evaluated for meibomian glands yielding liquid secretion (MGYLS) using the Meibomian Gland Evaluator [14]. For the independent sample, the abovementioned tests were employed, but in addition, lipid layer appearance using white light interferometry (Yokoi scale, [15] custom apparatus, and 1–5 scale) was assessed.

The classification scheme used to assign subjects as normal or EDED was identical to that reported previously [16]. In brief, a subject was classified as EDED related to MGD if the OSDI was ≥13, the TBUT was <6.0 seconds [16], combined corneal and conjunctival staining >6.0 (NEI system, [17] 0–33 total scale; 6/33 ≈ 18% of total scale), and either meibomian gland secretion grade using 0.1 scale unit increments of >1.0 or gland dropout >1.0 [10]. Subjects were classified as normal (i.e., not dry eye) if TBUT was >6.0 seconds, total NEI staining was ≤6.0, and secretion and gland dropout scores were <1.0.

2.1. Statistical Methods. Statistical analysis was undertaken using Minitab version 18 (Minitab LLC, State College, PA, USA). An *a priori* sample size estimate was made to compare normal and EDED subjects relative to a cumulative score comprised of functional and morphological assessments (index test) [13]. The composite score was comprised of eyelid marginal changes (0–5), mean lower eyelid meibomian gland secretion grade (0–3), and gland dropout using meiboscopy (0–4). This provided a semicontinuous scale of 0–12.

Relative to a receiver operating characteristic (ROC) curve, an area under the curve (AUC) of 0.80 (excellent discrimination) vs. the chance level of 0.50 [18] was the efficacy target. Assuming Type I and II error levels of 0.05 and 0.20, respectively, equal standard deviations in the normal and EDED groups, and a two-tailed hypothesis, 13 subjects per group provided 0.81 statistical power.

For both the index test and the independent sample analyses, multiple regression analysis (continuous variables) and polytomous logistic regression (ordinal variables) were undertaken to examine the effects of age, sex, and dry eye subtype (normal vs. EDED) on the parameters of interest. Comparisons of normal vs. EDED were controlled for age and sex if significant from the continuous or ordinal analysis. For continuous data, ANOVAs including age, gender, and dry eye type were conducted, with Tukey pairwise tests for significant factors between normal and EDED subjects. The *p* values were two-tailed and adjusted for multiple comparisons with $p < 0.05$ considered significant. 95% confidence intervals were constructed for each comparison. For ordinal data, age, gender, and dry eye subtype were compared using odds ratios and 95% CIs; those
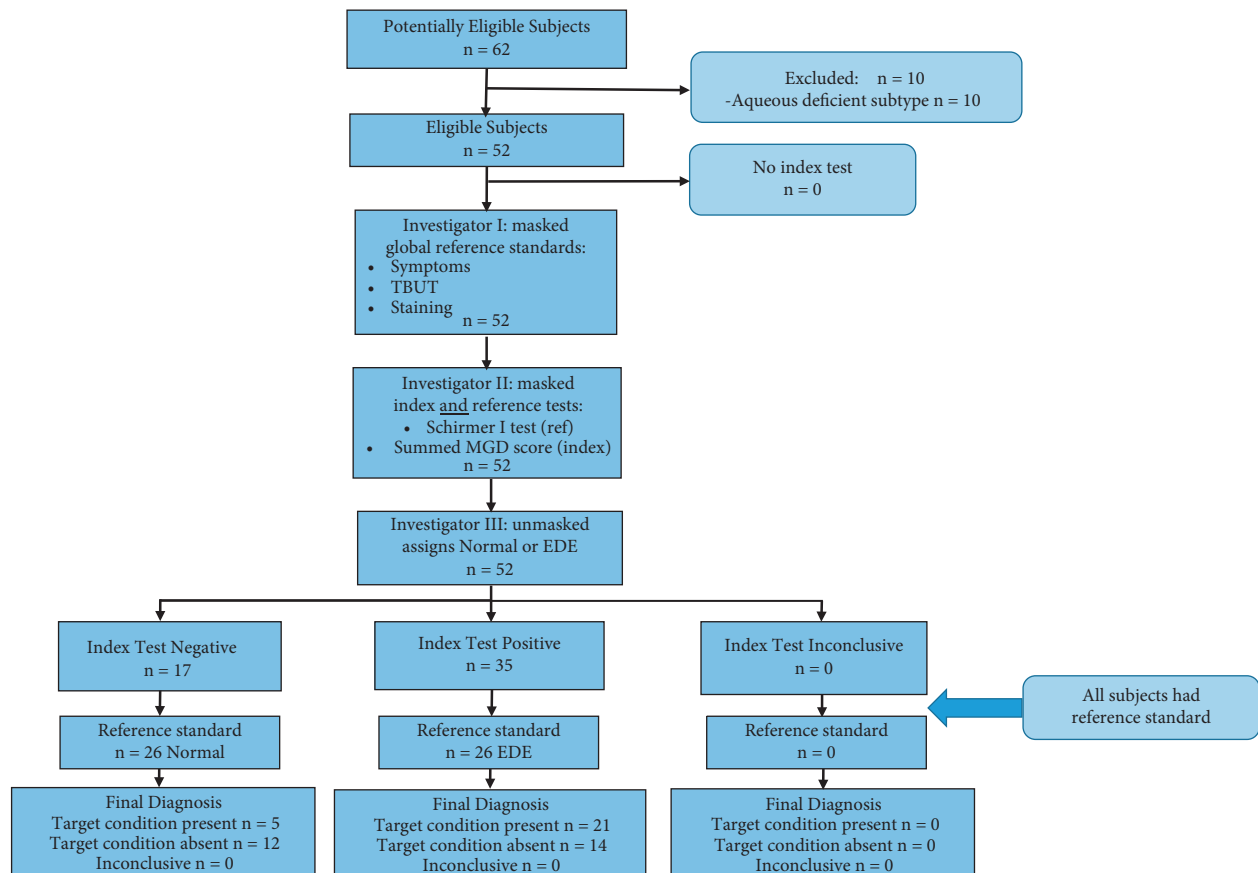
Figure 1: Participant flow diagram; STARD–2015 reporting guidelines.

CIs that included the null value of 1.0 were not considered significant.

The ROC curve analysis for AUC and optimum cut point (defined as maximal sensitivity and specificity, or the cut point with the greater sensitivity if these were unequal) was undertaken for the normal and EDED data.

3. Results

Twenty-six normal, 10 ADDED, and 26 EDED subjects completed the study. The mean ages (±SD) were 53.2 (±14.9), 55.7 (±6.9), and 61.0 (±17.1) for the normal, ADDE, and EDED subjects, respectively. No statistical difference was found for age in the three groups (ANOVA, $p = 0.184$). The ADDE subject data were eliminated from the data set so that only normal and EDED subjects were compared.

AUCs, cut points, sensitivity, and specificity values were derived from ROC analysis (Table 1). The index measure, summed MGD score, attained 0.81 sensitivity, but only 0.46 specificity and an AUC of 0.578, slightly better than chance [18]. The summed MGD score did not differentiate normal from EDED subjects ($p = 0.960$). The global dry eye tests of symptom questionnaires, TBUT, and staining scores achieved test sensitivities near or above 0.70, considered an acceptable level for an effective dry eye test [6], as opposed to the EDED-specific tests for a general clinic that did not achieve an acceptable level of discrimination.

Additional data were available from several prospective studies conducted concurrent with the efficacy study using identical test methods and classification criteria. The available data varied by test measure, up to a maximum number of 364 charts from clinically normal subjects and subjects having EDED. The EDED test data of this independent sample are summarized in Table 2 and were used for normal vs. EDED comparison and ROC curve and cut point determination.

Regression analysis was undertaken for marginal signs (0–5), gland secretion quality (0–3), and gland dropout (0–4), all from the lower eyelid of the right eye. This demonstrated a significant association with age for all three parameters (p values were <0.001 for marginal signs and secretion quality, and $p = 0.034$ for gland dropout).

Receiver operating characteristic (ROC) analysis was undertaken for the five EDED-specific clinical tests. Comparisons between normal and EDED subjects are presented in Table 2, and the ROC curves in Figure 2.

Cut points were determined on the basis of maximal values sensitivity and specificity.

Gland secretion: AUC 0.789 (95% CI: 0.734–0.844), cut point 1.1 (0–3 scale; 0.1 unit scale increments); sensitivity = 0.79, specificity = 0.78; and $n = 136$ normal, 228 EDED subjects

Marginal eyelid signs: AUC 0.729 (95% CI: 0.648–0.810), cut point 4.5 (0–5 scale);

TABLE 1: Efficacy study: test values and diagnostic parameters of EDED-specific and global dry eye tests.

EDE-specific tests	Scale range	Test parameter		AUC (95% CI)	Cut point	Sensitivity (CI); specificity (CI)	Significance[a] (95% CI)
		Normal $n = 26$ mean (SD or IQR)	EDED $n = 26$ mean (SD or IQR)				
Marginal signs	0–5	4 (3–5)	4 (3–5)	0.554 (0.40–0.71)	3.5	0.65 (0.47–0.83); 0.46 (0.27–0.65)	$p = 0.440$; OR 0.64 (0.21–1.97)[b,c]
Glands expressing	0–8	4 (2–5; ($n = 20$)	2 (1–4; $n = 23$)	0.643 (0.48–0.81)	3.5	0.70 (0.52–0.88); 0.55 (0.36–0.74)	$p = 0.508$; OR 0.66 (0.20–0.223)[b,c]
Gland secretion	0–3 in 0.1 unit steps	1.40 (0.6)	1.57 (0.6)	0.589 (0.44–0.74)	1.95	0.31 (0.13–0.49); 0.85 (0.71–0.99)	$p = 0.232p$ (−0.53–0.13)
Gland atrophy	0–4	1.34 (0.7)	1.57 (0.7)	0.612 (0.46–0.77)	1.25	0.69 (0.51–0.87); 0.58 (0.39–0.77)	$p = 0.590$ (−0.54–0.31)
Summed MGD score	0–12	6.35 (2.0)	6.94 (2.0)	0.578 (0.42–0.74)	5.35	0.81 (0.66–0.96); 0.46 (0.27–0.65)	$p = 0.960$ (−1.05–1.00)[b]
MGD-specific questionnaire	0–174	54.1 (37)	84.1 (32)	**0.739 (0.60–0.88)**	80.5	0.65 (0.47–0.83); 0.75 (0.58–0.92)	$p = 0.021$ (−44.8 to −3.8)
Global tests							
Modified Schein survey	0–24	7.7 (4.6)	11.2 (3.9)	**0.745 (0.61–0.88)**	9.5	0.73 (0.56–0.90); 0.69 (0.51–0.87)	$p = 0.026$ (**−5.48 to −0.37**)
OSDI	0–100	19.9 (16)	39.9 (23)	**0.757 (0.62–0.89)**	34.4	0.65 (0.47–0.83); 0.85 (0.71–0.99)	$p = 0.008$ (−27.68 to −4.28)
TBUT	Cont.	12.6 (9)	3.8 (1)	**0.916 (0.84–0.99)**	5.95	0.92 (0.82–1.00); 0.80 (0.65–0.95)	$p < 0.001$ (4.10–11.50)
NEI staining	0–33	5.1 (4)	11.9 (7)	**0.822 (0.70–0.94)**	7.50	0.77 (0.61–0.93); 0.81 (0.66–0.96)	$p < 0.001$ (−10.1 to −3.6)
Oxford staining	0–15	4.0 (2)	7.9 (3)	**0.838 (0.73–0.95)**	6.5	0.73 (0.56–0.90); 0.92 (0.82–1.00)	$p < 0.001$ (−5.38 to −2.04)

[a]Normal vs. EDED; polytomous logistic regression (ordinal data) or multivariable regression analysis (continuous data; Tukey simultaneous tests, controlled for age and gender; $p$values adjusted for multiple comparisons). [b]Significant for age ($p < 0.05$). [c]Significant for sex ($p < 0.05$).

TABLE 2: Descriptive and inferential statistical data (OD data only); independent sample analysis.

Test parameter	Scale range	Normal median (IQR) or mean (SD)	EDED median (IQR) or mean (SD)	Significance[a] (95% CI)
Marginal Signs Normal ($n = 94$) EDE ($n = 93$)	0–5	3 (2–4)	5 (3.25–5)	$p = 0.954$; OR = 1.02 (CI = 0.54–1.91)[b]
Gland Secretion Normal ($n = 136$) EDE ($n = 228$)	0–3	1.0 (0.6)	1.6 (0.6)	$p < 0.001$ (−0.67 to −0.40)[b,c]
Gland atrophy (meiboscopy) Normal ($n = 100$) EDE ($n = 229$)	0–4	1.0 (0.6)	1.4 (0.8)	$p < 0.001$ (−0.56 to −0.18)[b]
MGD specific Questionnaire Normal ($n = 57$) EDE ($n = 88$)	0–174	55.1 (42)	69.4 (38)	$p = 0.285$ (−20.22–5.99)[c]
Interferometry Normal ($n = 85$) EDE ($n = 190$)	1–5	2.32 (0.6)	2.49 (0.7)	$p = 0.176$ (−0.29–0.05)[b,c]

[a]Normal vs. EDED; polytomous logistic regression (ordinal data) or multivariable regression analysis (continuous data; Tukey simultaneous tests, controlled for age and gender; $p$values adjusted for multiple comparisons). [b]Significant for age ($p < 0.05$). [c]Significant for sex ($p < 0.05$).
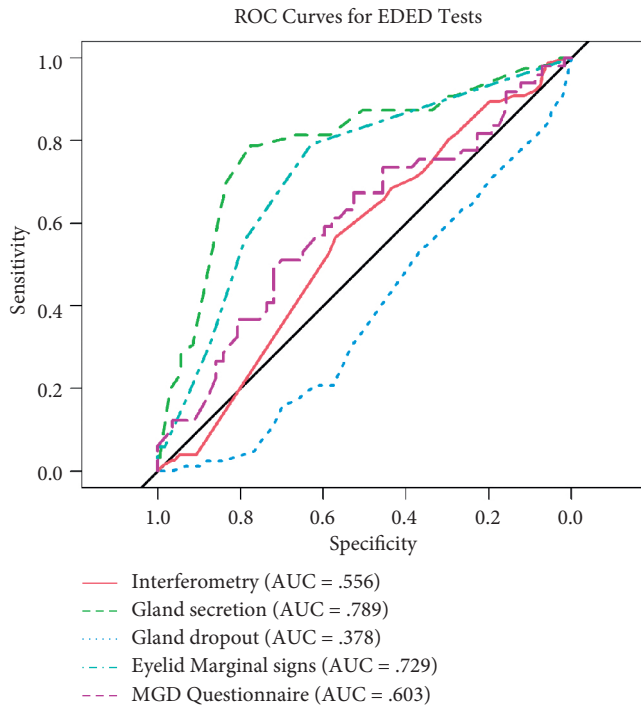
FIGURE 2: Receiver operating characteristic curves for EDE-specific tests, independent sample.

sensitivity = 0.79, specificity = 0.63; and $n = 94$ normal, 93 EDED subjects

MGD-specific questionnaire: AUC 0.603 (95% CI: 0.494–0.713), cut point 40.5 (0–174 scale); sensitivity = 0.51, specificity = 0.71; and $n = 57$ normal, 88 EDED subjects

Interferometry: AUC 0.556 (95% CI: 0.484–0.629), cut point 2.1 (1–5 scale; 0.1 scale unit increments); sensitivity = 0.57, specificity = 0.57; and $n = 85$ normal, 190 EDED subjects

Gland atrophy (meiboscopy): AUC 0.378 (95% CI: 0.308–0.449), cut point 0.95 (0–4; continuous scale by percent of scale); sensitivity = 0.54, specificity = 0.36; and $n = 100$ normal, 229 EDED subjects

95% confidence intervals, diagnostic scale cut points, and subject sample sizes are summarized in text.

4. Discussion

It was the purpose of these investigations to determine whether routinely available clinical methods (such as the slit lamp biomicroscope, a cotton bud or Meibomian Gland Evaluator for gentle determination of gland secretion quality, and Finhoff transillumination for gland atrophy) can reliably identify EDED related to MGD by examination of functional and morphological changes in the lower eyelid. Under rigorous study design (such as double investigator masking), only the global clinical tests of symptom questionnaires, TBUT, and staining scores demonstrated adequate test efficacy (sensitivity and specificity >70%) [6] and the ability to distinguish between normal and EDED subjects (Table 1).

However, in the independent sample, gland secretion, using the Bron scale [10, 19] with 0.1 unit scale increments, demonstrated test efficacy by AUC (0.789) (Figure 2), sensitivity and specificity of 0.79 and 0.78, respectively, and statistically significant differentiation of normal vs. EDED subjects (Table 2). The cut point of 1.1 on a scale of 0–3 aligns with the Bron and coauthor's recommendation of deficient secretion at Grade 1 or greater [10]. Recently, Xiao et al. [20] also reported excellent discrimination for gland secretion (AUC of 0.98), on a 0–24 scale for 8 glands on the lower eyelid, although they did not propose a diagnostic cut point. Altered gland secretion is an indicator of adverse functional change, and this simple test appears useful in EDED diagnosis.

Eyelid marginal signs were not greatly different in normal and EDED subjects in the efficacy study (Table 1), and the AUC was not sufficiently diagnostic, possibly due to limited sample size ($n = 26$ normal and MGD subjects). In the independent sample data (text and Table 2), eyelid marginal signs did show adequate AUC and discrimination of normal vs. EDED subjects, but the cut point was too great, at 4.5 on a 0–5 scale, to provide an effective diagnostic test threshold. As well, marginal signs are associated with increasing age, so in our data, these summed marginal score changes do not seem useful for diagnosis and classification of EDED. Arita and coworkers [21, 22] previously reported high AUCs for eyelid marginal signs, which suggests they are a useful general, if not severity level sign in MGD.

Meibomian gland dropout of the entire lower eyelid via meiboscopy (0–4 scale, in percent) does not appear to be a viable indicator of EDED given the low AUCs in both samples (Tables 1 and 2 and Figure 2). This measure is a rough estimate of gland loss, and we conclude that imaging (i.e., meibography), which has much greater test efficacy [20–22], is necessary to characterize this important morphological change in EDED.

White-light tear interferometry of the tear lipid layer has been recommended by the DEWS II diagnostic subcommittee [2] to assist in subtyping dry eye as being of evaporative etiology. We examined lipid interference grade using the scale recommended by Yokoi and coworkers [15] (1–5 scale, with 0.1 scale unit increments) and found no difference between normal and EDED subjects (mean grades of 2.32 and 2.49, respectively) (Table 2) and an AUC equivalent to a coin flip. This result may have occurred due to the significant thickness range responsible for the colored lipid patterns of the Goto scale [23].

Relative to developing core outcome sets (COSs) for clinical trials in dry eye, it appears that a combination of global and specific tests for EDED is necessary. The present and recently reported data suggest that the global tests of symptoms, osmolarity, tear stability, and corneal and conjunctival staining are effective in establishing the diagnosis and severity of EDED. However, given the high test efficacy of both tear stability measurement and staining, it does not appear necessary to also include tear osmolarity as an additional global indicator of EDED. The cost of this test also mitigates against its widespread use. Assessment of gland secretion using the 0–3 scale [19] in 0.1 unit increments is a

useful diagnostic indicator of meibomian gland function. Moreover, it represents a physiological measure due to the gentle pressure required to examine secretion opacity and viscosity. Meibomian gland functional assessment must be paired with morphological quantitation, which requires glandular imaging. With the exception of meibography, all of these tests plus the Schirmer I and tear meniscus height tests for aqueous production are suitable for a general clinic.

4.1. Study Limitations. These studies suffered from selection bias, or the use of the test under consideration to classify the condition, which tends to overestimate its efficacy [24]. Efforts should be made to characterize EDED with additional tests, keeping in mind the confounder of age, so that these and other clinical tests may be more accurately evaluated for efficacy.

In summary, it appears from the independent sample using clinical tests that only meibomian gland secretion quality is a useful specific indicator of the evaporative subtype of dry eye. Gland morphology assessed using meibography appears necessary to diagnose and quantitate changes associated with evaporative dry eye disease. Additional work should endeavor to more comprehensively assess the test efficacy of gland expressibility directly with the several available clinical methods and indirectly via the effect of gland patency on lipid layer thickness to establish cut points for diagnosis and treatment monitoring.

Data Availability

Data supporting this research article are available from the corresponding author on reasonable request.

Conflicts of Interest

The authors declare no conflicts of interest.

Acknowledgments

References

[1] F. Stapleton, M. Alves, V. Y. Bunya et al., "TFOS DEWS II epidemiology report," *Ocular Surface*, vol. 15, no. 3, pp. 334–365, 2017.

[2] J. S. Wolffsohn, R. Arita, R. Chalmers et al., "TFOS DEWS II diagnostic methodology report," *Ocular Surface*, vol. 15, no. 3, pp. 539–574, 2017.

[3] D. A. Schaumberg, J. J. Nichols, E. B. Papas, L. Tong, M. Uchino, and K. K. Nichols, "The international Workshop on meibomian gland dysfunction: report of the subcommittee on the epidemiology of, and associated risk factors for, mgd," *Investigative Opthalmology & Visual Science*, vol. 52, no. 4, pp. 1994–2005, 2011.

[4] S. Amano and K. Inoue, "Estimation of prevalence of meibomian gland dysfunction in Japan," *Cornea*, vol. 36, no. 6, pp. 684–688, 2017.

[5] I. J. Saldanha, J. T. Le, S. D. Solomon et al., "Choosing Core outcomes for use in clinical trials in Ophthalmology: perspectives from three Ophthalmology outcomes working groups," *Ophthalmology*, vol. 126, no. 1, pp. 6–9, 2019.

[6] A. Tomlinson, A. J. Bron, D. R. Korb et al., "The international Workshop on meibomian gland dysfunction: report of the diagnosis subcommittee," *Investigative Opthalmology & Visual Science*, vol. 52, no. 4, pp. 2006–2049, 2011.

[7] L. E. Downie, N. Rumney, A. Gad, P. R. Keller, C. Purslow, and A. J. Vingrys, "Comparing self-reported optometric dry eye clinical practices in Australia and the United Kingdom: is there scope for practice improvement?" *Ophthalmic and Physiological Optics*, vol. 36, no. 2, pp. 140–151, 2016.

[8] A. L. Xue, L. E. Downie, S. E. Ormonde, and J. P. Craig, "A comparison of the self-reported dry eye practices of New Zealand optometrists and ophthalmologists," *Ophthalmic and Physiological Optics*, vol. 37, no. 2, pp. 191–201, 2017.

[9] P. M. Bossuyt, J. B. Reitsma, D. E. Bruns et al., "Stard 2015: an updated list of essential items for reporting diagnostic accuracy studies," *BMJ*, vol. 351, p. h5527, 2015.

[10] G. N. Foulks and A. J. Bron, "Meibomian gland dysfunction: a clinical scheme for description, diagnosis, classification, and grading," *Ocular Surface*, vol. 1, no. 3, pp. 107–126, 2003.

[11] S. C. Pflugfelder, S. C. G. Tseng, O. Sanabria et al., "Evaluation of subjective assessments and objective diagnostic tests for diagnosing tear-film disorders known to cause ocular irritation," *Cornea*, vol. 17, no. 1, pp. 38–56, 1998.

[12] J. R. Paugh, J. Kwan, and M. Christensen, "Development of a meibomian gland dysfunction-specific symptom questionnaire," *Eye and Contact Lens: Science and Clinical Practice*, vol. 44, no. 1, pp. 6–14, 2016.

[13] C. Sade de Paiva, J. L. Lindsey, and S. C. Pflugfelder, "Assessing the severity of keratitis sicca with video-keratoscopic indices," *Ophthalmology*, vol. 110, no. 6, pp. 1102–1109, 2003.

[14] D. R. Korb and C. A. Blackie, "Meibomian gland diagnostic expressibility: correlation with dry eye symptoms and gland location," *Cornea*, vol. 27, no. 10, pp. 1142–1147, 2008.

[15] N. Yokoi, Y. Takehisa, and S. Kinoshita, "Correlation of tear lipid layer interference patterns with the diagnosis and severity of dry eye," *American Journal of Ophthalmology*, vol. 122, no. 6, pp. 818–824, 1996.

[16] J. R. Paugh, J. Tse, T. Nguyen et al., "Efficacy of the fluorescein tear breakup time test in dry eye," *Cornea*, vol. 39, no. 1, pp. 92–98, 2020.

[17] M. A. Lemp, "Report of the national eye institute/industry Workshop on clinical trials in dry eyes," *CLAO Journal: Official Publication of the Contact Lens Association of Ophthalmologists, Inc*, vol. 21, pp. 221–232, 1995.

[18] D. W. Hosmer and S. Lemeshow, "Chapter 5: assessing the fit of the model," in *Applied Logistic Regression* p. 162, John Wiley & Sons, Inc., New York, NY, USA, 2000.

[19] A. J. Bron, L. Benjamin, and G. R. Snibson, "Meibomian gland disease. Classification and grading of lid changes," *Eye*, vol. 5, no. 4, pp. 395–411, 1991.

[20] J. Xiao, M. Y. Adil, J. Olafsson et al., "Diagnostic test efficacy of meibomian gland morphology and function," *Scientific Reports*, vol. 9, no. 1, p. 17345, 2019.

[21] R. Arita, K. Itoh, S. Maeda et al., "Proposed diagnostic criteria for obstructive meibomian gland dysfunction," *Ophthalmology*, vol. 116, no. 11, pp. 2058–2063, 2009.

[22] R. Arita, I. Minoura, and N. Morishige, "Development of definitive and reliable grading scales for meibomian gland dysfunction," *American Journal of Ophthalmology*, vol. 165, pp. 125–137, 2016.

[23] E. Goto, "Quantification of tear interference image," *Cornea*, vol. 23, no. 8, pp. S20–S24, 2004.

[24] A. J. Bron, M. B. Abelson, and G. Ousler, "Methodologies to diagnose and monitor dry eye disease: report of the diagnostic methodology subcommittee of the international dry eye Workshop (2007)," *Ocular Surface*, vol. 5, pp. 108–152, 2007.

Research Article

Comparison of Consecutive Therapeutic Effects of Nanoemulsion and Emulsion Cyclosporin in Dry Eye Patients after Short-Term Treatment with Topical Fluorometholone

Yeon Sun Choi, Hae Jung Paik, and Dong Hyun Kim [ID]

Department of Ophthalmology, Gil Medical Center, Gachon University College of Medicine, Incheon, Republic of Korea

Correspondence should be addressed to Dong Hyun Kim; amidfree@gmail.com

Purpose. To compare the consecutive therapeutic effects of 0.05% emulsion and nanoemulsion cyclosporine (CsA) in dry eye patients after short-term treatment with unpreserved 0.1% fluorometholone (FML). *Methods.* A prospective, randomized, and double-blinded study of dry eye patients was conducted in a single center. Patients were assigned to the nanoemulsion CsA (group 1) and emulsion CsA (group 2) groups. To relieve discomfort, unpreserved 0.1% FML was used in both groups for 4 weeks and then changed to 0.05% CsA for the next 8 weeks. Symptom assessment in dry eye (SANDE) score, tear secretion, tear film breakup time (TBUT), corneal staining score (CSS), meibomian gland dysfunction (MGD) grade, and meibomian gland (MG) expression were evaluated at baseline and at 4 and 12 weeks after treatment. *Results.* Twenty-four patients completed the treatment (9 and 15 patients in groups 1 and 2); in both the groups, SANDE score, TBUT, MGD grade, and MG expression were significantly improved after treatment with unpreserved 0.1% FML (each $p < 0.005$), and the therapeutic effects were enhanced with changes in nanoemulsion or emulsion CsA compared with baseline (each $p < 0.001$). TBUT and CSS after treatment in group 1 were significantly improved compared to those in group 2 ($p = 0.003$ and 0.020, respectively). *Conclusion.* Consecutive therapeutic effects of nanoemulsion or emulsion CsA after short-term treatment with unpreserved FML were excellent in patients with dry eyes. Topical nanoemulsion CsA showed better improvement in TBUT and OSS than CsA. This trial is registered with KCT0006070.

1. Introduction

According to the TFOS DEWS II, dry eye disease (DED) is a multifactorial disease of the ocular surface characterized by a loss of homeostasis of the tear film accompanied by ocular symptoms in which tear film instability and hyperosmolarity, ocular surface inflammation and damage, and neurosensory abnormalities play etiological roles [1–3]. In addition, meibomian gland dysfunction is known as a representative cause of DED because it induces tear film abnormality and instability [4, 5].

Cyclosporine (CsA) is a lipophilic peptide composed of 11 amino acids that acts as a calcineurin inhibitor to prevent the infiltration of T cells and suppress several inflammatory cytokines. CsA binds to cyclophilin in the cytoplasm of T cells to form a CsA/cyclophilin complex that blocks calcineurin-mediated dephosphorylation of nuclear factor of activated T cells and interrupts the transcription of cytokines, including IL-2 and IL-4. Inhibition of IL-2 formation blocks T-cell proliferation and suppresses T-cell-mediated immune responses [6, 7]. In this manner, topical CsA is known to reduce the activated lymphocytes of the conjunctiva, inhibit the factors associated with inflammation and cell death, and increase the density of goblet cells in the conjunctiva; thus, it is used as a therapeutic agent for dry eye patients to improve tear production [5, 6]. Byun et al. reported that 0.05% CsA eye drops improved the clinical symptoms of dry eye patients, such as foreign body sensation, blurred vision, photosensitivity, and pain [8]. In another study, 0.05% CsA increased tear secretion and improved subjective symptoms in chronic DED patients [9]. Chang et al. reported that 0.05% CsA with 0.1% hyaluronic

acid (HA) improved the tear breakup time (TBUT) and tear osmolarity [10]. Meanwhile, topical corticosteroids are generally indicated for the treatment of ocular inflammatory diseases because they can inhibit proinflammatory cytokines and chemokines, stabilize macrophages and neutrophils, and repress the key enzymes involved in the initiation or maintenance of the inflammatory response [11]. Short-term topical 0.1% fluorometholone showed excellent therapeutic effects in patients with refractory DED or acute DED flares in our previous study [12].

Since CsA is insoluble in water, the 0.05% CsA eye drop (Restasis®, Allergan Inc., CA, USA) is in the form of an emulsion, with castor oil added to increase its solubility [13]. A well-known side effect of 0.05% CsA emulsion is a burning sensation, which decreases patient compliance [13]. In order to minimize this adverse effect, a 0.05% CsA in nanoemulsion form was developed. The nanoemulsion CsA eye drops were transparent, and their particle sizes were uniform. However, the therapeutic effects of emulsion and nanoemulsion CsA have not been fully investigated. Thus, we compared the consecutive therapeutic effects of 0.05% nanoemulsion and emulsion CsA after common short-term treatment with unpreserved fluorometholone (FML) in DED patients.

2. Materials and Methods

This study was approved by the Institutional Review Board (approval number GBIRB2016-238) according to the Declaration of Helsinki and was registered in the Clinical Research Information Service (https://cris.nih.go.kr). A prospective, randomized, and double-blinded study of dry eye patients was conducted in a single center, and 50 patients were enrolled from May 2018 to October 2019.

Patients older than 19 years who visited our clinic with complaints such as ocular dryness, burning, and hyperemia were examined to rule out DED, and we performed Schirmer's test without anesthesia and assessed tear film breakup time (TBUT) using standardized procedures. DED was diagnosed according to the diagnostic guidelines of the Korean Corneal Disease Study Group and TFOS II [1, 2]. Those with Schirmer's test outcome of <10 mm at the end of 5 min or a TBUT of <10 s participated in this study. Patients with a history of Sjogren's syndrome or who were taking systemic steroids or immunosuppressive agents, contact lens wearers, or patients who had DED induced by chronic drug usage, such as antidepressants and antihistamines, were excluded. Patients who had prior ocular surgery within 3 months or were on any other eye drops, such as lubricants or antiglaucoma medications, were also excluded.

Patients were randomly assigned to one of the two groups, nanoemulsion CsA (T-sporin®, Hanlim Pharm Co., Ltd., Seoul, Korea) group or emulsion CsA (Restasis®, Allergan Inc., Irvine, CA, USA) group using the block randomization method (groups 1 and 2). For rapid symptom relief, all patients in groups 1 and 2 were treated with unpreserved 0.1% FML (Fumelon®, Hanlim Pharm Co., Ltd., Seoul, Korea) four times a day for the first 4 weeks, and then, they were changed to 0.05% emulsion or nanoemulsion CsA twice a day for the next 8 weeks. All patients used 0.15%

hyaluronic acid artificial tears (Hyaluronmax®, Hanlim Pharm Co., Ltd., Seoul, Korea) four times a day for 12 weeks. The type of allocated drug (nanoemulsion or emulsion CsA) was masked to the examiner (DH Kim) and patients.

At baseline and 4 and 12 weeks after treatment, best-corrected visual acuity (BCVA), intraocular pressure, symptom assessment in dry eye (SANDE) score, TBUT, Schirmer's test, corneal staining score (CSS, National Eye Institute Scale, 0–15), MGD grade (0–4), and MG expression (0–3) were examined to compare the therapeutic effects between the two groups [7, 14–16].

Statistical analysis was performed using SPSS program version 22.0 (IBM Corp., Armonk, NY, USA). Data are presented as mean ± standard deviation (SD). The Wilcoxon signed-rank test and Mann–Whitney U test were used for intragroup and intergroup analyses. Differences were considered statistically significant at $p < 0.05$.

3. Results

A total of 50 patients (12 men and 38 women) were enrolled in the study, and the mean age of the patients was 61.2 ± 9.1 years. At the 12-week follow-up, 9 patients (4 men and 5 women) in group 1 and 15 patients (4 men and 11 women) in group 2 completed this clinical trial. Thirteen patients were excluded at 4 and 12 weeks (Figure 1). Fifteen patients no longer wanted to participate in this trial, nine patients were unable to be contacted, and two patients were excluded from the clinical trial because of acute viral conjunctivitis (Figure 1). The mean age of patients in groups 1 and 2 was 58.6 ± 11.4 and 62.1 ± 6.4 years, respectively ($p = 0.279$). The best-corrected visual acuity (BCVA), intraocular pressure, MGD grade, and MG expression at baseline were also not significantly different between the two groups ($p > 0.05$) (Table 1).

In groups 1 and 2, SANDE score, TBUT, MGD grade, and MG expression were significantly improved after treatment with unpreserved 0.1% FML for the initial 4 weeks (each $p < 0.005$, Table 2) and intraocular pressure did not increase significantly ($p = 0.873/0.723$, Table 2). CSS did not significantly change before and after 0.1% FML treatment (group 1/2: $p = 0.408/0.750$, Table 2). There was no significant increase in tear secretion in group 1, but there was a slight decrease in tear secretion in group 2 (group 1/2: $p = 0.396/0.008$, Table 2). After 4 weeks of FML treatment, BCVA, SANDE score, TBUT, CSS, MGD grade, and MG expression were not significantly different between groups 1 and 2 (each $p > 0.05$) but the tear secretion was reduced in group 2 compared to that in group 1 ($p = 0.037$, Table 2).

After consecutive treatment with 0.05% CsA for the next 8 weeks (12 weeks from baseline), both groups showed significant improvement in SANDE score, TBUT, MGD grade, and MG expression compared to baseline (each $p < 0.001$, Table 3). CSS showed no differences compared to baseline in both groups (group 1/2: $p = 0.563/0.750$, Table 3), and BCVA and intraocular pressure also showed no specific changes (each $p > 0.05$). There was some decrease in tear secretion in group 2 compared to baseline, but it was not statistically significant ($p = 0.070$, Table 3).
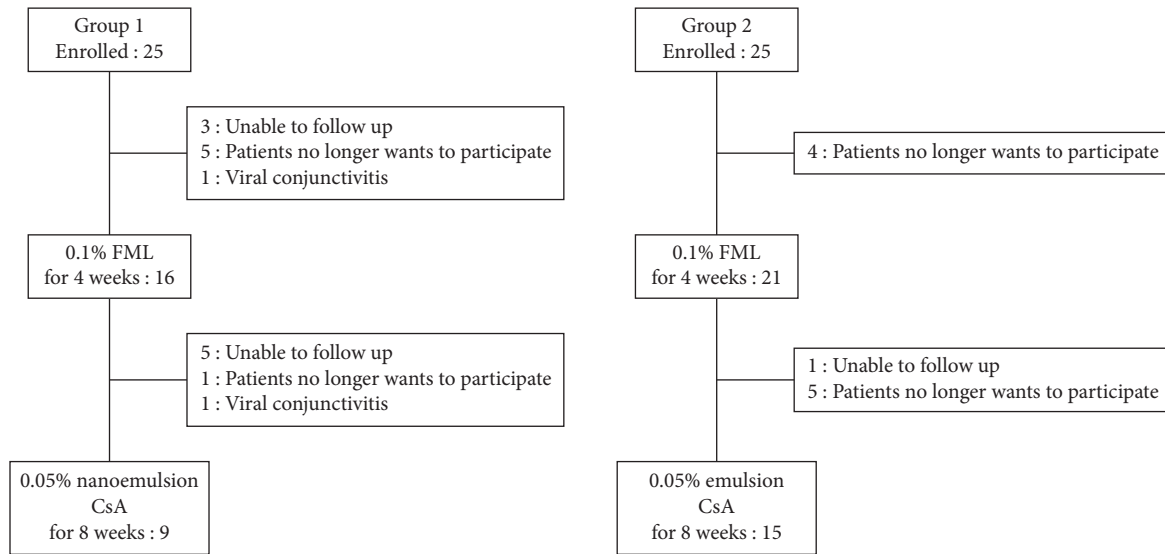
Figure 1: Schematic illustration of enrolled patients.

Table 1: Baseline characteristics in patients.

	Group 1 ($n = 9$) (nanoemulsion CsA)	Group 2 ($n = 15$) (emulsion CsA)	p value
Age (years)†	58.6 ± 11.4	62.1 ± 6.4	0.279
Sex (Male/female)‡	4/5	4/11	0.355
BCVA (logMAR)†	0.08 ± 0.11	0.12 ± 0.11	0.262
IOP (mmHg)†	9.4 ± 1.6	9.8 ± 2.4	0.643
SANDE score†	73.9 ± 17.8	67.8 ± 24.1	0.344
TBUT (sec)†	2.6 ± 1.1	2.3 ± 0.7	0.403
Schirmer (mm)†	9.0 ± 7.6	8.9 ± 7.2	0.077
CSS (pts)†	0.6 ± 1.1	0.3 ± 0.7	0.248
MGD stage (0–4)†	1.8 ± 0.4	1.9 ± 0.4	0.574
MG expression (pts)†	2.6 ± 1.1	2.3 ± 0.7	0.360

Values are presented as the mean ± standard deviation. †Mann–Whitney U test; ‡the chi-square test. CsA: cyclosporin; BCVA: best corrected visual acuity; IOP: intraocular pressure; SANDE: symptom assessment in dry eye; TBUT: tear film breakup time; CSS: corneal staining score (NEI scale, 0–15); MGD: meibomian gland dysfunction; MG: meibomian gland.

Table 2: Comparison of therapeutic effects at 4 weeks after treatment with topical FML between nanoemulsion and emulsion CsA groups.

	Group 1 (nanoemulsion CsA)			Group 2 (emulsion CsA)			p value‡
	Baseline	4 weeks after treatment	p value†	Baseline	4 weeks after treatment	p value†	
BCVA (logMAR)	0.08 ± 0.11	0.06 ± 0.07	0.348	0.12 ± 0.11	0.10 ± 0.10	0.407	0.132
IOP (mmHg)	9.4 ± 1.6	9.6 ± 1.4	0.873	9.8 ± 2.4	9.6 ± 2.1	0.723	0.731
SANDE (pts)	73.9 ± 17.8	51.2 ± 21.3	0.002*	67.8 ± 24.1	49.4 ± 15.8	<0.001*	0.588
TBUT (sec)	2.6 ± 1.1	4.3 ± 1.5	0.001*	3.1 ± 1.4	4.8 ± 1.5	<0.001*	0.296
Schirmer (mm)	9.0 ± 7.6	11.6 ± 10.0	0.396	8.9 ± 7.2	6.1 ± 4.9	0.008*	0.037
CSS (pts)	0.6 ± 1.1	0.4 ± 0.8	0.408	0.3 ± 0.7	0.4 ± 0.9	0.750	0.999
MGD grade	1.8 ± 0.4	1.1 ± 0.6	0.001*	1.9 ± 0.4	1.0 ± 0.3	<0.001*	0.536
MG expression (pts)	2.6 ± 1.1	1.4 ± 0.7	0.001*	2.3 ± 0.7	1.4 ± 0.5	<0.001*	0.752

Values are presented as mean ± standard deviation. †Intragroup analysis (Wilcoxon signed-rank test); ‡intergroup analysis (Mann–Whitney U test). FML: 0.1% fluorometholone; BCVA: best corrected visual acuity; IOP: intraocular pressure; SANDE: symptom assessment in dry eye; TBUT: tear film breakup time; CSS: corneal staining score (NEI scale, 0–15) MGD: meibomian gland dysfunction; MG: meibomian gland. *Statistically significant.

We compared the changes in SANDE score, TBUT, tear secretion, MGD grade, and MG expression from baseline between groups 1 and 2 at the time point of 12 weeks after treatment. TBUT and CSS were significantly improved in group 1 compared to those in group 2 (TBUT/CSS: $p = 0.003/0.020$, Figure 2, Mann–Whitney U test). However, there were no differences in SANDE score, tear secretion,

MGD grade, or MG expression between the two groups (each $p > 0.05$, Figure 2, Mann–Whitney U test).

Figure 3 shows the overall changes in SANDE score, TBUT, tear secretion, CSS, MGD grade, and MG expression at baseline and at 4 and 12 weeks after treatment between groups 1 and 2. In both groups, there were meaningful improvements in SANDE score, TBUT, MGD grade, and

TABLE 3: Comparison of therapeutic effects at 12 weeks after treatment with topical FML and CsA between nanoemulsion and emulsion CsA groups.

	Group 1 (nanoemulsion CsA)			Group 2 (emulsion CsA)			p value‡
	Baseline	12 weeks after treatment	p value†	Baseline	12 weeks after treatment	p value†	
BCVA (logMAR)	0.08 ± 0.11	0.06 ± 0.11	0.390	0.12 ± 0.11	0.10 ± 0.11	0.407	0.264
IOP (mmHg)	9.4 ± 1.6	9.2 ± 1.4	0.888	9.8 ± 2.4	9.3 ± 2.7	0.723	0.639
SANDE score	73.9 ± 17.8	37.0 ± 19.7	<0.001*	67.8 ± 24.1	41.3 ± 23.0	<0.001*	0.803
TBUT (sec)	2.6 ± 1.1	5.3 ± 1.1	<0.001*	3.1 ± 1.4	4.6 ± 1.4	<0.001*	0.037*
Schirmer (mm)	9.0 ± 7.6	11.1 ± 11.6	0.418	8.9 ± 7.2	6.7 ± 4.0	0.070	0.622
CSS (pts)	0.6 ± 1.1	0.1 ± 0.3	0.563	0.3 ± 0.7	0.5 ± 0.8	0.750	0.118
MGD grade	1.8 ± 0.4	0.9 ± 0.6	<0.001*	1.9 ± 0.4	0.9 ± 0.3	<0.001*	0.896
MG expression (pts)	2.6 ± 1.1	1.0 ± 0.5	<0.001*	2.3 ± 0.7	1.2 ± 0.4	<0.001*	0.274

Values are presented as the mean ± standard deviation. † Intragroup analysis (the Wilcoxon signed-rank test); ‡intergroup analysis (Mann–Whitney U test). FML, 0.1% fluorometholone; CsA, 0.05% cyclosporine; BCVA: best corrected visual acuity; IOP, intraocular pressure; SANDE, symptom assessment in dry eye; TBUT, tear film breakup time; CSS, corneal staining score (NEI scale, 0–15); MGD, meibomian gland dysfunction; MG, meibomian gland. *Statistically significant.
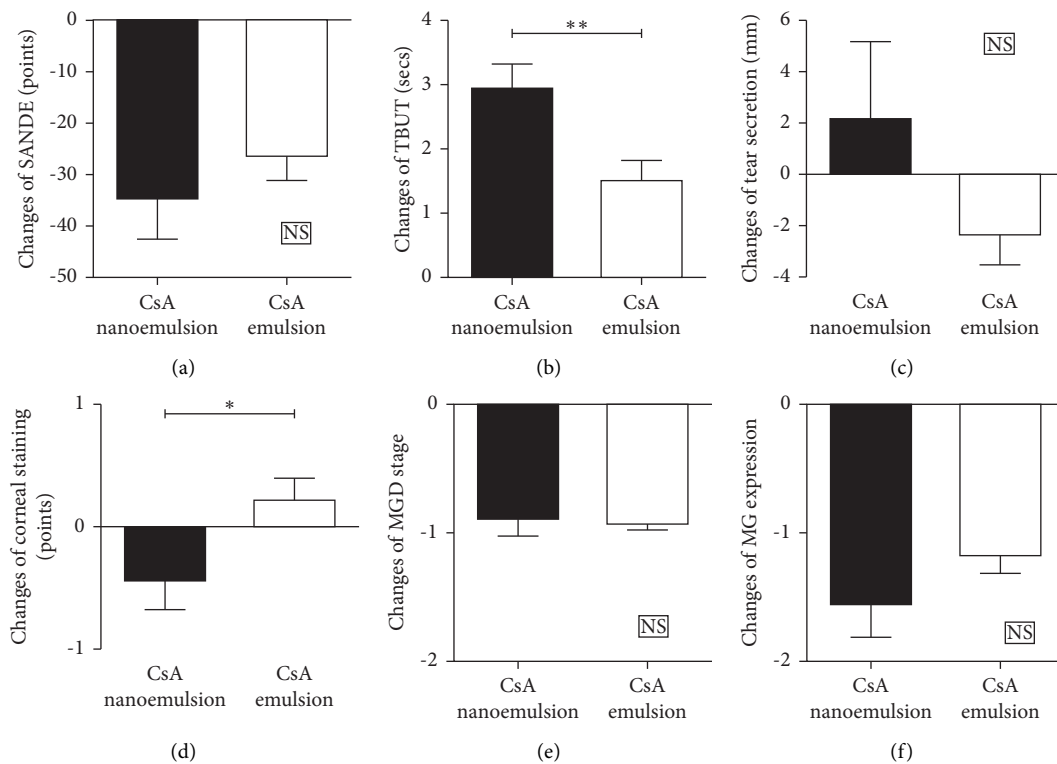
FIGURE 2: Comparison of changes in dry eye parameters between nanoemulsion and emulsion CsA groups at 12 weeks after treatment with initial topical steroid and consecutive topical CsA compared to baseline. CsA, cyclosporin; SANDE, symptom assessment in dry eye; TBUT, tear film breakup time; MGD, meibomian gland dysfunction; MG, meibomian gland.

MG expression at 4 weeks after treatment with FML compared to baseline and therapeutic effects were enhanced after treatment with nanoemulsion or emulsion CsA for an additional 8 weeks (each $p < 0.001$). Both groups showed no differences in tear secretion and corneal staining compared to the baseline (each $p > 0.05$).

4. Discussion

In this prospective, randomized, double-blinded study, unpreserved 0.1% FML for 4 weeks and consecutive 0.05% nanoemulsion or emulsion CsA for the next 8 weeks showed

excellent therapeutic effects in patients with DED. SANDE score, TBUT, MGD grade, and MG expression were significantly improved after treatment with 0.1% FML, and these therapeutic effects were greatly enhanced with changes in nanoemulsion or emulsion CsA. TBUT and CSS were more improved in the nanoemulsion CsA group than in the emulsion CsA group.

CsA is a lipophilic material that is separated from the fungus *Tolypocladium inflatum* and has the immunosuppressive function of inhibiting IL-2 to suppress T-cell proliferation [5, 7]. Systemic CsA has been used to prevent rejection of organ transplantation [5]. In the ophthalmic

FIGURE 3: Changes in dry eye parameters at baseline and 4 and 12 weeks after treatment. CsA, cyclosporin; SANDE, symptom assessment in dry eye; TBUT, tear film breakup time; MGD, meibomian gland dysfunction; MG, meibomian gland.
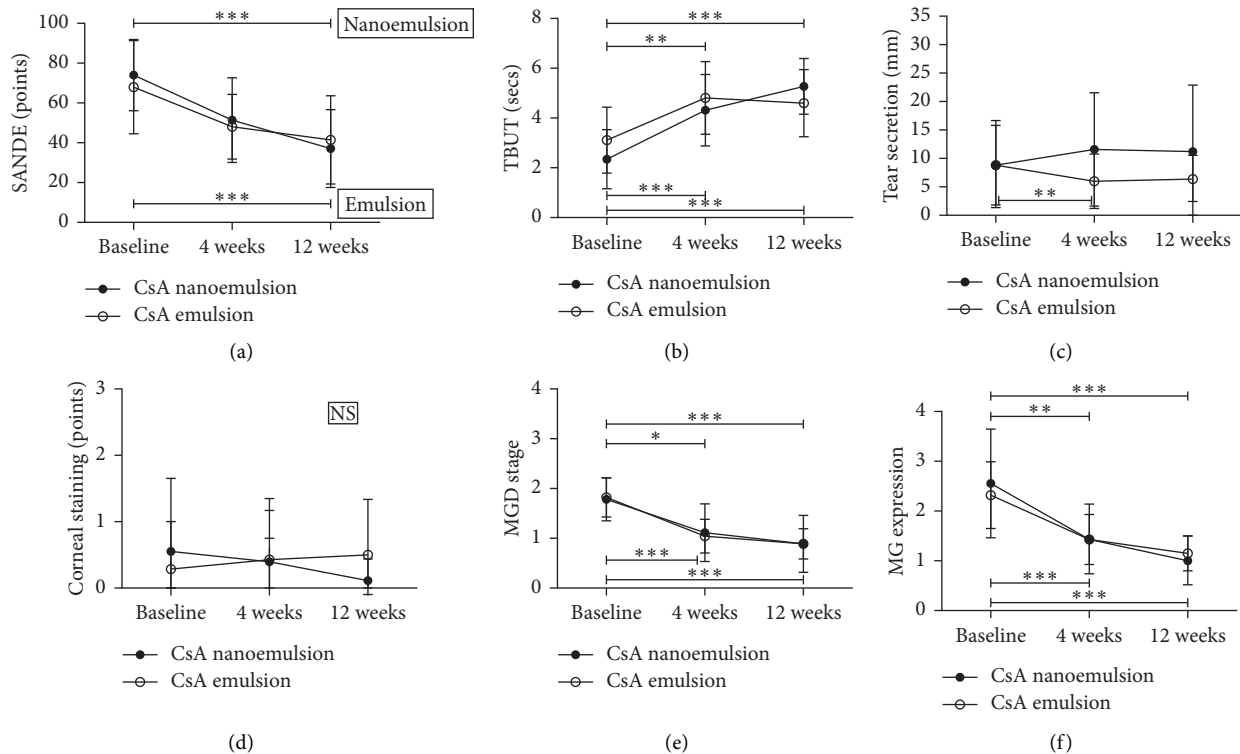
area, topical CsA has been used to prevent corneal graft rejection through immune suppression or to modulate inflammatory ocular surface diseases such as vernal keratoconjunctivitis, ocular GVHD, and Mooren's ulcer [5, 7, 8]. Topical CsA has been widely used, especially in patients with DED, since the emulsion type of CsA (Restasis®, Allergan Inc., Irvine, CA, USA) was released about 20 years ago. The molecules of CsA have a very hard structure due to hydrogen bonds associated with the ring structure due to C62H111N11O12; thus, the solubility in water is very low [13]. Olive oil or corn oil can be expected to induce better ocular penetration, but Williams reported that CsA, which is delivered in olive oil solution, is reported to cause a burning sensation in the conjunctiva [13]. Byun et al. reported that 72% of DED patients treated with CsA were satisfied and that the symptoms of DED and tear secretion were much improved, but there were definite side effects, including an irritating sensation after administration [8].

An emulsion is a liquid-liquid dispersion technology in which one or more liquids are dispersed in other liquids that are not mixed. It is an effective topical ophthalmic drug delivery method, especially oil-water emulsions, which are known to be effective in delivering lipophilic drugs. Owing to the recent development of a new emulsifier, emulsion technology is facing a new turning point in terms of the preparation of CsA [17, 18]. CsA has a large molecular weight, and its affinity for water is very low, making it difficult to use an effective agent as an existing ophthalmic drug delivery system. Therefore, various drug delivery technologies, such as hydrogels, in situ gelling systems, liposomes, nanoparticles,

and micelles, have been developed [17]. The Restasis® eye drops (Allergan Inc., Irvine, CA, USA) are an anionic oil-in-water emulsion without a preservative; CsA is dissolved in castor oil with an emulsifier, polysorbate [18]. However, as Restasis® is an anisotropic complex emulsion, when it comes in contact with the tear film, the surfactant may be released. In addition, there could be creamization or aggregation because of the uneven size of CsA particles, so the physical and chemical long-term stability is reduced. Therefore, side effects such as blurred vision, conjunctival congestion, and burning sensations after instillation have been frequently reported [19–21]. In addition, CsA is present in various phases, so that it cannot be sufficiently delivered to the tissue [19]. Meanwhile, Cyporin-N® (CsA, Cyporin-N®, Taejoon Pharm Co., Seoul, Korea) or 0.05% T-sporin® (CsA, T-sporin®, Hanlim Pharm Co., Ltd., Seoul, Korea) are nanoemulsion CsA products based on a self-nanoemulsifying drug delivery system (SNEDDS) method [22–25]. SNEDDS is an anhydrous homogenous mixture made by mixing oil, drugs, surfactants, and auxiliary surfactants. Its particle size is very small and even. As a transparent nanoemulsion in a nanometer unit, it is known to have excellent chemical and physical stability [22–25] (Figure 4).

Kim et al. reported that the nanoemulsion CsA was more effective in improving conjunctival damage and tear film stability than the emulsion CsA in patients with DED [22]. Shin et al. reported that the OSDI score and foreign body sensation were lower in the nanoemulsion CsA group, and both the nanoemulsion and emulsion CsA groups showed similar therapeutic effects in objective

(a)   (b)
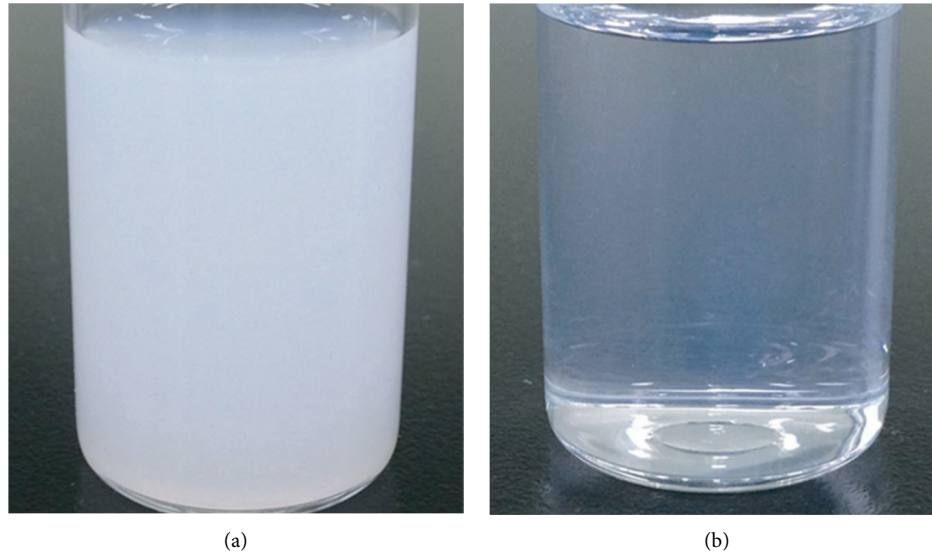
FIGURE 4: Comparison of transparency between emulsion and nanoemulsion CsA. (a) Emulsion CsA. (b) Nanoemulsion CsA. CsA, cyclosporin.

parameters of DED after 12 weeks of treatment [26]. In contrast with previous studies, this study showed significant improvement in MGD, which can be a major risk factor for DED. In addition, after the initial short-term FML treatment, we quickly alleviated the irritating symptoms of DED and then switched to the CsA protocol to continuously maintain ocular comfort and improve objective DED parameters. In particular, the nanoemulsion CsA group (group 1) showed better TBUT and CSS than the emulsion CsA group (group 2), even though there were slight differences.

Rye et al. showed that short-term corticosteroids can effectively improve objective findings and subjective symptoms in patients with acute exacerbation of DED or refractory DED [12]. One hundred thirty-seven DED patients treated with topical steroids for 4 weeks showed a significant improvement in SANDE score, TBUT, ocular surface staining, and MGD grade [12]. In particular, those effects were superior in tear MMP-9-positive patients [12]. CsA can also improve the symptoms and signs of DED, but improvement takes more than 2-3 months [12, 27]. Since up to 17% of patients complain of burning sensation, there are numerous clinical interventions to quickly improve the acute exacerbation of DED [28–31]. Sheppard et al. showed that two weeks of topical steroid usage before starting long-term topical CsA in chronic DED patients resulted in a rapid and effective decrease in the symptoms and signs of DED [32]. Also, prior use of a topical steroid reduces the burning sensation and discomfort due to CsA eye drops, resulting in an improvement in patient compliance so that the inflammatory response can effectively introduce CsA onto the ocular surface [32]. Byun et al. reported that the short-term use of topical steroid allows fast symptom relief in moderate-to-severe dry eye patients without any severe complications [33]. Singla et al. also reported that the combination of topical steroids and CsA had a better treatment effect than CsA single therapy in patients with

moderate dry eye syndrome [34]. Therefore, rapid symptom relief with short-term topical steroids and then switching to CsA could be a good treatment option to gain clinical efficiency and safety in DED patients with severe symptoms.

This study has several limitations. There were many drop-out patients, and the sample size was small. Quantitative analysis of reduced inflammation in the tear film and ocular surface was not performed. There were more drop-out patients in the nanoemulsion group than in the emulsion group, and it is necessary to analyze the cause, such as irritating sensation or discomfort in usage. However, we found that consecutive CsA treatment following short-term topical steroid administration rapidly improved and maintained long-term enhancement in DED symptoms and signs as well as MGD. In addition, more extensive studies are required to determine whether nanoemulsion CsA is superior to emulsion CsA.

5. Conclusions

In conclusion, the consecutive therapeutic effects of CsA after short-term, unpreserved topical steroid use were clinically excellent in DED patients. Topical nanoemulsion CsA showed better improvement in TBUT and OSS than emulsion CsA; hence, nanoemulsion CsA may be more helpful in DED patients.

Data Availability

The data that support the findings of this study are available from the corresponding author upon reasonable request.

Disclosure

Yeon Sun Choi and Hae Jung Paik should be considered the co-first authors.

Conflicts of Interest

The authors declare that there are no conflicts of interest regarding the publication of this paper.

Authors' Contributions

Yeon Sun Choi and Hae Jung Paik contributed equally to this study.

Acknowledgments

References

[1] J. Y. Hyon, H.-M. Kim, D. Lee et al., "Korean guidelines for the diagnosis and management of dry eye: development and validation of clinical efficacy," *Korean Journal of Ophthalmology*, vol. 28, no. 3, pp. 197–206, 2014.

[2] J. P. Craig, J. D. Nelson, D. T. Azar et al., "TFOS DEWS II report executive summary," *Ocular Surface*, vol. 15, no. 4, pp. 802–812, 2017.

[3] B. Ashley, D. J. John, and S. Lee, "Dysfunctional tear syndrome a Delphi approach to treatment recommendations," *Cornea*, vol. 25, pp. 900–907, 2006.

[4] S.-H. Lee and S. C. G. Tseng, "Rose Bengal staining and cytologic characteristics associated with lipid tear deficiency," *American Journal of Ophthalmology*, vol. 124, no. 6, pp. 736–750, 1997.

[5] D. W. Kim, Y. A. Kwon, S. W. Song, B. Y. Kim, and J. L. Chung, "Clinical usefulness of a thermal-massaging system for treatment of dry eye with meibomian gland dysfunction," *Journal of the Korean Ophthalmological Society*, vol. 54, no. 9, pp. 1321–1326, 2013.

[6] L. M. Periman, F. S. Mah, and P. M. Karpecki, "A review of the mechanism of action of cyclosporine A: the role of cyclosporine A in dry eye disease and recent formulation developments," *Clinical Ophthalmology*, vol. 14, pp. 4187–4200, 2020.

[7] Tear Film & Ocular Surface Society, "2007 Report of the international dry eye workshop (DEWS)," *Ocular Surface*, vol. 5, pp. 65–204, 2007.

[8] Y. J. Byun, T. I. Kim, and K. Y. Seo, "The short-term effect of topical cyclosporine A 0.05% in various ocular surface disorder," *Journal of the Korean Ophthalmological Society*, vol. 49, pp. 401–404, 2008.

[9] Y. S. Byun, E. J. Jeon, and S. K. Chung, "Clinical effect of cyclosporine 0.05% eye drops in dry eye syndrome patients," *Journal of the Korean Ophthalmological Society*, vol. 49, pp. 1583–1588, 2008.

[10] I. B. Chang, J. H. Park, M. S. Kim, and T. J. Kim, "Effect of sodium hyaluronate and cyclosporine A on tear film in dry eye syndrome," *Journal of the Korean Ophthalmological Society*, vol. 54, no. 2, pp. 231–236, 2013.

[11] A. E. Coutinho and K. E. Chapman, "The anti-inflammatory and immunosuppressive effects of glucocorticoids, recent developments and mechanistic insights," *Molecular and Cellular Endocrinology*, vol. 335, no. 1, pp. 2–13, 2011.

[12] K. J. Ryu, S. Kim, M. K. Kim, H. J. Paik, and D. H. Kim, "Short-term therapeutic effects of topical corticosteroids on refractory dry eye disease: clinical usefulness of matrix metalloproteinase 9 testing as a response prediction marker," *Clinical Ophthalmology*, vol. 15, pp. 759–767, 2021.

[13] P. Ames and A. Galor, "Cyclosporine ophthalmic emulsions for the treatment of dry eye: a review of the clinical evidence," *Clinical Investigation*, vol. 5, no. 3, pp. 267–285, 2015.

[14] D. A. Schaumberg, A. Gulati, W. D. Mathers et al., "Development and validation of a short global dry eye symptom index," *Ocular Surface*, vol. 5, no. 1, pp. 50–57, 2007.

[15] K. K. Nichols, G. N. Foulks, A. J. Bron et al., "The international workshop on meibomian gland dysfunction: executive summary," *Investigative Opthalmology & Visual Science*, vol. 52, no. 4, pp. 1922–1929, 2011.

[16] C. Putnam, "Diagnosis and management of blepharitis: an optometrist's perspective," *Clinical Optometry*, vol. 8, pp. 71–78, 2016.

[17] B. Yavuz, P. S. Bozdağ, and N. Unlü, "An overview on dry eye treatment: approaches for cyclosporine a delivery," *The Scientific World Journal*, vol. 2012, Article ID 194848, 2012.

[18] S. P. Bang, C. Y. Yeon, N. Adhikari et al., "Cyclosporine A eyedrops with self-nanoemulsifying drug delivery systems have improved physicochemical properties and efficacy against dry eye disease in a murine dry eye model," *PLoS One*, vol. 14, no. 11, Article ID e0224805, 2019.

[19] P. Agarwal and I. D. Rupenthal, "Modern approaches to the ocular delivery of cyclosporine A," *Drug Discovery Today*, vol. 21, no. 6, pp. 977–988, 2016.

[20] K. Sall, O. D. Stevenson, T. K. Mundorf, and B. L. Reis, "Two multicenter, randomized studies of the efficacy and safety of cyclosporine ophthalmic emulsion in moderate to severe dry eye disease. CsA Phase 3 Study Group," *Ophthalmology*, vol. 107, no. 4, pp. 631–639, 2000.

[21] T. G. Coursey, R. A. Wassel, A. B. Quiambao, and R. A. Farjo, "Once-daily cyclosporine-A-MiDROPS for treatment of dry eye disease," *Translational Vision Science & Technology*, vol. 7, no. 5, p. 24, 2018.

[22] H. S. Kim, T.-i. Kim, J. H. Kim et al., "Evaluation of clinical efficacy and safety of a novel cyclosporin A nanoemulsion in the treatment of dry eye syndrome," *Journal of Ocular Pharmacology and Therapeutics*, vol. 33, no. 7, pp. 530–538, 2017.

[23] T. Tadros, "Application of rheology for assessment and prediction of the long-term physical stability of emulsions," *Advances in Colloid and Interface Science*, vol. 108-109, pp. 227–258, 2004.

[24] F. U. Rehman, K. U. Shah, S. U. Shah, I. U. Khan, G. M. Khan, and A. Khan, "From nanoemulsions to self-nanoemulsions, with recent advances in self-nanoemulsifying drug delivery systems (SNEDDS)," *Expert Opinion on Drug Delivery*, vol. 14, no. 11, pp. 1325–1340, 2017.

[25] A. A.-W. Shahba, K. Mohsin, and F. K. Alanazi, "Novel self-nanoemulsifying drug delivery systems (SNEDDS) for oral delivery of cinnarizine: design, optimization, and in-vitro assessment," *AAPS PharmSciTech*, vol. 13, no. 3, pp. 967–977, 2012.

[26] E. H. Shin, D. H. Lim, C. M. Yang, and T. Y. Chung, "Comparison of efficacy and sensation of instillation between 0.05% cyclosporine nanoemulsion and microemulsion type," *Journal of the Korean Ophthalmological Society*, vol. 60, pp. 239–245, 2019.

[27] P. Marsh and S. C. Pflugfelder, "Topical nonpreserved methylprednisolone therapy for keratoconjunctivitis sicca in Sjögren syndrome," *Ophthalmology*, vol. 106, no. 4, pp. 811–816, 1999.

[28] S. C. Pflugfelder, S. L. Maskin, B. Anderson et al., "A randomized, double-masked, placebo-controlled, multicenter comparison of loteprednol etabonate ophthalmic suspension, 0.5%, and placebo for treatment of keratoconjunctivitis sicca in patients with delayed tear clearance," *American Journal of Ophthalmology*, vol. 138, pp. 444–457, 2004.

[29] P. D. O'Brien and L. M. Collum, "Dry eye: diagnosis and current treatment strategies," *Current Allergy and Asthma Reports*, vol. 4, pp. 314–319, 2004.

[30] S. C. Pflugfelder, G. Geerling, S. Kinoshita et al., "Management and therapy of dry eye disease: report of the management and therapy subcommittee of the international dry eye WorkShop (2007)," *Ocular Surface*, vol. 5, pp. 163–178, 2007.

[31] E. J. Holland, E. D. Donnenfeld, R. L. Lindstrom, S. C. Pflugfelder, J. D. Sheppard, and K. D. Solomon, "Expert consensus in the treatment of dry eye inflammation," *Ophthalmology Times*, vol. 32, pp. 1–12, 2007.

[32] J. D. Sheppard, E. D. Donnenfeld, E. J. Holland et al., "Effect of loteprednol etabonate 0.5% on initiation of dry eye treatment with topical cyclosporine 0.05%," *Eye and Contact Lens: Science and Clinical Practice*, vol. 40, pp. 289–296, 2014.

[33] Y. J. Byun, T. I. Kim, S. M. Kwon et al., "Efficacy of combined 0.05% cyclosporine and 1% methylprednisolone treatment for chronic dry eye," *Cornea*, vol. 31, no. 5, pp. 509–513, 2012.

[34] S. Singla, L. Sarkar, and M. Joshi, "Comparison of topical cyclosporine alone and topical loteprednol with cyclosporine in moderate dry eye in Indian population: a prospective study," *Taiwan Journal of Ophthalmology*, vol. 9, pp. 173–178, 2019.

Research Article

Changes of Lacrimal Puncta by Anterior Segment Optical Coherence Tomography after Topical Combined Antibiotic and Steroid Treatment in Cases of Inflammatory Punctual Stenosis

Islam Awny ⓘ,[1] **Elshimaa A. Mateen Mossa** ⓘ,[1] **Tasneem Mohammed Bakheet,**[2] **Hany Mahmoud** ⓘ,[1] **and Amr Mounir** ⓘ[1]

[1]*Sohag Faculty of Medicine, Ophthalmology Department, Sohag University, Sohag, Egypt*
[2]*Sohag Faculty of Medicine, Public Health and Community Medicine Department, Sohag University, Sohag, Egypt*

Correspondence should be addressed to Amr Mounir; dramrmonir@yahoo.com

Purpose. To evaluate the role of medical treatment and assessing its effect on resolving epiphora and improving punctum size by high resolution AS-OCT imaging comparing punctal parameters in patients before and after treatment with topical combined antibiotic and steroid treatment in cases of inflammatory punctual stenosis. *Patients and Methods*. Double-blinded controlled randomized study which was conducted on two groups of patients who had acquired punctal stenosis and epiphora presented to Ophthalmology Clinics of Sohag University Hospitals in the period between Jan 2021 and April 2021. The study included 44 eyes of 50 subjects complaining of epiphora. They were divided into two groups, the epiphora group one (EG1) received eye drops containing combination of antibiotics and steroids (orchadexoline eye drops, each ml contains 5 mg chloramphenicol, 1 mg dexamethasone sodium phosphate, 0.25 mg tetryzoline hydrochloride, 2 mg hydroxypropyl methyl cellulose, 10 mg α-tocopherol acetate (vitamin E), and 8 mg macrogol 400), 5 times daily for the first week, three times daily for the next two weeks, and one time daily for another one week. The second epiphora group (EG2) received preservative-free artificial tears (sodium hyaluronate-, polyethylene-, and propylene glycol-based), three times daily for four weeks. The patients were examined before treatment, one week, one month, and one and half months later. *Results*. Both groups were comparable regarding mean age (49 ± 13 vs 53 ± 11 years, *P* value = 0.2) and sex (males were 38.6% vs 31.8%, female were 61.4% vs 68.2%, *P* value = 0.6), respectively, with no statistically significant difference between both groups. Both groups were comparable regarding outer punctual diameter and length between the puncti before treatment. Outer punctal diameters were (EG1 228 ± 113 um, EG2 241 ± 115 um, *P* value = 0.5). Length between the puncti were (EG1 129 ± 73 um, EG2 137 ± 72 um, *P* value = 0.6). There was marked improvement of the outer punctual diameter (EG1 373 um ± 92 um, EG2 240 ± 109 um, (*P* value < 0.0001) and length between the puncti (EG1 217 ± 109 um, 136 ± 71 um (*P* value < 0.0002)) during the follow-up period. EG1 showed more improvement than EG2 when compared during the follow-up period. *Conclusions*. Topical combined antibiotic and steroid treatment was an effective method in treating cases of inflammatory punctual stenosis as found by monitoring of punctal parameter changes by AS-OCT. AS-OCT was found to be a useful method for evaluation of the lacrimal punctal parameters especially with different treatment modalities in epiphora cases.

1. Introduction

Lacrimal punctal stenosis is one of the least-evaluated etiologies of epiphora [1]. It is defined as narrowing or occlusion of the external opening of the lacrimal canaliculi, while the distal tear drainage system is free [2, 3]. It can also be defined more precisely as the punctum size less than

0.3 mm or inability to cannulate it with a 26G cannula without dilation [4].

Acquired punctal stenosis can result from variable causes, of which eye trauma, local or systemic drug toxicity, inflammatory or infectious diseases, malposition of the eyelid, tumors of upper and lower lid, or even the ageing changes could lead to that [5].

Various noxious stimuli can cause chronic inflammation with subsequent fibrosis and stenosis [6]. Punctal stenosis can be associated with canalicular, nasolacrimal sac and duct stenosis or obstruction in some cases [7].

Several methods were used for measuring normal punctum parameters, of which fitting different gauge cannulae (20–32G) but stretchable punctal walls during intubation made this method an unreliable predictor of punctal parameter measurements under normal physiological conditions [3].

Other methods approved photographing all four puncta by slit-lamp biomicroscopy and by using computer cursor punctal borders which are later mapped out, and the punctal area is measured by software-driven computer analysis [8].

Others used Ramsden eyepiece which has of a fixed transparent graduated scale positioned on the field and fitted to the slit-lamp with a fixed optical magnification of 32x results in a measurement of 0.03 mm [9].

AS-OCT parameters were $(614.6 \pm 195.6 \, \text{um})$ for the outer punctal diameter and $(545.8 \pm 270.1 \, \text{um})$ for the punctal depth. [10].

Anterior segment optical coherence tomography (AS-OCT) is accurate, noninvasive, objective, safe, and cross-sectional imaging method used to study various parts of the anterior segment of the eye including cornea, conjunctiva, angle, the lower tear meniscus height, and the lacrimal punctal parameters [10, 11].

In the literature, several methods were used for grading punctal stenosis. One of the most commonly used methods is Kashkouli's scoring system (grade 0 no punctum (agenesis), grade 1 punctal papilla is covered with a membrane (difficult to recognize), and the grade is less than the normal size but recognizable, grade 3 punctum is normal, grade 4 punctum is small slit (<2 mm), and grade 5 punctum is large slit (≤2 mm)) [12].

Munk scale for epiphora grading is another grading system (grade 0 no epiphora, grade 1 epiphora requiring dabbing less than twice a day, grade 2 epiphora requiring dabbing 2–4 times a day, grade 3 epiphora requiring dabbing 5–10 times a day, grade 4 epiphora requiring dabbing more than 10 times a day, and grade 5 is constant epiphora) [13].

The aim of this work was to evaluate the role of medical treatment and assessing its effect on resolving epiphora and improving punctum size by high resolution AS-OCT imaging comparing punctal parameters of the patients before and after treatment with topical combined antibiotic and steroids treatment in cases of inflammatory punctual stenosis.

2. Patients and Methods

The study included 44 eyes of 50 subjects; total coverage of epiphora patients fulfilled inclusion criteria and presented to the ophthalmology clinics of Sohag University Hospitals in the period between Jan 2021 and April 2021.

Patients included were aged 21 years or more who developed acquired inflammatory punctal edema and were complaining of epiphora. Punctal stenosis grading of the included groups was grade 2 according to Kashkouli's classification [12], and epiphora grading was 1 : 5 according to Munk's classification [13].

Patients who had a history of previous ocular and lacrimal surgery, trauma, lower lid margin malposition or laxity, dry eye (for the control group), glaucoma, corneal abnormalities (abrasions and keratitis), congenital punctal anomalies, nasolacrimal duct obstruction, mucocele, and pyocele were excluded.

The study design is a double-blinded controlled randomized study which was conducted on two group of patients, the first group, who had acquired punctal stenosis and epiphora (EG1) who received eye drops contains combination of antibiotics and steroids (orchadexoline eye drops, each ml contains 5 mg chloramphenicol, 1 mg dexamethasone sodium phosphate, 0.25 mg tetryzoline hydrochloride, 2 mg hydroxypropyl methyl cellulose, 10 mg α-tocopherol acetate (vitamin E), and 8 mg macrogol 400). The patients were advised to apply the drops 5 times daily for the first week, three times daily for the next two weeks, and one time daily for another one week. The second epiphora group (EG2) who received preservative-free artificial tears (sodium hyaluronate-, polyethylene-, and propylene glycol-based) three times daily for four weeks.

All patients were examined before treatment, one week, one month, and one and half months later. Orchadexoline eye drops were chosen due to its characteristic bitter taste to have a subjective method for evaluation of relieving of stenosis in addition to the objective method by AS-OCT. As the patients said that they felt bitter taste during treatment which is considered a sign of improvement.

Patients' selection was based on slit-lamp examination of the eye lids, corneal surface, bulbar and palpebral conjunctiva, tear meniscus, intraocular pressure (IOP) measurement, lower punctal examination, and grading of both punctal stenosis and epiphora according to Kashkouli's and Munk scoring systems [12].

2.1. Spectral Domain Anterior Segment-OCT Image Acquisition.
AS-OCT for lower puncti was performed using RTVue (Optovue Inc., Fermont, CA). OCT images of the width and length of the lower puncti of the participants were captured by the same operator on the same machine. The lower eyelid margin was gently everted using a cotton bud that was placed below the punctum. The punctum was everted perpendicular to the light source to allow alignment of the punctum depth with respect to the axis of the scanner's infrared beam. The punctum was imaged with the scan line placed horizontally along the mucocutaneous junction. Outer punctal diameter was measured as the distance between the two highest points on the nasal and temporal punctal orifice. Punctal depth is the vertical lumen; it was measured vertically between outer and inner punctal openings which appears closed.

This study was approved by the Ethical Committee of Faculty of Medicine, Sohag University, under IBR registration number S20-159 with clinical trial registration number NCT05028907 and was performed according to the

guidelines and Declaration of Helsinki. The aim of the study and intervention details were discussed with the participants, and informed written consent was obtained from them before inclusion.

2.2. Statistical Analysis. Statistical analysis was conducted using the SPSS software (version 26.0) (SPSS Inc., Chicago, IL, USA). All participants were chosen by using the systematic random sample technique from the attendees who fulfilled the inclusion criteria. The data were tested for normality using the Kolmogorov–Smirnov test and for homogeneity variances before further statistical analysis. Differences between groups for continuous measures were analyzed by an independent sample t-test and the chi-squared test for categorical measures. The Z test was used to compare 2 proportions.

3. Results

The study included 44 eyes of 50 subjects complaining of epiphora. They were divided into two groups, the epiphora group one (EG1) received eye drops containing combination of antibiotics and steroids (orchadexoline eye drops, each ml contains 5 mg chloramphenicol, 1 mg dexamethasone sodium phosphate, 0.25 mg tetryzoline hydrochloride, 2 mg hydroxypropyl methyl cellulose, 10 mg α-tocopherol acetate (vitamin E), and 8 mg macrogol 400).

The second epiphora group (EG2) received preservative-free artificial tears (sodium hyaluronate-, polyethylene-, and propylene glycol-based) three times daily for four weeks.

Both groups were comparable regarding mean age (49 ± 13 vs 53 ± 11 years, P value = 0.2) and sex (males were 38.6% vs 31.8%, female were 61.4% vs 68.2%, P value = 0.6), respectively, with no statistically significant difference between both groups (Table 1).

Mean duration of epiphora was measured in both groups before treatment (EG1 = 1.476 ± 0.51 months, EG2 = 1.57 ± 0.52 months) with no statistically significant difference (P value = 0.536).

Outer diameter and the length of the lower punctum of both groups before treatment and during the follow-up period comparing both groups were assessed objectively by AS-OCT and summarized in Table 2 and Figures 1(a)–1(d).

Both groups were comparable regarding outer punctal diameter and length between the puncti before treatment: outer punctal diameters (EG1 228 ± 113 um, EG2 241 ± 115 um, P value = 0.5) and length between outer and inner puncti (EG1 129 ± 73 um, EG2 137 ± 72 um, P value = 0.6). There was marked improvement of the outer punctual diameter (EG1 373 um ± 92 um, EG2 240 um ± 109 um, P value < 0.0002) and length between the puncti (EG1 217 ± 107 um, 136 ± 71 um (P value < 0.0008) during the follow-up period. EG1 showed more improvement than EG2 when compared during the follow-up period (Figures 2 and 3).

Subjective assessment of the improvement in both groups using Munk's test and the bitter taste of the orchadexoline eye drops were summarized in (Tables 3 and 4). Both groups showed significant objective improvement using Munk's test, which was more in EG1 when compared to EG2.

4. Discussion

The lacrimal punctum is an entry site for drainage of tears to the nasolacrimal duct [14]. Acquired and congenital abnormalities in the size and morphology of the lacrimal punctum and canaliculus may result in excess tears [3]. OCT is an established optical diagnostic technique that was employed for the first time for imaging the anterior segment in 1994 by Izatt [15].

OCT has many advantages, such as being noninvasive, painless, and contactless, with high resolution. Recently, OCT has been used to examine the proximal lacrimal system, and studies have investigated measurement of the anatomical parameters, evaluating the effect of punctoplasty and detecting lacrimal lesions [16, 17].

In this study, we evaluated the role of medical treatment and assessing its effect on resolving epiphora and improving the punctum size by high-resolution AS-OCT imaging comparing punctal parameters between patients and control subjects before and after treatment with topical combined antibiotic and steroid treatment in cases of inflammatory punctual stenosis.

The follow-up period was 6 weeks in both groups of the study. With clinical and OCT follow-up, we found marked improvement of the width and length of the lower puncti in group 1 (P value < 0.0001) with more improvement than group 2 when compared during the follow-up period.

In a study of Elalfy et al. [18], they evaluated prospectively the effect of medical treatment (preservative-free hydrocortisone sodium phosphate 3.35 mg/mL eye drops and preservative-free artificial tears based on sodium hyaluronate, polyethylene, and propylene glycol) in the management of inflammatory punctum stenosis guided by spectral domain anterior segment optical coherence tomography (OCT), and they concluded that a combination of preservative-free steroid eye drops and artificial tears causes significant widening of inflamed stenotic punctae and improvement of the epiphora.

We used anterior segment-OCT images for visualizing the lacrimal punctual structural changes as used previously [19] and performed quantitative measurements which help us to monitor disease prognosis and evaluate the efficacy of medical treatment.

The dexamethasone sodium phosphate used in the our study in group 1 exerts its anti-inflammatory effect in the surrounding conjunctival tissues of the ocular surface by decreasing the release of inflammatory mediators while chloramphenicol as a broad spectrum antibiotic eliminate any underlying subclinical infection.

In a study of Elshorbagy et al. [20], they investigated the role of anterior segment optical coherence tomography in the diagnosis of punctal stenosis and compared punctal parameters before and after medical treatment in the form of preservative-free methylprednisolone 5% eye drops. Their

TABLE 1: Demographic data of both groups.

		EG1, $n = 22$		Placebo group, $n = 22$		P value
Age	Mean + SD	49 ± 13		53 ± 11		0.2
Sex	Male	17	38.6%	14	31.8%	0.6
	Female	27	61.4%	30	68.2%	0.6

TABLE 2: Outer punctual diameter and length between the outer and inner punctum of both groups during follow-up period of six weeks.

		EG1, $n = 22$			EG2, $n = 22$			P value
		Mean	±	SD	Mean	±	SD	
	Before treatment	228 um	±	113	241 um	±	115	0.5
Outer punctual diameter	Two week after treatment	372 um	±	97	236 um	±	109	<0.0001
	Four weeks after treatment	396 um	±	87	243 um	±	110	<0.0001
	Six weeks after treatment	373 um	±	92	240 um	±	109	<0.0002
P1 value		<0.0001			0.9			
	Before treatment	129 um	±	73	137 um	±	72	0.6
Length between outer and inner punctum	Two weeks after treatment	211 um	±	108	131 um	±	69	<0.0006
	Four weeks after treatment	259 um	±	109	139 um	±	70	<0.0001
	Six weeks after treatment	217 um	±	107	136 um	±	71	<0.0008
P2 value		<0.0002			0.8			

[*]P[*]P value calculates the significant difference of the presented parameters between EG1 and EG2 and was calculated by the independent sample t-test. *P1* value calculates the significant difference in the outer punctual diameter in the EG1 and EG2 group before treatment and six weeks after treatment and was calculated by the paired sample t-test. *P2* value calculates the significant difference in the length between the outer and inner punctum in the EG1 and EG2 group before treatment and six weeks after treatment and was calculated by the paired sample t-test.
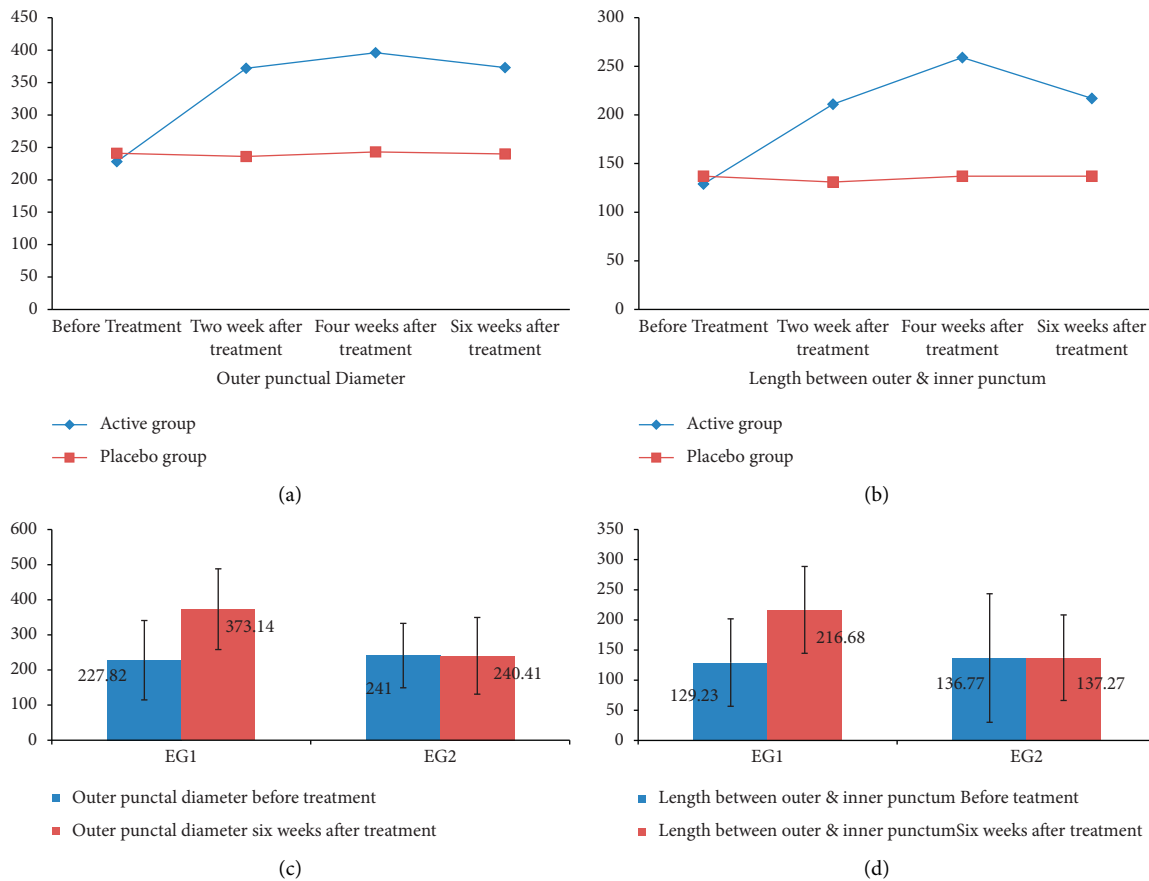

FIGURE 1: Comparison of outer diameter and the length of the lower punctum between both groups before treatment and during the follow-up period.
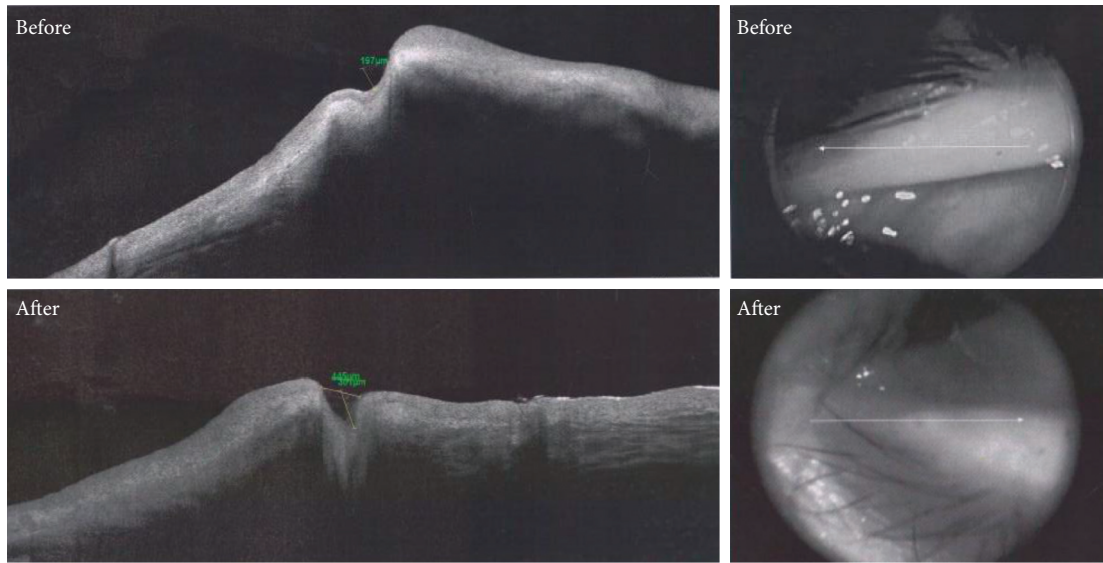
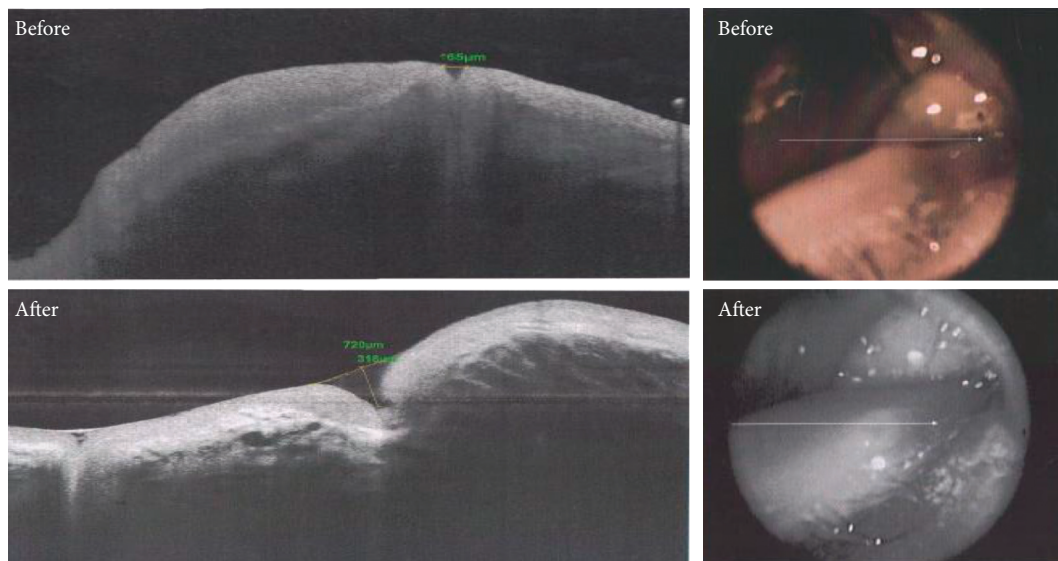FIGURE 2: Case 1: OCT punctal changes before and after treatment.

FIGURE 3: Case 2: OCT punctal changes before and after treatment.

TABLE 3: Munk's test results of both groups during follow-up period of six weeks.

Munk's test	EG1 $n = 22$	EG2 $n = 22$	P value
	Mean ± SD median (range)		
Before treatment	3.9 ± 1 4 (2–5)	3 ± 1.3 3 (1–5)	0.09
Two weeks after treatment	1 + 1 2 (0–4)	3 ± 1 4 (0–5)	<0.0001
Four weeks after treatment	1 + 1 2 (0–4|)	3 ± 1 4 (0–5)	<0.0001
Six weeks after treatment	1 + 1 1 (0–4)	3.4 ± 1.6 4 (0–5)	<0.0003
$P1$ value	<0.0002	<0.003	

$^*P$ $^*P$value calculates the significant difference of Munk's test between EG1 and EG2 and was calculated by Mann–Whitney U test. $P1$ value calculates the significant difference of Munk's test in the EG1 and EG2 group before treatment and six weeks after treatment and was calculated by Wilcoxon signed-ranks test.

TABLE 4: Bitter taste results of both groups before and after treatment.

Bitter taste		EG1 $n = 22$		EG2 $n = 22$		P value
		Count	%	Count	%	
Before treatment	No	28	63.6	28	63.6	0.8
	Yes	16	36.4	16	36.4	
Six weeks after treatment	No	6	13.6	26	59.1	<0.0009
	Yes	38	86.4	18	40.9	

P P value was calculated by Pearson chi-square. No, the patient did not felt bitter taste. Yes, the patient felt bitter taste.

results coincide with our results with improvement in AS-OCT parameters which were useful in monitoring and measuring the efficacy of medical treatment in reducing punctal edema, which results in subsequent reduction in the epiphora symptoms.

As regarding the OCT appearance of obstructed lacrimal puncti, OCT showed the narrow and small opening of the lacrimal punctum with fissure-like lumen of the vertical canaliculus (Figure 2), while in patients diagnosed with advanced punctal obstruction, OCT showed that the opening of the lacrimal punctum was covered by a membrane-like band (Figure 3). These results agree with the study of Hu et al. [21], who investigated the anatomical parameters of normal lacrimal puncta and vertical canaliculus using optical coherence tomography (OCT).

Limitations of this study included the small sample size of cases involved in the research (44 cases) and also, the short period of follow-up was another limitation (six weeks). Further studies are needed in the future with a larger sample size and longer follow-up period.

5. Conclusion

Topical combined antibiotic and steroid treatment was an effective method in treating cases of inflammatory punctal stenosis as found by monitoring of punctal parameter changes by AS-OCT. AS-OCT was found to be a useful method for evaluation of the lacrimal punctal parameters especially with different treatment modalities in epiphora cases.

Data Availability

The data used to support the results of this study are available from the corresponding author upon request.

Conflicts of Interest

The authors declare that they have no conflicts of interest.

References

[1] M. C. Hur, S. W. Jin, M. S. Roh et al., "Classification of lacrimal punctal stenosis and its related histopathological feature in patients with epiphora," *Korean Journal of Ophthalmology*, vol. 31, no. 5, pp. 375–382, 2017.

[2] U. Soiberman, H. Kakizaki, D. Selva, and I. Leibovitch, "Punctal stenosis: definition, diagnosis, and treatment," *Clinical Ophthalmology*, vol. 6, pp. 1011–1018, 2012.

[3] U. Soiberman, H. Kakizaki, D. Selva, and I. Leibovitch, "Punctal stenosis: definition, diagnosis, and treatment," *Clinical Ophthalmology*, vol. 6, p. 1011, 2012.

[4] R. H. Caesar and A. A. McNab, "A brief history of punctoplasty: the 3-snip revisited," *Eye*, vol. 19, no. 1, pp. 16–18, 2005.

[5] O. R. Ozgur, L. Akcay, N. Tutas, and O. Karadag, "Management of acquired punctal stenosis with perforated punctal plugs," *Saudi Journal of Ophthalmology*, vol. 29, no. 3, pp. 205–209, 2015.

[6] H. B. Fleit, "Chronic inflammation, pathobiology of human disease," in *Pathobiology of Human Disease*, L. M. McManus and R. N. Mitchell, Eds., Academic Press, San Diego, CA, USA, pp. 300–314, 2014.

[7] M. Kashkouli, F. Pakdel, and V. Kiavash, "Assessment and management of proximal and incomplete symptomatic obstruction of the lacrimal drainage system," *Middle East African Journal of Ophthalmology*, vol. 19, no. 1, p. 60, 2012.

[8] K. D. Carter, C. C. Nelson, and C. L. Martonyi, "Size variation of the lacrimal punctum in adults," *Ophthalmic Plastic and Reconstructive Surgery*, vol. 4, no. 4, pp. 231–234, 1988.

[9] S. Patel and I. Wallace, "Tear meniscus height, lower punctum lacrimale, and the tear lipid layer in normal aging," *Optometry and Vision Science*, vol. 83, no. 10, pp. 731–739, 2006.

[10] Y. Sung, J. S. Park, and H. Lew, "Measurement of lacrimal punctum using spectralis domain anterior optical coherence tomography," *Acta Ophthalmologica*, vol. 95, no. 7, pp. e619–e624, 2017.

[11] D. I. Park, H. Lew, and S. Y. Lee, "Tear meniscus measurement in nasolacrimal duct obstruction patients with Fourier-domain optical coherence tomography: novel three-point capture method," *Acta Ophthalmologica*, vol. 90, no. 8, pp. 783–787, 2012.

[12] M. B. Kashkouli, N. Nilforushan, M. Nojomi, and R. Rezaee, "External lacrimal punctum grading: reliability and interobserver variation," *European Journal of Ophthalmology*, vol. 18, no. 4, pp. 507–511, 2008.

[13] P. L. Munk, D. T. Lin, and D. C. Morris, "Epiphora: treatment by means of dacryocystoplasty with balloon dilation of the nasolacrimal drainage apparatus," *Radiology*, vol. 177, no. 3, pp. 687–690, 1990.

[14] M. J. Ali, D. K. Mishra, F. Baig, M. Lakshman, and M. N. Naik, "Punctal stenosis," *Ophthalmic Plastic and Reconstructive Surgery*, vol. 31, no. 2, pp. 98–102, 2015.

[15] J. A. Izatt, M. R. Hee, E. A. Swanson et al., "Micrometer-scale resolution imaging of the anterior eye in vivo with optical coherence tomography," *Archives of Ophthalmology*, vol. 112, no. 12, pp. 1584–1589, 1994.

[16] H. M. Timlin, P. A. Keane, A. C. Day et al., "Characterizing the lacrimal punctal region using anterior segment optical coherence tomography," *Acta Ophthalmologica*, vol. 94, no. 2, pp. 154–159, 2016.

[17] J. R. Wawrzynski, J. Smith, A. Sharma, and G. M. Saleh, "Optical coherence tomography imaging of the proximal lacrimal system," *Orbit*, vol. 33, no. 6, pp. 428–432, 2014.

[18] H. Y. Elalfy, M. A. Elsamkary, A. M. S. Elridy, T. M. Saad, S. M. Rashad, and S. M. Fawzy, "Medical treatment of inflammatory punctual stenosis monitored by anterior segment optical coherence tomography," *International Journal of Ophthalmology*, vol. 13, no. 7, pp. 1074–1078, 2020.

[19] D. Schmidl, A. Schlatter, J. Chua, B. Tan, G. Garhöfer, and L. Schmetterer, "Novel approaches for imaging-based diagnosis of ocular surface disease," *Diagnostics*, vol. 10, no. 8, p. 589, 2020.

[20] M. S. Elshorbagy, O. E. Shalaby, M. A. Eldesouky, and A. M. Awara, "Anterior segment optical coherence tomography (AS-OCT) guided reversal of edematous punctal occlusion," *Clinical Ophthalmology*, vol. 14, pp. 1467–1472, 2020.

[21] J. Hu, N. Xiang, G. G. Li et al., "Imaging and anatomical parameters of the lacrimal punctum and vertical canaliculus using optical coherence tomography," *International Journal of Medical Sciences*, vol. 18, no. 12, pp. 2493–2499, 2021.